

**POLYPROPYLENE PRODUCTION IN A  
FLUIDISED BED CATALYTIC REACTOR:  
COMPREHENSIVE MODELING, OPTIMISATION  
AND PILOT SCALE EXPERIMENTAL  
VALIDATION**

**MOHAMMAD JAKIR HOSSAIN KHAN**

**FACULTY OF ENGINEERING  
UNIVERSITY OF MALAYA  
KUALA LUMPUR**

**2016**

**POLYPROPYLENE PRODUCTION IN A FLUIDISED  
BED CATALYTIC REACTOR : COMPREHENSIVE  
MODELING, OPTIMISATION AND PILOT SCALE  
EXPERIMENTAL VALIDATION**

**MOHAMMAD JAKIR HOSSAIN KHAN**

**THESIS SUBMITTED IN FULFILMENT OF THE  
REQUIREMENTS FOR THE DEGREE OF DOCTOR OF  
PHILOSOPHY**

**FACULTY OF ENGINEERING  
UNIVERSITY OF MALAYA  
KUALA LUMPUR**

**2016**

**UNIVERSITY OF MALAYA**

**ORIGINAL LITERARY WORK DECLARATION**

**Name of Candidate : Mohammad Jakir Hossain Khan**

**(I.C/Passport No: [REDACTED])**

**Registration/Matric No : KHA 110038**

**Name of Degree : Doctor of Philosophy**

**Title of Project Paper/Research Report/Dissertation/Thesis ("this Work"):**

**POLYPROPYLENE PRODUCTION IN A FLUIDISED BED CATALYTIC  
REACTOR (FBCR): COMPREHENSIVE MODELING, OPTIMISATION AND  
PILOT SCALE EXPERIMENTAL VALIDATION.**

**Field of Study: Chemical Engineering**

**I do solemnly and sincerely declare that:**

- (1) I am the sole author/writer of this Work;
- (2) This Work is original;
- (3) Any use of any work in which copyright exists was done by way of fair dealing and for permitted purposes and any excerpt or extract from, or reference to or reproduction of any copyright work has been disclosed expressly and sufficiently and the title of the Work and its authorship have been acknowledged in this Work;
- (4) I do not have any actual knowledge nor do I ought reasonably to know that the making of this work constitutes an infringement of any copyright work;
- (5) I hereby assign all and every rights in the copyright to this Work to the University of Malaya ("UM"), who henceforth shall be owner of the copyright in this Work and that any reproduction or use in any form or by any means whatsoever is prohibited without the written consent of UM having been first had and obtained;
- (6) I am fully aware that if in the course of making this Work I have infringed any copyright whether intentionally or otherwise, I may be subject to legal action or any other action as may be determined by UM.

**Candidate's Signature**

**Date:**

**Subscribed and solemnly declared before,**

**Witness's Signature**

**Date:**

**Name:**

**Designation:**

## ABSTRACT

There is wide range of applications in chemical processes and energy generation in the experimental and numerical studies of multiphase flows. General uses include fluidised bed catalytic polymerization, fluidised bed reactors (type of chemical reactors), process parameters optimization, such as temperature, system pressure, monomer concentration, catalyst feed rate, superficial fluid velocity and vital technology breakthrough in various polyolefin based engineering. Via the use of Computational Fluid Dynamics (CFD) methods combined with mathematical and statistical model, this thesis concentrated on the investigation of bubble and emulsion phase dynamic transitions on polypropylene production rate. The use of ANNOVA (Analysis of variance) method with Response Surface Methodology (RSM) was used to statistically model the experiments to validate and identify the process parameters for polypropylene production was conducted by. Reaction temperature, system pressure and hydrogen percentage were the three important process variables and important input factors in the performed analysis of polypropylene production. Through the evaluation of the effects of the process parameters and their interactions, statistical analysis indicated that the proposed quadratic model had a good fit with the experimental results. The highest polypropylene production of 5.82% per pass was obtained at an optimum condition with temperature of 75 °C, system pressure of 25 bar and hydrogen percentage of 2%. With the combination of statistical model and CFD (computational fluid dynamic) method, a hybrid model was developed to explain the detailed phenomena of the process parameters. A series of experiments were also conducted for propylene polymerisation by changing the feed gas composition, reaction initiation temperature and system pressure in a fluidised bed catalytic reactor. During reaction, 75% monomer concentration (MC) was shown as the optimum propylene concentration. The multiphase reaction models tested in this research supposed that polymerisation

happened at both in the emulsion and the bubble phase. With respect to the experimental range of the superficial gas velocity and the catalyst feed rate, it was observed that the ratio of the polymer created during the bubble phase, as compared to the overall rate of production, was approximately in the range of 9.1-10.8%. This was a noteworthy quality and should not be looked over. Two different solvers were used to achieve fluid flow computation. One of them was ANSYS FLUENT which was a general-purpose CFD code expanded from UDF (user defined functions) method on a collocated grid. The expanded UDF had various physical models that could be used in a wide range of industries. The other solver was Design Expert which was developed for the optimization of a broad range of process parameters. Multiphasic model was a general-purpose hydrodynamic model that validated chemical reactions and dynamic profiles of gas-solid flow in real reaction situations that usually occurred in olefin polymerization and chemical processing reactors. It was observed that the enhanced hybrid and multiphasic models were able to forecast more constricted and safer windows at analogous conditions as compared to the experimental results. Conversely, the enhanced models had similar dynamic behaviour as the conventional model during the initial stages of the polymerisation but deviated as time progressed. Characterizations studies were conducted on the polypropylene and resulted in detailed information on the effects of the different process parameters on the product.

## ABSTRAK

Semenjak sedekad yang lalu, kajian secara eksperimen dan numerik terhadap pelbagai aliran telah menunjukkan peningkatan yang luar biasa terutamanya pada aliran gas-pepejal. Kajian terbabit telah banyak diaplikasikan di dalam proses kimia, penjaan tenaga dan sebagainya. Aplikasi yang biasa adalah merupakan pempolimeran reaktor lapisan berpemangkin, reaktor lapisan bendalir (sejenis reaktor kimia), pengoptimuman parameter proses, seperti suhu, tekanan sistem, kepekatan monomer, kadar kemasukan pemangkin, had laju bendalir dan kejayaan menemukan teknologi penting dalam pelbagai produk kejuruteraan asas polyolefin. Kajian yang diketengahkan dalam tesis ini menumpukan penyiasatan terhadap transaksi dinamik fasa gelembung dan emulsi kepada kadar pempolimeran melalui penggunaan kaedah Computational Fluid Dynamics (CFD) yang digabungkan dengan model matematik. Tindak balas pelbagai fasa yang dilaksanakan di dalam kajian ini menganggarkan pempolimeran berlaku di dalam kedua-dua fasa gelembung dan emulsi. Dapat diperhatikan bahawa dengan merujuk kepada julat eksperimen had laju bendalir dan kadar kemasukan pemangkin, nisbah polimer yang terhasil kepada kadar keseluruhan penghasilan produk adalah dianggarkan di antara 9.1-10.8%. Ini adalah satu jumlah yang besar dan tidak boleh diabaikan. Pengiraan aliran bendalir dapat dilaksanakan dengan menggunakan dua perisian yang berbeza. Satu daripadanya ialah ANSYS FLUENT, kod umum CFD berdasarkan kaedah pembentukan UDF (fungsi takrifan pengguna) pada himpunan grid. Pembentukan UDF menawarkan pelbagai model fizikal yang boleh diaplikasikan oleh pelbagai bidang industri. Dapat disimpulkan bahawa model dua-fasa yang berpeningkatan dan model CFD dapat membuat pneganggaran yang lebih tepat dan selamat pada keadaan yang sama jika dibandingkan dengan keputusan eksperimen. Pemodelan statistik dengan pengesahan eksperimen terhadap parameter proses

penghasilan polypropylene dijalankan menggunakan kaedah ANNOVA (Analysis of variance) kepada Response Surface Methodology (RSM). Tiga pembolehubah proses i.e., suhu tindak balas, tekanan sistem dan peratusan hidrogen dipertimbangkan sebagai faktor input yang penting dalam penghalisan polypropylene terhadap analisis yang dilaksanakan. Analisis statistik menunjukkan kuadratik model yang dicadangkan bersesuaian dengan keputusan dari eksperimen. Penghasilan polypropylene tertinggi diperolehi iaitu 5.82% setiap pas pada keadaan optimum bersuhu 75 °C, tekanan sistem 25 bar dan 2% peratusan hidrogen. Model hybrid dicadangkan, menggabungkan kombinasi model statistik dengan kaedah CFD (computational fluid dynamic), digunakan bagi menerangkan fenomena parameter-parameter proses, dan eksperimen bersiri dijalankan bagi pemolimeran propylene dengan mengubah komposisi gas, suhu awal tindak balas, dan tekanan sistem, di dalam reaktor lapisan bendalir berpemangkin, 75% kepekatan monomer (MC) merupakan kepekatan propylene yang optimum dan perlu dikekalkan sepanjang tindak balas. Kajian ini adalah unik kerana pembentukan model bersepadu ini juga mampu memberikan idea yang jelas berkaitan dengan dinamik parameter lapisan untuk memisahkan fasa-fasa dan juga mampu menghitung kadar tindak balas kimia bagi setiap fasa di dalam tindak balas tersebut. Selain itu, model yang berpeningkatan ini juga menunjukkan perlakuan dinamik yang sama berbanding model konvensional, pada peringkat awal tindak balas pemolimeran; akan tetapi, ia menyimpang seiring dengan peningkatan waktu. Kajian pencirian juga telah dijalankan terhadap polypropylene; iaitu memberikan maklumat yang lengkap terhadap kesan perubahan parameter proses kepada produk.

## ACKNOWLEDGEMENTS

First of all and foremost, I thank to my ALLAH almighty for giving me strength, will-power, patience against many odds and fulfilling my prayers, ALHAMDULILLAH. All of my best wishes are always given to the Holy Prophet Muhammad S. A. W, his families, and all of us as their followers until the end of time.

I would like to express my special appreciation and thanks to my supervisor, Professor Dr. Ir. Mohd Azlan Hussain: you have been a tremendous mentor for me. I would like to thank you for encouraging my research and for allowing me to grow as a research scientist. The scholastic guidance of Professor Iqbal M Mujtaba from University of Bradford, UK on both research as well as on my career have been priceless. I would remember their immense support throughout my life.

I also wish to sincerely thank to University of Malaya and Ministry of Education, Malaysia for funding my PhD research described in this thesis through the HIR Grant (UM.C/HIR/MOHE/ENG/25) and Commonwealth Scholarship and Fellowship Plan (CSFP) in Malaysia. It is a pleasure to express a gratitude to the Project Directorate of Bangabandhu Fellowship Project, Bangladesh, for the assistance and support throughout my study period. I also would like to offer my gratitude to my younger brother, sister and fellow friends who have contributed ideas and suggestion to the success of this thesis. Words fail me to express my appreciation to my wife and my beloved son, for their endless love and understanding, through the duration of my studies. Without them with me, it would not have been possible to complete my studies.

Finally, I would like to thank everybody who had been important to the successful realization of thesis, and I would like to express my apology that I could not mention them personally one by one. This thesis is dedicated to my lovely mom,dad, wife and son.

**Mohammad Jakir Hossain Khan**



## TABLE OF CONTENTS

TITLE PAGE.....	i
ORIGINAL LITERARY WORK DECLARATION.....	ii
ABSTRACT (ENGLISH).....	iii
<i>ABSTRAK</i> .....	v
ACKNOWLEDGEMENTS.....	viii
TABEL OF CONTENTS.....	ix
LIST OF FIGURES.....	xiii
LIST OF TABLES.....	xiv
<b>CHAPTER 1: INTRODUCTION.....</b>	<b>1</b>
1.1 Background.....	1
1.2 Problem statement .....	3
1.3 Objectives of the research .....	4
1.4 Workflow of the thesis .....	5
 <b>CHAPTER 2: LITERATURE REVIEW.....</b>	 <b>9</b>
2.1 Introduction.....	9
2.1.1 The process of fluidization and fluidized bed reactors.....	9
2.1.2 Scope of the review .....	10
2.2 Computational modeling of fluidized bed reactor .....	15
2.2.1 Theoretical framework .....	15
2.2.1.1 The eulerian model .....	18
2.2.1.2 The mixture model .....	18
2.2.1.3 The vof model .....	19
2.2.1.4 Combined approaches.....	19
2.3 CFD software packages .....	22
2.4 Coding and models for CFD.....	40
2.4.1 Supporting tools for CFD software .....	43
2.5 Aspects and mechanisms in fluidized bed reaction .....	45
2.5.1 Modeling of hydrodynamic behavior of fluidized bed reactor.....	45
2.5.2 Fluid flow modeling .....	46
2.5.3 Mixing models .....	50
2.5.4 Bubble modeling .....	54

2.6 Elevated pressure processes .....	61
2.7 CFD study on heat transfer phenomena and modeling of polyolefin reaction.....	63
2.8 Electrostatic modeling of polymerization .....	72
2.9 Modeling of agglomeration in fluidized bed reactors .....	79
2.10 Summary.....	88
<b>CHAPTER 3: POLYPROPYLENE PRODUCTION OPTIMIZATION IN FLUIDIZED BED CATALYTIC REACTOR (FBCR): STATISTICAL MODELING AND PILOT SCALE EXPERIMENTAL VALIDATION.....</b>	<b>91</b>
3.1 Introduction .....	91
3.2 Experimental Studies .....	95
3.2.1 Pilot plant description and operation.....	95
3.2.2 Pilot plant instrumentation.....	97
3.3 Experimental design and optimization.....	98
3.4 Results and Discussion.....	100
3.4.1 Verification on Statistical Models .....	100
3.4.2. Model Fitting.....	102
3.4.2.1 Diagnostic Statistics for Model Adequacy.....	105
3.5 3D Response Surfaces and their corresponding analysis.....	110
3.6 Conclusion.....	112
<b>CHAPTER 4: DEVELOPED HYBRID MODEL FOR PROPYLENE POLYMERISATION AT OPTIMUM REACTION CONDITION.....</b>	<b>114</b>
4.1 Introduction.....	114
4.2 Experimental study.....	117
4.2.1 Description of experimental setup .....	117
4.2.2 Measurement and analysis system.....	120
4.2.3 Model development for optimization.....	121
4.3 CFD Modelling of Gas–Solid Phenomenon in FBCR.....	123
4.3.1 Phase Sequestration.....	124
4.3.2 Mass balance model.....	127
4.3.2.1 Conservation of Momentum.....	127
4.3.3 Solids Pressure.....	129
4.4 Results and Discussion.....	130
4.4.1 RSM analysis.....	131

4.4.2 Effect of Process Conditions on Bed Structure during Reaction..	134
4.4.3 Boundary condition.....	135
4.5 Model Validation and Grid Sensitivity Analysis.....	136
4.5.1 Grid Independent Analysis.....	138
4.6 Examining the model accuracy.....	143
4.6.1 Interaction graphs.....	146
4.6.2 Perturbation graph.....	147
4.7 Statistical diagnosis of the model through ANNOVA analysis .....	148
4.8 Financial Benefits.....	150
4.9 Conclusion.....	151
<b>CHAPTER 5: MULTIPHASIC REACTION MODELING FOR</b>	<b>154</b>
<b>POLYPROPYLENE PRODUCTION IN A PILOT-SCALE</b>	
<b>CATALYTIC REACTOR.....</b>	
5.1 Introduction.....	154
5.2 The Reactions and Kinetic Model for Polymerization.....	158
5.2.1 The Multiphasic Hydrodynamic Models.....	160
5.2.2 The Emulsion Phase Model.....	165
5.2.3 The Bubble Phase Model.....	166
5.2.4 The Inter-Phase Hydrodynamic Model.....	168
5.2.5 Coupling Steps of Multiphasic CFD-Based Reaction model.....	173
5.2.6 Grid Sensitivity Analysis.....	174
5.3 Experimental Facilities.....	176
5.3.1 The Catalyst Dosing Measurement System.....	178
5.4 Results and Discussion.....	180
5.4.1 Hydrodynamic Model in the Absence of Polymerization.....	181
5.4.2 Bubble Emulsion Phase Distribution and Model Verification.....	183
5.4.3 Model Validation Based on the Effect of Superficial .....	188
5.4.4 Effect of Catalyst Feed Rate.....	192
5.4.5 Effect of the Feed Composition.....	194
5.5 Conclusions.....	196

<b>CHAPTER 6: EFFECT OF DYNAMIC PROCESS PARAMETERS ON PRODUCTION RATE OF POLYPROPYLENE AND THEIR MECHANICAL FEATURES: FROM VALIDATING MODELS TO PRODUCT ENGINEERING .....</b>	<b>201</b>
6.1 Introduction.....	201
6.2 Choice of measurement technique.....	205
6.3 Experimental setups .....	207
6.4 Model development .....	208
6.5 Sample preparation for mechanical testing .....	217
6.5.1 Impact property testing of plastics.....	218
6.5.2 Dynamic mechanical analysis.....	218
6.6 Results and Discussion.....	219
6.6.1 Dual phase (bubble-emulsion) dynamics behaviour.....	219
6.6.2 Dynamics of temperature on reaction system and production.....	221
6.7 Real-time pressure profile during reaction .....	223
6.8 Hydrogen flow rate profile.....	225
6.9 Mechanical and thermal characterisations.....	227
6.9.1 Izod impact strength.....	228
6.9.2 Tensile and flexural properties.....	229
6.9.3 Morphological transformations.....	231
6.9.4 Dynamic Mechanical Analysis (DMA).....	232
6.10 Conclusions.....	236
<b>CHAPTER 7: CONCLUSIONS AND RECOMMENDATIONS.....</b>	<b>238</b>
7.1 Conclusions.....	238
7.2 Recommendations and future works.....	240
<b>REFERENCES .....</b>	<b>241</b>
<b>LIST OF PUBLICATIONS.....</b>	<b>266</b>

## LIST OF FIGURES

Figure 2.1:	(a) Schematic of a fluidized bed polypropylene reactor with multiphase reaction steps; (b) influence of catalyst particles inside phases.....	12
Figure 2.2:	Typical surface temperature profile inside the pilot plant....	39
Figure 2.3:	Typical concentration profile of ethylene.....	39
Figure 2.4:	Typical mesh (a) original mesh performing using GAMBIT, (b) refined mesh in FLUENT only for the height of fluidized section.....	44
Figure 2.5:	Void fraction contours and solid flux vectors of the bed with a porous plate distributor.....	51
Figure 2.6:	Comparison between experiment and model results in terms of (a) bubble shape and (b) particle velocity profile of polyethylene. The unit vector above particle velocity profile plot corresponds to a particle velocity of 1 m/s and minimum fluidization velocity 1.25 m/s.....	56
Figure 2.7:	Void fraction of solids at specific cutoff for different time steps.....	57
Figure 2.8:	Simulation with time step of 0.00025 s, first order up-wind (Courant number was below 0.15, at constant cell value). With condition of gas velocity 12.6 cm/s, gas density 1.21 kg/m <sup>3</sup> , pressure 101325 Pa and minimum fluidization velocity 0.093 m/s.....	59
Figure 2.9:	Bubble and particle behaviors at three different fluidization conditions. (a) normal gas-inlet mode, (b) gas entering the core zone exclusively, and (c) gas entering the annulus zone exclusively.....	61
Figure 2.10:	Instantaneous particle time line temperature distribution in a fluidized regime at minimum fluidization velocity 1.6 ms <sup>-1</sup> .....	69
Figure 2.11:	Snapshots showing the heating process of particles by hot air uniformly injected at the bed bottom in different flow regimes: (a) fixed bed ( $u_f/u_{mf} = 0.5$ ); (b) expanded bed ( $u_f/u_{mf} = 1.4$ ); and (c) fluidized bed ( $u_f/u_{mf} = 6.0$ ). Particles are colored by their dimensionless temperatures. The dimensionless temperature $T$ of individual particles is obtained according to $(T_i - T_0)/(T_{in} - T_0)$ , where $T_0$ is the initial bed temperature and $T_{in}$ is the air temperature at the inlet.....	71
Figure 2.12:	Scheme of the electric charge transporting process during the fluidization: (a) occurred charging via particle–gas friction, (b) occurred charging via smooth and purities particle–particle contact, and (c) occurred charging via roughness and impurities particle–particle contact.....	74
Figure 2.13:	Effect of particle charge (mono-charged) on the bubble hydrodynamics in the bed at $U_0 = 1.2$ m/s.....	76
Figure 2.14:	Instantaneous contours of electric field for two-dimensional	77

	simulation of pilot plant fluidized-bed reactor for standard deviation=0.01 at t=129.5 s: (a) radial direction, (b) axial direction (same scale), (c) axial direction (reduced scale)	
Figure 2.15:	Electrostatic effects on the particles in a quasi-2D fluidized bed.....	79
Figure 2.16:	The snapshots of agglomerate formation in the bed.....	83
Figure 3.1:	Schematic diagram of fluidization of the polypropylene production system.....	96
Figure 3.2:	Detailed experimental set up of a pilot scale fluidized bed catalytic reactor (3D).....	97
Figure 3.3:	Normal probability plot.....	107
Figure 3.4:	Linear correlation between actual and predicted values.....	107
Figure 3.5:	The residuals and predicted response plot for propylene polymerization.....	107
Figure 3.6:	Outlier <i>t</i> plot for propylene polymerization per pass.....	108
Figure 3.7:	Deviation graph of process parameters.....	109
Figure 3.8:	3D Response surface and contour plot of hydrogen concentration vs. pressure on polypropylene production (%)......	111
Figure 4.1:	Detailed process diagram of fluidization of polypropylene production system .....	118
Figure 4.2:	Sampling and Analysis system integrated with a pilot scale fluidized bed catalytic reactor.....	118
Figure 4.3:	3D Response surface 3(a) with 2Dcontour plot 3(b) of reaction temperature (RT) and system pressure (SP) .....	131
Figure 4.4:	3D Response surface 4(a) with 2Dcontour plot 4(b) of reaction temperature (RT) and monomer concentration (MC).....	132
Figure 4.5:	3D Response surface 4.5(a) with 2Dcontour plot 4.5(b) of Bubble diameter and pressure on polymerisation.....	134
Figure 4.6(a)	Changes of polymerization rate at node number 101,343 at various pressure and amount of monomer (propylene). y-axis indicates the polymerization changes.....	138
Figure 4.6 (b)	Changes of polymerization rate at node number 101,343 at various pressure and amount of monomer (propylene). y-axis indicates the polymerization changes.....	139
Figure 4.6(c):	Changes of polymerization rate at node number 87,009 , at various pressure and amount of monomer (propylene). y-axis indicates the polymerization changes.....	139
Figure 4.7:	General computational domain and mesh generation ; (a) Framework of the gas-phase fluidized bed polymerization reactor used in simulation, (b) Generated Mesh for fluidized bed simulation, (c ) Computational region marked.....	140
Figure 4.8:	Bed dynamic conditions at various process combinations at inlet gas velocities.....	142
Figure 4.9:	Normal % probability and residual plot for propylene polymerization (%)......	144
Figure 4.10:	The residuals and predicted response plot for propylene polymerization.....	145
Figure 4.11:	Outlier <i>t</i> plot for propylene polymerization (%) per pass.....	146
Figure 4.12:	(a) Interaction between temperature and pressure; (b)	147

	Interaction between temperature and propylene concentrations; (c) Interaction between pressure and propylene concentration.....	
Figure 4.13:	Deviation of individual parameter from the response.....	148
Figure 5.1:	Steps of CFD-based multiphasic reaction model development.....	174
Figure 5.2:	(a) Changes of the polymerization rate at node number 111,143 at various superficial gas velocities. Contour lines indicate the polymerization (%) changes; (b) Changes of the polymerization rate at node number 89,101 at various superficial gas velocities. Contour lines indicate the polymerization (%) changes; (c) Changes of the polymerization rate at node number 56,834, at various superficial gas velocities. Contour lines indicate the polymerization (%) changes.....	175
Figure 5.3:	General computational domain and mesh generation. (a) Framework of the gas-phase fluidized bed polymerization reactor used in the simulation; (b) Generated mesh for the fluidized bed simulation; (c) Computational region marked.	176
Figure 5.4:	Image of the pilot-scale FBCR for polypropylene production where the experiments were conducted for this study (detailed dimensions have been shown in mm).....	178
Figure 5.5:	A Real-time data acquisition system for the pilot-scale FBCR for polypropylene production.....	178
Figure 5.6:	Pressure and temperature profile measurement scheme for real-time data acquisition system (fluidized bed has been shown before gas mixer introduction in the system).....	179
Figure 5.7:	The catalyst dosing measurement device. (1) An elective touchscreen with a dose-controlling optional button; (2) A dual-wire reading meter; (3) A changeable and a rotatable converter consisting of a rapid connector technique; (4) Horn antennas (made of stainless steel); (5) A flange plate protector (needed for aggregating products) with extension services; (6) A single converter for many applications.....	179
Figure 5.8:	Dynamic bed behavior analysis between multiphasic and conventional model (without reaction).....	182
Figure 5.9:	Dynamic effect of superficial gas velocity on phase (bubble and emulsion) formation before catalyst injection.....	185
Figure 5.10:	Mass fraction of monomer (propylene) during reaction at $U_0 = 0.2$ m/s.....	187
Figure 5.11:	The dispersal transformation of hydrogen mass fraction due to alteration of time in the FBR at $U_0 = 0.2$ m/s.....	189
Figure 5.12:	Effect of superficial gas velocity on the production rate (at optimum catalyst dosing 0.2 g/s).....	190
Figure 5.13:	Effect of superficial gas velocity on the production rate of emulsion phases at various catalyst feed rates predicted by the multiphasic model.....	190
Figure 5.14:	The ratio of polymer production in the bubble phase to the total production rate.....	191
Figure 5.15:	Snapshot of the solid volume fraction of catalyst particles with different time intervals in the FBR.....	194
Figure 5.16:	Effect of catalyst feed rate on polypropylene production	194

	comparison and validation.....	
Figure 5.17:	Effect of monomer composition (mol %) on polypropylene production.....	195
Figure 6.1 :	Pressure and temperature profile measurement scheme for real-time data acquisition. (fluidised bed has been shown before gas mixer introduction in the system).....	206
Figure 6.2:	Detailed schematics of the pilot scale fluidised bed reactor for polypropylene production , 2 (a) and pilot scale fluidised bed reactor at University of Malaya, 2 (b) .....	207
Figure 6.3:	Schematic of online data acquisition system .....	204
Figure 6.4:	Produced granular Polypropylene (6.4.a) and dog-bone shape polypropylene bars (6.4.b) for thermo-mechanical testing.....	217
Figure 6.5:	Dynamic phase transformation of fluidised bed during propylene polymerisation.....	221
Figure 6.6:	Online temperature monitoring during reaction and effect on reaction rate. (system pressure 25 bar and hydrogen concentration at 2 mol%)	222
Figure 6.7:	Real-time pressure dynamics profile of propylene polymerisation in a pilot scale fluidised bed reactor at 75 °C temperature and 2 mol% of hydrogen.....	225
Figure 6.8:	Real-time Hydrogen consumption dynamics in the pilot scale fluidised polymerisation reactor.....	226
Figure 6.9:	Izod strength profile of different grades of polypropylene (PP-2, PP-4 and PP-8) .....	229
Figure 6.10:	Tensile strength analysis of PP-2, PP-4 and PP-8 (ASTM D 638).....	230
Figure 6.11:	SEM images on morphological changes of produced polypropylene .....	231
Figure 6.12(a):	DMA analysis of PP-2 (s=Sample Size: 17.5000 x 10.2000 x 2.4200 mm, Method: SOP 05202, Single Cantilever Ramp 5.00 °C/min, Instrument: DMA Q800 V20.24 Build 43).....	233
Figure 6.12(b):	DMA analysis of PP-4 (s=Sample Size: 17.5000 x 10.2000 x 2.4200 mm, Method: SOP 05202, Single Cantilever Ramp 5.00 °C/min, Instrument: DMA Q800 V20.24 Build 43).....	233
Figure 6.12(c):	DMA analysis of PP-8 (s=Sample Size: 17.5000 x 10.2000 x 2.4200 mm, Method: SOP 05202, Single Cantilever Ramp 5.00 °C/min, Instrument: DMA Q800 V20.24 Build 43).....	234



## LIST OF TABLES

Table-2.1:	Recent applications of CFD approach on fluidization and fluidized bed reactors.....	24
Table 2.2:	Equations used for CFD analysis in ANSYS FLUENT for polyolefin fluidized bed reactors.....	33
Table 2.3:	Multi-category usages of MFIX.....	43
Table 2.4:	Equations for calculating heat flux .....	71
Table 3.1:	Coded levels for independent variables used in the experimental design.....	100
Table 3.2:	Central Composite Design (CCD) experimental design and results of the response surface.....	101
Table 3.3:	Model selection.....	102
Table 3.4:	Statistical parameters for sequential models.....	103
Table 3.5:	<i>t</i> -Test result for testing the significance of individual parameters.....	104
Table 4.1:	Range of the independent process variables employed in the experimental design and physical properties of the reaction system.....	122
Table 4.2:	Dynamic Correlations and Formulas Applied for the CFD Model for the Bubble and Emulsion Phase.....	125
Table 4.5:	Statistical parameters for developed model and process parameters.....	149
Table 5.1:	Kinetic mechanism of gas-phase catalytic propylene polymerization.....	162
Table 5.2:	Dynamic correlations and formulas applied for the multiphasic model.....	164
Table 5.3:	Transport equations for dynamic multiphasic fluidized bed reaction system.....	170
Table 5.4:	Features of the catalyst dosing system.....	180
Table 5.5:	System boundary and operating conditions used for simulation..	181
Table 6.1:	Computational conditions for modelling.....	216

## CHAPTER 1: INTRODUCTION

### 1.1 Background

Over the last few decades, polymer-based materials have been the focus of research due to the noticeable advancement in improved material properties in comparison to other conventional micro- and macro-level materials (Arencón & Velasco, 2009; Delva et al., 2014; Tian, Xue et al., 2013). Among polymer-based materials, polypropylene is known as a high-class thermoplastic polymer resin generated from olefins (Galli & Vecellio, 2004; Nguyen et al., 2015). Polypropylene has been positioned as the leading polymer due to its extensive application from home appliances to all-encompassing industrial usages (Bikiaris, 2010; Umair, Numada et al., 2015). Due to its greater physiochemical properties, numerous traditional materials have been replaced by polypropylene and various industrial sectors have directly benefited from its use in composites (Pracella et al., 2010). For example, fuel usage has been remarkably reduced in the automobile sector by substituting metals with polypropylene since it is lighter. Consumers are impressed with its other physiochemical properties such as cutting-edged structural stability, superior dielectric vitality and better corrosion resistance and competency, making polypropylene is the best alternative to conventional materials (Glaß et al., 2013; Hisayuki et al., 2008). Nevertheless, polypropylene and polypropylene based materials only comprise 20% of the polyolefin market share although it has wide acceptability in the global material market. Therefore, from a scientific and economic point of view, it is vital that proper studies on modelling, optimisation and experimental validation of polypropylene production are carried out to expand its use and market share (Balow et al., 2003).

To better understand the complicated flow behaviours and process parameters necessary for enhancing the reactor performance, multidisciplinary efforts have been made to create the polymerisation process and its procedures, (Gharibshahi et al., 2015; Syamlal et al., 1993). For example, the fluidisation technique was commercially utilised and is a well-known technology. Some of the special features of fluidised bed reactors are excellent mass and heat transfer rates, uniform particle mixing and the ability to achieve diverse chemical reactions (Ahmadzadeh et al., 2008; Aysar et al., 2011; McAuley et al., 1994). Several researchers had acknowledged gas phase polymerisation as a more sustainable and user-friendly technology. The polymer fluidisation performance is influenced by a number of factors such as fluidised bed components, system temperature, and gas-solid alignment. Ironically, all these impelling factors make reaction regime analysis difficult. Yet, these factors have a big influence on the quality control of different grades of polypropylene. The overall operating conditions have a broad influence on the exothermic nature and system pressure sensitivity of the propylene polymerisation reaction (Shamiri et al., 2011). It is important to develop a valid model to clarify the functional relationship among the process variables to allow for the design of a robust reaction system to carry out safe reactions and to produce uniform, consistent and quality products. In many industrial applications, the model would also support better decision making (Ahmmed et al., 2009; Jang et al., 2010; Kaushal & Abedi, 2010).

At the moment, little evidence is available from literature on hand to indicate any optimisation study being carried out so far after taking into account the integrated process parameters, multiphasic fluid dynamics and reaction rate with the CFD method on propylene polymerisation. This thesis sought to bridge this research gap. The objective of this research was to study the specific operating parameters from

multidimensional approaches, i.e., the statistical, mathematical and CFD point of views, for propylene polymerisation in a real reaction pilot-scale environment and to identify the best process parameters for the combination of a predictive CFD coupled model and experimental validation. Reaction temperature (RT), system pressure (SP), monomer concentration and hydrogen concentration were the chosen operating parameters. Also included in this research was an industrial standard characterisation study. The experiments were carried out in a pilot-scale plant which was a stand-in example of an industrial-scale plant and equipped with a full-range production facility under the Malaysian National Petroleum Authority (PETRONAS). To give an idea of the impact of this hybrid model based production optimization study, a financial analysis was also carried out. An additional 6,411,981.74 TPA of polypropylene can be produced at industrial scale to meet this global demand based on the estimates in this study. In the global market, this would generate profits in excess of 7,675.14€ million in 2016 alone.

## **1.2 Problem statement**

Extreme nonlinearities in the dynamics of the reactor were due to the complicated reaction, heat and mass transfer mechanisms as well as the complex gas and solid flow characteristics in the fluidized bed reactor. These variables pose a huge challenge in the modelling and optimization of such a process.

The basic reaction modelling in the propylene polymerization fluidized bed reactor was made even more difficult by the presence of strong interaction between process variables that conventional process modelling and optimization strategies could not cope. Limited studies were done on the reaction coupled dynamic modelling and optimization of specifically the gas phase polypropylene catalytic reaction in pilot scale fluidized bed reactor even though available literature point to the fact that research was

done of the basic modelling and control of polymerization process in fluidized bed reactors.

It is often assumed that the emulsion phase that develops at minimum fluidization and bubbles are completely solid-free in most conventional models. On this premise, it was impossible to forecast the influence of the dynamic gas–solid allocation on the apparent reaction and heat/mass transfer rates in the fluidized beds properly at velocities higher than minimum fluidization. Yet, experimentally (Aoyagi & Kunii, 1974) and theoretically (Gilbertson & Yates, 1996), the presence of solids in the bubbles had been proven. The emulsion phase may contain more gas at higher gas velocities and also did not remain at minimum fluidization conditions (Abrahamsen & Geldart, 1980). Improved assimilation of the two phases will cause more solid particles to enter the bubbles, resulting in more gas entering the emulsion phase while the superficial gas velocity increased in a fluidized bed reactor. Hence, a comprehensive model was required to give a more realistic perception of the encountered phenomena in bed hydrodynamics and enhance the quantitative knowledge of the real process.

In order to get the real picture behind the dynamic nonlinearities and difficulties involved in the gas phase propylene polymerization rate phenomena in a fluidized bed reactor, it is essential to come up with an efficient real-time process dynamics monitoring scheme and product engineering strategy over modelling and simulation concept.

### **1.3 Objectives of the research**

The objectives of this research was to come up with a comprehensive model for optimization of a gas-phase propylene polymerization in a fluidized-bed catalytic reactor (FBR).

This research included the salient factors of the polymerization of propylene while incorporating mathematical and experimental approaches to describe the dynamic process parameters and behaviour of a fluidized bed reactor with reaction modelling. Every experimental and validation aspects were also taken into account. Lastly, real-time observations of process parameters and their effects on product quality were also studied.

Below are the specific objectives and approaches:

- 1- To predict the optimum operating conditions for polypropylene production through a statistical model.
- 2- To examine the influence of reaction temperature, system pressure and monomer concentration on the polypropylene production rate and on fluidised bed dynamics by incorporating statistical model with CFD model.
- 3- To develop a multiphasic reaction model to predict the reaction rate in every phase in real reaction conditions.
- 4- To characterise the polypropylene produced by varying the hydrogen concentration at optimum conditions.

#### 1.4 Workflow of the thesis

Below are the topics in relation to the various aspects relevant to the thesis:

**Chapter 1:** This chapter detailed a short introduction on the comprehensive modelling of gas phase polymerization fluidized bed reactors along with the related circumstance of the research. It was then followed with the problem statements which highlighted the direction of the research. The objectives and scope of the study were then elaborated in detail based on the defined problem statements.

**Chapter 2:** Chapter 2 gave a general overview of multidimensional modelling of fluidized bed reactor and its applications in olefin polymerization. This chapter provided a brief review on the modelling of gas-solid fluidized bed systems and recent researches that had been carried out. The information in this chapter was published in the **Journal of Industrial and Engineering Chemistry**.

**Chapter 3:** Polypropylene Production Optimization in Fluidized Bed Catalytic Reactor (FBCR): Statistical Modelling and Pilot Scale Experimental Validation

This chapter described a strategy to examine the relationship among various operating parameters in order to come up with the optimum process environment for propylene polymerization in a pilot scale fluidized bed via RSM modelling and Central Composite Design (CCD) technique. This work was published in the journal named '**Materials**'.

**Chapter 4:** Developed a Hybrid Model for Propylene Polymerisation at Optimum Reaction Conditions.

This chapter described an integrated method to identify optimum process parameters and dynamic transformations of the fluidized bed for propylene polymerisation. To

explain the fluidised bed dynamic behaviour, a two-phase gas–solid model was analysed at optimum process conditions. The CFD (computational fluid dynamics) based optimization model was created to integrate the dynamic gas-solid flow dynamics and process parameter interaction effects on polymerization. In order to simulate a multiphase flow, the Eulerian-Eulerian approach was applied in this work. The built-in PBM (population balance model) and a moment method were utilised to measure the percentage of the polymer production. This work was published in the journal called ‘**Polymers**’.

**Chapter 5:** Multiphasic Reaction Modelling for Polypropylene Production in a Pilot-Scale Catalytic Reactor.

In this chapter, an innovative polyolefin-based engineering process model, which reduced the computational and the experimental bids in the presence of a novel pilot-scale experimentation design, was established. Momentum method was used to explain the polypropylene production rate factors. The required mass balance equations for reacted monomers (that were described by a sequence of differential and algebraic equations) were individually applied for the different emulsions during the bubble phase because the plug flow reactor had very active catalyst sites. This was an improved representation of the conditions faced by the heterogeneous Ziegler-Natta catalysts. This study was published in the ‘**Polymers**’ journal.

**Chapter 6:** Model based real-time process parameters monitoring for polypropylene production and their effects on product quality.

A common but distinctive online data acquisition system was set up and used to attain real-time data for the important process parameters, i.e., pressure, temperature and feed rate of hydrogen, on the dynamics of polypropylene (PP) production in a catalytic Fluidized Bed Reactor (FBR) in this study. An industrial level characterisation analysis



was also carried out to assess the outcomes of the process parameters on the quality of polypropylene. The manuscript of this chapter was submitted to the **Advances in Production Engineering & Management (APEM)** journal for publication and is now under review.

### **Chapter 7: Conclusions and Recommendations**

Results and findings of this study were summarized in the last chapter and were followed by a list of recommendations for further studies.

University of Malaya

## CHAPTER 2: LITERATURE REVIEW

### NOTATION:

$A$	cross sectional area of the fluidized-bed ( $m^2$ )
$A_r$	pre-exponential factor (consistent unit)
ANOVA	analysis of variance
CFD	computational fluid dynamics
$CV$	coefficients of variation
$D$	diameter of the fluidized-bed reactor (m)
$D_v$	the electric displacement vector
DEM	discrete element method
DPM	discrete particle model
$E$	electric field (V/m)
$E_r$	Activation energy for the reaction (J/Kmol)
EDC	eddy dissipation concept
FBR	fluidized bed reactor
GFM	granular flow model
$H$	total enthalpy (J/kg, J/mole)
$H_b$	Bed Height
IPSA	inter phase slip algorithm
KTGF	kinetic theory of granular flow
MGM	multi grain model
$P$	induced polarization
PEA	partial elimination algorithm
$P_{MW}$	Propylene molecular weight (kg/kmol)
TFM	two fluid model

VOF	volume of fluid
$MnS_{RG}$	mean of square regression
$N_r$	apparent order of reaction
$P_n$	bulk partial pressure of gas (Pa)
$D_{0,r}$	diffusion coefficient for reaction ( $m^2/S$ )
$DgF$	degree of freedom
$C_p$	heat capacity at constant pressure (joule/ kelvin)
$H_{reac}$	heat released by surface reaction ( $^{\circ}C$ )
$Y_j$	mass fraction of species j in particle
$T_p$	particle temperature ( $^{\circ}C$ )
$R_v, R_j$	radius of particle (m)
$\bar{R}_{j,r}$	rate of particle species depletion (kg/s)
$R_{kin,r}$	rate of reaction (units vary)
$R_{j,r}$	rate of species reaction per unit area ( $kg/m^2s$ )
$S_g$	source term in gas phase scalar equation
$T_{f\Omega}$	local temperature of fluid ( $^{\circ}C$ )
$A_p$	surface area of particle ( $m^2$ )
$D_b$	bubble diameter (m)
$H_a$	Hamaker constant (erg)
$J_s$	dissipation of granular energy ( $m^2/s^3$ )
$N_c$	Courant number
Pr	Prandtl number

Re	particle Reynolds number
SSQ	sum of squares,
$T_\infty$	system temperature ( $^{\circ}\text{C}$ )
$q_{i,wall}$	conductive heat flux between particle i and wall ( $\text{W}/\text{m}^2$ )
$q_{i,f}$	conductive heat flux between particles i and f ( $\text{W}/\text{m}^2$ )
$q_{i,j}$	conductive heat flux between particles i and j ( $\text{W}/\text{m}^2$ )
$k_e$	effective fluid thermal conductivity (kelvin-meters per watt)
$q_{i,rad}$	flux between particle i and its local surrounding environment ( $\text{W}/\text{m}^2$ )
$f_h$	fraction of heat absorbed by particle
$m_p$	mass of particle
$n_r$	effectiveness factor (dimensionless)
$k_{f\Omega}$	number of particles in a domain $\Omega$
$k_p$	thermal conductivity of particle (kelvin-meters per watt)
$t_a$	time lag (s)
$t_c$	time of particle–particle collision (s)
$d_p$	particle diameter (m)
Es	particle-particle restitution coefficient
g <sub>0</sub>	gravitational acceleration ( $\text{m}/\text{s}^2$ )
$h_b$	height of the fluidized bed (m)
K	thermal conductivity (kelvin-meters per watt)

$p_s$	particulate phase pressure (bar)
$V$	velocity of phase (Pa.s)
$v'$	fluctuating particle velocity (Pa.s)
$v_b$	total bed volume (m <sup>3</sup> )
$w_p$	polymer mass fraction

*Greek Letters:*

$\varepsilon$	the void volume of the fluidized bed
$\Sigma$	surface tension, (N/m)
$\Theta$	porosity of the polymer particle
$\eta_r$	effectiveness factor
$\alpha_s$	volume fraction of solid
$\rho$	charge density (c·m <sup>-2</sup> )
$\rho_s$	solid density (kg/m <sup>3</sup> )
$\Theta_s$	granular temperature (m <sup>2</sup> /s <sup>2</sup> )
$\lambda_s$	solid bulk viscosity (kg/m <sup>2</sup> s <sup>-1</sup> )
$\alpha_g$	volume fraction of gas
$\alpha_{s,max}$	maximum volume fraction of solid phase
$\phi$	sphericity
$\mu$	dynamic viscosity (Pa.s)
$\dot{\gamma}$	shear rate (1/s)
$\mu_0$	zero shear viscosity (Pa.s)
$\gamma_s$	dissipation due particle–particle collision(m <sup>2</sup> s <sup>-3</sup> )

$\varphi$	electric potential (V)
$\Gamma_g$	gas phase diffusion coefficient
$\rho_g$	density of gas phase (kg/m <sup>3</sup> )
$\rho_f$	density of fluid (kg/m <sup>3</sup> )
$\epsilon_0$	permittivity of vacuum (F/m)
$\chi_e$	electric susceptibility (m/V) <sup>n-1</sup>
$\epsilon_m$	relative permittivity of mixture (F/m)
$\epsilon_s$	relative permittivity of solid phase (F/m)
$\epsilon_g$	relative permittivity of gas mixture (F/m)
$\Delta t$	time step in simulation (s)
$\Delta_p$	pressure drop (Pa)
$\Delta x$	dimension of the grid

*Subscripts*

Kin	Kinetic
Eff	Effective

## 2.1 Introduction

### 2.1.1 The process of fluidization and fluidized bed reactors

The physiochemical phenomenon called, ‘fluidization’, conveys the idea of converting a bed of fine particulate materials into a fluid-like state by passage of a gas or liquid through it. Transport phenomena in fluidized beds have several complex features which can be utilized to great benefit in various processes. If a fluid is passed through a bed of fine particles, at lower velocities the fluid simply percolates through the void spaces between particles and this is known as a fixed bed. When displacement of particles occurs by increasing the flow rate of the fluid, it is known as an expanded bed. Particles are suspended at a higher velocity in the fluid. The buoyancy force acts as the balancing force between gravitational and drag forces when the bed is in suspended form. When the pressure drop across the bed becomes equal to the weight of particles, the bed is considered as fluidized and the superficial fluid velocity at which this situation is observed is called the minimum fluidization velocity. This phenomenon can be expressed mathematically by the following equation (Geldart et al., 2009; Puettmann et al., 2012; Yang et al., 2003):

$$\Delta p = H_b(1 - \varepsilon)(\rho_s - \rho_f)g \quad (2.1)$$

The section with a clear surface or upper limit of the fluidized bed is regarded as the dense phase. Further increment of velocity of the fluid may cause the surface to lose its distinct character. There are a number of influential factors for controlling the quality of fluidization. In general, properties of solids and fluid determine the smoothness of fluidization. Moreover, solids mixing, bubble size, bed geometry, gas flow rate, particle size, distributor type and vessel interiors are other factors affecting fluidization.

FBRs have been frequently used in various processes. Implementation of fluidization technology can be categorized into chemical and physical processes. Olefin polymerization (propylene and ethylene), a wide range of synthesis reactions, manufacturing of silicon, gasoline synthesis (Fischer-Tropsch), coking (Fluid and Flexi), combustion, gasification and catalytic cracking of heavy hydrocarbons are examples of chemical processes. Physical processes involving fluidization include heat exchange, drying, coating, granulation, solidification and purification of gases with adsorbent (Bi et al., 2000; Yang et al., 2007).

Different types of reactors, like continuous stirred tank reactor (CSTR ) (Ali et al., 2011), tubular loop, autoclave and fluidized bed reactor (FBR), have been used to produce polyolefins. However, recently FBRs have drawn the attention of engineers, scientists and researchers. As a result, gas–solid fluidized-bed reactors are broadly used for producing polyolefin as well as other petrochemical products. Employing gas phase fluidized beds in polyolefin production processes is beneficial due to its low investment requirement and low operating cost compared to other processes. This technology also provides some significant engineering advantages. For example, it involves no solvent separation, has great heat exchange potential and has ability to utilize various types of catalysts to manufacture a wide range of products (Rokkam et al., 2010). Diverse benefits of fluidized bed reactors, like their capabilities to carry out a wide range of multiphase chemical reactions, excellent mixing performance of particles, significant mass and heat transfer, as well as their ease of operation in both batch and continuous states have established this type of reactors as one of the most extensively used reactors for polyolefin production.



Union Carbide can be credited as the first commercial user of the fluidized bed polymerization reactor for producing high density polyethylene (HDPE) in 1968. The same manufacturer extended its production line for production of linear low density polyethylene (LLDPE) in 1975 and for polypropylene (PP) in 1985. Several simulation and experimental studies have been accomplished in order to understand the observable fact of fluidization for improving and optimizing their design (Xie et al., 1994). Effective fluidization ensures proper gas-solid contact, homogenous temperature profile and minimum gas bypassing (Choi et al., 1988). Consequently, Hypol, Innovene, Unipol, Spheripol, which are widely used commercial technologies, have been producing polyolefin through fluidization (Kunii et al., 1991; Geldart et al., 1986).

### **2.1.2 Scope of the review**

Polyolefin reaction mechanism models are classified based on several factors. Constant bubble size model (Choi & Ray, 1988), well-mixed model (Kiashemshaki et al., 2006; W. C. Yang, 2003), bubble growth model (Shamiri et al., 2010), catalyst phase model (Ahmed et al., 2009), well-mixed and constant bubble size dynamic model (Shamiri et al., 2011) and multiple active sites model (Davidson et al., 1963) are significant types of models for describing olefin polymerization phenomena in many studies. Numerous references are available for mathematical modeling and simulation of gas-phase olefin polymerization in fluidized condition. In this type of reactor, mechanism of reaction, physical transport methods, reactor design and operating conditions have great influence on the quality of the polymer product. In most cases, polymerization processes are widely categorized into heterogeneous and homogeneous processes. Homogeneous reaction method implies that the polymerization occurs within a single phase while in heterogeneous systems reactants and polymerization reaction are presented in different phases (Shamiri et al., 2010). Pseudo-homogeneous models of polyolefin production are

simple and can be used in catalytic batch reactors. In this model it is assumed that only a single (liquid or gas) phase exists in the reactor. On the other hand, heterogeneous models are mostly practical for simulation of gas phase semi-batch reactors. Such models are widely used in olefin polymerization reactors. Due to the multi-phase nature of polymerization (liquid–solid phase or gas–solid phase), the heterogeneous catalysis reaction model should be solved simultaneously with a hydrodynamic model describing inter-phase heat transfer, mass transfer and mixing. It is well established that a fluidized bed should be considered as a two-phase system. These phases are emulsion and bubble, also known as the dense and lean phases, respectively. Although bubbles are often assumed to be solid-free, they usually carry a small quantity of solids. Each gas bubble carries a considerable amount of solids behind it which is called wake. Solids in the wake are dragged up with the bubble, consequently, the rest of solids within the emulsion phase flow downward.

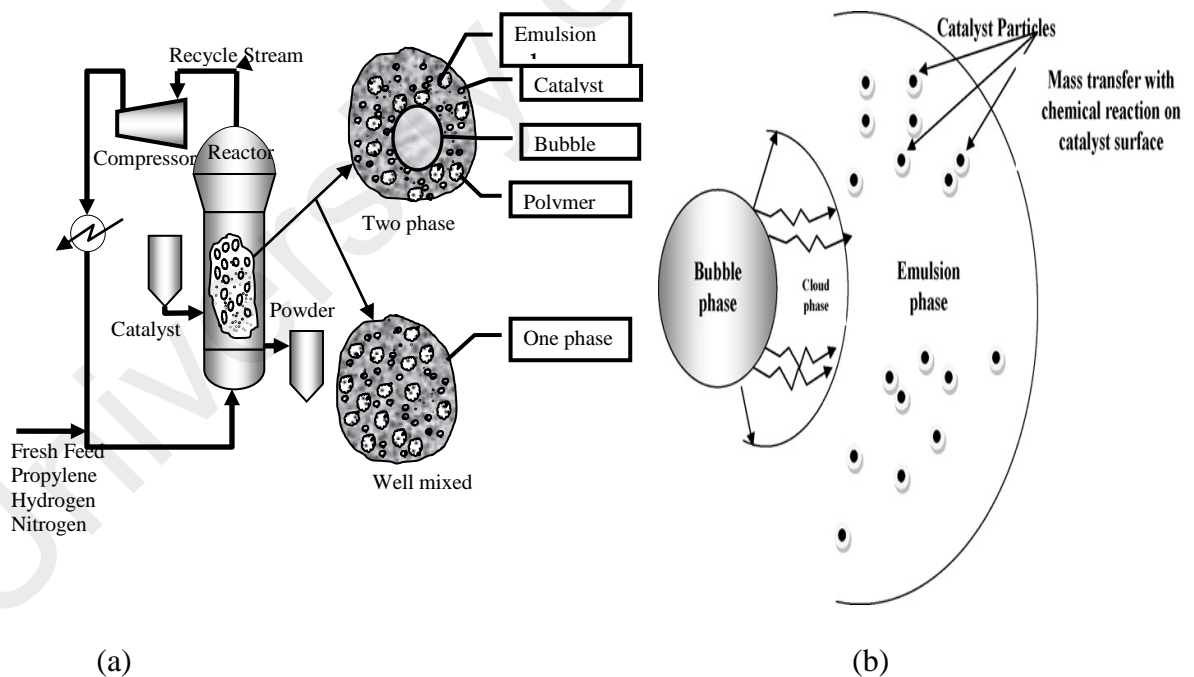


**Figure 2.1:** (a) Schematic of a fluidized bed polypropylene reactor with multiphase reaction steps (Shamiri et al., 2011); (b) influence of catalyst particles inside phases. Reproduced with permission from Elsevier (Ahmed et al., 2009).

Each bubble is surrounded by a cloud which is also rich in solids and moves with the same velocity as the bubble. Polyolefin reaction modeling is illustrated schematically in Figure 2.1. This figure illustrates the expositions of multiphase reactions in a fluidized bed reactor for olefin polymerization reaction. Reactant gases, blown into the bed from the bottom, form bubbles in a fluidized bed. While bubbles rise in the bed, mass transfer of reactant gases takes place between cloud and bubble as well as cloud and emulsion. After transfer of reactant gases from bubble to emulsion, chemical reaction takes place in the emulsion and on the surface of the catalyst particles. The rate of mass transfer of reactants from bubble to emulsion diametrically affects the polymer production rate. Many researchers have mentioned that reactor modeling should be done based on the type of the catalyst and the value of porosity (Chatzidoukas et al., 2003; Zavala et al., 2005). The superficial gas velocity, as well as the catalyst dosing rate, can severely affect the molecular weight of polymer in the emulsion phase, concentration of monomer and temperature inside the emulsion phase (Xu et al., 2006; Xuejing et al., 2006).

In a gas-phase polymerization process, monomers in the gas phase react with the solid catalyst in the emulsion phase to form polymer particles (Luo et al., 2009). Since the reaction takes place in a mixture of gas and solid phases, a two phase model was considered in many cases for describing this process. Reports about simulation of industrial scale or even pilot scale polymerization process are limited in the open literature. Gobin et al. (Gobin et al., 2012) simulated large polymerization reactors and mainly focused on the ability of the simulator to explain the complex flow behavior of the large-scale reaction system.

Advanced process modeling and simulation tools, like the CFD approach, are required to understand the effect of numerous changes that are required for the scale-up process such as bed diameter, rising of bed height and fluidization velocity, distributor types and adding of in-bed heat exchanger tubes along with baffles, as well as experimental data for validation. Therefore, several research groups have been involved in developing non-intrusive measurement techniques in the laboratory scale polymerization reactors to obtain statistically and mathematically significant data for validation of CFD models (Hulme et al., 2005)

Earlier models of FBRs were not capable of being used for scale-up purposes but to a certain extent were proposed for interpretation of experimental data (Anderson & Jackson, 1967; Rokkam et al., 2010; Yiannoulakis et al., 2001). The use of CFD analysis is also in its initial stage, especially in the field of polyolefin reactions. Although, there are broad applications of the CFD in recent studies of chemical reactors, current CFD simulations include too much simplification and paid inadequate attention to the multi scale structure (for example, homogenous assumption in hydrodynamics, mass transfer and reaction models and 2D instead of 3D models). These simplified treatments may miss the real mechanisms underlying the complex states of motion. To conquer this problem, CFD with consideration of meso-scale structures has been proposed in recent years. This method can help to understand the structure-oriented coupling between flow, heat/mass transfer and reactions. This combination, the so-called multi-scale CFD (MSCFD), characterizes the sub-grid meso-scale structure with stability criteria in addition to conservation equations. This approach is demonstrated by the energy minimization multi-scale (EMMS) model and its extensions, e.g., EMMS/matrix for flow modeling and EMMS/mass for reaction

modeling and can be a promising approach in industrial and scale up simulations (Wang et al., 2010).

In this study, the background of these computational models, considering various aspects involved in polyolefin reactions in a fluidized bed reactor, are discussed.

## **2.2 Computational modeling of fluidized bed reactor**

### **2.2.1 Theoretical framework**

Development of CFD, which can be used to solve conservation and momentum equations in multiphase flows (Hosseini et al., 2012), is an advanced research area for visualizing fundamental phenomena without carrying out real-time experiments (Paul et al., 2004). In case of a polymerization reactor, an extra advantage of CFD is that it can provide information on turbulent zones. Information in these zones is vital because the reactants are mostly introduced to these areas and the reaction yield is higher. Although, experimental analysis of the flow pattern in polymerization reactors remains vital, the irregular mechanism of mixing of reactive fluids makes the flow visualization more complex. CFD studies had been initially criticized for their limitations in adequate analyzing the polymerization process. A mentionable drawback of the CFD modeling of a polymerization procedure is its high computational time. Since transport equations in a polymerization reaction are highly coupled in nature, it is extremely challenging to solve the related equations and simplification of the reaction mechanism as well as dependency of the transport properties on the variables is essential (Patel et al., 2010).

Although initial CFD studies have limitations in analyzing different polymerization processes, this approach was able to provide dynamic simulation of FBRs. Continuous development of supercomputers and invention of computer units with continually

increasing power have facilitated solving these complicated equations numerically. The effort required for experimental design and data acquisition have been significantly reduced by the CFD analysis. Recent developments in the research field of multiphase flow of gas-solid modeling suggest substantial process developments that have the potential to advance plant operations significantly. Forecasting of gas-solid flow pattern in certain production systems, such as pneumatic transport lines, fluidized bed reactors, hoppers and precipitators, is critical to control the operation parameters of a majority of process plants. The lack of ability to precisely model these fluidization regimes has slowed down the progress of simulations for these operations. Hence, in recent years, researchers involved in the development of CFD softwares have been paying attention to significant points to propose updated modeling techniques for simulating gas-solid flows with a higher level of consistency. Implementation of CFD for analyzing multiphase flows have been widely accepted and have directed researchers to develop CFD codes for simulating fluidized beds. Consequently, engineers involved in olefin polymerization industries are beginning to use these latest methods to make significant upgrading by considering alternatives although it would be too expensive or time consuming to obtain the real plant size results (Reh et al., 1999).

Although gas-solid flow modeling techniques are based on conservation equations, but it has also been reported that conventional models are not yet adequately improved to be effective tools for the design of industrial FBRs. The reason for this drawback remains first in the complexity of the gas-solid flow pattern in reacting systems which makes computations very difficult and time consuming. Adding chemical reactions to this complexity requires additional computational resources and particularly handling of large geometries of industrial reactors clearly exceeds the currently available computing capacities (Gidaspow et al., 1994; Ryu et al., 2013; Shi et al., 2010). Furthermore, to

provide comprehensive information on complex fluid dynamics, CFD possesses a great potential and has been considered as a promising technique (Zhao et al., 2000; Mountain et al., 2001).

Two forms of CFD models, i.e., Lagrangian and Eulerian methods, are generally used to describe gas-solid fluidized reactors. The Lagrangian model solves equations of motion (Newton's second law) for every particle in the system in which particle-particle collisions and various forces acting on the particle are taken into account. In the Eulerian model, both phases (solids and gas) are counted as continuum (fluid) and momentum and continuity equations are considered for both phases (Ahuja et al., 2008; Wang et al., 2006). The Eulerian-Lagrangian approach, which is also recognized as discrete particle model (DPM) or discrete element method (DEM), considers the fluid as a continuum while the solids are considered as the dispersed phase. The DPM uses the Eulerian framework to model the continuous phase and the trajectories of particles are simulated in the Lagrangian framework. The continuous phase can be modeled by averaging its properties over a wide range of trajectories. However, to obtain a momentous average of all quantities, an abundant of particle trajectories is suggested to be simulated. In some software packages, such as ANSYS FLUENT, the Eulerian-Lagrangian approach is capable of modeling dispersed multiphase flow surrounded by a low volume fraction of solid particles (Vejahati et al., 2009). Gas and emulsion phases are assumed to be continuous in the Eulerian-Eulerian approach while is considered entirely interpenetrating in every control volume. Three different Euler-Euler multiphase models are accessible to explain fluidized bed olefin polymerization: the Eulerian model, the mixture model and the volume of fluid (VOF) model as described in the following section.

### **2.2.1.1 The eulerian model**

In the Eulerian model, both phases are considered as continuum and momentum and continuity equations for multi-phase flow are solved. A single pressure field is considered for all phases. Interphase exchange coefficient and pressure are important parameters for coupling these equations. Based on the relevant phases, different types of coupling methods are available. Fluidized beds, risers, bubble columns and particle suspensions can be covered by the Eulerian multiphase model. For calculation of the fluid-solid momentum exchange coefficient, ANSYS FLUENT suggests utilizing Syamlal-O'Brien and Gidaspow (O'Brien & Gidaspow, 1989) correlations for use in the granular flow while Wen and Yu (Wen & Yu, 1966) correlation can be used if the system media is dilute. The Eulerian-Eulerian approach is applicable to determining the hydrodynamics of fluidized beds in which volume fraction of phases are of the same order. This computationally cost effective approach is also convenient where body forces (like gravity) act to split the phases or interact within and between the phases. This method is limited by hardware memory constraints and convergence issues.

### **2.2.1.2 The mixture model**

The mixture model is simpler than the Eulerian model. This approach was developed for modeling of two or more phases (interpenetrating continua). Momentum equations are solved by this model and evaluate relative velocities to describe the flow of dispersed phases. Cyclone separator, sedimentation, particle-laden flow with low loading and bubbly flow are examples of application of the mixture model. Homogeneous multiphase flows can also be modeled without relative velocities for the dispersed phase by the mixture model.



### **2.2.1.3 The vof model**

The VOF approach is applied to model multi immiscible fluids. In this model, momentum equations, equations of continuity for all fluids through the flow field and tracking the volume fraction of each of fluids are considered. Calculation of motion of large bubbles in a liquid, motion of fluid through a system, jet breakup and steady or transient movement of multi fluid phases are typical applications of this model. There are, however, some limitations in application of the VOF model. For instance, all control volumes are required to be filled with either a single fluid or a combination of phases, that is, void regions where no fluid is present and cannot be defined in this model and only a single phase can be described as a compressible ideal gas. The VOF cannot model the streamwise periodic flow including specified mass flow rate and specified pressure drop. User-defined function of ANSYS FLUENT is the option to explain compressible fluids behavior with the help of VOF model. However, if a system is highly sensitive to pressure, then the VOF approach is not advisable. The VOF model also cannot be used with the DPM model for gas-solid reaction modeling in which particles are analyzed in parallel.

### **2.2.1.4 Combined approaches**

Although the Eulerian–Eulerian model has become the primary choice of most researchers to investigate the performance of the polymerization reaction fluidized beds, some researchers combined the Eulerian–Eulerian approach and the granular flow model (GFM) (Ding & Gidaspow, 1990; Wei et al., 2011; Yan et al., 2012). In this approach, both phases are governed by conservation equations of mass and momentum. Describing inter-phase forces, i.e., drag, lift and virtual mass forces, is important to couple momentum balances of two phases. It has been shown that due to the large difference between densities of emulsion and fluid phases, the lift force and the virtual

mass force are less significant and can be neglected (Jakobsen et al., 1997; Krishna & van Baten, 2001). Consequently, in most CFD analyses of fluidization, only drag force was considered (Ahuja & Patwardhan, 2008).

In the gas–solid flow, particles are considered as exaggerated molecules with the intention that an analogy of their behavior with gas molecules can be stipulated. The GFM approach typically does not provide the trajectory of particles and its averaging in a computational cell but can be perfectly accomplished at a hypothetical level which requires extensive modeling efforts. Formulation of the governing equations involves various averaging issues. As a result, the Eulerian–Eulerian model is applicable to multiphase flow processes containing large volume fractions of the dispersed phase (Fan et al., 1998; Ranade et al., 2001). Conversely, the 2D Eulerian-Eulerian model extended with the kinetic theory of granular flow (KTGF) was applied (Lu et al, 2002) to simulate the behavior of bubbles in a gas-solid FBR. Their simulated results were compared with bubble sizes obtained from the equation of Darton (Darton, 1977) and the model of Davidson (Davidson, 1963). Several studies on behavior of bubbles in a free and agitated gas-solid FBR via 2D and 3D Eulerian models were also carried out (Antonio et al., 2009). Vegendla et al. (Vegendla et al., 2011) performed a comparative study of Eulerian–Eulerian and Eulerian–Lagrangian method on two-phase gas–solid riser flow behavior by considering gas phase as a continuous phase and the solid phase as a dispersed phase. Solids volume fraction, solids velocity, gas phase turbulent kinetic energy and its dissipation were elaborately studied at certain operating conditions. They concluded that the simulation results, when applying Eulerian–Lagrangian method, fits better to the experimental data whereas the Eulerian–Eulerian method showed more deviation from the experimental data. A combined CFD approach using DEM along with Navier–Stokes equations has been suggested to explain

multiphase flow behavior and heat transfer amid particles and between the gas and the particles for methanol-to-olefins (MTO) production in FBR (Zhuang et al., 2014). The same study claimed that this hybrid approach can provide real-time particle activity by tracing the movement vector of the catalyst particle coupled with heat transfer equations.

However, some CFD studies have been reported recently on the flow structure of phases in fluidized bed polymerization reactors (Sun et al., 2012; Vun et al.2010), since there are many important parameters in the modeling which can notably influence the simulation results (Perryet et al.,1998). Chen et al. (Chen et al., 2011) applied a CFD model to describe the gas–solid two-phase flow in fluidized bed polymerization reactors. They considered complete hydrodynamics of the FBR, such as solid holdup distribution, behavior of bubbles and solids velocity. Many researchers also performed advanced investigations on the influence of operation conditions and geometry of the reactor, like type of distributor, size of solid particles, gas velocity and operating pressure on the hydrodynamics of the reactor, for accurate scale-up and design of reactors (Aldaco et al., 2007; Cabezaset al., 2003; Doroodchi et al., 2005).

### **2.3 CFD software packages**

Among different CFD software packages, only a few are capable of modeling complex multiphase flows. Pheonics, Fluent, CFX, Star-CD, Ester-Astrid, COMSOL and MFIIX are some common software packages that have been used in CFD analysis of olefin polymerization since the last decade. These computational tools can be used for interfacing the user-defined function (UDF) to enhance the modeling and to get more realistic simulation results. Preprocessing is considered as the first step for developing and analyzing the flow model. The prerequisite for preprocessing is to propose the

model with the support of a computer aided design (CAD) package, generating a mesh and entering the data. For this purpose, GAMBIT is well accepted by researchers as a preprocessing tool. The CFD solver is capable of performing the calculations and generates the results after preprocessing. Among several CFD packages, ANSYS FLUENT has been used in most industrial simulation practices. Moreover, Flow Wizard is the earliest wide-ranging function of CFD product for designers introduced by ANSYS FLUENT. Some particular industrial sectors, like material processing industries, also use specific CFD packages such as FIDAP and POLYFLOW for their process development and scale up purposes (Addagatla et al., 2008; Li et al., 2012; Wang et al., 2007).

In the recent years, the commercial CFD package ANSYS FLUENT seems to be the first choice for a number of researchers for modeling fluidized bed reactors. In fact, ANSYS FLUENT is one of the most inclusive softwares offered to the CFD community because of its wide range of industrial applications, from airflow over aircraft wings to the modeling of gas-solid flows in fluidized beds. A large number of research articles have been published in recent years on the application of ANSYS FLUENT in the CFD analysis of fluidized bed reactors of polyolefin production. Table 2.1 shows some of significant researches on CFD approach applied to polyolefin production in the fluidization research field.

**Table-2.1:** Recent applications of CFD approach on fluidization and fluidized bed reactors

Factors studied	CFD package and algorithm	CFD approach	Remarks	Reference
Bubble dynamics of Geldart D particles, the effect of bubble coalescence (size and frequency), bubble rise velocity, and pressure drop.	FLUENT 6.3.26. for grid structure GAMBIT	Euler-Euler full 3D unsteady CFD simulations	Euler-Euler transient full three-dimensional computational fluid dynamic simulations helped to shape an understanding of the impact of specific geometry	(Wardag & Larachi, 2012)
Effect of nature of reactor wall (flat- and corrugated)	FLUENT 6.3.26 & GAMBIT-generated grid structure	3-D transient Euler-Euler CFD simulations	Corrugated wall offered more stable gas-solid fluidization operation than flat wall	(Khan & Larachi, 2012)
Solid volume fraction, axial solid velocity, radial solid velocity, power spectrum, normal Reynolds stresses, turbulent kinetic energy, granular temperature and energy spectrum	FLUENT 6.3.26	Eulerian approach with KTFG	The obtained results gave a close comparison of the simulated factors.	(Chalermssinwan et al., 2012)
Interchange due to gas advection between the emulsion phase and bubbles.	MFIX code with the KTFG	Two-fluid modeling approach with classical potential flow theory	Suitable for high gas velocity rates.	(Hernández-Jiménez et al., 2013)
Physical values of fluid and particle phases.	In-house CFD/DEM code (DEMEST) and MATLAB.	Euler-Lagrange approach combined discrete element Method (DEM)	This combined model can predict accurately the particles motion and the pressure gradients in the bed. But only applicable in small scale with relative large particles.	(Alobaid et al., 2013)
Fluid-particle interaction (porosity and momentum)	DEM program "DEMEST" and	Euler-Lagrange approach in	Is able to simulate the highly complex hydrodynamic behavior of the dense gas-solid	(Alobaid & Epple, 2013)

**Table-2.1:** Recent applications of CFD approach on fluidization and fluidized bed reactors

Factors studied	CFD package and algorithm	CFD approach	Remarks	Reference
transfer)	MATLAB codes	combination with a deterministic collision model.	flow in the fluidized bed.	
Electrostatic charges on single bubble	MFIX	Two Fluid Model (TFM) coupled with the Srivastava and Sundaresan frictional model [209]	This model showed that electrostatic charges are predicted to cause the bubble to elongate and rise more quickly.	(Jalalinejad et al., 2012)
Hydrodynamic behavior of binary particle mixtures differing in size and density and effect of wall boundary condition	Fluent 6.3.26 and high-order discretization scheme-QUICK	Multi-fluid Eulerian model incorporating the kinetic theory of granular flow.	Particle-wall restitution coefficient only plays a minor role in predicting the segregation and mixing of binary particle mixtures in bubbling fluidized beds.	(Zhong et al., 2012)
Particle-particle heat transfer between different particle classes in a dense gas-solid fluidized bed of binary particles.	FLUENT 6.3.26 and SIMPLE algorithm	Multi-fluid Eulerian – Eulerian and KTGF in combination with stochastic collision frequency method and conductive heat transfer theory,	This model considers gas phase as the primary phase, whereas the particle phases are considered as secondary or dispersed phases.	(Chang et al., 2012)
Solid wall boundary conditions and granular temperature models	FLUENT 13.0.0 for CFD simulation and the 3D geometrical	Full three-dimensional two-fluid Euler framework with standard per-phase k-	KTGF model yielded better prediction of gas holdup profile; RNG dispersed modes predicted better flow pattern of three-phase fluidized beds; the third order MUSCL scheme was recommended for simulating complex flow	(Hamidipour et al., 2012)

**Table-2.1:** Recent applications of CFD approach on fluidization and fluidized bed reactors

Factors studied	CFD package and algorithm	CFD approach	Remarks	Reference
	meshing was achieved by using the GAMBIT (version 2.4.6)	$\epsilon$ turbulence model and RNG dispersed modes	patterns in three-phase fluidized beds; no significant improvement was observed with the laminar flow model	
Gas–solid flow, solid-phase properties, Momentum exchange coefficients, Pressure drop and bed expansion ratio, time-average local voidage and velocity profiles	Fluent version 6.3; MFIX , Open-FOAM; two phase Euler Pimple Foam	Eulerian–Eulerian model, KTGF	The flow fields showed a very good agreement between the MFIX and Fluent simulations, but did not conform to those of Open FOAM (Open Source Field Operation and Manipulation).	(Herzog, Schreiber, Egbers, & Krautz, 2012a)
Mixing of gas and solids phases, inlet gas velocity and solids circulation rate, particle properties (i.e., density and diameter), The residence time distribution (RTD)	FLUENT with the SIMPLE algorithm	2D Eulerian–Eulerian model based on the KTGF coupled with a k– $\epsilon$ turbulent mode	The developed model can predict the hydrodynamic behavior including the solids volume fraction and the gas and solids velocities. Comparisons with available experimental results showed good matching.	(Khongprom et al., 2012)
Flow behavior and conversion, solid phase viscosity and pressure of fluid, cohesive inter-particle forces and heat transfer	In-house code FLOTRACS-MP-3D in Cartesian coordinate system	Eulerian–Eulerian approach and KTGF	The model is fairly successful in bringing forth the effect of hydrodynamics on conversion in a bubbling bed of Geldart A particles and in the process highlights the strength of computational fluid dynamics in capturing vital details of complex flow patterns in fluidized beds.	(Yusuf et al., 2012)
Gas phase turbulence, diffusive species transfer, rate of conversion	FLUENT 12.1, coupled with SIMPLE	Eulerian-granular framework; 2D planar model	The model could predict the correct trend when a much less reactive carrier gas is injected. In this case, reaction rate was the limiting factor	(Cloete et al., 2012)

**Table-2.1:** Recent applications of CFD approach on fluidization and fluidized bed reactors

Factors studied	CFD package and algorithm	CFD approach	Remarks	Reference
	algorithm and QUICK scheme	employing the KTGF	and the accurate hydrodynamic resolution of the gas-emulsion interface was of lesser importance.	
Bubble properties such as aspect ratio, diameter and rise velocity as well as bed expansion	ANSYS FLUENT 12.1; SIMPLE algorithm, QUICK and second order upwind scheme were also employed	Eulerian–Eulerian Two-Fluid Model (TFM) with closure equations based on the kinetic theory of granular flow (KTGF)	3D simulations were in better agreement with experiments than the corresponding 2D simulations while bubble aspect ratio showed that the deviation of the predicted bubble properties using 2D simulations were more pronounced at higher bed height and higher superficial velocities.	(Asegehegn et al., 2012)
Various bed thicknesses with respect to particle packing, bed expansion, bubble behavior, solids velocities, and particle kinetic energy.	open-source code, MFIx-DEM.	Eulerian–Lagrangian simulations with the discrete element method (DEM)	Due to the inherent limitations of CFD–DEM approach, a direct numerical simulation (DNS) is advised to be preferable to accurately investigate the transition from 2D flow to 3D flow.	(Yan, Li, et al., 2012)
Random motion of particles, solid pressure, conductivity of fluctuating energy and viscosity, tangential restitution coefficient and normal restitution coefficient	KTRS-FIX code [162] (Kinetic Theory of Rough Spheres-Flow with Interphase eXchange) ,	Two-fluid model with a kinetic theory of rough spheres (KTRS), implicit continuous Eulerian (ICE) approach and KTGF.	An agreement between numerical simulations and experiments by was achieved by using this model with the consideration of particle rotation where kinetic theory is applicable.	(Shuai, Zhenhua, Huilin, Yunchao, et al., 2012)
Particulate systems consisting of a compressible gas and solid particles with complex and/or	SIMPLE algorithm	Immersed boundary method (IBM) [221] incorporated into the	DEM-CFD-IBM approach is capable to handle large objects or arbitrary shaped boundaries	(Guo, Wu, & Thornton, 2013)



**Table-2.1:** Recent applications of CFD approach on fluidization and fluidized bed reactors

Factors studied	CFD package and algorithm	CFD approach	Remarks	Reference
moving boundaries		coupled discrete element method and computational fluid dynamics (DEM-CFD) approach.		
Gas distributor plate angles, presence of a heat exchange tube bundle, superficial fluidizing velocities and initial solid packing heights	ANSYS Fluent 12.1, SIMPLE” algorithm, and QUICK scheme	Eulerian–Eulerian model (EEM) with KTGF	This model can capture the key features of a fluidized bed system, fast fluidization, bubbling fluidization in the reactor and solid circulation between the various parts of reactor column.	(Feng et al., 2012)
Simulation and characterization of bubble behavior and bed dynamics	Fluent 6.3 and SIMPLE	Eulerian–Eulerian three dimensional (3-D), KTGF and maximum entropy method (MEM)	The bubble behavior in a cylindrical fluidized bed in the bubbling regime is characterized and explained in this simulation study.	(Acosta-Iborra et al., 2011)
Effect of inlet boundary conditions , solids acceleration process and flow, the effects of particle size on the flow	Fluent 6.3, Gambit 2.4, SIMPLE algorithm and QUICK	Eulerian_Eulerian approach coupled with KTGF	This model is effective to specify the inlet boundary conditions for the simulations of gas-solids two-phase flows in a circulating fluidized bed.	(Peng et al., 2011)
Bed height, the bed expansion ratio and solid volume fraction, turbulent granular temperature.	FLUENT 6.2.16,	Energy Minimization Multi-Scale (EMMS) interphase exchange coefficient model with Eulerian model and KTGF.	To evaluate the third dimension of the system and compare the results with the corresponding data obtained from the 2-D analysis for validation, the use of this model is highly efficient.	(Chalermssinuwat et al., 2011)

**Table-2.1:** Recent applications of CFD approach on fluidization and fluidized bed reactors

Factors studied	CFD package and algorithm	CFD approach	Remarks	Reference
Effect of using different inter-phase drag model, solid volume fractions, expansion height, and pressure drop inside the fluidized bed at different superficial gas velocities.	FLUENT 6.3 and Phase-Coupled Semi Implicit Method for Pressure Linked Equations (PC-SIMPLE) algorithm,	Multi-fluid Eulerian–Eulerian model along with finite volume method and KTGF	Although three-dimensional simulation takes more time and computing processors than two-dimensional simulation, this simulation gives more accurate results when the models are compared with experimental data.	(Esmaili & Mahinpey, 2011)

ANSYS FLUENT has shown its excellent potential on solving the governing equations for the fluid flow as well as heat and mass transfer since launched in 1983. A wide range of models on incompressible and compressible as well as laminar and turbulent fluid flows can be efficiently solved by this software in either steady or transient state (Bhuiya, Chowdhury, Ahamed, et al., 2012; Bhuiya, Chowdhury, Islam, et al., 2012). ANSYS FLUENT is capable of modeling transport phenomena (including heat and mass transfer) with chemical reaction in complex geometries which is essential for analysis of fluidized bed reactors of polyolefin production. The set of free surface and multiphase flow models is one of the very constructive group of models in ANSYS FLUENT that can be used for analysis of gas-liquid, gas-solid, liquid-solid and gas-liquid-solid flows. This option also covers the volume-of-fluid (VOF), mixture, Eulerian and DPM approaches. Different types of heat transfer mechanisms can be modeled by ANSYS FLUENT, including natural, forced and mixed convection, with or without conjugate heat transfer, porous media, etc. Additional physical phenomena, for instance buoyancy and compressibility, can be broadly modeled in addition to the turbulence model. Extended wall functions and zonal models can address the issues of near-wall accuracy with more precision.

Conservation equations of mass and momentum for flows related to fluidization can be solved by ANSYS FLUENT including heat transfer or compressibility to the problem requires addition of a supplementary equation of energy conservation. For modeling the turbulent flow, additional transport equations should be solved. Both incompressible and compressible turbulent flows can be described by this general form of equation. Mixing and transport of chemical species can be modeled through convection, diffusion and reaction sources for each component. Various concurrent chemical reactions can be

modeled, including reactions occurring in the bulk phase (volumetric reactions) and/or on wall or particle surfaces and in the porous region. ANSYS FLUENT has both pressure-based and density-based solvers with options for convection and diffusion components. The user should specify mass fraction of inlet species to determine the convection component of the rate of mass transfer. On the other hand, diffusion term can be evaluated from the gradient of inlet species. In the pressure-based solver, both convection and diffusion components are considered for evaluating the net rate of transport of species at the inlet.

ANSYS FLUENT (version 14.5) provides three models for generalized finite-rate formulation reaction modeling:

**Laminar finite-rate model:** Arrhenius kinetic expression is used to determine reaction rates by ignoring the effect of turbulence. This kinetic expression is computationally expensive.

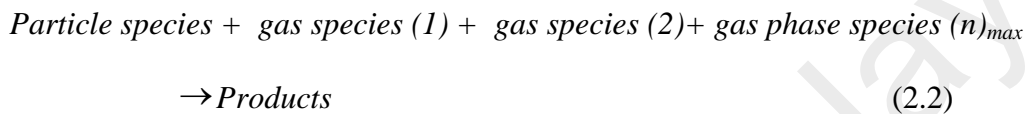
**Eddy-dissipation model:** In this model, Arrhenius kinetic calculations can be avoided as the rate of reaction is assumed to be controlled by the turbulence. As a result, this model is computationally inexpensive. This model also requires products to initiate reaction which is one of the main steps in of the polymerization catalytic reaction.

**Eddy-dissipation-concept (EDC) model:** The EDC model can integrate detailed Arrhenius chemical kinetics with turbulent flames. Consequently, featured chemical kinetic calculations are computationally expensive (*FLUENT 14.5.7*, 2013).

Since polymerization of olefins is a pressure dependent reaction, known as the “fall-off” reaction, one of these three methods can be used to represent the rate expression (Caspar & Meyer, 1983; *FLUENT 14.5.7*, 2013; Stewart, Larson, & Golden, 1989). The method introduced by Magnussen and Hjertager in ANSYS FLUENT has been suggested to be the basis to model turbulence-chemistry interactions (Hjertager, 1976). Catalytic

polymerization is an exothermic reaction and ANSYS FLUENT affords to solve directly this exothermic reaction modeling in a fluidized bed.

Polymerization reaction involves more than one type of gas reactant, including carrier ( $N_2$ ), polymer chain cutting ( $H_2$ ) and reaction closure ( $CO_2$ ) gases. In the case of multiple gas phase reactants, ANSYS FLUENT suggests that the reaction stoichiometry must be extended as follows:



Gas-solid catalyzed reaction is widely used for industrial scale polymer production. For example, Ziegler–Natta catalyst is used in polypropylene and polyethylene production. The reactant gases (propylene/ethylene, nitrogen and hydrogen) are converted on the polymer particles to produce a broad distribution of polymer molecules. The porous catalyst particles, composed of small sub fragments which includes active metal. Polymerization occurs on the active sites of the catalyst surface by diffusion through the porous catalyst (Shamiri et al., 2011; Zacca, Debling, & Ray, 1996). Table 2.2 (*FLUENT 14.5.7*, 2013) shows the necessary equation applicable for olefin polymerization through fluidization.

**Table 2.2:** Equations used for CFD analysis in ANSYS FLUENT for polyolefin fluidized bed reactors (*FLUENT 14.5.7, 2013*)

Type of equations used	Mathematical expression	Significant factors	Remarks
Conservation of mass or continuity equation	$\frac{\partial \rho}{\partial t} + \nabla \cdot (\rho \vec{v}) = S_m$	Is valid for incompressible as well as compressible flows	Mass added to the continuous phase from the dispersed phase
Continuity equation for 2D axisymmetric geometries	$\frac{\partial \rho}{\partial t} + \frac{\partial}{\partial x} (\rho v_x) + \frac{\partial}{\partial r} (\rho v_r) + \frac{\rho v_r}{r} = S_m$	Incompressible, compressible flows and any user-defined sources.	Both axial and radial velocity are considered
Momentum conservation equations	$\frac{\partial}{\partial t} (\rho \vec{v}) + \nabla \cdot (\rho \vec{v} \vec{v}) = -\nabla p + \nabla \cdot (\vec{\tau}) + \rho \vec{g} + \vec{F}$	Static pressure, stress tensor, external body forces	Momentum vector considers porous-media and user-defined sources
Stress tensor	$\vec{\tau} = \mu \left[ (\nabla \vec{v} + \nabla \vec{v}^T) - \frac{2}{3} \nabla \cdot \vec{v} I \right]$	Effect of volume dilation	molecular viscosity and unit tensor is very effective
2D axisymmetric geometries momentum conservation equations	$\frac{\partial}{\partial t} (\rho v_x) + \frac{1}{r} \frac{\partial}{\partial x} (r \rho v_x v_x) + \frac{1}{r} \frac{\partial}{\partial r} (r \rho v_r v_x) = -\frac{\partial p}{\partial x} + \frac{1}{r} \frac{\partial}{\partial x} \left[ r \mu \left( 2 \frac{\partial v_x}{\partial x} - \frac{2}{3} (\nabla \cdot \vec{v}) \right) \right] + \frac{1}{r} \frac{\partial}{\partial r} \left[ r \mu \left( \frac{\partial v_x}{\partial r} + \frac{\partial v_r}{\partial x} \right) \right] + F_x$	Axial and radial momentum	swirl velocity is main concern
User-defined scalar (UDS) transport			

**Table 2.2:** Equations used for CFD analysis in ANSYS FLUENT for polyolefin fluidized bed reactors (*FLUENT 14.5.7, 2013*)

Type of equations used	Mathematical expression	Significant factors	Remarks
equations			
Single phase flow	$\frac{\partial \rho \phi_k}{\partial t} + \frac{\partial}{\partial x_i} \left( \rho u_i \phi_k - \Gamma_k \frac{\partial \phi_k}{\partial x_i} \right) = S_{\phi_k}$ $k = 1, \dots, N$	Arbitrary scalar, diffusion coefficient,	In the case of anisotropic diffusivity tensor may change
Multiphase flow	$\frac{\partial \alpha_k \rho_k \phi_k^k}{\partial t} + \nabla \cdot (\alpha_k \rho_k \bar{u}_k \phi_k^k - \alpha_k \Gamma_k^k \nabla \phi_k^k) = S_k^k$ $k = 1, \dots, N$	Volume fraction, physical density, velocity of phase.	Two categories of scalars: per phase and mixture is considered. Solves the transport equation inside the volume occupied by certain phase.
Periodic flows			
Momentum conservation equation for swirl velocity	$\frac{\partial}{\partial t} (\rho w) + \frac{1}{r} \frac{\partial}{\partial x} (r \rho u w) + \frac{1}{r} \frac{\partial}{\partial r} (r \rho v w) = \frac{1}{r} \frac{\partial}{\partial x} \left[ r \mu \frac{\partial w}{\partial x} \right]$ $+ \frac{1}{r^2} \frac{\partial}{\partial r} \left[ r^3 \mu \frac{\partial}{\partial r} \left( \frac{w}{r} \right) \right] - \rho \frac{v w}{r}$	Radial velocity, swirl velocity and axial velocity	For 3D problems no particular inputs and special solution procedures required throughout the problem setup
Compressible flow equation	$\rho = \frac{P_{op} + p}{\frac{R}{M_w} T}$	Operating pressure, local static pressure, molecular weight, temperature,	Follow ideal gas law
Energy conservation equation	$\frac{\partial}{\partial t} (\rho E) + \nabla \cdot (\bar{v} (\rho E + p)) = -\nabla \cdot (\sum_j h_j J_j) + S_h$	Energy factor, conservative	For inviscid flows energy conservation

**Table 2.2:** Equations used for CFD analysis in ANSYS FLUENT for polyolefin fluidized bed reactors (*FLUENT 14.5.7, 2013*)

Type of equations used	Mathematical expression	Significant factors	Remarks
		vectors	equations are reduced because of the absence of molecular diffusion
Mass diffusion equation (Laminar flow)	$\vec{J}_i = -\rho D_{i,m} \nabla Y_i - D_{T,i} \frac{\nabla T}{T}$	Diffusion flux, concentration gradients, mass and (Soret) diffusion coefficient,	Fick's law is used for modeling
Mass diffusion equation (turbulent flow)	$\vec{J}_i = -\left(\rho D_{i,m} + \frac{\mu_t}{Sc_t}\right) \nabla Y_i - D_{T,i} \frac{\nabla T}{T}$	Schmidt number, turbulent viscosity, turbulent diffusivity	Turbulent diffusion generally overwhelms laminar diffusion
Laminar finite-rate model equation	$\hat{R}_{i,r} = \Gamma(v_{i,r}'' - v_{i,r}') \left( k_{f,r} \prod_{j=1}^N [C_{j,r}]^{\eta_{j,r}'' + \eta_{j,r}'} \right)$	Rate exponent for product species, reactant species and molar concentration of species.	Only applicable for a non-reversible reaction
Eddy-dissipation model equation	$R_{i,r} = v_{i,r}' M_{w,i} A \rho \frac{\varepsilon}{k} \min_{\mathfrak{R}} \left( \frac{Y_{\mathfrak{R}}}{v_{\mathfrak{R},r}' M_{w,\mathfrak{R}}} \right)$	Mass fraction of any product species and particular reactant,	ANSYS FLUENT permits multi-step reaction mechanisms with the eddy-dissipation models.



For modeling of this type of reaction, ANSYS FLUENT suggests the following equations for the surface reaction rate and mass fraction of the surface species calculation:

*Rate of reaction:*

$$\bar{R}_{j,r} = A_p n_r y_j R_{j,r} \quad (2.3)$$

$$R_{i,r} = R_{kin,r} \left( P_n - \frac{R_{j,r}}{D_{0,r}} \right)^N \quad (2.4)$$

*Kinetic rate of reaction:*

$$R_{kin,r} = A_r T_p \beta_r e^{-(E_r / RT_p)} \quad (2.5)$$

*Rate of particle surface species depletion for reaction order  $N_r, n=1$ :*

$$\bar{R}_{j,r} = A_p \eta_r Y_j p_n \frac{R_{kin,r} D_{0,r}}{D_{0,r} + R_{kin,r}} \quad (2.6)$$

*For reaction order  $N_r = 0$ :*

$$\bar{R}_{j,r} = A_p \eta_r Y_j R_{kin,r} \quad (2.7)$$

Another CFD software, COMSOL also provides effective simulations to study the gas phase fluidization. Material, energy and momentum balance equations of ethylene polymerization process can be found in the literature ( Incropera et al., 2007; Li et al., 2008; Bird et al., 2002). The following equations below are applicable for gas phase polymerization process specially used in COMSOL. The feed to the reactor was considered primarily of ethylene as the monomer and nitrogen as the carrier gas (homopolymerisation).

### Material balance

The steady state material balance for ethylene through the fluidized bed reactor is given by:

$$D_i \left[ \frac{1}{r} \frac{\partial}{\partial r} \left( r \frac{\partial C_i}{\partial r} \right) + \frac{\partial^2 C_i}{\partial z^2} \right] + r_{C_2H_4} = \frac{\partial}{\partial z} (v_z C_i) + \frac{1}{r} \frac{\partial}{\partial r} (r v_r C_i) \quad (2.8)$$

where the subscript “*i*” indicates ethylene species. The reaction rate of ethylene is given by:

$$r_{C_2H_4} = -k_r C_{C_2H_4} \quad (2.9)$$

where the reaction rate constant is:

$$k_r = .085 \exp \left[ \left( -\frac{9000}{1.98} \right) \left( \frac{1}{T} - \frac{1}{360} \right) \right] \quad (2.10)$$

Eq. (8) should be solved according to the following boundary conditions:

$$\text{Reactor walls: } (r = R); \quad -\frac{\partial C_i}{\partial r} = 0 \quad (2.11)$$

$$\text{Ethylene initial feed concentration: } (z = 0); \quad C_{C_2H_4} = C_{C_2H_4}^o \quad (2.12)$$

$$\text{Convective flux: } (z = L); \quad -\frac{\partial C_i}{\partial z} = 0, \quad (2.13)$$

### Energy balance

The energy balance inside the FBR can be obtained by employing conduction and convection heat transfer equations:

$$\rho_g C_{pg} \left( v_r \frac{\partial T}{\partial r} + v_z \frac{\partial T}{\partial z} \right) = k_g \left[ \frac{1}{r} \frac{\partial}{\partial r} \left( r \frac{\partial T}{\partial r} \right) + \frac{\partial^2 T}{\partial z^2} \right] + r_{C_2H_4} \Delta H_{rxn} \quad (2.14)$$

This equation should be solved according to the following boundary conditions:

$$\text{Symmetry: } r = 0, \frac{\partial T}{\partial r} = 0 \quad (2.15)$$

$$\text{Symmetry: } r = R, T = T_w \quad (2.16)$$

$$\text{Inlet temperature: } z = 0, T = T_0 \quad (2.17)$$

$$\text{Convective heat flux: } z = L, \frac{\partial T}{\partial z} = 0 \quad (2.18)$$

### *Momentum balance*

At steady state condition, velocity profiles in the r and z directions can be obtained from:

r-direction:

$$\rho_g \left( v_r \frac{\partial v_r}{\partial r} + v_z \frac{\partial v_r}{\partial z} \right) = -\frac{\partial p}{\partial r} + \mu_g \left[ \frac{\partial}{\partial r} \left( \frac{1}{r} \frac{\partial}{\partial r} (r v_r) \right) + \frac{\partial^2 v_r}{\partial z^2} \right] \quad (2.19)$$

z-direction:

$$\rho_g \left( v_r \frac{\partial v_z}{\partial r} + v_z \frac{\partial v_z}{\partial z} \right) = -\frac{\partial p}{\partial z} + \mu_g \left[ \frac{1}{r} \frac{\partial}{\partial r} \left( r \frac{\partial v_z}{\partial r} \right) + \frac{\partial^2 v_z}{\partial z^2} \right] \quad (2.20)$$

These equations should be solved subject to the following boundary conditions:

$$\text{No slip at reactor walls: } r = R, v_z = 0, v_r = 0 \quad (2.21)$$

$$\text{Symmetry: } r = 0, \frac{\partial v_r}{\partial r} = 0, \frac{\partial v_z}{\partial r} = 0 \quad (2.22)$$

$$\text{Inlet velocity: } z = 0, v_z = v_o, v_r = 0 \quad (2.23)$$

$$\text{Reactor exit: } z = L, \frac{\partial v_z}{\partial z} = 0, v_r = 0 \quad (2.24)$$

The above set of model equations can be solved by COMSOL Multiphysics software which is a finite element solver. COMSOL Multiphysics also offers an extensive interface to MATLAB and its toolboxes for a large variety of programming, preprocessing and post processing possibilities. This software allows for entering coupled systems of partial differential equations and the equations can be entered directly or using the so-called weak form. Physical properties of ethylene and nitrogen gas are also available in COMSOL.

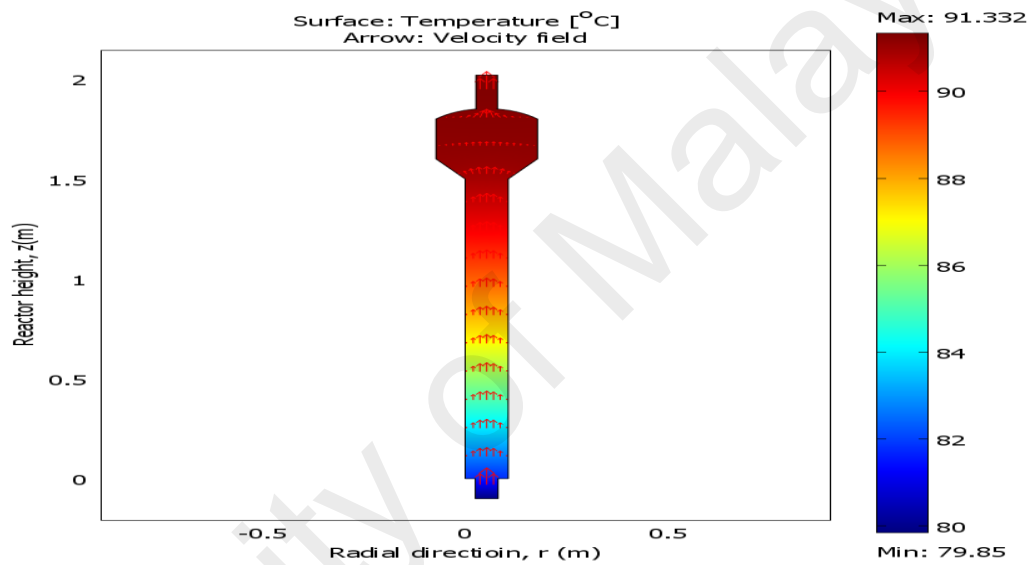


**Figure 2.2:** Typical surface temperature profile inside the pilot plant.

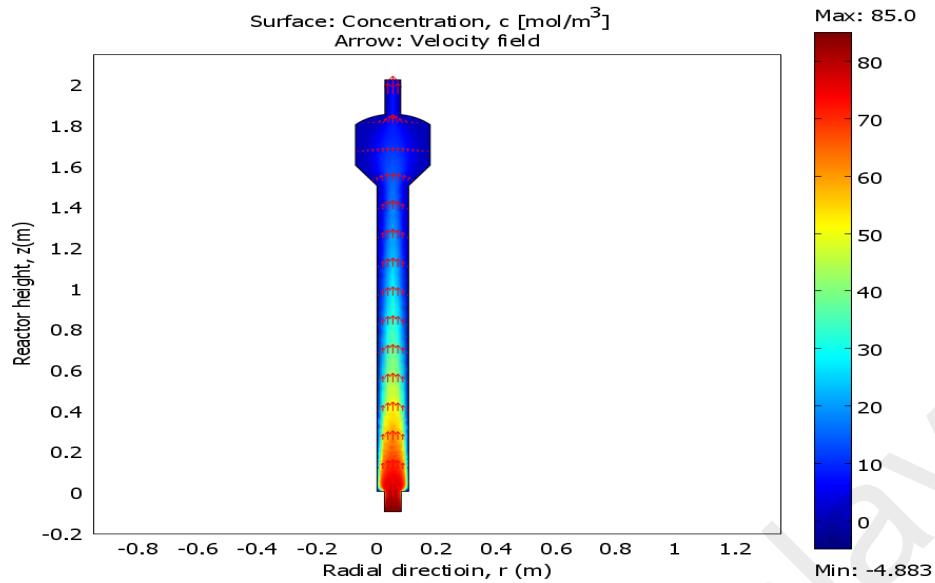


**Figure 2.3:** Typical concentration profile of ethylene.

Figure 2.2 illustrates a typical temperature profile through the pilot plant fluidized reactor for which the above set of partial differential equations were solved with COMSOL Multiphysics software package (McAuley et al., 1990). Increase in the reactor temperature is owed to the heat of ethylene polymerization for the exothermic reaction. Detailed operating conditions can be found elsewhere (McAuley et al., 1990; McAuley et al., 1994). Figure 2.3 illustrates the typical changes in ethylene concentration along the reactor height. This diagram demonstrates that ethylene concentration decreases along the reactor height due to progress of the polymerization reaction. The arrows in Figure 2.3 illustrate the profile and demonstrate that the velocity is uniform throughout the bed and decreases in the enlargement zone to give a chance to the polymer particle to return back to the reactor.

## 2.4 Coding and models for CFD

Kuipers et al. (Kuipers et al., 1993) presented a constructive overview on the progress of CFD codes. They highlighted the development of CFD techniques, particularly in the field of chemical reaction engineering research and identified the importance of CFD as a “workhorse” used in this area (Kolaczowski et al., 2007). However, they pointed to constraints and drawbacks of CFD courses in the curricula of technical universities. Papers on the application of CFD codes in modeling chemical reactions taking place in a mixing environment has also emerged in literature (Frassoldati et al., 2005; Goh et al., 2003). In order to investigate complexities of particle overheating in a gas-phase polymerization reactors, the commercial ANSYS FLUENT CFD software has been used by many researchers (Davidson et al., 1963; Eriksson & McKenna, 2004; Gerogiorgis & Ydstie, 2005; Warnecke et al., 1999).

In the polymerization reaction, the polymer particle grows on the surface of the catalyst. Reactants diffuse through the gas phase from bubble to emulsion, then through the pores of the particle and finally react on active sites of the catalyst to produce polymer product. In many models proposed for the polymerization reactor, transport of species in the gas phase was neglected and only momentum and energy balances for the gas phase and the energy balance of the solid phase were considered (Canu & Vecchi, 2002). Canu and Vecchi (Canu & Vecchi, 1997) employed CFX software to simulate the catalytic polymerization reaction. In their simulation, they did not consider diffusion and reaction in the catalyst separately but used a simplified surface reaction expression that lumps all complexities into one term. They kept default values of the CFD code to model non-ideal flow structure with complex geometry. FEMLAB, widely known as equation solver for the partial differential equation, has also been satisfactorily used for solving for reaction and diffusion equations of catalytic reactions (Lettieri et al., 2003).

The above discussion clarifies that there are several options in a CFD code and it is the user's decision to select the appropriate condition. Commercial codes offer default settings which can be really helpful. Although a number of research groups have shared their knowledge about the CFD simulation of chemical reactors since the last two decades, new researchers still face difficulties when attempt to utilize these tools (Sahu et al., 2010). Generally, there is not enough published data with the completed simulations to demonstrate how to organize a commercial CFD code for simulation of the performance of a catalytic reactor. The CFD software FLUENT 6.0 was used for many numerical simulations accompanied with various drag forces used to calculate the momentum exchange coefficient (Herzog et al., 2012).

At the present time, numerous general-purpose CFD codes are available. The choice of number of governing equations to be used and selection of codes solely depends on the purpose of the model. Three types of gas-solid regimes are considered to be handled by ANSYS FLUENT: (i) particle-laden flow (ii) pneumatic transport (iii) fluidized bed (both fluidized bed reactors and circulating fluidized beds). Application of CFX-4 commercial code for simulating of gas-fluidized beds has been detailed by Lettieri et al. (Lettieri et al., 2003). The particle-bed model and the Eulerian granular model were their main considerations. Taghipour et al. (Taghipour et al., 2005) conducted both experimental and simulation studies on a gas–solid fluidized bed system. They used a 2D fluidized bed column to provide a meaningful understanding of the hydrodynamics of the reactor. It is worth mentioning that, compared to Taghipour et al. (Taghipour et al., 2005) and Herzog et al. (Herzog et al., 2012a) carried out their simulations with a more recent version of Fluent and achieved results that match much better with the numerical results of MFIX. Their analysis showed that the Eulerian–Eulerian model of

OpenFOAM (Open Source Field Operation and Manipulation) has not been fully developed until now, whereas, Londono et al. (Londono et al., 2007) made initiatives to benchmark the OpenFOAM module based only on global values. However, this module is an addition to the development of Passalacqua and Fox (Passalacqua & Fox, 2011).

Literature survey has shown that a small number of publications and discussion exists regarding open source (OS) software development in computational research of olefin fluidization. In fact, verification of a complex software is a critical and difficult task. Syamlal et al. (Syamlal et al., 2008) carried out an elaborated case study on application of the computational research software. They studied the cause for the small number of researchers engaged in computational science and engineering and stated that the main reason is the 'effectiveness' along with the 'sustainability' of the OS development. The theory manual of MFIX contains equations (Syamlal et al., 1993) while the user's manual contains code architecture, numerical technique and user instructions (Syamlal, 1994). The first set of gasifier simulations by OS codes were carried out in 1995 (Syamlal, 1996). Gas-solids flow models in MFIX is a continuing development process like other recognized mathematical models and numerical techniques. Hydrodynamics, heat transfer and chemical reactions in fluid-solids systems can be described directly by MFIX general-purpose computer code (Guenther, 2002). This code can solve commonly recognized set of partial differential equations for conservation of mass, momentum, species and energy for multiple phases (Gidaspow, 1994). Table 2.3 illustrates the applicable categories of MFIX and shows the multicategorical applications of MFIX as a CFD tool.



**Table 2.3:** Multi-category usages of MFI (Syamlal et al., 2008)

<b>Sector</b>	<b>Considered factors</b>	<b>Fraction of usages in percentage (%)</b>
Energy	Coal gasification and combustion, Biomass combustion	28%
Fluidization	Bubbling fluidized beds, risers, particle flow, gas-solids flow	20%
Chemical reactors	Fluid catalytic cracking, fluid bed reactors and polymerization	12%
Multiphase flows	Multiphase, micro-fluidics, slurry flow, gas-liquid	14%
Geophysical	Volcanic granular flows	8%
Other applications	Micro-channel heat exchanger, Powder flow	18%

## **2.5 Aspects and mechanisms in fluidized bed reaction**

### **2.5.1 Modeling of hydrodynamic behavior of fluidized bed reactor**

Profound knowledge of fluidized bed hydrodynamics is important for proper gas-solid reaction modeling and, thus, a proper fluidization process design. Modeling of gas-solid flow patterns, together with the volume, size and velocity of bubbles is a challenging issue. Uniform gas distribution in the reaction zone of the reactor with a desirable interfacial surface area between the gas and solids is important to achieve better conversion. Higher gas velocity is a must for higher production rate and for balancing purposes staging and baffling is also considered. Furthermore, strong control over heat exchange is essential to avoid potential dead spots (Fan, 2005).

Development of hydrodynamic models for describing fluidization process started in early 1960s. The precedent studies mainly focused on the stability of fluidization as well as formation and motion of bubbles. Literature survey disclosed that researchers have attempted to obtain a better understanding of the hydrodynamics of FBRs by carrying out laboratory scale experiments. However, laboratory scale data are not necessarily enough for accurate scale up. For clear understanding of the hydrodynamics in a commercial scale fluidized bed reactor, the study on a vessel of that size is a must. As such, computational modeling is needed to decrease the capital cost and attain featured

engineering design guidance (Hsiaotao, 2007). Most of designs of FBRs have been performed based on the data from the laboratory scale or pilot scale units. Accurate hydrodynamic models, considering fundamental laws of mass, energy, momentum and species conservation, can link the gap between laboratory scale experimental data and industrial scale reactors (Taghipour et al., 2005). Although polyolefin systems have been the focus of numerous researchers since the last three decades, the nonideality of the particle behavior makes it difficult to utilize a CFD model to study effects of its parameters on the system behavior.

### **2.5.2 Fluid flow modeling**

Small number of studies are available on the dynamics of fluid flow in fluidized bed polymerization reactors, especially for influences of modeling parameters and operation/reactor conditions on the flow behavior (Shi, et al., 2011; Darelius et al., 2008; Zhang et al., 2005; Zhang et al., 2008). Two dimensional Eulerian–Eulerian model, combined with the KTGF approach, was applied to simulate the flow fields in a gas–solid FBR (Antoni et al., 2009; Gera & Gautam, 1995; Kuipers et al., 1993; Pain et al., 2001; Peirano et al., 2001; Shen et al., 2004).

CFD has become a very attractive option besides experimental techniques. However, this numerical method needs a very effective and careful validation procedure. Eulerian–Eulerian and Eulerian–Lagrangian approaches are two approaches that are frequently used for formulation of multi-fluid flow and motion of dispersed phase, respectively (Yong et al., 1999; Panneerselvam et al., 2007). CFD models for various systems, like solid-liquid, gas–solid and particle-fluid, have been used since two decades ago (Cheung et al. 2007; Jiradilok et al., 2007; Laborde et al., 2009). The two-fluid model (TFM), based on the Eulerian–Eulerian approach, has been adopted to solve

various multiphase flow dilemmas. The TFM requires a package of empirical or physical models for closing the conservation equations (Sun et al., 2011). Nowadays, the KTGF has become the top choice for the closure law to explain solid phase dynamics (solid viscosity, solid pressure, solid shear stress) along with the TFM (Hosseini et al., 2010). However, some researchers considered a drag force model to obtain precise simulation results. Recently, some researchers applied drag force model combined with the KTGF-based TFM model for calculation of dynamic parameters and simulation hydrodynamics of gas–solid fluidized bed (Hamzehei & Rahimzadeh, 2009; Li et al., 2009). Several momentum exchange coefficients in the gas–solid flow were also developed (Gidaspow et al., 1994; Syamlal et al., 1989). Hosseini et al. (Hosseini et al., 2009) examined different drag models at high gas velocities using combined 2D Eulerian-Eulerian approach and the KTGF. They showed that particles motion and bubbles behavior are satisfied by experimental data.

In the gas phase olefin polymerization, porosity and effect of temperature on performance of the reactor is significant (Miroliaei et al., 2012). Ding and Gidaspow (Ding & Gidaspow, 1990) pioneered the study on prediction of instantaneous porosity and evaluation of the porosity distribution in fluidized beds experimentally. Jung et al. (Jung et al., 2006) analyzed various types of granular temperature in a 2D model fluidized bed with a combination of KTGF-based code and MFIX and showed that the results are in agreement with their earlier experimental study. Energy spectrum of particle turbulence, phase dispersion, granular temperature, Reynolds stresses and phase dispersion have been evaluated in risers of fluidized bed (Jiradilok et al., 2008; Jiradilok et al., 2006). However, very few researchers have focused on the organized analysis of fluidization dynamic parameters with complete investigation on the multiphase gas–solid flow. Nevertheless, the TFM (Eulerian–Eulerian model) integrated with the KTGF

is accepted by many researchers to simulate the flow behavior in the gas–solid fluidized bed. Since the RNG-k- $\epsilon$  model requires an impractical higher turbulent viscosity and is hard to converge, the typical k- $\epsilon$  turbulence model with high computation speed and acceptable speed of convergence is normally chosen to solve the transport equations of k and  $\epsilon$ . FLUENT offers double precision option and can provide a better solution for these complexities. In this case, discretization of the momentum equation can be done by the second order upwind scheme in the ANSYS FLUENT package (Tagliaferri et al., 2013; Jung et al., 2005).

Turbulence is an important phenomenon in gas-solid fluidized beds. This phenomenon can affect mixing as well as heat and mass transfer. Proper knowledge of turbulent energy power spectrum is required to simplify and investigate the turbulent flow (Rao & Sivashanmugam, 2010). According to the cascade theory of turbulence, the turbulent energy spectrum is divided into energy-containing range, inertial range and dissipation range. Reynolds number and the Kolmogorov  $-5/3$  law are key tools for calculation and classification of flow behavior. For instance, a flow with a high Reynolds number is categorized under inertial range which also can be observed by the Kolmogorov  $-5/3$  law (Gidaspow et al., 1994; Kashyap et al., 2011; Sun et al., 2011; Wadner er al., 2012). Flow at lower Reynolds numbers, inhomogeneous and irregularity is observed for the spatial and temporal distribution of instantaneous turbulent dissipation. For a flow with lower Reynolds number, Kolmogorov  $-5/3$  law is not suitable whereas the Levy–Kolmogorov law can be considered (Onishi et al., 2013; Rathore & Das, 2013; Wang et al., 2013; Xiong et al., 2012) while constitutive equations are applied in the TFM to explain the rheology of the solid phase (pressure gradient and viscosity) (Cui & Fan, 2004a, 2004b; Mudde et al., 1997).

Concepts of fluid kinetic theory can be introduced to explain the functional stresses in the solid phase follow-on from particle streaming collision contribution if the particle motion is enough to be dominated by particle collision interaction (Boemer et al., 1997; Liu et al., 2013). Concepts of kinetic theory developed by Lun et al. (Lun et al., 1984) were adopted in some studies for explanation of constitutive functions for the solid-phase stress. Moreover, some significant KTGF equations for study of flow behavior have been accepted widely as follows:

$$p_s = \alpha_s p_s \theta_s [1 + 2g_0 \alpha_s (1 + e_s)] \quad (2.25)$$

$$\lambda_s = \frac{4}{3} \alpha_s^2 d_s g_0 (1 + e_s) \sqrt{\frac{\Theta_s}{\pi}} \quad (2.26)$$

where

$$g_0 = \frac{1}{1 - (\alpha_s / \alpha_{s,\max})^{1/3}} \quad (2.27)$$

It is also necessary to consider transport equation for the granular temperature (Ding & Gidaspow, 1990):

$$\frac{\partial}{\partial t} (\rho_s \alpha_s \Theta_s) + \nabla (\rho_s \alpha_s \bar{v}_s \Theta_s) = \frac{2}{3} [(-\rho_s \bar{I} + \bar{\tau}_s) \nabla \bar{v}_s + \nabla (k \nabla \Theta_s) - \gamma_{\Theta_s} + \phi_{gs}] \quad (2.28)$$

Lun et al. (Lun et al., 1984) provided the following correlation for the collision dissipation of energy:

$$\gamma_{\Theta_s} = \frac{12(1 - e_s^2) g_0 p_s \alpha_s^2 \Theta_s^{1.5}}{d_s \sqrt{\pi}} \quad (2.29)$$

Double precision mode of ANSYS FLUENT can be applied to solve the stated equations. For coupling of velocity and pressure, SIMPLE (Semi-Implicit Method for Pressure-Linked Equations) algorithm with phase-coupled mode can be used. GAMBIT is convenient for grid generation and 3D geometries visualization in different system environments.

### 2.5.3 Mixing models

Fluidized beds are generally useful devices for various applications of particle mixing. Motion of bubbles is considered as the main driving force for particle mixing. On the other hand, segregation also occurs at certain conditions. In gas–solids olefin polymerization reactor, perfect mixing is always advisable. To initiate polymerization, mixing of granulated polymer particle, reactant gas, carrier gas and polymer chain cutting gas is mandatory (Cooper & Coronella, 2005; Shamiri et al., 2011). Mixing and segregation take place simultaneously and at the equilibrium state when a moderately homogeneous distribution of particles is desired (Jang et al., 2010). During fluidization, bubbles move from the bottom towards the top of the bed which results in both mixing and segregation of particles. These phenomena are fully supported by the two-phase theory of fluidization (Mostafazadeh et al., 2013).

Due to traveling of bubbles up throughout the bed, particles are drawn into a sluggish zone trailing the bubbles, known as the wake (Basesme & Levy, 1992; Fernandes et al., 2001). Particle penetration in the wake causes axial mixing and consequently fresh particles permeate from the dense adjoining region. Particles adjacent to the wake will be deposited at the surface of the bed due to the upward movement of bubbles. As a result, particles at the bottom of the bed can be mixed with the particles at the top. The adjoining fluid surrounding the rising bubble is considered as the main motive of particle mixing (Tsuchiya et al., 1990). In the intervening time, the bubble at its rising moment leaves a void behind (Gibilario et al. 1974). Mixing of solids in a bubbling fluidized bed is highly affected by collision and coalescence of bubbles. Bubbles and emulsion can be considered as source and sink of kinetic energy for particles, respectively. Energy transfer from source to sink occurs through the drift region. This

energy transfer produces circulation of solids, in the scale of bubble diameter, in the drift zone. Therefore, both gross and internal circulations are the cause of solids mixing in the bed (Norouzi et al., 2011; Norouzi et al., 2012; Norouzi, Mostoufi et al., 2012).

Norouzi et al. (Norouzi et al., 2011) investigated the behavior of the solid phase in fluidized beds using a 2D CFD-DEM simulation to get more information on mixing and motion of solids. Their typical results are shown in Figure 2.5 which demonstrates evolution of void fraction contours and solids flux vectors in a fluidized bed with a porous plate distributor at superficial gas velocity of  $1 \text{ m.s}^{-1}$ .

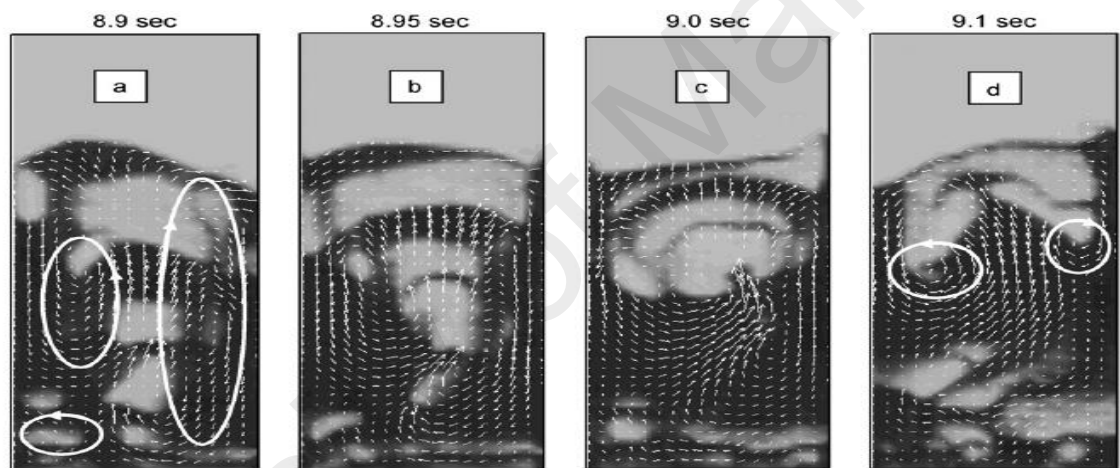


**Figure 2.5:** Void fraction contours and solid flux vectors of the bed with a porous plate distributor. Reproduced with permission from Elsevier ( Norouzi et al., 2011) .

Formation of bubbles at the vicinity of the distributor, growth of bubbles, their coalescence and breakage can be seen in this figure. Norouzi et al. (Norouzi et al., 2011) showed that the bubble breakage affects internal circulation of particle which develops in rapid local mixing of particles. Heat of polymerization reaction is mainly removed through mixing. It has been found through experiments in polymerization reactors that the quality of mixing in a specific reactor has a significant influence on the rate of polymerization as well as product properties. CFD has the advantage that is capable of presenting precise information on turbulent zones in the reactor. These information can

help to obtain a better reaction yield by introducing reactants into regions with intense turbulence.

The non-linear behavior of reactive fluids can further complicate the formulation of quantitative analysis along with flow visualization during lab scale experiments. Hence, although experimental investigation of the flow behavior in polymer reactors is very important, every parameter related to the mixing process is not manageable with experimental analysis, especially for the desired spatial resolution (Javad et al., 2004; Kemmere et al., 2001; Zhang & Ray, 1997). In spite of successful efforts to solve various problems on the effect of mixing on kinetics of polymerization, there are also difficulties identifiable on modeling of mixing in polymerization reactors. On the other hand, improvement of CFD methods has provided the opportunity to visualize the mixing dynamics such that the necessity to carry out real-time experiments can be bypassed (Azadi et al., 2011; Paul et al., 2004). To make simulation faster, Wells and Ray (Wells & Ray, 2005) proposed a CFD model in combination with a compartment model while ignoring back mixing. Kolhapure and Fox (Kolhapure & Fox, 1999) performed a CFD simulation of ethylene polymerization in a tubular reactor and showed that uneven mixing reduces the polymer conversion but increases the polydispersity index. However, their modeling approach can be criticized for using randomly defined mixing parameters that limited the application of the model. Substantial effect of bubble motion on different aspects of mixing, such as wake, cross solid mixing, interaction and coalescence of adjacent bubbles, dispersion of particles in the wake and eruption of the bubble were explained through the CFD approach (Rhodes et al., 2001). The CFD-DEM technique was applied for investigation of mixing and the particle motion in the flat-bottom spout bed. Both mixing and segregation phenomena were explained with clear justifications with the help of CFD-DEM (Zhang et al, 2009; Zhang et al., 2010).



Wu and Zhan (Wu & Zhan, 2007) investigate the mixing of particles for various configurations in the reactor inlet by employing hard-sphere DEM. Effect of mixing of polydisperse fluidized inert powders was studied with the support of multifluid model option of ANSYS FLUENT by Mazzei et al. (Mazzei et al., 2012). In their study, they proposed and applied a novel quadrature method of moments (QMOM) into ANSYS FLUENT code considering all particles possess different velocity.

The population balance equation (PBE) is one of the widely accepted methods to explain mixing based on variation of particle size. The change of particle size distribution (PSD) with respect to time and space can highly influence physical and chemical phenomena of the gas phase polymerization processes. Variation of the PSD can be linked to significant parameters of segregation which can cause uneven mixing of particles in the bed. For analysis of the mixing performance, particle population can be categorized by diameter and velocity. Consequently, two internal coordinates, a scalar and a vector, should be used for this purpose (Ahmadzadeh et al., 2008). To explain the population of particles, a volume density function (VDF) has been proposed. Since, the PBE and the moments are linear in the VDF, mixing is also a linear process and these values may be accurately calculated through their transport equations in the numerical code. To solve this problem, ANSYS FLUENT correlates user defined scalars either with a specific phase (the fluid or any granular phase) or with the mixture of all phases (Kotoulas & Kiparissides, 2006).

To reduce the computational time in simulation of a fluidized bed polymer reactor, a vessel may be considered whose height is double the static height of the powder. This height possibly is enough to let small size particles to fall back into the dense bed. In

this case, these particles bypass the computational domain and are irreversibly lost (Mazzei et al., 2010).

It has been reported that polymerization requires an extremely viscous medium which can affect flow pattern in a polymerization system (Shuai et al., 2012; Shuai et al., 2012; Yiwei et al., 2013). Therefore, the mass viscosity is highly recommended to be considered for polymerization reactor modeling. The apparent viscosity of the mixture can be calculated from (Moritz et al., 1989; Shuai et al., 2012):

$$\mu = \frac{\mu_0}{(1 + \mu_0 \dot{\gamma}^{1.2} / 35000)^{0.6}} \quad (2.30)$$

and the density of the mixture can be calculated from (Soliman et al., 1994):

$$\rho = (1174 - 0.918T)(1 - wp) + (1250.0 - 0.605T)wp \quad (2.31)$$

#### 2.5.4 Bubble modeling

Bubbling is involved in most gas fluidized beds. Therefore, to understand the governing phenomena of bubble formation, it is highly important to understand the fluidization features in the olefin polymerization process. Complete fluidization of the bed is required for bubble formation which spreads throughout the bed in the form of high void fraction regions. Generally, the shape of a bubble depends on its velocity, not the bed dimension. A slow bubble is spherical and starts to deform by increasing its velocity. The size of a bubble can be determined by an effective spherical radius which includes the wake region (Hulme & Kantzas, 2004). The nature of bubble formation and movement in fluidized beds can influence the hydrodynamics of fluidization. Thus, bubble diameter, distribution of bubbles and their collision are considered as significant

parameters (Dong et al., 2013). A number of comprehensive studies have been carried out on various bubble properties. It has been found that the bubble wake is one of the influential aspects accountable for inherent transport properties in the system. Therefore, investigating the bubble wake have drawn attention of researchers for many years. Ever-increasing computer power along with employment of CFD approach has gained considerable attention for investigating bubble behavior in polymerization process through CFD modeling (Almendros et al., 2010; Busciglio et al., 2010; Fung & Hamdullahpur, 1993).

However, still inadequate understanding of multiphase flows has been gained due to complex phenomena involving fundamental interactions between phases, for instance, particle-bubble interaction or particle-particle collision (Mitra-Majumdar, Farouk, & Shah, 1997). Geldart and Kelsey (Geldart & Kelsey, 1972) investigated the bubble motion in two-dimensional and three-dimensional beds with different thicknesses in an effort to show a relationship between three and two dimensional bubble sizes for the first time. For quantitative comparison, some successful CFD simulations, e.g., Syamlal-O'Brien (Syamlal & O'Brien, 2003), Laux-Johansen (Laux & Johansen, 1998) and many other cases can be considered (Reuge et al., 2008). Time step, partitioning schemes, solid stress closure equations and frictional stress are influential parameters on bubble properties. Boemer et al. (Boemer et al., 1997) conducted experiments on various bubble parameters like size of bubble, bubble velocity, angle of wake, pressure distribution and voidage. Although they obtained useful results, not much data points were reported for bubble properties. Particle velocity is one of the most significant parameters on the formation of bubble and it is possible, through CFD-DEM, to provide information on the velocity profile of particles in bubbles (Bokkers et al., 2004; Hassani et al., 2013). The comparison on particle velocity and bubble shape is shown in Figure

2.6 for both simulation and experimental runs. Figure 2.6 (a) illustrates the significant interface between bubble and emulsion phase, which is also predicted through the CFD model.

Experimental results achieved by the model are also shown in Figure 2.6 (b). Electrostatic effect between particles, diameter of bubble and solids diffusivity was also considered in this study.

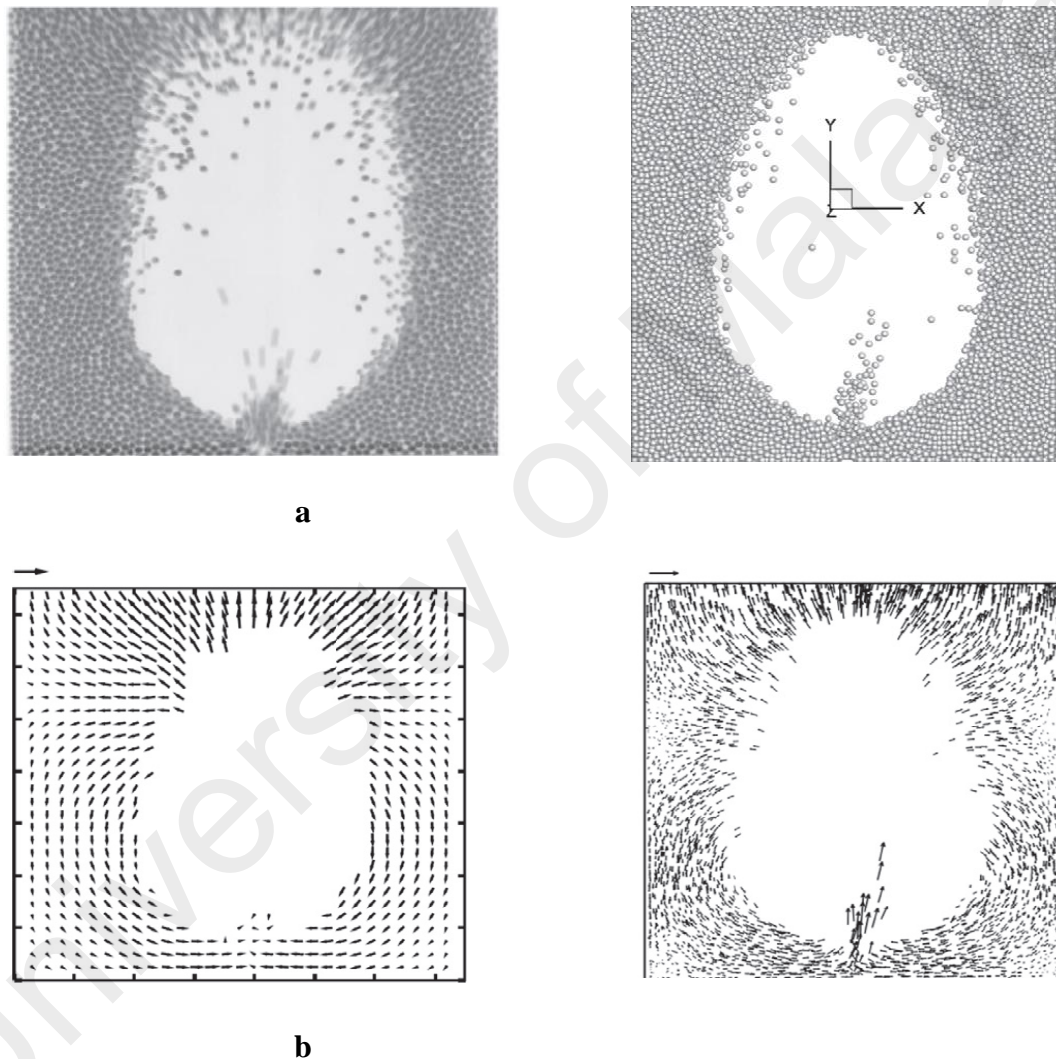


**Figure 2.6:** Comparison between experiment (Bokkers et al., 2004) and model results in terms of (a) bubble shape and (b) particle velocity profile of polyethylene. The unit vector above particle velocity profile plot corresponds to a particle velocity of 1 m/s and minimum fluidization velocity 1.25 m/s . Reproduced with permission from Elsevier.

Bubbles can be identified from the void fraction images produced by ANSYS FLUENT. Example of such images can be seen in Figure 2.7. In addition, a specific program is required to track the bubbles from a frame to another.

It is advised that discontinuation of void fraction to be fixed by the user in order to compare the simulation results.

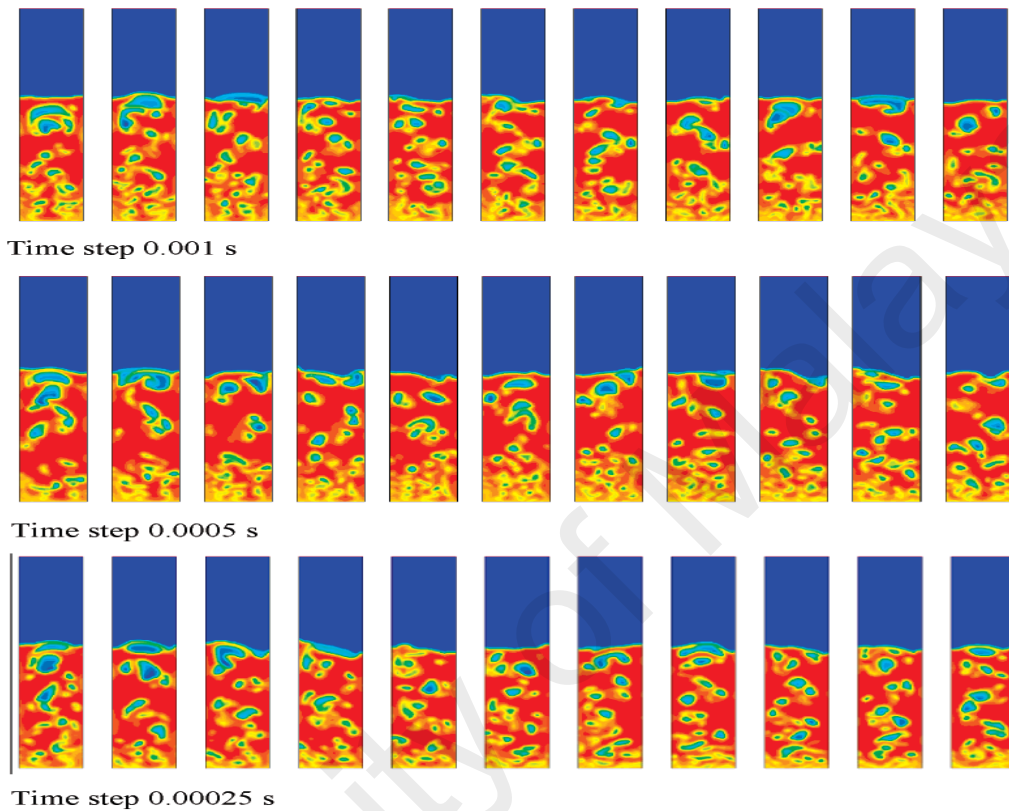


**Figure 2.7:** Void fraction of solids at specific cutoff for different time steps. Reproduced with permission from ACS. (Hulme et al., 2005)

Setting up the time step has an important effect on the accuracy of bubble simulation. In order to obtain transient simulations, the governing equations should be solved to propagate the solution at specific time steps.

Computational time and convergence are usually affected by the time step. ANSYS FLUENT offers the ‘first order semi-implicit’ real time solution technique, thus, a smaller time step is appropriate for a more precise solution. Since computational time is a major issue in studying of bubbles in the gas phase polymerization process, prolonged simulation of a few real seconds becomes key consideration as simulation of bubble

dynamics in a fluidized bed can take more than one week for a simple geometry. For comparing different time steps, the dimensionless Courant number can be used (Gobin et al., 2001). The Courant number reflects the part of a cell that the fluid traverses by advection in a time step:

$$N_c = \vec{v} \frac{\Delta t}{\Delta x} \quad (2.32)$$

When advection is dominant over dispersion, the Courant number should be kept small to reach a better accuracy and minimize the numerical dispersion. It is recommended to set the Courant number to 0.3 for obtaining convergence at a proper calculation speed for continuing “good” behavior in the computations.

The differencing scheme is another parameter that affects properties of bubbles in the simulation of an olefin polymerization reactor. There are first-order upwind and second-order upwind options available in ANSYS FLUENT. It is shown in Figure 2.8 that bubbles appear at the beginning of simulation, but fade away at longer times since the bubbles cannot be detected when the differencing scheme was changed from the second-order upwind to the first-order upwind. Discretization of voidage derivatives by the second-order differencing scheme is preferred since it does not assure cell uniformity and calculate a gradient between the cell nodes, thus, bubble boundaries can be determined distinctively.

If the cell value is kept constant as in first order differencing scheme the solution would become fundamentally smoothed in successive time steps as shown in Figure 2.8.

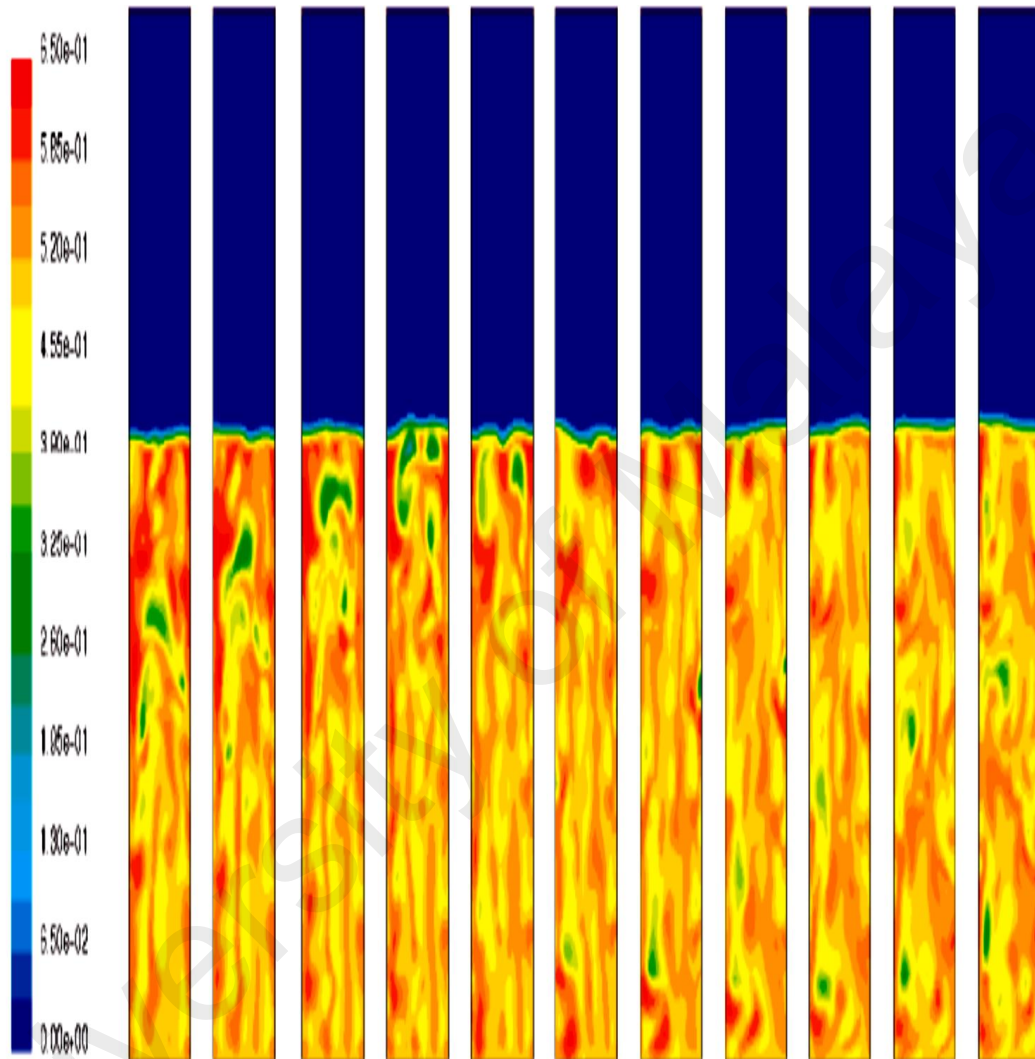


**Figure 2.8:** Simulation with time step of 0.00025 s, first order up-wind (Courant number was below 0.15, at constant cell value). With condition of gas velocity 12.6 cm/s, gas density 1.21 kg/m<sup>3</sup>, pressure 101325 Pa and minimum fluidization velocity 0.093 m/s. Reproduced with permission from ACS (Hulme et al., 2005).

Van Wachem et al. (van Wachem et al., 1998) established a CFD model in conjunction with the Eulerian-Eulerian gas-solid model for a freely bubbling fluidized bed using the commercial CFX package. Renzo et al. (Renzo et al., 2011) carried out CFD simulation of a bubbling FBR by considering the chemical kinetic aspects and focused on

multiphase fluid dynamics, polydisperse particle distributions, intra-particle heat and mass transfer rates.

Bed height is another important parameter for bubble modeling. Height of the bed increases due to formation of bubbles. Coalescence of bubbles takes place during their rise and produce larger bubbles. At the same time, deformation of bubble occurs due to wall effects and interaction with other bubbles. Experiments have indicated that small bubbles are formed near the bottom of the bed and they grow larger as a result of coalescence when rising in the bed (Lyczkowski et al., 2009). Modified Sitnai's methodology has also been used to give details on the fundamental procedure for the analysis of hydrodynamic properties of bubbles (Sitnai et al., 1982). Based on this model, it was concluded that for the hypothetical transient pressure field created by the theoretical Davidson model (Davidson, 1963) for a single noninteracting bubble in a bed with no internals, the time lag,  $t_a$ , determined from autocorrelation yields the ratio of the bubble diameter,  $D_b$ , to the vertical bubble velocity,  $V_b$ , given by:

$$t_a = \frac{D_b}{V_b} \quad (2.33)$$

This equation can be used to calculate the ratio of bubble diameter to bubble velocity from the time lag obtained from the experimental and computed autocorrelations. The bubble diameter may then be determined from:

$$D_b = v_b t_a \quad (2.34)$$

where the bubble velocity can be determined from the well-known equation of Davidson and Harrison (Davidson & Harrison, 1963):

$$v_b = 0.71\sqrt{(gD_b)} \quad (2.35)$$



The type of the gas distributor influences bubble formation and motion which in turn affects the mixing in fluidized bed of olefin polymerization. Particle size distribution in the axial direction is affected by circulation of solids. There are two possible flow paths in a fluidized bed in the upper zone and the bottom zone. Most of the small particles move in the upper part of the bed while large particles flow around in the bottom section. It is noticeable that the number of gas bubbles occurring steadily during the fluidization changes when the geometry of the gas distributor is changed. The gas bubbles merge to grow in size and proceed to the center of the fluidized bed steadily. Bigger bubbles complete their circulation cycle as they burst adjacent to the bed surface. Correspondingly, intense upward flow trend is observed in the case of smaller particle which also proceed to the center progressively (Zhou et al.2013). Flow pattern of bubble and emulsion phases in a fluidized bed for various types of gas distributor is shown in Figure 2.9. It can be seen in this figure that the path of the emulsion phase is more complex than the gas phase. Bubbles are formed as the gas passes through the distributor. Coalescence of bubbles occurs as they flow up and gradually inclined toward the center and burst at the surface of the bed. In a same way, particles at the bottom of the bed flow up and shift to the center through movement of bubbles.

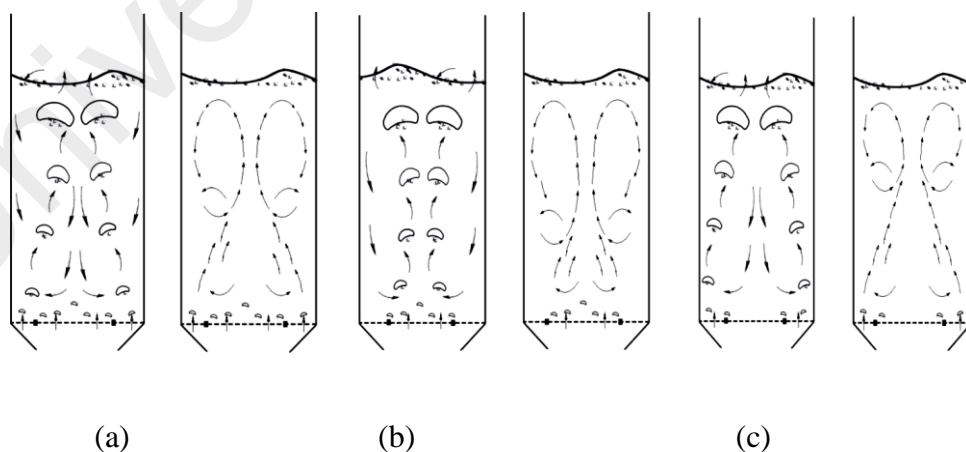


**Figure 2.9:** Bubble and particle behaviors at three different fluidization conditions. (a) normal gas-inlet mode, (b) gas entering the core zone exclusively, and (c) gas entering the annulus zone exclusively. Reproduced with permission from Elsevier (Zhou et al., 2013).

Once the particles reach the top surface of the bed, they mainly move downward gradually in the region close to the wall. Two circulation zones are virtually of the same dimensions and the gas flows evenly in these zones [Fig. 2.9 (a)]. Particle motion and bubble formation are shown in Figures. 2.9 (b) and (c) in which the gas is injected through the core and annulus regions, respectively, of the distributor.

## **2.6 Elevated pressure processes**

Since the polymerization process occurs at elevated pressure, there is a need for fundamental knowledge of variation of the flow structure against pressure. Li and Kuipers (Kuipers et al., 2002) numerically investigated the influence of pressure on the regime transition in dense gas fluidized bed using the DEM. Their results showed that increasing the pressure decreases the incipient of fluidization, increases the homogeneity of the bed and the bed height and leads to a quick transition to turbulent regime of fluidization. They also found that particle-particle collision, compared to particle-fluid interaction, is reduced at elevated pressures. Godlieb et al. (Godlieb et al., 2008) considered the relationship between operating pressure and granular temperature by performing a full 3D DEM-CFD simulation. They found that the granular temperature increases by increasing the pressure and that the pressure has influences the granular temperature mainly in the vertical direction. Zhang et al. (Zhang et al., 2000) investigated motions of bubble and particle in a three-phase fluidized bed at elevated pressures. The Eulerian volume-averaged method, the Lagrangian dispersed particle method and the VOF method were used to describe the motion of liquid, solid particles and gas bubbles, respectively. Furthermore, bubble-induced force model, continuum surface force (CSF) model, Newton's third law and close distance interaction (CDI) model were applied to illustrate, respectively, the coupling effect of particle-bubble, gas-liquid, particle-liquid interactions and the particle-particle collision analysis. Their

simulation results indicated that the bubble trajectory is more tortuous at high pressure than at low pressure. Mansourpour et al. (Mansourpour et al., 2010) studied the effect of pressure on the bubble dynamics (i.e., bubble diameter, rise velocity and its path of rise) in a gas fluidized bed based using the DEM-CFD technique. Their results showed that at elevated pressure, bubbles rise slower and become smaller while bubble break-up rate increases. Consequently, the bed homogeneity enhances at higher pressures. Furthermore, the bubble path becomes twisty through the bed at elevated pressures. Norouzi et al. (Norouzi et al., 2012) developed a comprehensive mathematical model based on the DEM-CFD technique to investigate mixing and segregation of particles in fluidized beds at high pressure. Their results showed that the bed transforms from a segregated state to partially mixed condition by increasing the pressure and vertical segregation at low pressure becomes substituted by horizontal segregation at high pressure. Also, they examined the effect of volume fraction of small particles at different pressures. They showed that the rate of segregation decreases by increasing the mass fraction of small particles at the same pressure.

## **2.7 CFD study on heat transfer phenomena and modeling of polyolefin reaction**

Design of a gas phase polymerization reactor is generally based on considering an arrangement of single or multiple pseudo-homogeneous phases in which mass and heat transfer between phases are taken into account. High rate of the polymerization reaction (normally in the order of 5 to 50 kg of polymer per gram of catalyst per hour) and its exothermic nature (heat of reaction of 100 kJ/mol) makes removing the generated heat at increased yields difficult in industrial reactors. This problem is more serious in gas-phase reactions since the heat transfer characteristics of gas-phase reactors are poor (Floyd et al., 1986).

It is well known that heat transfer problems in fluidized beds are related to particle-particle interactions (McKenna et al., 1998) and researchers can provide knowledge of this local phenomena through modeling. Fitting the model for a polyolefin reactor involves the combination of a wide range of particle growth models (Timothy et al., 2001). Therefore, researchers have investigated effect of local deviations in flow rate, gas composition and initiation temperature of reaction on both particle growth and reactor performance. Coupling heat transfer and reaction kinetics in modeling polyolefin reactors is unavoidable and academic and industrial communities have encountered difficulties inherent in this problem. For example, the DEM was used in simulation of both ethylene and propylene polymerization process in a lab scale reactor (Eriksson & McKenna, 2009; Tioni et al., 2009). Kaneko et al. (Kaneko et al., 1999) verified temperature of particles and gas in a fluidized bed reactor for polyolefin production by the DEM. In their study, the reaction rates were simplified to zero-order kinetic expressions. In this model the reaction rate depends only on the temperature profile in the reactor, but the effect of reactant concentration on the reaction rate was not considered. Karimi et al. (Karimi et al., 2011) developed a DEM-CFD technique combined with equations of conservation of mass and energy to study the behavior of a gas-phase polyethylene reactor. The comprehensive reaction mechanism of McAuley et al. (McAuley et al., 1990) and the corresponding kinetics was employed in their model. Effect of operating conditions of the reactor on temperature distributions of gas and solids was also investigated to examine the possibility of hot spot formation. Their simulations showed that temperature of particles decreases by increasing the gas velocity due to an increase in the heat transfer rate. It was also shown that increasing the pressure results in a higher bed homogeneity and more efficient contact between reactants and the catalyst.

Many researchers have attempted to couple mass and energy balances for a single particle through a modified two-dimensional mass, momentum and energy balance equations in a FBR (Ibrehem et al., 2009). They showed that there is a need for more accurate explanation of the FBR hydrodynamics in order to obtain a full-scale integrated reactor model and to present practical information about heat transfer and its relationship with particle growth and fluidization conditions. By applying the direct QMOM, CFD packages can solve PBEs in the reactor (Behjat et al., 2008). For a laboratory scale fluidized bed, temperature distribution and void fraction can be calculated by CFD softwares. Rapid heat generation among the multiphase environment (gas, solid, emulsion, etc.) causes the overheating of bigger particles which would likely result in hot spots in the reactor. Consequently, multigrain model (MGM) is the model which has attracted several research groups to explain the hot spot phenomena. The MGM considered agglomeration of concentric layers of micro particles, in which the reaction occurs inside the polymer particles. Considerable results can be achieved from modeling studies by the MGM approach. For instance, it can be shown that intraparticle temperature gradients and external heat transfer resistances can be neglected for low active catalyst or small extent of the reaction and that heat transfer resistances are much more important at early stages of polymerization. However, McKenna et al. (McKenna et al., 1998) pointed the disadvantages of the MGM approach such as its deficiency to calculate changes in rapidly evolving particles with physically impractical predictions, for example melting of particle cores. In addition, they demonstrated that conventional heat transfer models, such as empirical correlation of Ranz-Marshall, may contain assumptions which give rise to physically unrealistic results, especially when applying to highly dynamic polymerization processes. Therefore, McKenna et al. (McKenna et al., 1998) used the CFD approach to analyze the heat transfer and geometric scale

effects at the same time in the gas-phase olefin polymerization for complex operating conditions.

Since measurements in industrial reactors are not easy to carry out, the CFD technique has been used as a useful tool for displaying details that cannot be obtained directly from the experiment (Hutchinson & Ray, 1987). However, only a limited number of successful CFD modeling of fluidized bed hydrodynamics including heat transfer have been reported. Studies on hydrodynamics of two dimensional non-reactive gas-solid fluidized bed reactor with heat transfer, both experimentally and computationally, can be found which are mainly focused on the influences of temperature and particles size on the hydrodynamic condition of the bed and gas-solid heat transfer. A multifluid Eulerian model, integrated with the kinetic theory of solid particles, can be used to simulate the gas-solid flow in a wide range of superficial gas velocity and diverse particle sizes. Ranz-Marshall equation is widely applied to calculate particles gas heat transfer coefficient and can provide reasonable results for particle and gas temperatures during bubble formation and rise in gas-solid fluidized beds. Another challenge is detecting formation of hot spots which mainly occurs due to nonlinear exchanging of heat at the distributor and near the wall of the fluidized bed (Hamzehei & Rahimzadeh, 2009).

A multifluid Eulerian model, associated with the KTGF approach, was applied by Huilin et al. (Huilin et al., 2003) to describe hydrodynamics of bubbling fluidized beds. They demonstrated, with simulation results, that the hydrodynamics of a bubbling fluidized bed is severely affected by distribution of particle size as well as the magnitude of energy dissipation in particle-particle interactions. It was shown by Mickley and Fairbanks (Mickley & Fairbanks, 1955) that the particle-wall contact time

is an important factor in calculating the heat transfer coefficient between wall and fluidized bed. Although their theoretical work is reasonably verified with the experimental data, their correlation is applicable only to limited operating conditions. Di Natale et al. (Natale et al, 2009) presented an experimental study on heat transfer coefficients between a fluidised bed of fine particles and a submerged surface using different shapes of immersed tubes within the fluidized bed. Their findings highlighted the strong influence of the surface shape on the heat transfer coefficient in addition to thermal properties of the gas and solid.

Dong et al. (Dong et al., 2010) employed the TFM for simulation of gas-solid two-phase flow in fluidized beds. Conservation of mass, momentum and energy for both solid and gas phases were considered. Their model also utilized the KTGF for describing solid properties such as solids shear stresses and solids viscosity based on the granular temperature that determines the oscillating behavior of the particles. Interaction between particles can be represented by solids pressure and bulk viscosity to obtain normal forces and the shear viscosity for tangential forces, respectively, in collisions. The collisions probability is adjusted with the radial distribution function. The CFD package ANSYS FLUENT was used for simulation purposes which offers the energy equations on the basis of enthalpy balance. For calculating the rate of energy transfer between solid and gas phases, the rate was considered as the function of average particle diameter, gaseous thermal conductivity, temperature difference, Nusselt number and volumetric fraction. The interphase heat transfer coefficient of Gunn (Gunn, 1978) was exercised which is associated by particle Reynolds number and Prandtl number. For determination of the local instantaneous heat transfer coefficient,  $h$ , the operative thermal conductivity of both phases is considered which can be calculated by

correlations of Kuipers et al. (Kuipers et al., 1993) and Patil et al. (Patil et al., 2006) as follows :

$$K_g^{eff} = \left( \frac{1 - \sqrt{\alpha_s}}{\varepsilon_g} \right) K_g \quad (2.36)$$

$$K_g^{ef} = \frac{1}{\alpha_s} K_g [\omega A + (1 - \omega) \Gamma] \quad (2.37)$$

$$\Gamma = \frac{2}{1 - B/A} \left[ \frac{A-1}{(1 - B/A)^2} \frac{B}{A} \ln\left(\frac{A}{B}\right) - \frac{B-1}{1 - B/A} - \frac{B+1}{2} \right] \quad (2.38)$$

$$A = \frac{K_s}{K_g}, B = 1.25 \left( \frac{\alpha_s}{\alpha_g} \right), W = 7.2 \times 10^{-3} \quad (2.39)$$

The grid refinement technique suggested by Kuipers et al. (Kuipers et al. 2001) is usually employed for mesh generation to subdivide the region near heated surfaces as a substitute of the uniform sub cell dimensions proposed by Syamlal and Gidaspow (Syamlal & Gidaspow, 1985) .

Detailed heat transfer study on particle level in fluidization with CFD validation is very rare. Brown and Lattimer (Brown & Lattimer, 2013) studied heat transfer characteristics of fluidized particles. Their study included both CFD simulation and experimental data. They showed that the apex surface of the bed usually exhibits the maximum particle temperatures due to higher bed-to-wall heat flux, lower residence time of bed particle in gas channel and convective gas-to-particle heat transfer at the top of the bed. Figure 2.10 illustrates the time dependent fluctuations of particles within the fluidized state. It is noticeable that entrainment of the fluidized bed particles occurs above the temporal outlines. Upward movement above the jet zone and downward movement in the moving section is the main cause for these phenomena. The escalating surface temperature of particle restrains the heat exchange rate of gas-to-particle. At the



fluid inlet point, a greater heat flux was noticed from bed to wall that also caused energy loss.

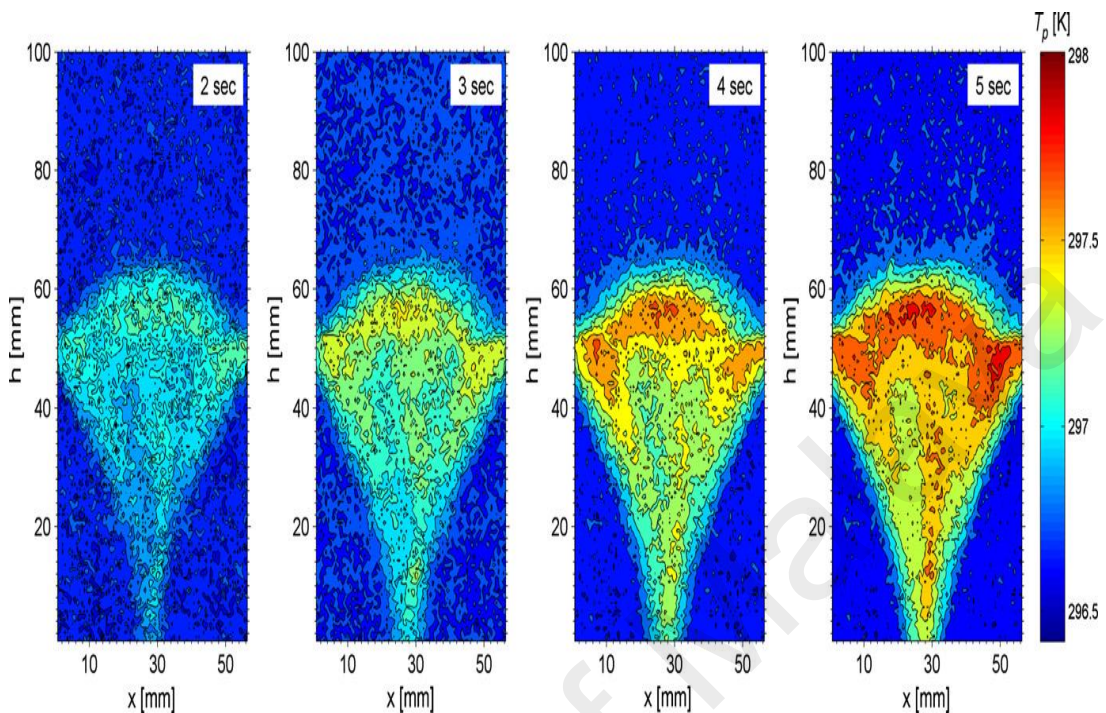


**Figure 2.10:** Instantaneous particle time line temperature distribution in a fluidized regime at minimum fluidization velocity  $1.6 \text{ ms}^{-1}$  Reproduced with permission from Elsevier (Brown & Lattimer, 2013).

Many researchers discussed about the reports on CFD simulation of individual particles and their interactions in the system and the few models to describe overall behavior of the reactor (Dehnavi et al., 2008). Dehnavi et al. (Dehnavi et al., 2010) investigated the hydrodynamics and heat transfer of the fluidized bed of polyethylene particles based on the Eulerian–Eulerian approach. Their findings proved that the Eulerian–Eulerian model is good fitting for scale up of industrial fluidized bed reactors for polyethylene production.

Various commercial softwares have been suggested by researchers for CFD simulation of heat transfer in a bed of polyolefin particles. The calculation domain provided by ANSYS FLUENT is divided into a finite number of non-overlapping control volumes. The main grid points, positioned in the center of each control volume, consist of certain

significant scalars, like pressure, volume fraction, density and granular temperature, while velocity components are stored at the cell surfaces. A simple discretization for governing equations can be carried out with the help of a staggered grid to ease numerical instabilities. Integration of conservation equations are carried out in time and space. The integration is executed by applying the first order upwind differencing in space and complete implicit techniques in time. For solving the discretized equations, a specialized phase coupled algorithm, called PC-SIMPLE (Phase-Coupled Semi-Implicit Method for Pressure-Linked Equations) was used.

Drag force is one of the dominant hydrodynamic parameters in heat transfer analysis of olefin polymerization reactors. Due to the strength of the drag force, the two-phase partial elimination algorithm (PEA) was simplified for the gas-solid flow and was used to decouple the drag forces. The interphase slip algorithm (IPSA) was applied for ensuring the coupling between velocity and the continuity equation. The feed gas/gases (ethylene/ propylene) were considered as the continuous phase. It was shown that particle shape in the case of inter-particle heat transfer is significant. The dispersed phase surrounding spherical particles, whose average diameter is presumed to be uniform and constant, showed comparatively linear changes of heat transfer fluctuations (Chiesa et al., 2005). Researchers (Hou et al., 2012; Zhuang et al., 2014) investigated heat transfer characteristics of powders with diverse properties in gas-solid fluidization by means of the combined CFD-DEM approach incorporated with a heat transfer model. They extended the model of Zhou et al. (Zhou et al., 2009) by applying a cohesive force model.

In order to apply the heat transfer equation, most researchers commonly have considered three modes: conduction between the wall and particles, convection between

fluid and particles and radiation between particles and their local surrounding environment. For instance, according to the heat balance, the governing equation for particle numbered as  $i$  can be written as (Zhou et al., 2009):

$$M_p C_{p,i} \frac{dT_i}{dt} = \sum_j q_{i,j} + q_{i,f} + q_{i,rad} + q_{i,wall} \quad (2.42)$$

This is widely known as the lumped formulation in which thermal resistances inside the particle are neglected. Equations required for calculating the heat fluxes are listed in Table 2.4.

**Table 2.4:** Equations for calculating heat flux

Heat flux	Equation
Convective	$q_{i,f} = (2 + a \text{Re}_i^b \text{Pr}^{1/3}) k_f A_i \Delta T / d_{pi}$ $q_{f,wall} = 0.037 \text{Re}^{0.8} \text{Pr}^{1/3} k_f A_w \Delta T / L$
Conductive	$q_{i,j} = 4r_c (T_j - T_i) / (1/k_{pi} + 1/k_{pj})$
Radiative	$q_{i,rad} = \sigma e A_i (T_{local,i}^4 - T_i^4)$ $q_{f,rad} = \sigma e_f A_f (T_{local,i}^4 - T_i^4)$

Inter particle and amid fluid heat transfer elaborately can be portrayed by the CFD approach with combination of the DEM. Figure 2.11 shows the evolution of temperature of a fluidized bed at various operating conditions.

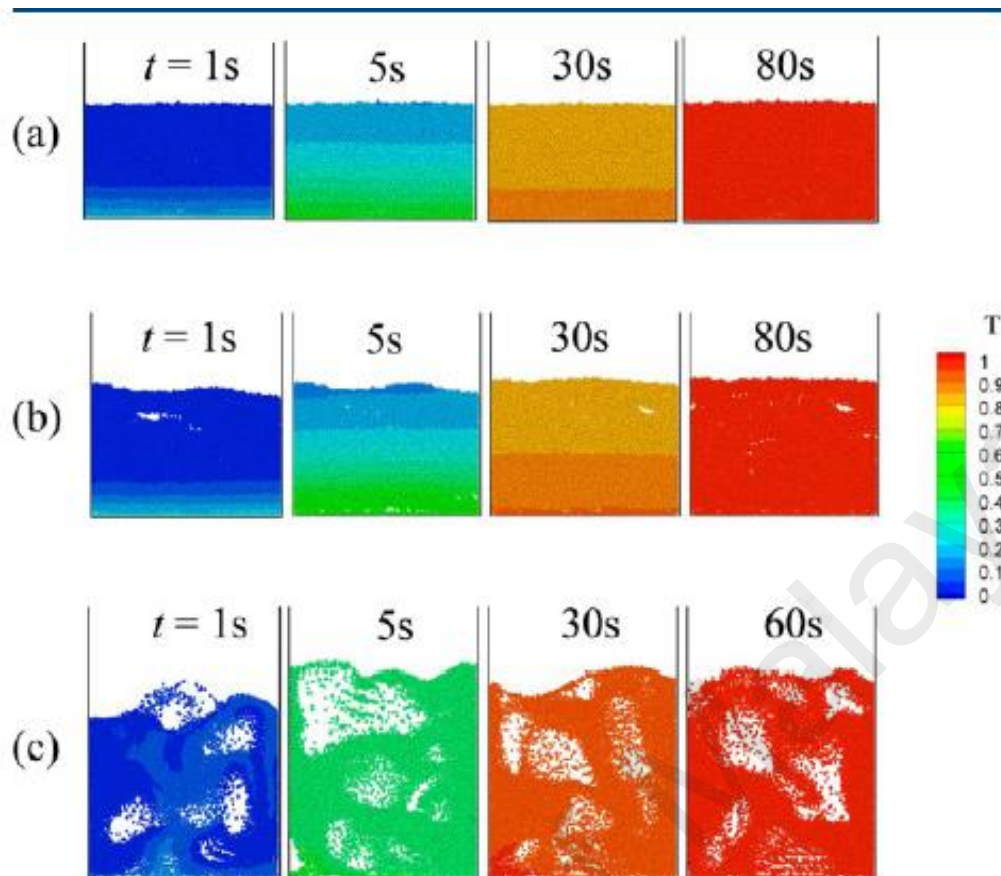


**Figure 2.11:** Snapshots showing the heating process of particles by hot air uniformly injected at the bed bottom in different flow regimes: (a) fixed bed ( $u_f/u_{mf} = 0.5$ ); (b) expanded bed ( $u_f/u_{mf} = 1.4$ ); and (c) fluidized bed ( $u_f/u_{mf} = 6.0$ ). Particles are colored by their dimensionless temperatures. The dimensionless temperature  $T$  of individual particles is obtained according to  $(T_i - T_0)/(T_{in} - T_0)$ , where  $T_0$  is the initial bed temperature and  $T_{in}$  is the air temperature at the inlet. Reproduced with permission from ACS (Hou et al., 2012).

It can be seen in this figure that temperature of the bed increases as the hot gas flows upward. At the initial stage of heating, no considerable transform of bed structure is detected when  $u_f < u_{mf}$  (Figure 2.11a). When  $u_{mf} < u_f < u_{mb}$ , the bed is transformed from a fixed bed to a static expanded bed (Figure 2.11b). A small change can be noticed in the expanded bed frame-up during the heating process. Alteration of gas properties, which depend on local temperature and forces acting on particles, is the cause of this change. Particles move faster in the fluidized bed when  $u_f > u_{mb}$  and rapid and homogeneous heating can be noticed (Figure 2.11c). Consequently, rapid heat transfer occurs between fluid and particles, thus, the bed temperature increases rapidly.

## 2.8 Electrostatic modeling of polymerization

Regular collision between particles is frequent in fluidization. Therefore, generating electrostatic charge is unavoidable in fluidized bed of nonconducting materials. In the olefin polymerization process, finding particles sticking to the wall, also recognized as wall sheeting, is very common. The wall sheeting also causes formation of large aggregated particles and alteration of the hydrodynamics (Hendrickson et al., 2006). Solids circulation and fines entrainment are also affected by electrostatics. Electric charge in polymer particles is produced by particle–particle and particle–wall contacts as well as gas–solid friction. The polymerization reaction is exothermic and wall sheeting causes a decrease in the heat dissipation. As a result, solids attached to the wall become molten and form sheets. Consequently, electrostatic charge minimization in industrial scale fluidized bed reactors is required for which injection of antistatic chemical agents to fluidized beds can be suggested (Salama et al., 2013; Yao et al., 2002). However, controlling the dose of the antistatic agent is vital since an excessive dose can affect the catalyst activity. It has been reported that the charge dissipation occurs due to increasing the relative humidity in the fluidizing system. Addition of fine particles to large dielectric particles can neutralize the electric charge of the system (Boland & Geldart, 1972).

It has been proven that the fines particles are largely positively charged, whereas large particles and the system wall are mostly negative in nature (Giffin & Mehrani, 2010). As a result, fine particles adhere to the wall due to their positive charge. Griffin et al. (Giffin & Mehrani, 2010) and Sowinski et al. (Sowinski et al., 2010) conducted experiments in fluidized beds packed with polyethylene particles and measured charges of particles by the Faraday cup. Some researchers found that certain the electrostatic

charge in a fluidized bed may increase by increasing the static bed height and the gas velocity since solids motion and rate of solids collision are affected by these two parameters. In a fluidized bed of polymer, the electrostatic charge increases as the temperature is increased which directs particle for agglomeration (Fang et al., 2008; Tiyaiboonchaiya et al., 2012). As agglomerate formation is a cause of extra overhead cost in polymer production, it is essential to recognize the charge arrangement, dissipation progression and entrainment to manage electrostatic effects. Numerous research projects have been conducted from industrial and academic point of view on the effect of electrostatic forces in fluidized beds, especially in fluidized polymerization reactors. Significant amount of entrainment was observed in the neutral bed while in a fluidized bed of fine polymer, elutriation was decreases in gas phase polyethylene production. Adhesion of fine particles to larger particles forms a polymer layer on the reactor wall due to slow entrainment (Briens et al., 1992). Failure to control electrostatic charge may also cause wall fouling in fluidized bed polymer reactor. Wall fouling may take place just above the bed surface on the reactor wall which is caused by induction charging and deposits (Sharmene et al., 1998). Desired fluidization achieved by boosting the scale of electrification with the rise of system pressure and temperature (Moughrabiah et al., 2008). The scheme of the charging mechanism and transport is shown in Figure 2.12.

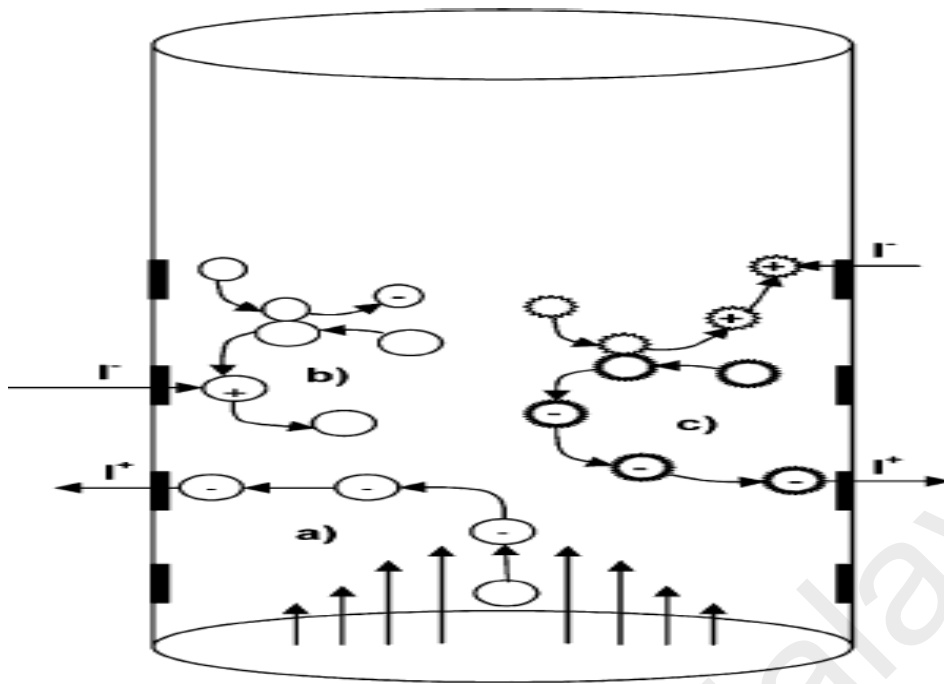


**Figure 2.12:** Scheme of the electric charge transporting process during the fluidization: (a) occurred charging via particle–gas friction, (b) occurred charging via smooth and purities particle–particle contact, and (c) occurred charging via roughness and impurities particle–particle contact. Reproduced with permission from ACS (Tiyapiboonchaiya et al., 2012).

Desired fluidization state can be achieved by boosting the scale of electrification with the rise of system pressure and temperature. From the above discussion, it is clear that the modeling of electrostatics in gas–solid fluidized beds, particularly in the polymerization process, is extremely important. Therefore, some researchers have focused on incorporating electrostatic phenomena in modeling of gas–solid fluidized beds by either Eulerian–Lagrangian or Eulerian–Eulerian approach which are especially suitable for fluidized bed catalytic polymerization reactor. Al-Adel et al. (Al-Adel et al., 2002) studied gas–particle flow by fixing the charge for the entire particles and neglecting hydrodynamic segregation in the riser fluidized bed. They carried out two fluid modeling and simulations to explain the effect of electric field on size and shape of bubbles considering fixed charge on particles. The electrostatic model combined with the multi-fluid CFD code for studying the polydispersity by computing electric field at each grid point and time step was proposed by Rokkam et al. (Rokkam et al., 2010)

where the QMOM was applied for relating it to the distribution of polymer particle size. The particle charge is a function of its size and is considered as an input to the electrostatic model whereas charge dissipation and charge generation are not usually considered for this type of CFD modeling (Shih et al., 1987).

Lim et al. (Lim et al., 2006) numerically studied pneumatic transport of granular materials through inclined and vertical pipes in the presence of an electrostatic field using a coupled DEM-CFD technique and a simple electrostatic field model. They showed that in the presence of a mild electrostatic field, reversed flow of particles can be found in the dense region close to the bottom wall of the inclined conveying pipe and forward flow in a more dilute region in the region above. At sufficiently strong electrostatic field, complete backflow of solids in the inclined pipe may occur and applying a higher inlet gas velocity is necessary to maintain a net positive flow along the pipe. Hassani et al. (Hassani et al., 2013) added inter-particle electrostatic forces among charged particles and between charged particles and the wall to their 3D DEM-CFD code. They investigated effects of electrostatic forces on hydrodynamics of fluidization in terms of bubble behavior, probability distribution of porosity, solids diffusivity and solids circulation in beds filled with mono-charged and bipolar-charged particles. They explored the effect of existence of mono-charged particles on bubble properties by comparing fluidized bed with and without charged particles. Their results are shown in Figure 2.13 which demonstrates that by increasing the charge of particles, a significant change in the bed hydrodynamics should be expected. Bubbles become smaller and the sharp interface between emulsion and bubble phases vanishes when charge of particles increases from 0 to 30 pC due to the effect of repulsive forces between charged particles in the emulsion phase.



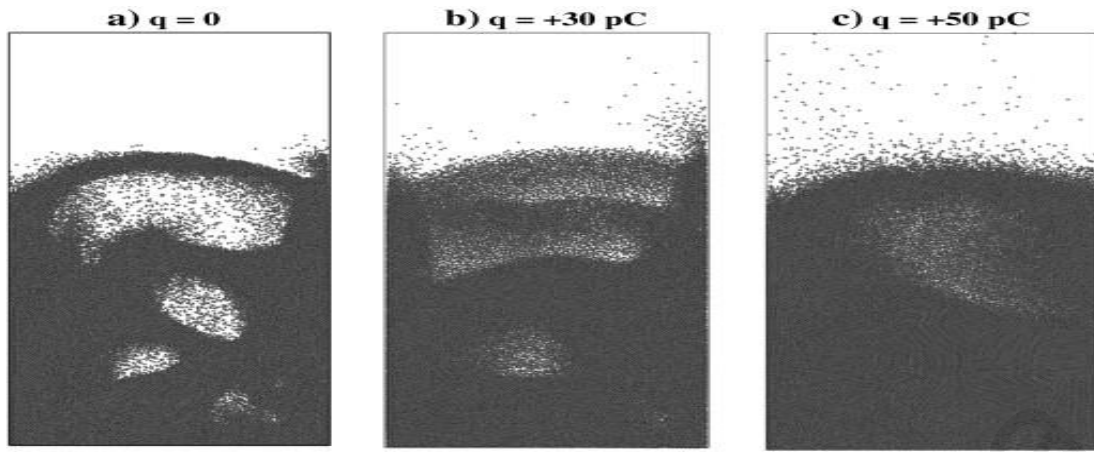


**Figure 2.13:** Effect of particle charge (mono-charged) on the bubble hydrodynamics in the bed at  $U_0 = 1.2$  m/s . Reproduced with permission from Elsevier. (Hassani et al., 2013)

Prediction of hot spots, chemical reactor modeling, polymer particle size distribution and variation of reactor temperature have also been carried out by the Eulerian–Eulerian approach combined with the QMOM (Fan, 2007). Multiphase CFD model, based on the Eulerian–Eulerian approach, can be used for describing segregation of polymer particles caused by charge and/or size. ANSYS FLUENT 6.3 provides options for electrostatic modeling and verification. A set of equations should be introduced for describing of electrostatic effects in the CFD study of fluidized bed polymerization reactors which can be solved by the user defined scalar (UDS) in ANSYS FLUENT 6.3 and onward versions. The UDS for a multiphase system in ANSYS FLUENT is in the form (Rokkam et al., 2010):

$$\frac{\partial(\epsilon_g \rho_g \phi)}{\partial t} + \nabla \cdot (\epsilon_g \rho_g \mu_g \phi - \epsilon_g \Gamma_g \nabla \phi) = S_g \quad (2.43)$$

This Poisson equation is coupled with the multi-fluid CFD model through the volume fractions of the gas and solid phases, thus, must be solved at every time step during the simulation. Gauss's law was used to evaluating the force acting on a charged particle in the gas–solid flow. This law in the differential form is:

$$\nabla \cdot D_v = \rho \quad (2.44)$$

The relationship between the electric displacement and the electric field is:

$$D_v = \epsilon_0 E + P \quad (2.45)$$

The following constitutive relation was used to relate the induced polarization and electric field for an isotropic medium:

$$P = \epsilon_0 \chi_e E \quad (2.46)$$

where  $\chi_e$  is the electric susceptibility of the medium. The value of  $1 + \chi_e$  is the relative permittivity which can be measured and its value can be found in literature (Rokkam et al., 2010). The electric field is related to the charge density as follows:

$$\nabla \cdot \epsilon_m \epsilon_0 E = \rho \quad (2.47)$$

The relative permittivity  $\epsilon_m$  for a gas–solid mixture can be obtained from the Bruggeman equation :

$$\epsilon_g = \left( \frac{\epsilon_s - \epsilon_m}{\epsilon_s - \epsilon_g} \right) \left( \frac{\epsilon_g}{\epsilon_m} \right)^{\frac{1}{3}} \quad (2.48)$$

Finding out the location of the density electrostatic forces in the reaction system is very important. The electric field in radial and axial directions in a reactor is shown in Figure 2.14.

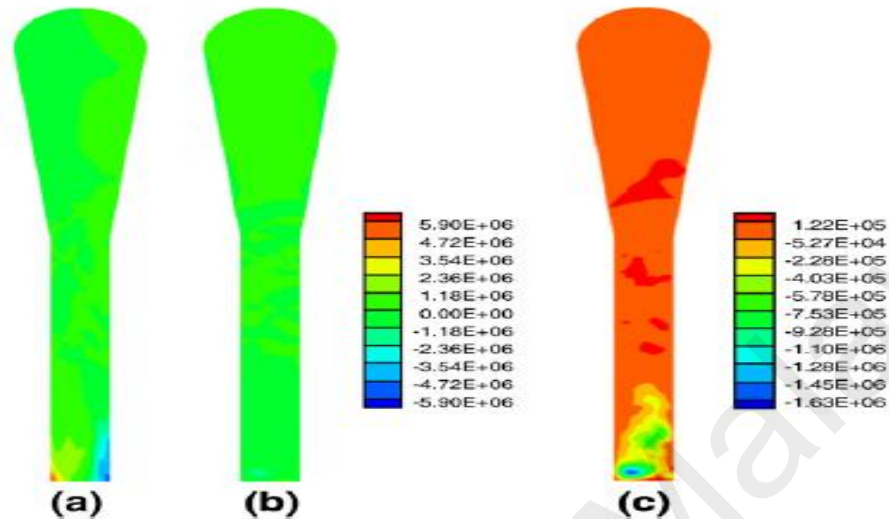


**Figure 2.14:** Instantaneous contours of electric field for two-dimensional simulation of pilot plant fluidized-bed reactor for standard deviation=0.01 at  $t=129.5$  s: (a) radial direction, (b) axial direction (same scale), (c) axial direction (reduced scale) Reproduced with permission from Elsevier (Rokkam et al., 2010).

Highly dense electric field can be founded close to the wall and near the distributor plate. The electric potential gradient seems to be greater in the radial direction compared than in the axial direction. As mentioned earlier, fine particles are attracted toward walls of the reactor by the electrostatic forces. It is clear in Figure 2.14 that the strongest electric field effect is located in the axial direction close to the distributor plate.

Fouling of the reactor wall due to electrostatic charges was analyzed through CFD modeling in the industrial scale by Sowinski et al. (Sowinski et al. 2012). They argued that smaller particles create more wall fouling as they posses higher charge. Particle sizes from  $600$  to  $710 \mu\text{m}$  show an affinity to stick to the column wall. At high gas velocity, there is a tendency for particles to either adhere to the column wall or to be

dislodged with the tapping of the column and remain within the dropped particles by the influence of the quantity of generated electrostatic charge inside the fluidized bed.

Since interaction of particles is highly influenced by the electrostatics and the hydrodynamics is directly related to the particle interaction, it is important to figure out how to control the electrostatic potential distribution in a gas–solid fluidized bed (Liao et al., 2011; Sowinski et al., 2009). The electrostatic effect makes the particles to form coherent structures and reminds one of the continuous behavior of the liquid. Figure 2.15 shows the electrostatic effect on the particles in a quasi-2D fluidized bed.

University of Malaya

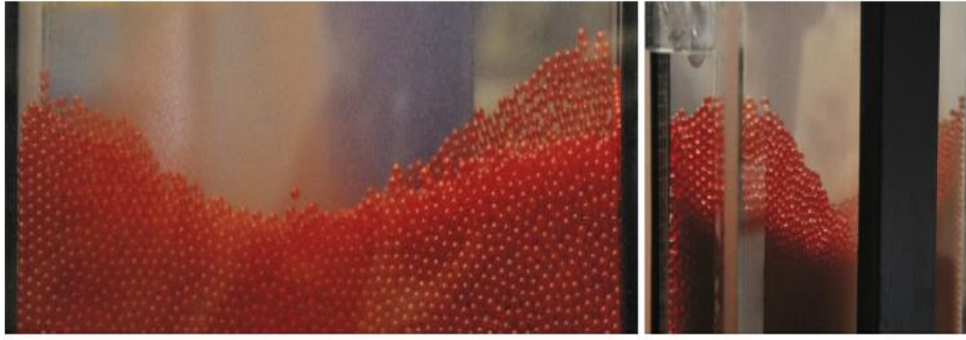


**Figure 2.15:** Electrostatic effects on the particles in a quasi-2D fluidized bed. Reproduced with permission from Elsevier. (Jalalinejad et al., 2012)

The degree of electrostatic effect can be clearly recognized in this figure, where the electrostatic effect can be clearly observed in the measurement, the particles form coherent structures and exhibits liquid like behavior . Zhou et al. (Zhou et al., 2013) also found different flow patterns inside the fluidized bed when considering electrostatic field distribution where tuning of gas velocity for individual zone and adjustment of gas bubbling and particle motion usually is reformed.

## **2.9 Modeling of agglomeration in fluidized bed reactors**

Occurrence of agglomeration is one of the most important technical difficulties in industrial fluidized polymerization reactors. Among different adhesive forces (including liquid bridging force, van der Waals force and solid bridging force), agglomeration of polymer particles in fluidized bed reactors is usually caused by solid bridge force at high temperatures. Therefore, a sufficient knowledge of agglomeration and related phenomena, such as segregation, is vital for studying fluidized beds reactors. Experiments in these systems are tedious and expensive while numerical simulation provides a powerful tool for investigating the agglomeration phenomenon. A variety of modeling tools, such as population balance in the Eulerian framework and DEM in the Lagrangian framework, have been used to predict the dynamic evolution of particle size distribution in fluidized bed reactors. Population balance was utilized to simulate the

particle size distribution by many researches (Ashrafi et al., 2012; Ashrafi et al., 2008; Chen et al., 2011; Rabinovich & Kalman, 2011; Yan et al., 2012; Yan et al., 2012). The DEM was addressed in a number of previous studies to simulate the agglomeration phenomenon. Mikami et al. (Mikami et al., 1998) developed a model for wet powder fluidization. To take into account the liquid bridge force between particles, a regression expression for the liquid bridge force was developed as a function of dimensionless liquid bridge volume and the separation distance based on numerical solutions of the Laplace-Young equation. Fluidization behavior of wet particles is completely different from that of dry particles and the minimum fluidization velocity, the bed voidage and pressure fluctuations in a wet fluidized bed are higher than those in a dry fluidized bed. Kuwagi et al. (Kuwagi & Horio, 2002) developed a two-dimensional DEM to study the mechanism of fine particles agglomeration in which van der Waals interaction was taken into account as the cohesive force. They showed that agglomerates are formed in the bubble wake region while they break in the upper region of bubbles. Wet granulation processes were conducted in a rotating drum with the DEM approach by Mishra et al. (Mishra et al., 2002). By applying this technique, steady state size distribution of agglomerates was obtained. Gröger et al. (Gröger et al., 2003) performed a cohesive DEM to investigate the internal tensile strength and shear strength. Inter-particle cohesion was taken into account by modeling the liquid bridge. Their results showed that the surface roughness has a great influence on the stresses in wet particle systems.

A mechanistic study of de-fluidization based on the DEM-CFD simulation was conducted by Wang and Rhodes (Wang & Rhodes, 2004). They applied an artificial cohesive force between particles and investigated effect of a wide range of inter-particle forces as well as mobility of individual particles on the fluidization condition of the bed.

They found that transition from free-bubbling to de-fluidization state by increasing the inter particle force is gradual and de-fluidization occurs more gradually at higher excess velocities. A mathematical model based on the DEM was developed by Limtrakul et al. (Limtrakul et al., 2007) to simulate the hydrodynamics of a vibrated fluidized bed. Effects of vibration, particle type, amplitude and frequency of vibration and superficial gas velocity on improvement of fluidization quality were studied in their work. Their results showed that the fluidization state can be observed by enough total forces of vibration and fluid provided to the particles. Yang et al. (Yang et al., 2008) presented a numerical study based on the DEM in which the agglomeration of fine particles was considered with van der Waals attraction. Agglomerate structure, packing density, coordination number and tensile strength were analyzed with particular reference to the effect of particle size associated with the van der Waals attraction. Their results showed that the spherically formed agglomerates were not homogenous, but had the packing density and coordination number decaying exponentially with the agglomerate radius. Li et al. ( Li et al., 2011) reviewed recent advancement of the DEM technique in adhesive particulate flows and compared the DEM approach with other similar Lagrangian methods.

Although many reports exist on simulating the agglomerating phenomenon in fluidized beds by evaluating the cohesive force between particles through liquid bridging and interaction of particles with van der Waals force, a few reports exist on simulation of the whole mechanism of agglomeration in fluidized beds at high temperature. Kuwagi et al. (Kuwagi & Horio, 2002) developed a model for metallic solid bridging by the surface diffusion mechanism, including the effect of surface roughness, by the DEM-CFD technique in a fluidized bed with uniform temperature distribution. They described the agglomeration process of particles and observed a decrease in the pressure

fluctuations. Mansourpour et al. (Mansourpour et al., 2013) proposed a model to improve the simulation of agglomeration process at high temperature compared to previous models. They used a DEM-CFD approach in which agglomerates were tracked as real objects and their translational and rotational motions were calculated according to the multi-sphere method. In simulations of Mansourpour et al. (Mansourpour et al. 2011), particles stick together and form agglomerates with an irregular shape, instead of clusters of primary particles as defined in previous researches. Their model included the energy balance equations for both gas and particles in order to consider the effect of temperature distribution on the agglomeration phenomenon. The cohesive force employed by Mansourpour et al. (Mansourpour et al., 2013) was based on a time dependent model, developed for solid bridging by the viscous flow. The surface of the particle becomes sticky when its temperature increases to a value greater than the softening point. Colliding particles with sticky surfaces join together and form larger agglomerates by forming permanent solid bridges. Applying these improvements resulted in gradually de-fluidization of the bed in simulations of Mansourpour et al. (Mansourpour et al. 2011).

Figure 2.16 illustrates snapshots of agglomerate formation in a fluidized bed of polyethylene particles (Mansourpour et al., 2013). The agglomerates are colored according to the number of particles in agglomerates. This figure demonstrates gradual defluidization of the bed by the progress of agglomeration of particles. At early stages of fluidization ( $t = 1$  sec.), agglomerates have not been formed and the bed is completely fluidized. Formation of bubbles at the distributor, their rise and grow through the bed and their burst at the bed surface can be seen in this figure.



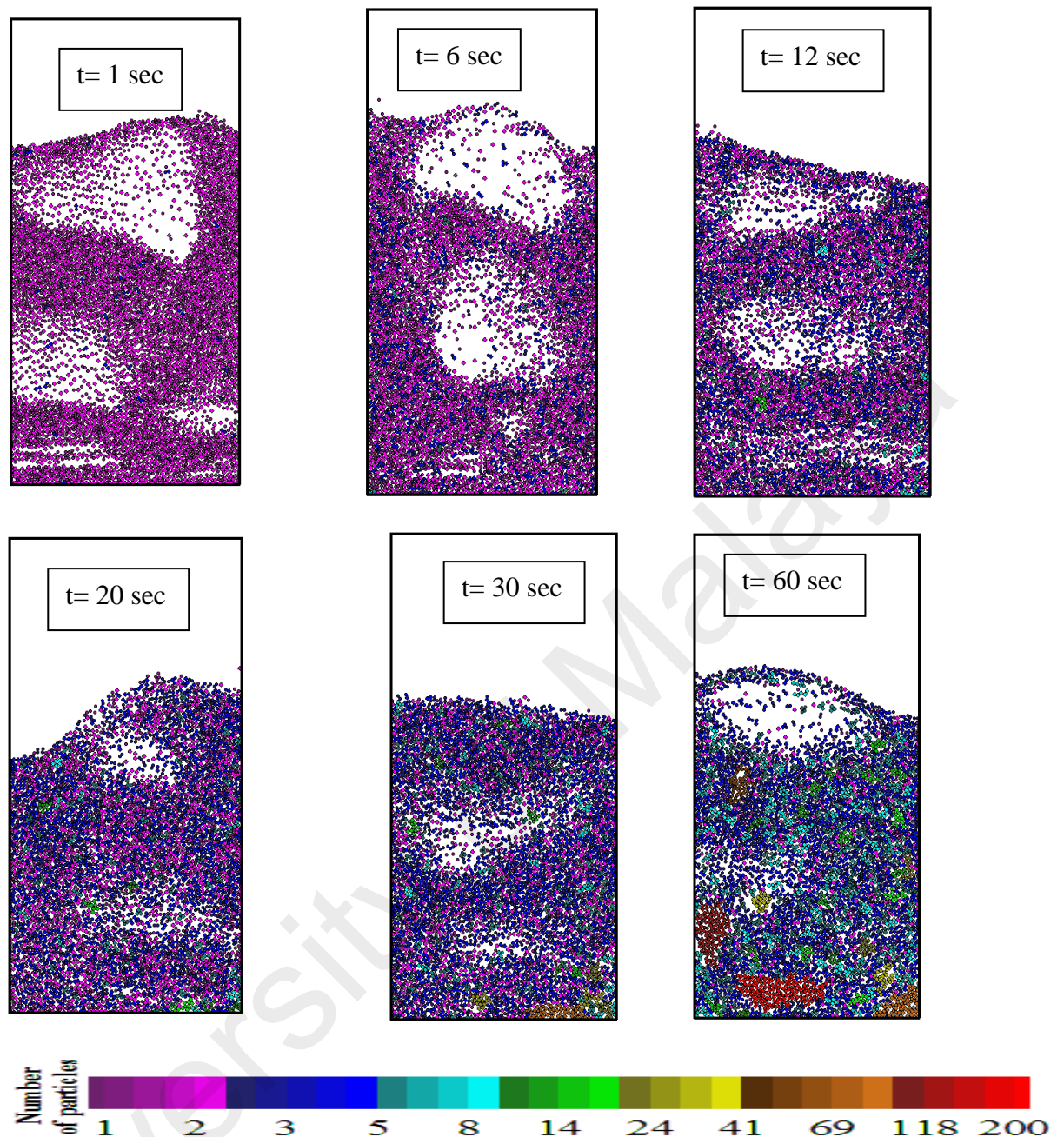


**Figure 2.16:** The snapshots of agglomerate formation in the bed. Reproduced with permission from John Wiley and Sons (Mansourpour et al., 2013).

After elapsing 6 seconds of fluidization, small agglomerates (containing two or three particles) are formed in the dense regions as well as the vicinity of the distributor. Increasing the number of agglomerates in the bed boosts the possibility of particle-agglomerate and agglomerate-agglomerate contacts. When these agglomerates grow in size, their movement becomes more restricted. Consequently, bed expansion and size if

bubbles are reduced ( $t = 20$  sec.). In this situation, the gas passing through the bed cannot exert enough drag force on the agglomerates to compensate their weight. On the other hand, large agglomerates hinder the movement of smaller species in the bed. Therefore, the majority of the gas injected to the bed passes through the channels formed by agglomerates. It can be seen in Figure 2.16 that at  $\sim 60$  sec., massive agglomerates are accumulated at the bottom and a de-fluidized layer is formed on the distributor. Nevertheless, in this situation particles and agglomerates at a higher level are still fluidized and the height at which bubbles are formed is shifted to the top of the de-fluidized layer. De-fluidization due to agglomeration occurs as a consequence of two different mechanisms: agglomeration and segregation. Formation of large agglomerates which have minimum fluidization velocities higher than the gas velocity leads to accumulation of a large fraction of agglomerates at the bottom of the bed. This is likely to be the cause of beginning of segregation with worsening the fluidization quality and eventually occurrence of de-fluidized zones at the bottom of the bed. It is worth noting that the agglomeration is probably promoted by a reduction in momentum of particles which is a result of segregation. Moreover, segregation influences the hydrodynamics of the fluidized bed as it influences the bubble characteristics.

In order to gain more insight in the effects of segregation on the fluidization behavior, several numerical investigations based on the CFD concepts were conducted. Dahl and Hrenya (Dahl & Hrenya, 2005) investigated segregation of particles with Gaussian and log-normal size distributions by the DEM technique. Annaland et al. (Annaland et al., 2009) calculated the rate of particle segregation in a bi-disperse freely bubbling fluidized bed with both a novel multi-fluid model (MFM) based on the KTGF for multi-component mixtures and the DEM. The granular temperature of the segregating system, as calculated with the MFM, agrees reasonably well with the granular temperature

found in the DEM simulation. Fan and Fox (Fan & Fox, 2008) integrated the direct QMOM into the multi-fluid model to represent the PSD with a finite number of nodes in MFI-X. They compared their simulation results with results of Dahl and Hrenya (Dahl & Hrenya, 2005) and showed that the multi-fluid model can capture occurrence of segregation along the bed height while this model cannot detect horizontal segregation. Tagami et al. (Tagami et al., 2009) used CFD–DEM to investigate the fluidization behavior of binary and ternary mixtures. They indicated that momentum transfer is enhanced when the size ratio of particles is increased in polydispersed systems. It was also shown that a wide size distribution enhances bubble growth and rise velocity of bubbles through the bed. Norouzi et al. (Norouzi et al., 2012) conducted a numerical study for investigating size segregation of particles in the presence of fines in a bubbling gas–solid fluidized bed based on the DEM technique. They investigated the effect of adding fines at different concentrations and with various sizes and showed that segregation is enhanced by adding fine particles. Furthermore, reducing the size of fines initially enhances the final extent of segregation while further decrease in size of fines diminishes the segregation.

## 2.10 Summary

The incredible advancement in the computer hardware engineering, upshot in boosted memory with capability of high performance computing workstations, has facilitated solving equations of momentum, heat and mass transfer with a wide range of numerical methods. These progresses inspired the beginning of more practical numerical techniques resulting the arrangement of a sequence of CFD codes. Due to the well-built accomplishment achievement in single phase flow simulation, CFD is regarded as a significantly promising tool for modeling multiphase flow. Nevertheless, CFD is still being considered at the level of verification and validation for modeling multiphase flows for modeling multiphase flow systems such as fluidized beds and more progress concerning the flow dynamics and computational models are needed to make it a standard tool in designing large scale industrial reactors. The up to date issues in the CFD modeling and its applications in fluidized bed of olefin polymerization system design and various reaction parameters have been shown in this study. The hydrodynamic behavior in fluidized beds was found to be non-linear and complex as well. It was shown that conventional mathematical modeling and hypothesis of these hydrodynamic are not convenient enough for pilot to large industrial-scale reactors. The cost effectiveness and prompt solution capability have made the CFD approach as the best choice option for researchers and industrial users. Therefore, CFD models seem to be properly fitted to scale up the full-scale reactor with detailed reaction mechanism. Availability of wide-ranging and multipurpose CFD commercial softwares has the proven track record to fulfill the requirements of giving details on complete fluidization factors. These are adequate to put up to any kind of analysis condition from prediction of fluid flow behavior, mixing effect, bubble phenomena, mass and momentum incident, inter-particle charging and so on to integrated reactor design and optimization. Among these softwares, ANSYS FLUENT has been most widely employed for

simulating fluidized bed polymerization reactors, reaction mechanism and production optimization studies. Moreover, CFD simulation of a bubbling fluidized bed reactor has been carried out by several research groups who also included the chemical kinetics, bed dimensions and bubble formation confrontations into multiphase fluid dynamics. The axisymmetric of the reactor has given way to chaotic transient generation of bubble formation within certain time durations. Exothermic nature of the polymerization reaction causes heat transfer problems in particle-particle interactions and requires a full scale modeling approach. More detailed CFD investigations can provide results about the effect of gas temperature and particle size on gas-solid heat transfer and bed hydrodynamics. A more clear understanding of effect of electrostatic charge on polymeric systems through a numerical implementation can be carried out in ANSYS FLUENT. CFD modeling is more feasible to obtain criteria for regulating the distribution of electrostatic potential by changing and observing its effect on the hydrodynamics of the gas–solid fluidized bed. Using porous media models for simulating the gas phase catalytic reaction through a multi-phase reacting system is common in mathematical modeling of such reactors. These models can be modified based on the scale and requirements of the simulation as well as the accuracy associated with their numerical implementation. It was also pointed out in this review that there is still a gap between experimental and CFD results in pilot and industrial scale systems. Experimental validations are extremely necessary to ensure that CFD simulations are more than just theoretical exercises. In the recent years, some studies have been carried both in the laboratory, closely resembling that in the industry . New technologies, such as particle image velocimetry, have also shown to provide valuable data for validating CFD predictions. Nevertheless, successful validation has been reported in many cases and even where there are discrepancies, deficiencies in the model or measurement technique were readily identifiable.

## **CHAPTER 3: POLYPROPYLENE PRODUCTION OPTIMIZATION IN FLUIDIZED BED CATALYTIC REACTOR (FBCR): STATISTICAL MODELING AND PILOT SCALE EXPERIMENTAL VALIDATION**

### **3.1 Introduction**

Polypropylene is a type of thermoplastic polymer resin and a superior quality polymer material that originates from olefins (Galli & Vecellio, 2004; Tian et al., 2013). Polypropylene and its composites have been given priority over all other polymers by engineers due to its diversified applications (Arencón & Velasco, 2009) from household stuffs to a wide range of industrial appliances (Bikiaris, 2010), as structural plastic or a fiber-type plastic. A number of conventional materials like steel, aluminum wood etc. have also been replaced by polypropylene and its composites since its superior physical and chemical properties such as its light weight, sophisticated structural stability, greater dielectric vitality, better mechanical strength, corrosion resistance capability and flexibility are better than these traditional materials (Glaß et al., 2013; Kennedy & Knill, 1994). However, Polypropylene and its composites hold only 20% share over the gross world polyolefin production (Balow, 2003) and hence an optimization study on polypropylene production is important from a scientific and economical point of view to enhance its usages and to improve its share of the market. For its production, fluidization is considered as a well-established technology used in most cases. The capability to carry out a variety of chemical reactions, homogeneous particle mixing and extra ordinary mass and heat transfer characteristics are some of the major advantages of using Fluidized Bed Catalytic Reactors (FBCR) in industrial scale polypropylene production. Furthermore, the gas phase fluidization process has been recognized as an environmental friendly and convenient technology by a number of researchers (Lesage et al., 2012; Luo et al., 2009; Martinez et al., 2010). Very important operating

conditions like temperature, pressure and composition can influence significantly the process of polymer fluidization and these operating conditions are necessarily to be controlled to produce different grades of polyolefin (Kumar et al., 2000; Prasetya et al., 1999). Being an exothermic reaction, propylene polymerization generates heat when the reaction starts which principally influences the other operating factors and product quality. As a result of these mechanisms, proper process modeling to cater to these complicated reactions, hydrodynamic aspects as well as mass and heat transfer in the fluidized bed reactor, is necessary to engage engineers and scientists to design technically efficient and operationally feasible reactors for these facilities (Jang et al., 2010; Li et al., 2010; Khan et al., 2014). Furthermore, the optimization of these operating parameters also requires functional relationship among the process variables through available process modeling techniques.

A classical model for chemical engineering process which comprises chemical kinetics, physical property interactions, mass and energy balances is made up of a number of differential as well as algebraic equations for both dynamic and steady state processes. (Jarullah et al., 2012; Villarreal et al., 2013). Some researchers considered the polyolefin reactor as a well-mixed reactor and just proposed a purely mathematical model where the temperature and monomer concentration in the reactor were calculated (McAuley et al., 1994; Shamiri et al., 2010; Xie et al., 1994). On the basis of a mixing cell framework a comprehensive mathematical model has also been proposed for simulation of transient behavior of a fluidized bed polypropylene reactor by using steady state population balance equation coupled with the proposed dynamic model along with incorporating multisite polymerization kinetics of multi-monomer (Harshe et al., 2004). Ibrehem et al. (Ibrehem et al., 2009) recently proposed that emulsion and solid phases are the stages where polymerization reactions take place during fluidization

and reports that alteration of catalyst particles with different porosity affects the rate of reaction and hence the model has been obtained taking these effects into consideration. However, all these models generally take into account partial assumptions on reaction rates which do not cover all reaction conditions and circumstances and are normally not validated experimentally. Furthermore, it is also challenging to formulate precise mathematical models to take all these operation and design aspects under consideration for such a complex polymerization process (Sassi & Mujtaba, 2013).

Another feasible modeling approach is through statistical techniques that have been applied with the purpose to predict the optimum operating conditions in chemical processes to obtain the highest yield of desired product by a number of researchers (Basiri et al., 2013; Gonzalez et al., 2011; Hafizi, Ahmadpour, Koolivand et al., 2013). In fact, Response surface methodology (RSM) has been described as a very functional statistical tool for determination of optimum processes parameters both for lab scale to industrial scale, as highlighted by various workers (Kukreja et al., 2002; Rajković et al., 2013; Srivastava et al., 2002). RSM covers experimental design, process optimization and empirical modeling where targeted response may fluctuate by numerous process variables (termed factors). RSM is principally appropriate for problems where the explanation of the process mechanism is inadequate and difficult to be characterized by first-principles mathematical model. Being contingent on definite objectives in reality, these RSM methods generally vary in the experimental design system, the selection of appropriate models and the mathematical equations of the optimization problem. Thus a precise design of experiment (DoE) is vital for a prolific experimental study (Shuaeib et al., 2007). The classical factorial and central composite designs can be utilized to investigate the interactions of process factors depending upon the polynomial models obtained in this method.



However, from literature studies, no work has been reported so far for the optimization of process variables of propylene polymerization in a fluidized bed catalytic reactor (FBCR) by applying these statistical modeling techniques. Also very few works have been reported to study a pilot scale catalytic reactor although this is extremely important for predicting and validating the set of appropriate significant process variables and parameters for industrial use (Ibrehem et al., 2009; Shamiri et al., 2011; Shamiri et al., 2010). Hence, the objective of our work is to investigate the relationship among various operating parameters and to find out the optimum process parameters for propylene polymerization in a pilot scale fluidized bed using RSM modeling and Central Composite Design(CCD) technique. This novel pilot plant is a prototype of an industrial scale polypropylene production plant which is now in operation under management of the National Petroleum Corporation, Malaysia. Another novelty of our plant is that sampling of the gases in the system was conducted with an online Refinery Gas Analyzer (RGA). This type of real time and sophisticated sampling facilities is globally very rare even in industrial scale set up, although being highly necessary. To the best of our knowledge, this is the first attempt to conduct research on polypropylene production applying RSM for process parameter optimization under various parameter interactions in an original designed FBCR pilot plant.

## **3.2 Experimental Studies**

### **3.2.1 Pilot plant description and operation**

The pilot plant developed in our lab to produce polypropylene consists of a fluidized bed reactor zone and a disengagement zone designed for polymerization purposes which is shown schematically in Figure 3.1 and its 3D figure shown in Figure 3.2. The inner diameter and height of the fluidized bed zone are 10 cm and 150 cm, respectively. The diameter is based upon the capacity of the production and the height of the reactor based on the fluid residence times. The disengagement zone has a diameter of 25 cm and a height of 25 cm. Catalyst particles were injected at 9 cm above the distributor plate located at the feed gas entrance point. In this polymerization reactor, the bubbling fluidized bed operates by the mixed gas fluidization process. Granulated polymer particle was used as the bed material because of its suitable mechanical stability. The operating temperature range in the center of the fluidized bed is maintained at about 70-80 °C. A heater was used to regulate the gas inlet temperature of the reactor for startup condition to reach the required reaction temperature. Unreacted Gas mixture from the top of the reactor is recycled and cooled by a shell and tube heat exchanger. One cyclone and four filters were fitted at the top of the reactor to remove fines entrained from the reactor. A buffer vessel is installed to control the pressure fluctuations in the system.

Propylene, hydrogen and nitrogen are used as the main input gases during the fluidization process which acts as the medium of heat transfer as well as the reactants for the growing polymer particles during polypropylene production in the fluidized bed catalytic reactor. Continuous charging of catalyst and co-catalyst is carried out into the reactor which activates the reactants (propylene and hydrogen) to produce an outspread distribution of polymer particles. The cocatalyst is also used to keep the moisture below

2 ppm while activating the catalyst, which is the requirement for producing industrial grade polypropylene. After the bed has been fluidized, unreacted gases are separated in the disengaging section of the plant. The disengaged gases are recycled and mixed with fresh feed gases consisting of propylene, nitrogen and hydrogen. This gas mixture passes through the heat exchanger in order to remove excess heat and is recycled through the gas distributor. The finished product is collected from the adjacent collection cylinder, whose connecting line is positioned just above the distributor plate. Propylene can be converted to polypropylene as much as 2% to 3% per pass under fluidization conditions while the overall conversion can reach up to 98% (McAuley et al., 1994; Shamiri et al., 2011). The system is designed to run at a maximum pressure of 30 bar.

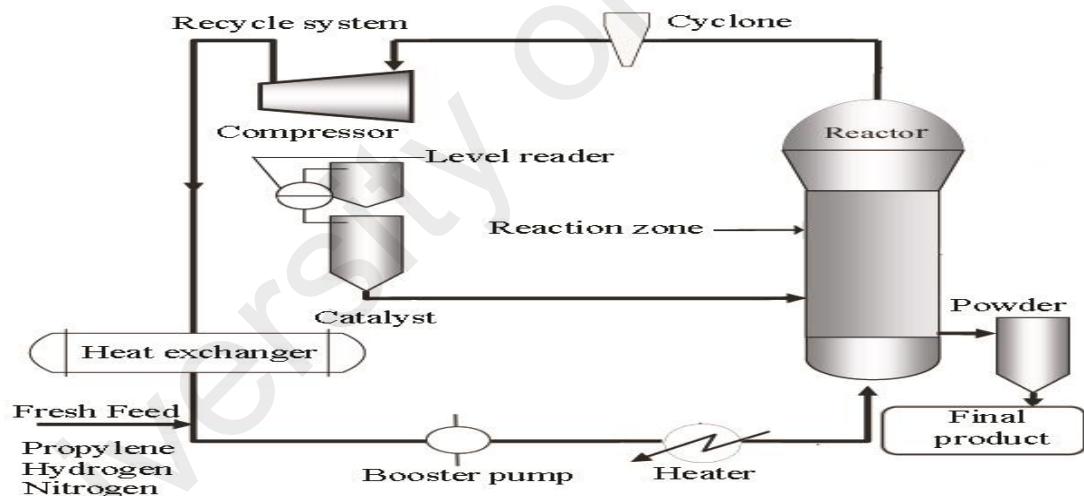


**Figure 3.1:** Schematic diagram of fluidization of the polypropylene production system.

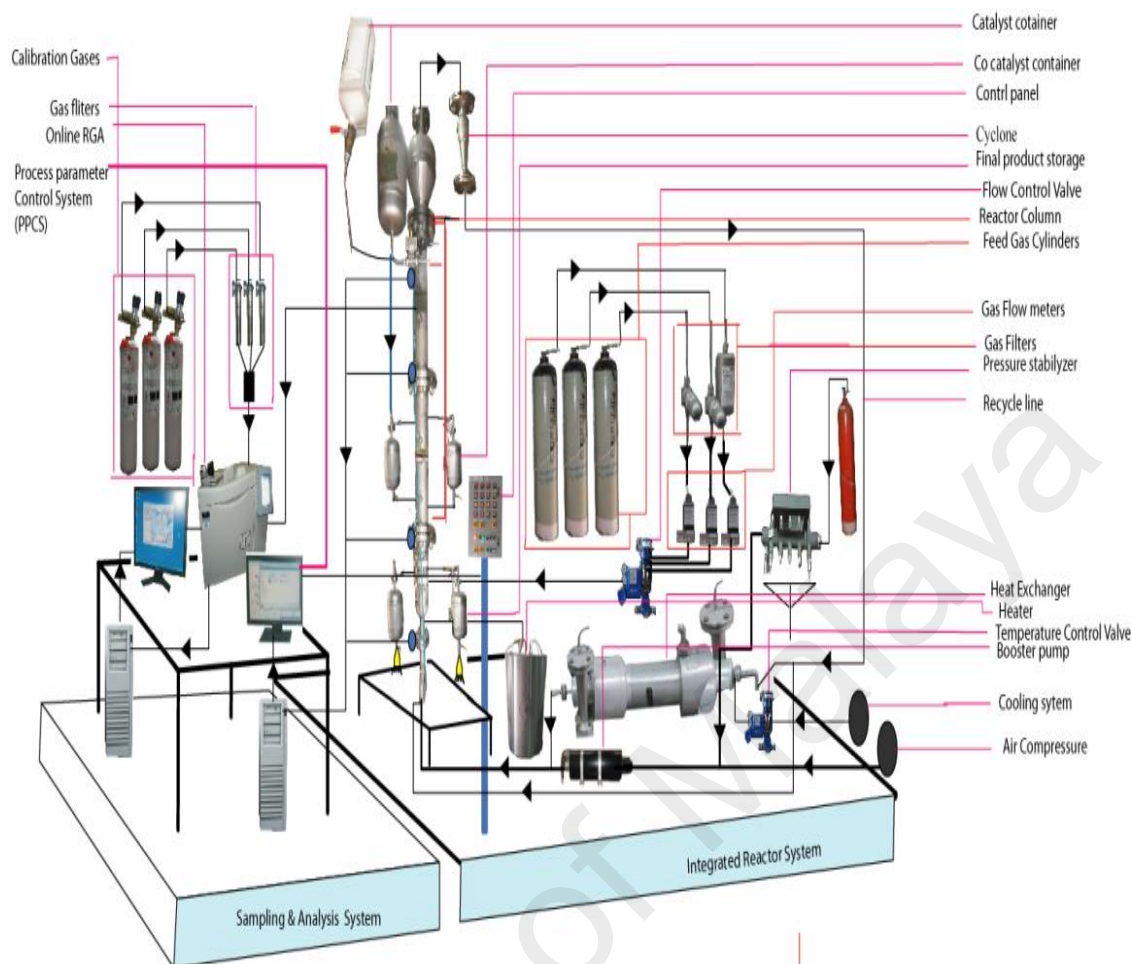


**Figure 3.2:** Detailed experimental set up of a pilot scale fluidized bed catalytic reactor (3D).

### 3.2.2 Pilot plant instrumentation

Temperatures in the reactor were measured at 6 different vertical positions, starting at 16 cm above the distributor plate. A temperature controller is used to control the temperature of this recycled gas entering the reactor. The air driven piston compressor was used to compensate for the pressure drop through the system. A flow meter and control valves were added just before the gas enters the reactor to regulate and measure the flow rate and circulation flow through the reactor system. The flow of catalyst is adjusted by a measuring valve, which revolves at a constant speed and inserts the catalyst into the reactor. Pressure and differential pressure indicators were placed in different points to check the pressure changes in the system and over pressure is avoided by placing a relief valve on the top of the reactor set at 30 bar.

An online integrated Refinery Gas Analyzer (RGA) was used for analyzing the gas composition analysis where wide-ranging automatic data recording devices and measuring equipment were employed in the pilot plant. The gas components consisting of hydrogen, nitrogen and propylene were analyzed online (with accuracy of  $\pm 0.03\%$ ) with a real time Refinery Gas Analyzer (RGA), a device of Perkin Elmer Clarus 580 series. The Gas chromatography engineering software which was developed by Perkin Elmer was used for the gas composition analysis that analyzes the multi component hydrocarbon and light gases. The three channel model in the data acquisition system provides a guaranteed analysis of the compositions of hydrogen, nitrogen, oxygen, carbon monoxide, carbon dioxide and propylene in approximately 8.5 minutes using two thermal conductivity detectors (TCD/TCD) and a flame ionization detector (FID).

### 3.3 Experimental design and optimization:

In this study, the statistical analysis of propylene polymerization was performed using the Stat-Ease software where the CCD (Center Composite Design) is applied to analyze the interactions among the process variables and to identify the optimum process condition (Islam et al., 2007; Setiabudi et al., 2013). After collection of experimental data along with the design procedures, an empirical model was developed according to the RSM procedure. In this work, the polynomial function is to be fitted with the data at the initial stage after which the factor values are identified to optimize the objective function. The accuracy of the polynomial model fitting was determined by the coefficient of determination  $R^2$  and  $R^2_{adj}$  in Eqs. (3.1) and (3.2) correspondingly:

$$R^2 = 1 - \frac{SSQ_{residual}}{SSQ_{mod} + SSQ_{residual}} \quad (3.1)$$

$$R_{adj}^2 = 1 - \frac{SSQ_{residual}/DgF_{residual}}{(SSQ_{mod} + SSQ_{residual})/(DgF_{mod} + DgF_{residual})} \quad (3.2)$$

The performance of the system was evaluated by analyzing the response of percentage of propylene conversion per pass and the following is the mathematical equation related to the composite design i.e.

$$Y = \beta_0 + \sum_{i=1}^k \beta_i \chi_i + \sum_{i=1}^k \beta_{ii} \chi_i^2 + \sum_{i=1}^{k-1} \sum_{j=i+1}^k \beta_{ij} \chi_i \chi_j + \varepsilon \quad (3.3)$$

where,  $Y$  is the response vector, taking into account the main, pure-quadratic, and two-factor interaction effects while  $\varepsilon$  is the error vector. Regression and graphical analysis of the experimental design data and evaluation of the statistical significance of the various equations obtained were carried out in this analysis. The optimum preparation conditions were estimated through regression analysis and three-dimensional response surface plots of the independent variables with each dependent variable. Furthermore, the P-value is considered as a feature to measure the level of significance of all independent variables which at the same time signify the interaction intensity between all independent variables where the smaller P-value indicates the higher level of significance of the related variable.

The consequence of the second-order regression models was tested by the use of ANOVA and F-value analysis. This calculated F-value can be expressed from the following equation:

$$F = \frac{MnS_{RG}}{MnS_{RD}} \quad (3.4)$$

where the meaning of these terms can be referred to the nomenclature.

The *DgF* based F distribution for residual and regression is applied to compute the F-value in the particular point of importance. From these analysis, regression coefficients are obtained based on their significances with respect to the P-value

The coefficient of variation (CV) indicates the extent of error of any model which is measured as the percentage of standard deviation over mean value given as:

$$C.V = \frac{S.D}{mean} \times 100 \quad (3.5)$$

If the CV of a model does not exceed 10%, the model can be rationally regarded as reproducible.

### **3.4 Results and Discussion**

#### **3.4.1 Verification on Statistical Models**

The independent variables considered important in this process are reaction temperature (A), system pressure (B) and hydrogen concentration (C). Reaction temperature refers to the temperature used during the initiation of the polymerization process, while system pressure refers to the required pressure of 20 bar process maintained at the starting point of reaction even though the system can be sustained at 30 bar. The range and coded level of the polymerization process variables studied are listed in Table 3.1. The independent variables were coded to the (-1, 1) interval where the low and high levels were coded as -1 and +1, respectively. According to the CCD, the total number of experiments required to be conducted is 20 runs. The polynomial equations were further used to plot three dimensional (3-D) surfaces and two-dimensional (2-D) contours to visualize the individual and interactive effects of the process factors on the response variables within their predefined ranges.

**Table 3.1:** Coded levels for independent variables used in the experimental design.

Factor	Name	Units	Type	Low Coded	High Coded	Low Actual	High Actual
A	Temperature	°C	Numeric	-1.000	1.000	70.00	80.00
B	Pressure	bar	Numeric	-1.000	1.000	20.00	30.00
C	Hydrogen (%)	%	Numeric	-1.000	1.000	2.00	10.00

Batch experiments for 20 runs with different combinations of the process variables were carried out in the experiments. The percentage of polypropylene production was considered as the response. The proposed combination parameters for the experimental design and consequent results of the response using CCD are listed in Table 3.2. The Mean Square Error ( $MnS_{er}$ ) of the center point is 0.00005, which shows the accuracy of the data points taken and justify the use of these data to obtain the model coefficients in Eq 3.7.

Experimental results showed that the polymer conversion ranged from 3.1% to 5.82%. The maximum yield (5.82%) was found under the experimental conditions of A=75°C, B=25 bar and C=2% which shows that for achieving perfect coordination of experimental parameter for propylene conversion, precise optimum process conditions are mandatory to be observed.



**Table 3.2:** Central Composite Design (CCD) experimental design and results of the response surface.

Run	Factor A, Temperature (°C)	Factor B, pressure (bar)	Factor C, Hydrogen (%)	Response, Y, Polymer conversion (%) (Experimental result)
1	70	20	10	3.10
2	70	20	2	5.20
3	75	20	6	4.53
4	80	20	10	3.32
5	80	20	2	5.40
6	75	25	10	3.86
7	70	25	6	5.00
8	75	25	6	5.20
9	75	25	6	5.20
10	75	25	6	5.21
11	75	25	6	5.20
12	75	25	6	5.21
13	75	25	6	5.19
14	75	25	2	5.82
15	80	25	6	5.10
16	70	30	2	5.38
17	70	30	10	3.10
18	75	30	6	5.00
19	80	30	2	5.68
20	80	30	10	3.57

### 3.4.2. Model Fitting

By the analysis of variance (ANOVA) method, the consequent F-value and P-value analysis were utilized. The summary of the Linear, Quadratic, 2FI (2 Factor Interaction) and Cubic model is shown in Table 3.3. The linear model represents the sequential sum of squares for the linear terms (A, B and C). The 2FI model implies the sequential sum of squares for the two-factor interaction terms (AB, BC and AC). Quadratic model exhibits the sequential sum of squares for the quadratic ( $A^2$ ,  $B^2$  and  $C^2$ .) terms. For all the above models small P-value (Prob>F) indicates that selected model terms can improve the model significance. The F-value is also associated with these models. The larger F-value indicates more of the variance can be explained by the model; a small number says the variance may be more due to noise.

**Table 3.3:** Model selection.

Source	Sum of squares	Degrees of freedom	Mean square	F-value	p-value
Linear	11.39	3	3.80	21.55	<0.0001
2FI	0.025	3	$8.446 \times 10^{-3}$	0.039	0.9891
Quadratic	2.73	3	0.91	130.90	<0.0001
Cubic	0.066	4	0.016	28.79	0.0005

It is observed from Table 3.3 that the quadratic model is the best fit model in terms of its significance and for this experimental design, the 2<sup>nd</sup> order model is suggested as the P-value of this model is also smaller than that of other models.

For the proposed quadratic equation, the independent variables matched were also tested for the integrity of fit. The suitability of the fitted model was assessed using numerous indicators and the outcomes were presented in Table 3.4.

To evaluate the appropriateness of the model, the  $R^2$ , the adj.  $R^2$ , CV and F-value were used (Chen et al., 2012). According to the Table 3.4, the F-value of model at 226.46 indicates the significance of this model, which also shows negligible tendency towards noise (Ayeni et al., 2013; Chatterjee et al., 2012). The probability value was found to be extremely low (P-value < 0.0001) since less than 0.0500 for the P-value indicates that the model terms chosen are considerably important. The value for the coefficient of determination,  $R^2$  can be used to judge the precision and accuracy of the proposed model. The acquired value at 0.9951 specify that 99.51% of the variability in the dependent variable could be justified through the model, and only 0.49% of the overall variations cannot be clarified (Dora et al., 2013; Kumar et al., 2000). Furthermore, the obtained value of the adjusted determination coefficient (adj.  $R^2$ ) is 0.9907, which shows good relationship among the independent variables. In the current work, an incredibly low value of CV (1.75%) indicates a high level of accuracy and an excellent consistency of the model for the experimental results. The results shown in Table 3.4 proves that all the linear terms (A, B & C) and the quadratic terms ( $A^2$ ,  $B^2$  &  $C^2$ ) were important model terms due to their small P-value.

**Table 3.4:** Statistical parameters for sequential models.

Source	Sum of Squares	df	Mean Square	F-Value	<i>p</i> -value (Prob >F)
Model	14.14	9	1.57	226.46	<0.0001
A-Temperature	0.17	1	0.17	23.98	0.0006
B-pressure	0.14	1	0.14	20.06	0.0012
C-Hydrogen	11.09	1	11.09	1597.78	<0.0001
AB	0.015	1	0.015	2.21	0.1683
AC	$4.513 \times 10^{-3}$	1	$4.513 \times 10^{-3}$	0.65	0.4388
BC	$5.513 \times 10^{-3}$	1	$5.513 \times 10^{-3}$	0.79	0.3937
$A^2$	0.038	1	0.038	5.49	0.0411
$B^2$	0.45	1	0.45	64.27	<0.0001
$C^2$	0.30	1	0.30	42.56	<0.0001

Lack of Fit: 0.069; R-Squared: 0.9951; Adj. R-Squared: 0.9907; CV%: 1.75.

In order to show the significance of the individual parameters on the response, another effective statistical tool, t-test, has been carried out. The t-test can show the level of significance of every individual parameter. From Table 3.5 it can be observed that P-value obtained from the t-test analysis is much more lower than 0.05 for every individual factor (A,B, & C) which indicates that each of the factor [temperature, pressure and hydrogen (%) ] taken under consideration is a highly significant factor for this polypropylene production process.

**Table 3.5:** *t*-Test result for testing the significance of individual parameters.

<b>One-Sample Test (Individual Parameter)</b>			
<b>Factor</b>	<b><i>t</i></b>	<b>DgF</b>	<b><i>p</i>-value</b>
Factor, A	92.466	19	0.00001
Factor, B	30.822	19	0.00001
Factor, C	9.247	19	0.00001

The subsequent second order polynomial equation was established by the application of least squares method and multiple regression study on the obtained data and given by Eq (3.7) below i.e.

$$\text{Polymer conversion (\%), } Y = (0.13 \times A) + (0.12 \times B) - (1.05 \times C) + (0.044 \times A \times B) + (0.024 \times A \times C) - (0.026 \times B \times C) - 0.12 \times A^2 - 0.40 \times B^2 - 0.33 \times C^2 + 5.19 \quad (3.7)$$

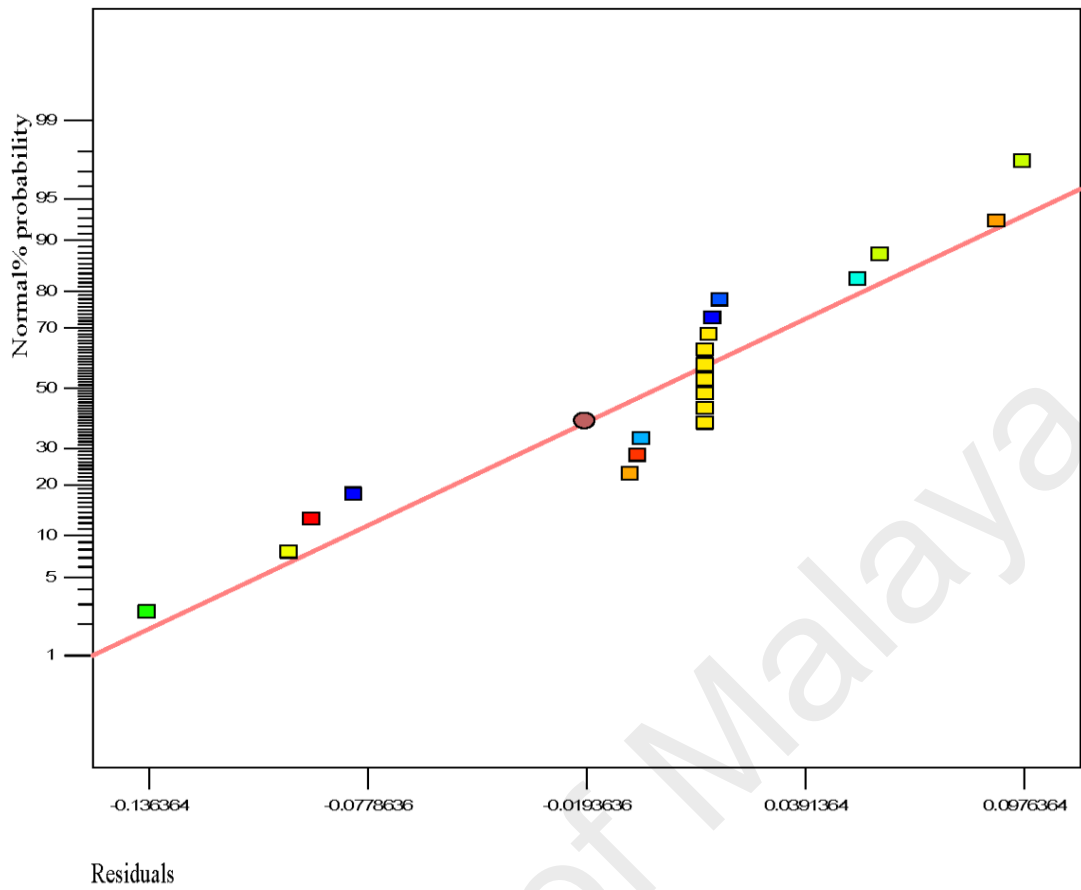
Where Y is the predicted percentage of polypropylene conversion, whilst A (temperature), B (pressure) and C (Hydrogen) are the coded form of independent variables of the model.

### 3.4.2.1 Diagnostic Statistics for Model Adequacy

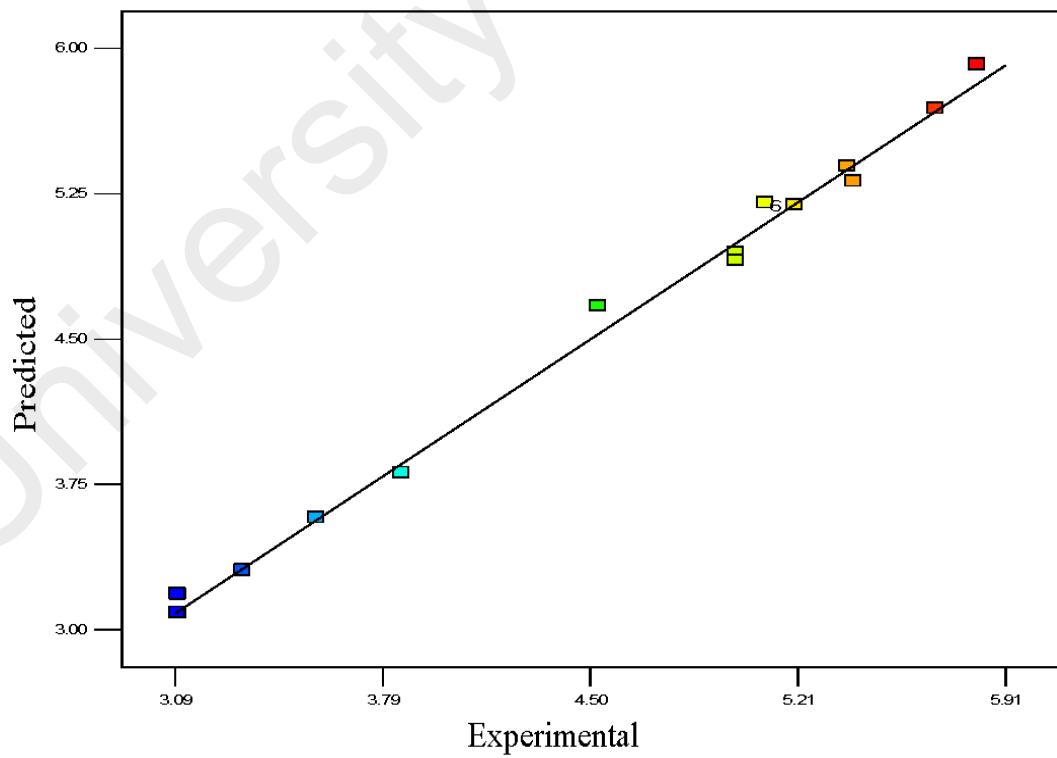
Usually, it is essential to confirm first whether the fitted model provides an adequate approximation to the actual values or not. Even though the model explains an acceptable fit, further continuation with the analysis and optimization of the integrated response surface tends to prevent inadequate or misleading results. In this study, several diagnostic tools have been used to check the adequacy and process parameters. The appropriateness of the models was also estimated by the influence plots and the residuals (difference among the anticipated response value and the actual value) in order to determine the coefficient for the data obtained experimentally in this work. Residuals are usually considered as components of variations, imprecisely fitted to the model and subsequently it is predicted that they behave according to a normal distribution feature. For the evaluation of normality of the residuals, a graphical visualization for the normal probability plot is considered as the proper method. In Figure 3.3, the scrutinized residuals are plotted against the predicted values, where, they lie rationally close on a straight line and exhibit no digression of the variance. By this way, the normal distribution of data can be confirmed. Furthermore, the regression model was used to calculate the predicted values of the polypropylene production (%) and were compared with the experimental results which are shown in Figure 3.4. As shown in Figure 3.4, there is a suitable relationship between the experimental values and the predicted values that were distributed comparatively adjacent to the straight line. This phenomenon proves that the presented regression equation used for fitting the data was appropriate, and the CCD model in conjunction with the experimental design is efficiently functional for optimization of the polypropylene conversion (%).

Figure 3.5 shows the residuals and predicted polymerization capacity per pass of the batch reaction. The general trend is that the plot is scattered randomly, suggesting that the variance of the real findings is constant for every response value and the results indicate that the response variable does not require any modification since this result does not indicate any existence of large biased errors in the experiments performed, which can also be seen in the results of Table 3.2

The outliers would be cautiously tested in the experimental design, since they may correspond to data acquisition error or rather of more severe error (Aktaş et al., 2006). The batch runs of polypropylene polymerization rate in percentage per pass are shown in the outlier  $t$  plot in Figure 3.6. The plot of outlier  $t$  is a calculation of the degree of the standard deviation i.e. intensity of deviation of actual value from the predicted value. Maximum standard residuals are required to be in the range of  $\pm 3.50$  and any observed value alongside a standardized residual beyond this value is not totally related to its experimental response (Montgomery, 2006). In this study almost all values for outlier  $t$  are lower than the interval of  $\pm 3.50$  which proves that the estimation of the fitted model against the response surface is justifiably good enough without biased unknown errors. Only one data was found to be beyond this value which contributed to the lesser significant term of the model (Myers & Cook, 2009).



**Figure 3.3:** Normal probability plot.



**Figure 3.4:** Linear correlation between actual and predicted values.

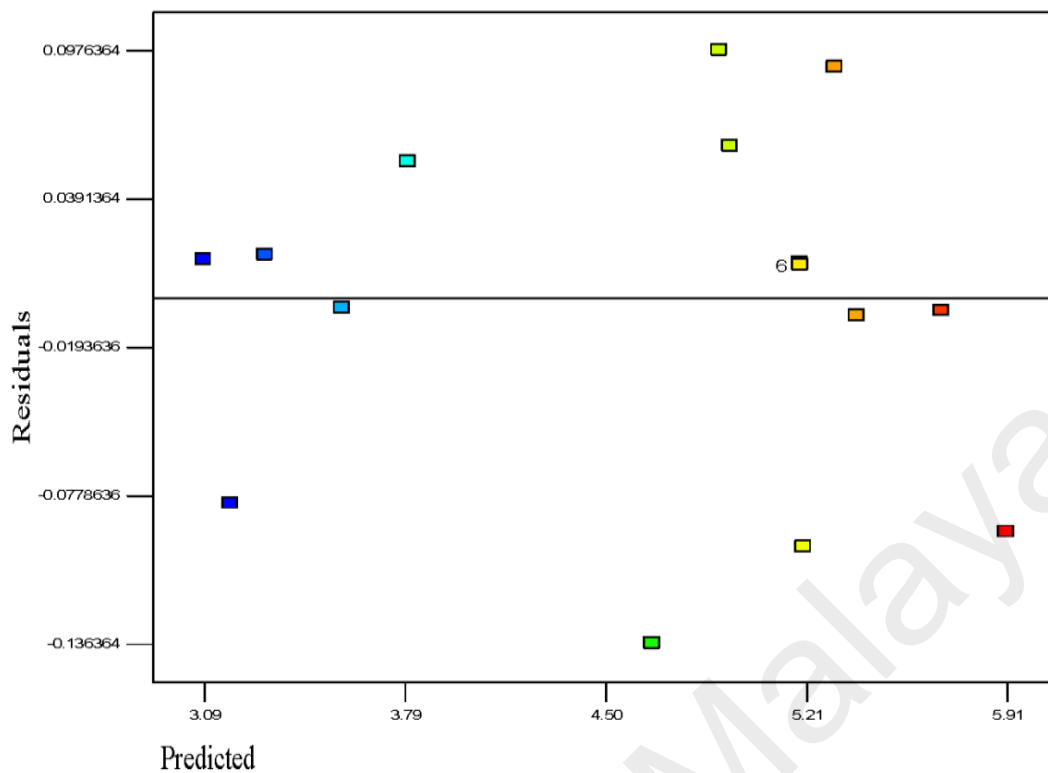


**Figure 3.5:** The residuals and predicted response plot for propylene polymerization.

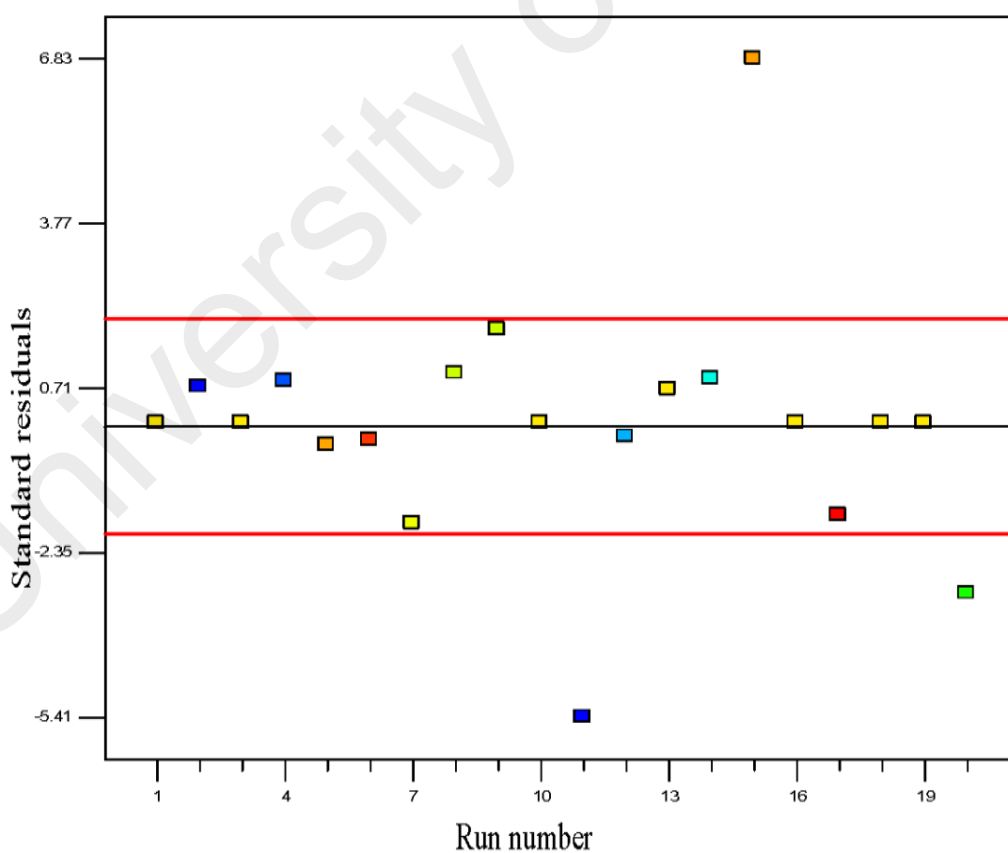


**Figure 3.6:** Outlier  $t$  plot for propylene polymerization per pass.



The perturbation diagram for the polypropylene production rate with respect to the three input process factors is shown in Figure 3.7 where the influence of a process variable around a specific point in the design range is illustrated by the perturbation plot. In this method the response (the value of Y) is plotted with respect to only one variable of the overall process one at a time over its range considering the additional process variables remaining constant in its center point. A steep slope or curvature in a factor shows that the response is sensitive to that factor and a flat line demonstrates insensitivity to modification in that specific factor. The relative effects of every independent variable on the response (polypropylene production, %) can be seen in the perturbation plot of Figure 3.7. The sharp curvature of temperature (A), pressure (B) and hydrogen concentration (C) obtained, demonstrates that the propylene production (%) was responsive to all three process variables as expected. However, the perturbation analysis clearly shows that among three parameters, hydrogen concentration (C) affects the value of Y more than the other two parameters as would be expected in such a process. This is also clearly shown for the value of coefficients as indicated in Eq. 7.

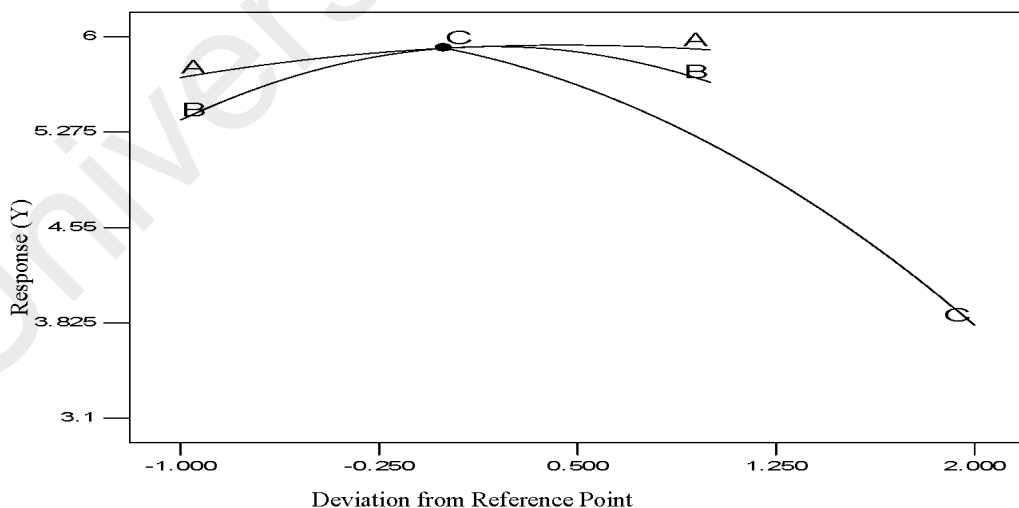


**Figure 3.7:** Deviation graph of process parameters.

### 3.5 3D Response Surfaces and their corresponding analysis

RSM provides several benefits in observing the effect of interaction within independent parameters and to recognize the effects of binary combination of linking two independent factors efficiently. However, it is easier to understand the interactions between factors graphically and the application of three-dimensional plots of the model is further useful for the graphical explanation of the interactions in this study (Mason et al., 2003). Here the 3-D response surfaces were plotted by applying Eq. (7) in order to show the polypropylene production rate which was affected by the various levels of other process variables. The interaction character between two process parameters can be explained by the response surfaces whilst the other process parameter remained constant at their center point. To identify the optimum levels of process parameters, the 3D plot line can also be used to find the optimum response of polymer conversion yield at the highest point of the surfaces. In these figures, the color line levels indicate the various effects on the polypropylene production rate.

The polypropylene production rises with the decrease of hydrogen percentage. It can be observed from Figure 3.8 that the hydrogen percentage showed a positive linear influence on the polypropylene production and the production increased notably in lower concentrated hydrogen regions. From the 3D graph of Figure 3.8 it is depicted that the combination of temperatures of  $75^{\circ}\text{C}$ , pressure of 25 bar and hydrogen of 10% shows a 3.86% polypropylene production per pass whereas at temperature of  $75^{\circ}\text{C}$  and pressure of 25 bar with hydrogen of 6% and 2% shows the polypropylene production at 5.2% and 5.82% respectively.

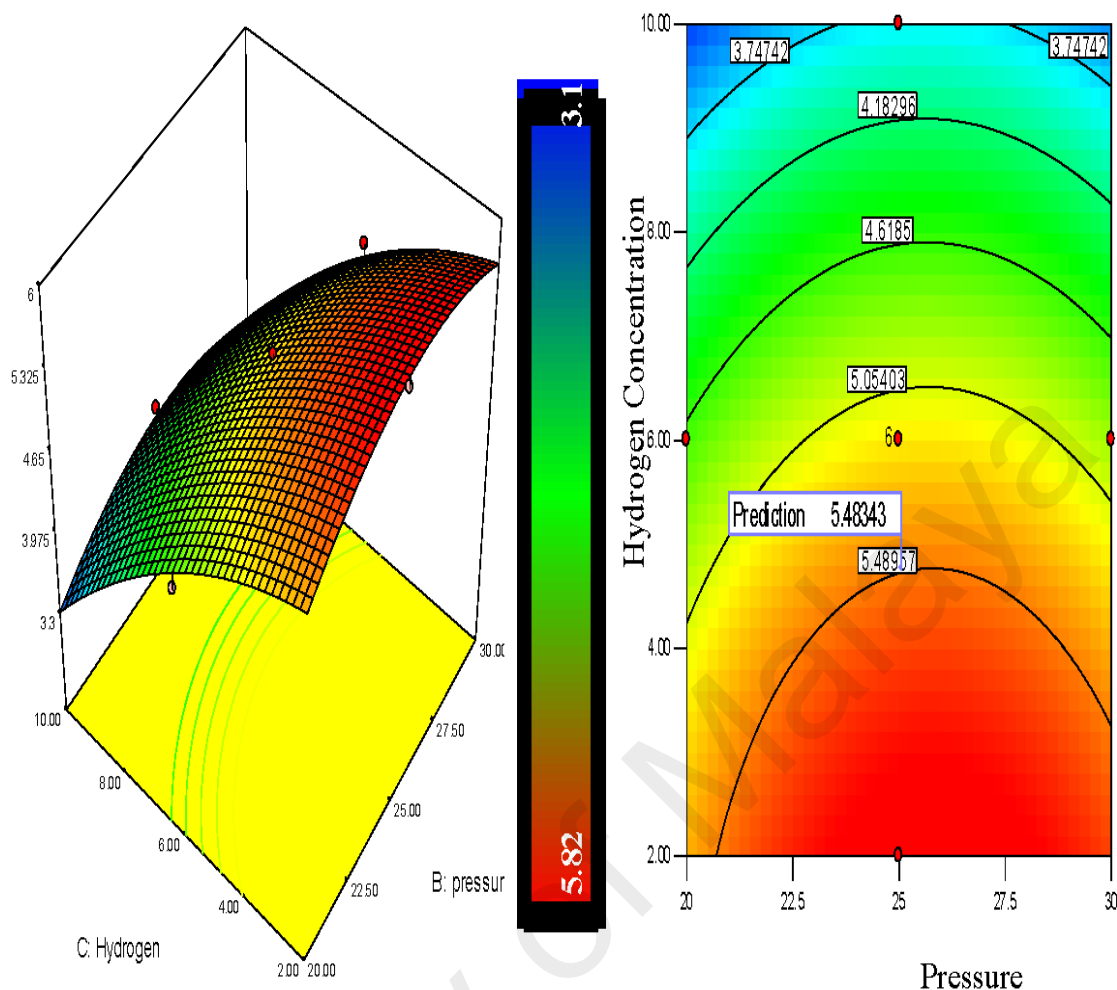


**Figure 3.8:** 3D Response surface and contour plot of hydrogen concentration vs. pressure on polypropylene production (%).

Figure 3.8 shows the response surfaces of the combined effect of hydrogen concentration and pressure on the polymer conversion. Hydrogen concentration and system pressure both showed positive effect on polypropylene production. From the contour plot, it can be clearly seen that decrease of hydrogen concentration increases the polypropylene production percentage while the increase of pressure also speeds up polypropylene production. The red colour zone indicates the optimum results while the other colors shows the lower values of the response.

Hydrogen is well recognized for its role as a chain transfer agent in industrial scale polypropylene production. The initial insertion of hydrogen decreases the molecular weight of polypropylene, which increases the diffusion rate of monomer on to the

catalyst active site. It is also reported that the nature of catalyst, monomer, and reaction conditions can also significantly affect the hydrogen effect on polypropylene production (Alshaiban & Soares, 2012; Faldi & Soares, 2001). Researchers have also shown that the polypropylene polymerization rate significantly increases due to the increase in hydrogen concentration in the system up to a certain extent and further increment of hydrogen concentration did not show any change for the polypropylene production rate (Guastalla & Giannini, 1983). The adsorption of hydrogen on the catalyst surface was identified as the cause of this phenomenon.

In the literature, the local bed pressure variation has been reported as one of the major parameters for olefin polymerization in gas phase catalytic fluidization (Sedighikamal & Zarghami, 2013; Shamiri et al., 2011; Shamiri et al., 2010). The reason is that pressure fluctuations can influence the effect of the dynamic phenomena taking place in the fluidized bed, such as from gas turbulence, bubbles hydrodynamics, and bed operating conditions (Shamiri et al., 2010). The effect of pressure can also significantly affect the fluidized bed polymerization through the minimum fluidization velocity and particle size. Naturally a pressure increase raises the inlet gas momentum and reduces the bubble surface tension, which boosts the disengagement of the bubble and the pressure intensification also enhances the fluid viscosity and reduces the buoyancy force, which slows down the detachment of the bubble from the particles (Fan et al., 2001).

### **3.6 Summary**

The optimum experimental conditions for the production of polypropylene in a pilot scale fluidized bed catalytic reactor (FBCR) was verified by response surface methodology coupled with central composite design. The set of equations and predicted value from the statistical model were compared with experimental data. Independent

variables such as temperature, pressure and hydrogen concentration were identified as the most important parameters that need to be determined to optimize the polypropylene production. The optimum condition for polypropylene production was found to be at a temperature of 75<sup>0</sup>C, pressure of 25 bar, and hydrogen concentration of 2% from this study. The projected polypropylene production from the statistical model was found to be at 5.2% , whereas from the experimental data it gives 5.82%. Correlation between system pressure and reaction initiation temperature shows interaction among them and the outcomes of various statistical techniques applied in this study have proven that the proposed model is an excellent alternative to conventional first principle models. Finally we can conclude that the excellent correlation coefficients obtained for the developed correlations for the three responses can be successfully used with over 95% confidence, for operation of the process to produce optimum polypropylene production in the real plant. This would in turn accelerate the global usage and availability of this versatile plastic which is inexpensive and an excellent alternative for many other materials in the market.

## CHAPTER 4 : DEVELOPED HYBRID MODEL FOR PROPYLENE POLYMERISATION AT OPTIMUM REACTION CONDITIONS

### 4.1 Introduction

Polymer-based materials have been a focal point in researches over the last few decades, due to noticeable advancement in improved material properties, compared to other conventional micro- and macro-level materials (Arencón & Velasco, 2009; Delva et al., 2014; Tian et al., 2013). Among polymer-based materials, polypropylene is considered a high-class thermoplastic polymer resin, generated from olefins (Galli & Vecellio, 2004; Nguyen et al., 2015). The extensive applications, from home appliances to all-encompassing industrial usages, have positioned polypropylene as the leading polymer (Bikiaris, 2010; Umair et al., 2015). Numerous traditional materials have been replaced by polypropylene, due to its greater physiochemical properties. Several industrial sectors have directly benefited by using polypropylene and its composites (Pracella et al., 2010). For example, fuel consumption has been reduced remarkably in the automobile sector by replacing metals with polypropylene, as it is lighter. Other physiochemical properties such as cutting-edged structural stability, superior dielectric vitality, and better corrosion resistance competency, have impressed consumers, and the choice of polypropylene is the best alternative to conventional materials (Glauß et al., 2013; Hisayuki et al., 2008). Although it has wide acceptability in the global materials market, polypropylene and polypropylene base materials comprise just 20% of the polyolefin market share. Therefore, from a scientific and economic perspective, it is relevant to conduct research on optimising propylene polymerisation, to increase its application and expand its market share (Balow, 2003).

Multidisciplinary efforts have been made to develop the polymerisation process and its procedures, to better understand of the complicated flow behaviours and process parameters are necessary for improving the reactor performance (Gharibshahi et al., 2015; Syamlal et al., 1993). As an example, the fluidisation technique has been applied commercially and is a well-recognised technology. Excellent mass and heat transfer rates, uniform particle mixing, and an ability to achieve diverse chemical reactions, are some of the special features of fluidised bed reactors (Ahmadzadeh et al., 2008; Aysar et al., 2011; McAuley et al., 1994). Gas phase polymerisation has been acclaimed as a more sustainable and user-friendly technology by several researchers. A number of factors such as fluidised bed components, system temperature, and gas–solid alignment, can influence the polymer fluidisation performance. Ironically, all these impelling factors make reaction regime analysis difficult. However, the quality control of different grades of polypropylene is highly correlated with these factors. The exothermic nature and sensitivity to system pressure of the propylene polymerisation reaction, can also be broadly influenced by the overall operating conditions (Shamiri et al., 2011). The development of a valid model to clarify the functional relationship among the process variables is vital, to design a robust reaction system to carry out the reaction safely, and to produce uniform and consistent product quality. The model would also support better decision making in many industrial applications (Ibrehem et al., 2009; Jang et al., 2010; Ajarullah et al., 2012; Kaushal & Abedi, 2010).

Statistical modelling with response surface methodology (RSM) has been employed in lab-scale to industrial-scale research, to ascertain the optimum operating conditions of a process by several research groups (Mansouri et al., 2014; Sulaiman, 2013). RSM is typically suitable to solve complexities where the explanation of the process dynamics is indistinct, and it is complicated to justify it by a first-principles mathematical model.

Under RSM, the standard factorial and Central Composite Design (CCD) are generally proposed to scrutinise the interactions of process factors, based on polynomial models (Özer et al., 2009; Wachem et al., 2001). Alternatively, purely mathematical models have also been described, by assuming the hydrodynamics of the fluidised bed reactor in propylene polymerisation (Shamiri et al. 2012b; Sridhar et al. 2001). However, it has also been reported that developing a mathematical model for a pilot-scale polyolefin production plant is difficult, as the rate of polyolefin production is very sensitive to the essential process parameters of temperature, pressure, feed concentration, and the geometry of the reaction unit (Shamiri et al., 2010).

Correspondingly, the literature does not provide any evidence that any optimisation study has been carried out so far, by considering the integrated process parameters with CFD method on propylene polymerisation. Although conducting pilot-scale research is very important for any industrial decision making procedure, it is rarely reported. The purpose of this study is to examine the multidimensional approaches (from the statistical and CFD point of views) among specific operating parameters for propylene polymerisation in a real reaction pilot-scale environment, and to identify the optimum process parameters by the combination of a predictive CFD coupled RSM model and experimental validation. The operating parameters that have been chosen are reaction temperature (RT), monomer concentration (MC), and system pressure (SP).

An integrated method for identification of optimum process parameters and dynamic transformations of bed for propylene polymerisation has been described in this study. The experiments were conducted in a pilot-scale plant which is a prototype of an industrial-scale plant, and is currently in the full-range production facilities under the Malaysian National Petroleum Authority (PETRONAS). The sampling and



measurement facilities confirmed the uniqueness of our engineered pilot plant, as this system was integrated with a real time data acquisition system and cutting-edge online sampling capacities by a Refinery Gas Analyser (RGA). On a global scale, this type of pilot plant is very exceptional, although it is demanded in industrial production facilities. As there are no indications to the contrary, we consider this to be unique research on the optimisation of propylene polymerisation by employing RSM and investigational validation, in a novel engineered pilot-scale plant.

One of the main concepts of the hypothesis is to apply the well-recognised central composite design (Ahmadzadeh et al., 2008; Armstrong et al., 2010) to propose easy to understand and industrially applicable optimum process parameters, together with their detailed interaction along with fluidized bed dynamic behaviours. The robustness of the experimental design is also discussed in terms of the composite design, and emphasis on constructing an adequate precision ratio, the analysis of variance (ANOVA), and the significance of second-order models, determined by the *F*-value, normal percentage probability, and an interaction graph. The quadratic model provides better evaluation capability for the response surface, and is given in general and actual equations. The face-centred option was chosen to attain the least possible number of experimental runs and the highest possible 3D value.

## **4.2: Experimental study**

### **4.2.1 Description of experimental setup**

A pilot-scale fluidised bed catalytic reactor was built to conduct the gas phase polypropylene production, comprising of a fluidised bed and a disengagement section. The detailed schematic diagram and a 3D illustration of the production process are shown in Figures 4.1–4.2 respectively. The height of the fluidised bed was 150 cm and

the diameter was 10 cm. The volume of the disengagement region was fixed at 625 cm<sup>2</sup>. A specially-fabricated catalyst container was installed at a point 9 cm higher than the metallic distributor mesh. The final product haul out points were set at three different heights above the distributor plate. To maintain proper mechanical stability inside the reactor system, the granulated polymer powder was always retained.

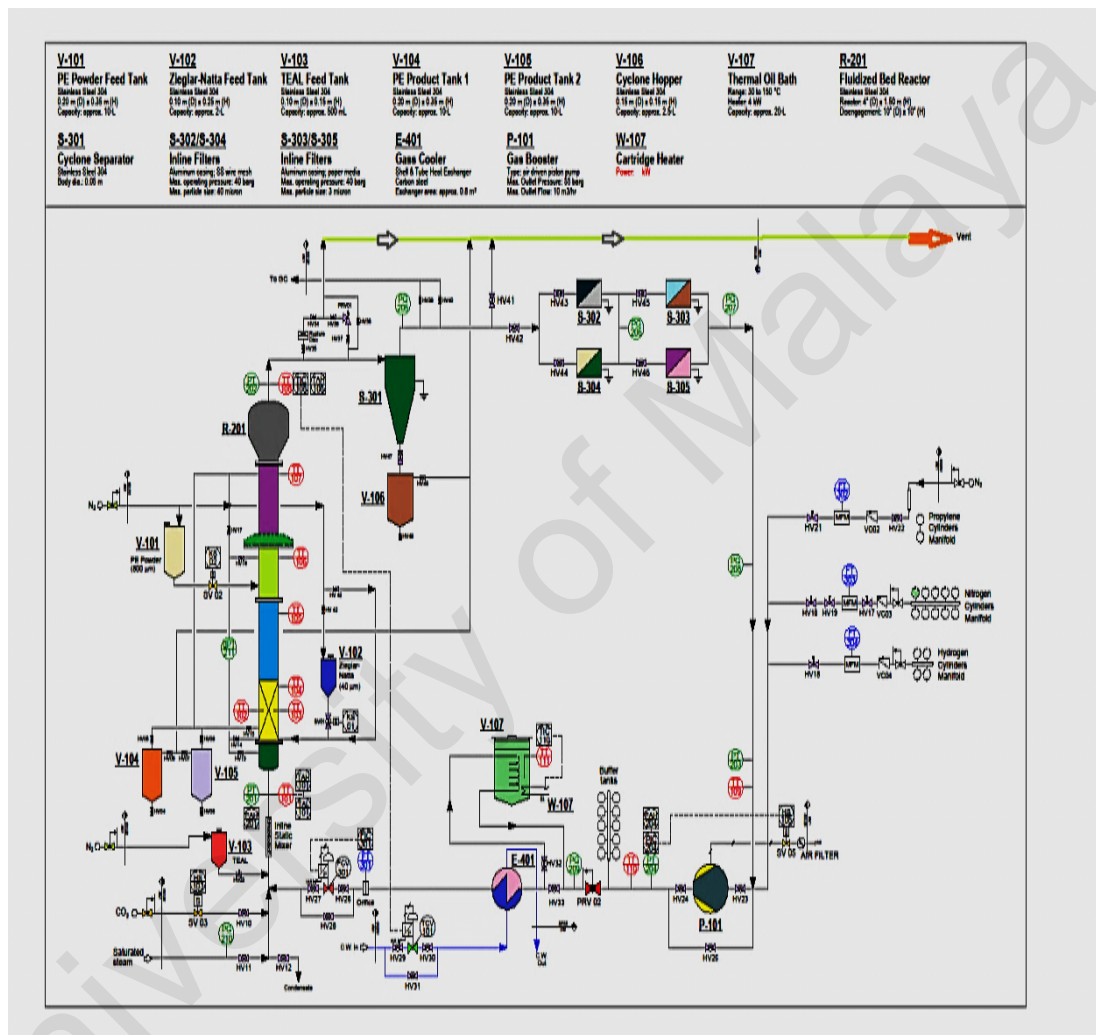


**Figure 4.1:** Detailed process diagram of fluidization of polypropylene production system

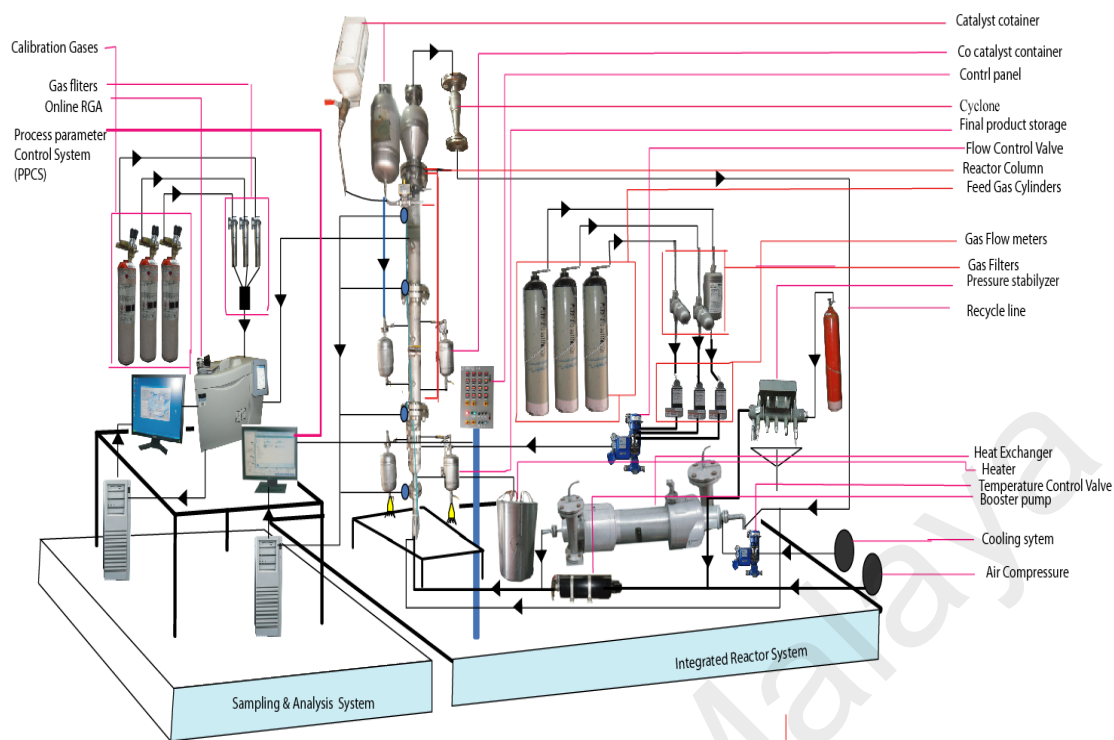


**Figure 4.2:** Sampling and Analysis system integrated with a pilot scale fluidized bed catalytic reactor

As temperature control is a very sensitive issue for fluidised catalytic polymerisation reactions, the system was kept within a 70–80 °C range. To achieve the reaction initiation temperature, a heater was used to heat up the inlet gas mixture. To obtain a detailed temperature profile in the system, six temperature sensors were installed vertically at different points of the pilot plant, starting at 16 cm above the metallic mesh. The unused gases were passed through a heat exchanger to be cool down, as the mixture had a higher temperature than required. The cyclone was integrated with four filters, equipped to eliminate fines entrained from the reactor. For the purpose of keeping the system pressure always stable, an air plunge compressor was used. A control valve was attached to the reactor system, to regulate the inlet flow and flow circulation inside the reactor. A nitrogen gas cylinder, used as a buffer container, was installed to balance pressure fluctuations. Several gas cylinders of propylene, nitrogen, and hydrogen were used for feedstock loading. The co-catalyst was dosed after confirming and fixing the

gas composition. The objective of injecting the co-catalyst was to keep the moisture level below 2 ppm and activate the catalyst, which is a prerequisite for manufacturing commercial grade polypropylene. The mass flow for the co-catalyst was adjusted by the control valve, which revolved at a regular, very fast speed, and injects the co-catalyst into the reactor. In the pilot plant, unreacted gases were recycled through the cyclone and four filters described earlier. The Ziegler–Natta catalyst container was always kept above atmospheric pressure with nitrogen, to avoid contamination. Three different gas purifiers were added to the source line of propylene, hydrogen, and nitrogen, to remove traces of O<sub>2</sub>, H<sub>2</sub>O, CO. Three flow meters were used to measure the flow feed gases. The system was fabricated to withstand a maximum pressure of 30 bar. A relief valve, pre-set at 30 bar to avoid over pressure inside the system, was placed at the top of the reactor.

Propylene, nitrogen, and hydrogen, used as feed gases in the fluidised bed reactor, all work as heat transfer agents. Nitrogen is used as the reactant carrier gas, and hydrogen as the polymer chain disassembly agent. These gases were passed through the distributor flanking the bottom of the reactor. The disengaging region of the reactor system is where unreacted gases and solid particles are separated from each other. Fresh feed gases are introduced with the solid-free gases, and recycled back into the system through the metallic mesh. The polypropylene produced is continuously withdrawn from the product discharge line, located at the bottom of the reactor. The propylene polymerisation can fluctuate 2–3% per cycle, while the complete reaction cycle can produce nearly 98% polymerisation, if the gas–solid fluidisation techniques have been adopted (Shamiri et al., 2011).

#### **4.2.2 Measurement and analysis system**

To test the gas composition, the online refinery gas analyser was connected to the sampling line of the reactor system. A set of comprehensive computing equipment and hi-tech data logging tools, were deployed at the pilot plant. The real time data on components of H<sub>2</sub>, N<sub>2</sub>, and propylene, were examined through updated RGA (PerkinElmer Clarus® 580 HYBRID series). Engineering gas chromatography software upgraded by PerkinElmer, USA and University of Malaya, Malaysia, which is capable of analysing a wide-range of hydrocarbons and light gases, investigated the gas composition. The real time data, delivered by this integrated measuring system, were collected. At intervals of 8.5 min, the data acquisition system delivered three types of data, channelled through double Thermal Conductivity Detectors (TCD) and a single Flame Ionisation Detector (FID). The TCD channel displayed data mainly on the carrier gas (nitrogen) and hydrogen. The FID channel provided data for a wide range of hydrocarbons. However, in this study we will only consider the data for propylene.

#### **4.2.3 Model development for optimization:**

The response surface methodology is an assemblage of both statistical and mathematical approaches that comprise the experimental blueprint, for expressing the scope of the input variables, and observed mathematical model, in order to examine a suitable estimating relationship amid the achieved responses (Cloete et al., 2015; Cloete et al., 2013). This methodology can also anticipate the optimisation structures, for accomplishing the optimum outputs for the process variables that generate the predicted response.

If each independent input parameter ( $x_1, x_2, \dots, x_k$ ) is determinate, governable, and random in the experiment environments, with slight minimum error, then linear yield (response)  $Y_R$  can be expressed as:

$$Y_R = f(x_1, x_2, \dots, x_k) + \varepsilon \quad (4.1)$$

Additionally, in the RSM the relationships can be given by the polynomial equation expressed as:

$$Y_R = \beta_0 + \sum_{i=1}^k \beta_i \chi_i + \sum_{i=1}^k \beta_{ii} \chi_i^2 + \sum_{i=1}^{k-1} \sum_{j=i+1}^k \beta_{ij} \chi_i \chi_j + P_{rt} + \varepsilon \quad (4.2)$$

where  $\beta_0, \beta_i, \beta_{ij}$  represent the regression coefficients which might be determined by mathematical model. The value of  $P_{rt}$  has been showed in later section.

CCD was employed to study the interaction of the process parameters and to predict the optimum polymerisation conditions. After completion of the data acquisition from the experimental study, the next step was to explain an empirical model for the response surface. The level of fit of the polynomial model can be explained by the coefficients of determination  $R^2$  and  $R^2_{adj}$ , determined by equations 3 and 4 respectively.

$$R^2 = 1 - \frac{SSQ_{residual}}{SSQ_{model} + SSQ_{residual}} \quad (4.3)$$

$$R^2_{adj} = 1 - \frac{SSQ_{residual} / DgF_{residual}}{(SSQ_{model} + SSQ_{residual}) / (DgF_{model} + DgF_{residual})} \quad (4.4)$$

In equations 3 and 4, SSQ is the sum of squares, and  $DgF$  the degrees of freedom from the ANOVA table. The three-factor experiments were conducted at the design centre to evaluate the pure error and were carried in randomised order, as required in many design procedures. Reaction temperature (A), system pressure (B), and monomer concentration (C), were selected as the input process variables. Reaction temperature refers to the temperature maintained at the reaction start-up point, while system pressure refers to the prerequisite pressure inside the system. For fluidised bed polymerisation, a

minimum pressure of 20 bar is mandatory for a reaction, although pressure can be raised to 30 bar. The coded value with lowest (-1) and highest (+1) icons of the polymerisation process are given in Table 4.1.

**Table 4.1:** Range of the independent process variables employed in the experimental design and physical properties of the reaction system.

Code of the Factor	Factor Name	Units	Type	Low Coded	High Coded	Low Actual	High Actual
A	Reaction Temperature (RT)	°C	Numeric	-1.000	1.000	70.00	80.00
B	System Pressure (SP)	bar	Numeric	-1.000	1.000	20.00	30.00
C	Monomer Concentration (MC)	%	Numeric	-1.000	1.000	70.00	80.00

### Physical properties

bubble diameter (m)	$550 \times 10^{-6}$
gas velocity (m/s)	0.50
gas density ( $\text{kg/m}^3$ )	23.45
gas viscosity (Pa s)	$1.14 \times 10^{-4}$
polymer density ( $\text{kg/m}^3$ )	1000
void fraction of the bed at minimum fluidization	0.45

### 4.3 CFD Modelling of Gas–Solid Phenomenon in FBCR

A two-phase gas-solid model was analysed to explain the fluidized bed dynamic behaviour at optimum process conditions. The commercial software package, ANSYS 16.1 (latest version), was used as it provides integrated and parallel computational facilities for complex multi-phase flows and process parameter optimizations under the options of FLUENT and Design Exploration, respectively. In the present work, in order to simulate a multiphase flow, the Eulerian-Eulerian approach was applied. A built-in model, known as the PBM (population balance model), and a moment method were used to measure the polymer production percentage.

The method includes mathematical evaluation of the emulsion and bubble phases, classifying them as intrusive sequences, whose dynamics is responsible for the value of the production proportion. In the cases when the method of moment and population balance are used, the polymer's physiochemical properties, including monomer conversion, active site information and polymer production rate, can be conjectured.

Below is the population balance characteristic of living chains dwelling on active sites, whose dimensions are  $r = 1$ :

$$\frac{dN(1, s)}{dt} = k_i(s)N(0, s)[M] + Y(0, s)[k_{fm}(s)[M] - N(1, s) \times [k_p(s)[M] + k_{fm}(s)[M]] + k_{fst}(s) + k_{da}(s) + k_{dl}(s)[l_m] + \frac{Y_{ppc}}{\sum \zeta_{eb}} \quad (4.5)$$

Living chains, whose length is more than 1, have population balance of:

$$\frac{dN(r, s)}{dt} = k_p(s)[M]N(r-1, s) - N(r, s) \times [k_p(s)[M] + k_{fst}(s) + k_{da}(s) + k_{dl}(s)[l_m] + \frac{Y_{ppc}}{\sum \zeta_{eb}} \quad (4.6)$$

Dead chains are characterised by length smaller than 2 and their population balance is:

$$\frac{dQ(r, s)}{dt} = N(r, s) \{ [M]k_{fm}(s) + k_{fst}(s) + k_{da}(s) + k_{dl}(s)[l_m] + \frac{Y_{ppc}}{\sum \zeta_{eb}} Q(r, s) \quad (4.7)$$

By merging Eqs. (5), (6) and (7) and summing upon all  $r$  values, the subsequent mass balance on  $Y(0, s)$  can be obtained:

$$\frac{dY(0, s)}{dt} = [M] \{ k_i(s)N(0, s) \} - Y(0, s) \{ k_{fst}(s) + k_{da}(s) + k_{dl}(s)[l_m] + \frac{Y_{ppc}}{\sum \zeta_{eb}} \} \quad (4.8)$$

The equation used in the RSM model has considered the population balance as constant for response calculation purposes. The model has also adopted the notions of multisite polymerisation kinetics and rigorous multi-monomer.



### 4.3.1 Phase Sequestration

This function was calculated as the volume quadratic mean of the volume fraction (solid-gas) over the bed apportioned by the preliminary static bed height. Greater values of this function measurement specified greater volume fraction oscillations throughout the averaging procedure, and consequently the substantial solids volume fraction showed heterogeneities in the two phases. The phase sequestration measurement is also an indicator of the quality of the gas–solid contact attained in the reactor. A high degree of phase sequestration implies improved contact between the solid and the gas and thereby, an enhancement in the performance of the reactor (Shamiri et al. 2012a). The necessary correlations involved in the fluidization of both the phase models are given in Table 4.2:

It was assumed that propylene consumption took place immediately after the catalyst dosing, where hydrogen depletion transpired due to the engagement of hydrogen in the polymer chain expurgation.

$$\int P_{rt} = \sum_{i=1}^2 P_{mw} R_i \quad (4.9)$$

$R_i$  is the instantaneous rate of polymerization

The mass, momentum and energy interactions between both phases were also taken into account. The energy equation was considered in this case since the flow was in exothermal conditions. Here, the noticeable forces on the particles were the drag and gravity, while the virtual mass and lift effects were neglected due to the higher density ratio of the solid to the gas phase. The standard  $k - \epsilon$  turbulence model was used to model the solid phase. It should be highlighted that the granular temperature was solved for each phase. The solid shear viscosity consisted of collisional, kinetic and frictional effects. Schaeffer's expression (Armstrong et al., 2010) was used to model the frictional viscosity in the dense cases. The solid pressure consisted of two terms. The first term represented the kinetic term and the second term, which accounted for the particle

collisions, was calculated using the Maxwellian distribution. The radial distribution function modified the probability of the particle collisions as the phase became denser (Akbari et al., 2014). A two-dimensional physical model of the reactor system must be available in order to study the pilot FBR plant. Although it has been pointed out that the differences between 2D and 3D-simulated void fractions, the 2D model is still recommended to reduce the cost of calculation while maintaining accuracy (Bi & Grace, 1995; Xie et al., 2008a). In addition, the 2D simulation has always been applied for much cheaper numerical costs and less computational time (Alchikh et al., 2015; Armstrong et al., 2010; Xie et al., 2008b). The next sections describe the main governing equations behind the developed model.

**Table 4.2:** Dynamic Correlations and Formulas Applied for the CFD Model for the Bubble and Emulsion Phase:

parameter	formula	Ref.
Bubble velocity	$v_b = v_o - v_e + v_{br}$	(Lucas et al., 1986)
Bubble rise velocity	$v_{br} = 0.7119(gd_b)^{1/2}$	(Kunii et al., 1991)
Emulsion velocity	$v_e = \frac{v_o - \partial v_b}{1 - \partial}$	(Mostoufi et al., 2001)
Bubble diameter	$d_b = d_{br}[1 + 27(v_o - v_e)]^{1/3}(1 + 6.84H)$ $d_{br} = 0.0085$ (Geldard B category)	(Silva et al., 2001)
bubble phase fraction	$\partial = 0.534[1 - \exp\left(-\frac{v_o - v_{mf}}{0.413}\right)]$	(Cui et al., 2000)
emulsion phase porosity	$\chi_e = \chi_{mf} + 0.2 - 0.059 \exp\left(-\frac{v_o - v_{mf}}{0.429}\right)$	(Cui et al., 2000)
bubble phase porosity	$\chi_b = 1 - 0.146 \exp\left(-\frac{v_o - v_{mf}}{0.439}\right)$	(Cui et al., 2000)
volume of polymer phase in the emulsion phase	$\zeta_{pe} = AH(1 - \chi_e)(1 - \partial)$	(Shamiri et al., 2011)
volume of polymer phase in the bubble	$\zeta_{pb} = AH(1 - \chi_b)\partial$	(Akbari et al., 2014)

**Table 4.2:** Dynamic Correlations and Formulas Applied for the CFD Model for the Bubble and Emulsion Phase:

parameter	formula	Ref.
phase volume of the emulsion	$\zeta_e = AH (1 - \chi_b)$	(Shuya et al., 2014)
phase volume of the bubble	$\zeta_b = A\delta H$	(Kunii, 1991)
Minimum fluidization velocity	$\beta e_{mf} = [(29.5)^2 + 0.357 Ar]^{1/2} - 29.5$	(Kunii, 1991)
Mass transfer coefficient	$K_{sg} = 4.5 \left( \frac{\beta e_{mf}}{d_{pr}} \right) + 5.85 \frac{PPC \cdot g^{1/4}}{d_{pr}^{5/4}}$ $K_{gs} = 6.77 \frac{D_g^{0.45} v_b}{d_{pr}^3}$	(Ibrehem et al., 2009)
Momentum exchange coefficient	$K_{mm} = 150 \frac{\alpha_s^2 v_g}{\alpha_g d_{pr}} + 1.75 \frac{\alpha_s \rho_g}{d_{pr}}  v_b - v_e $	(Syamlal, 1993)

### 4.3.2 Mass balance model

The continuity equation for the gas and solid phases are as follows:

The continuity equation for gas phase:

$$\frac{\partial}{\partial t} \alpha_g \rho_g + \nabla \cdot (\alpha_g \rho_g \vec{v}_g) = \sum_{s=1}^n (\dot{m}_{sg} - \dot{m}_{gs}) \quad (4.10)$$

The continuity equation for solid phase:

$$\frac{\partial}{\partial t} (\alpha_s \rho_s) + \nabla \cdot (\alpha_s \rho_s \vec{v}_s) = \sum_{g=1}^n (\dot{m}_{gs} - \dot{m}_{sg}) \quad (4.11)$$

### 4.3.2.1 Conservation of Momentum

The momentum balance for gas phase

$$\frac{\partial}{\partial t} \alpha_g \rho_g \bar{v}_g + \nabla \cdot \alpha_g \rho_g \bar{v}_g \bar{v}_g = \alpha_g \nabla P + \nabla \cdot \bar{\tau}_g + \alpha_g \rho_g \bar{g} + \sum_{s=1}^n \bar{R}_{sg} \dot{m}_{sg} \bar{v}_{sg} - \dot{m}_{gs} \bar{v}_{gs} + \bar{F}_g + \bar{F}_{lt,g} + \bar{F}_{vr,g} \quad (4.12)$$

Where  $\bar{\tau}_g$  is considered as the specific gas phase stress-strain tensor and can be defined as

$$\bar{\tau}_g = \alpha_g \mu_g \nabla \bar{v}_g + \nabla \bar{v}_g^T + \alpha_g \lambda_g \frac{2}{3} \mu_g \nabla \cdot \bar{v}_g \bar{I} \quad (4.13)$$

The momentum balance for solid phase

$$\frac{\partial}{\partial t} (\alpha_s \rho_s \bar{v}_s) + \nabla \cdot (\alpha_s \rho_s \bar{v}_s \bar{v}_s) = \alpha_s \nabla P + \nabla \cdot \bar{\tau}_s + \alpha_s \rho_s \bar{g} + \sum_{g=1}^n \bar{R}_{gs} \dot{m}_{gs} \bar{v}_{gs} - \dot{m}_{sg} \bar{v}_{sg} + \bar{F}_s + \bar{F}_{lt,s} + \bar{F}_{vr,s} \quad (4.14)$$

Stress-strain tensor solid phase:

$$\bar{\tau}_s = \alpha_s \mu_s \nabla \bar{v}_s + \nabla \bar{v}_s^T + \alpha_s \lambda_s \frac{2}{3} \mu_s \nabla \cdot \bar{v}_s \bar{I} \quad (4.15)$$

The solid phase stresses were described according to the KTGF theory [(Batchelor, 1967)], where the random particle motion is modelled by analogy with the thermal motion of molecules in a gas using the concept of granular temperature.

The given solids' granular temperature is corresponds to the kinetic energy of the particles' random motion. The equation below is derived from the kinetic theory for granular temperature:

$$\frac{3}{2} \frac{\partial}{\partial t} (\alpha_s \rho_s \Theta_s) + \nabla \cdot (\alpha_s \rho_s \bar{v}_s \Theta_s) = (-p_s \bar{I} + \bar{\tau}_s) : \nabla \bar{v}_s + (\nabla \cdot k_{\Theta_s} \nabla \Theta_s) - \lambda_{\Theta_s} + \phi_{gs} \quad (4.16)$$

where  $-p_s \bar{I} + \bar{\tau}_s$  is the generation of energy by the polypropylene particle stress tensor;

$k_{\Theta_s} \nabla \Theta_s$  = diffusion of energy ( $k_{\Theta_s}$  is the diffusion coefficient);  $\lambda_{\Theta_s}$  = collisional

dissipation of energy;  $\phi_{gs}$  = energy exchange between the certain point of gas phase and

solid phase or vice-versa.

Equation 16, comprises the term  $(k_{\Theta_s} \nabla \Theta_s)$ , relating the diffusive flux of granular energy. When the default Gidaspow et al. (Gidaspow et al., 1991) model is enabled the ANSYS FLUENT uses the following expression:

$$k_{\Theta_s} = \frac{150\rho_s d_s \sqrt{\Theta_s}}{384(1+e_{ss})g_{o,ss}} \left[ 1 + \frac{6}{5} \alpha_s g_{o,ss} (1+e_s) \right]^2 + 2\rho_s \alpha_s^2 d_s (1+e_{ss}) g_{o,ss} \sqrt{\frac{\Theta_s}{\pi}} \quad (4.17)$$

Where,  $e_{ss}$  refers to the restitution coefficient of the granulated solid particle (particle-particle),  $g_{o,ss}$  refers the radial distribution function and  $\Theta_s$  represents the polymer's granular temperature. ANSYS FLUENT is characterised by a 0.9 default. However, it can be tailored with accordance to the particle type. Several research groups (Cloete et al., 2013; Van Wachem et al., 1998; Van Wachem et al., 2001) support the notion that the diffusive terms and the convection can be disregarded, given a local occurrence of the granular energy's dissipation and its constant condition. Taking into account the complicatedness of the partial differential equation, overlong computational hours and instabilities in the solution method, the algebraic type of the equation has been suggested by many research groups for simulating fluidized beds (Bi & Grace, 1995; Klimanek et al.; Syamlal et al., 1993). Therefore, an algebraic equation can be derived to calculate the granular temperature on the basis of Equation 4.16

$$0 = (-p_s \dot{\gamma} + \dot{\tau}_s) : \nabla \vec{v}_s - \lambda \Theta_s \quad (4.18)$$

The granular temperature can be wholly or partially computed using the options and preferences listed below:

- the default algebraic equation based on Equation 4.16, which disregards any diffusion and convection in transport;
- a partial equation of the differential based on Equation 4.16, which uses various property options;
- the constant value of the granular temperature which can be applied in the cases of small arbitrary variations;

### 4.3.3 Solids Pressure

The total solid pressure was calculated and included in the mixture momentum equation:

$$P_{\sum \text{ solid}} = \sum_{s=1}^N p_{gr} \quad (4.19)$$

For the granular particulate flow in the fluidized bed regime, the solid pressure was calculated independently and used for the pressure gradient term,  $\nabla p_s$  in the granular-phase momentum equation. The solid pressure was composed of a kinetic term and a second term due to particle collisions:

$$p_{gr} = \alpha_s \rho_s \Theta_s + 2\rho_s (1 + e_{s'}) \alpha_s^2 g_{0,s'} \Theta_s \quad (4.20)$$

The value of  $e_{s'}$  in this study was set at 0.9, but the value can be adjusted according to the particle type. The granular temperature  $\Theta_s$  is proportional to the kinetic energy of the fluctuating particle motion. The function  $g_{0,s'}$  is a distribution function that governs the transition from the minimum fluidization velocity. The simulation criteria for the pilot scale fluidization study generally suggest and advise that the gas velocity be varied from 3 to 7 times that of the minimum fluidization velocity. (Dompazis et al., 2008; Syamlal et al., 1993) Since the ANSYS FLUENT provides a default value of 0.63 for  $g_{0,s'}$  a minimum fluidization value of 0.1 m/s was considered for the simulation in this study.

#### 4.4 Results and Discussion:

According to the design, 20 batch experiments were performed with various combinations of the process parameters. The propylene polymerisation percentage ( $Y_{ppc}$ ) was considered the response to the developed model.

**Table 4.3:** Experimental design and results of the response surface design:

Run	Factor A (°C)	RT (bar)	Factor B	SP (%)	Factor CMC	Response, (Actual )	$Y_{ppc}$ , (%)
1	70		25		75		5.96
2	70		25		75		4.83
3	70		20		70		4.53
4	80		30		70		5.10
5	75		20		75		5.90
6	70		30		70		4.57
7	75		25		70		5.62
8	75		25		75		5.98
9	75		25		80		5.94
10	70		20		80		5.63
11	75		25		75		5.96
12	75		25		75		5.97
13	75		25		75		5.95
14	80		25		75		5.89
15	70		30		80		5.53
16	75		25		75		5.95
17	75		30		75		5.92
18	80		30		80		5.95
19	80		20		70		4.98
20	80		20		80		5.93

The design of the experiment on the process parameters under consideration and the achieved results are listed in Table 4.3.

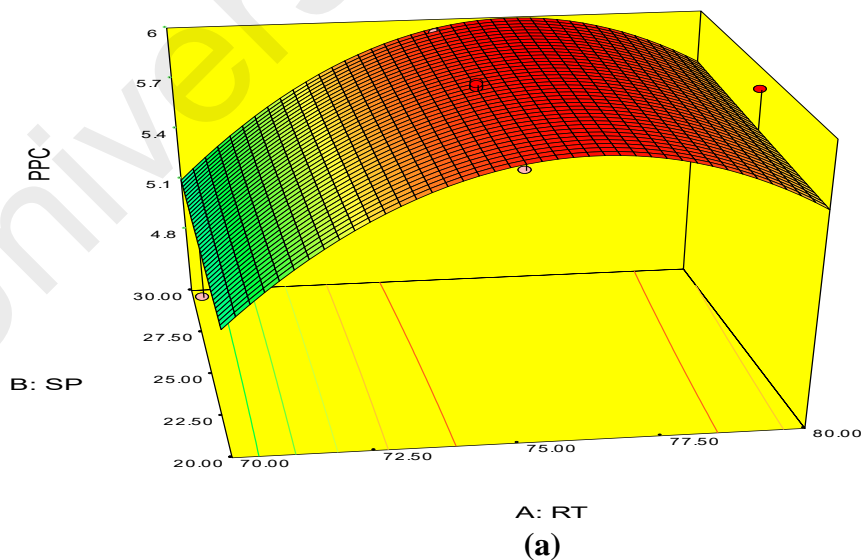
#### 4.4.1 RSM analysis

It is highly desirable to study the correlations between process variables and responses, and RSM is exceptional well-suited for extensive chemical reactions comprising single or multiple responses (Chen et al., 2012; Thouchprasitchai et al., 2011). The RSM-based quadratic model for the propylene conversion rate can be presented by Equation 21:

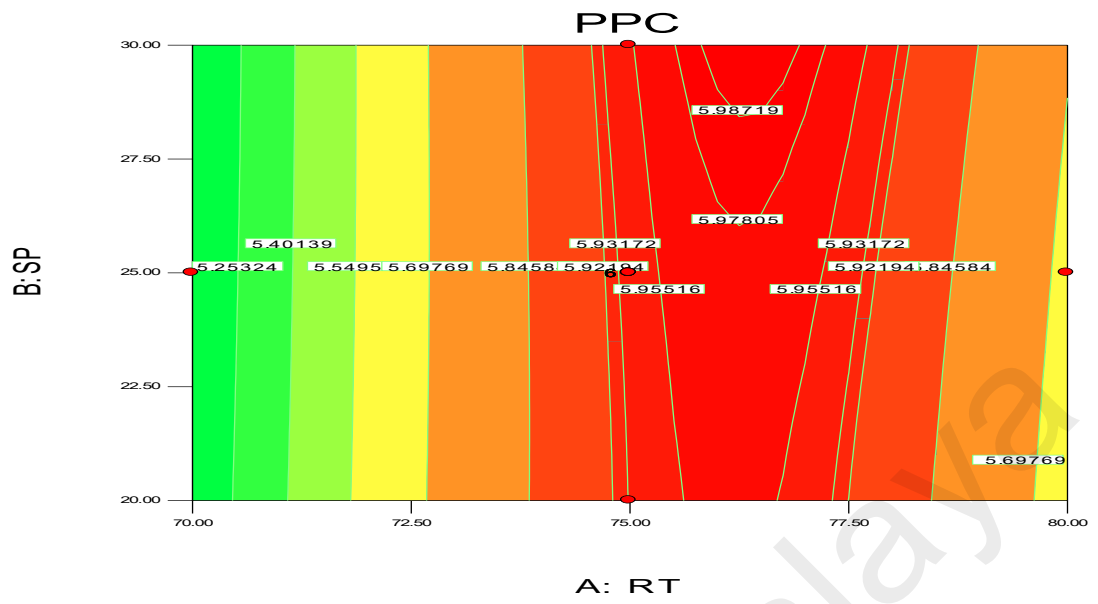
$$Y_{ppc} = (0.28 \times A) + (0.002 \times B) + (0.42 \times C) + (0.025 \times AB) - (0.032 \times AC) - (0.030 \times BC) - 0.55 \times A^2 + 0.038 \times B^2 - 0.13 \times C^2 + 5.94 \quad (4.21)$$

where  $Y_{ppc}$  is predicted monomer concentration and A, B, and C, are reaction temperature, system pressure, and monomer concentration respectively.

The 3D surface and 2D contour plots are shown in Figures 4.3–4.4. The interaction structure of two process parameters can be explained by setting another fixed parameter at the central level by applying Equation 21. The 3D plot in conjunction with the contour investigation has also been employed to verify the optimum process parameters for the highest response of polymer conversion yield at the surfaces.

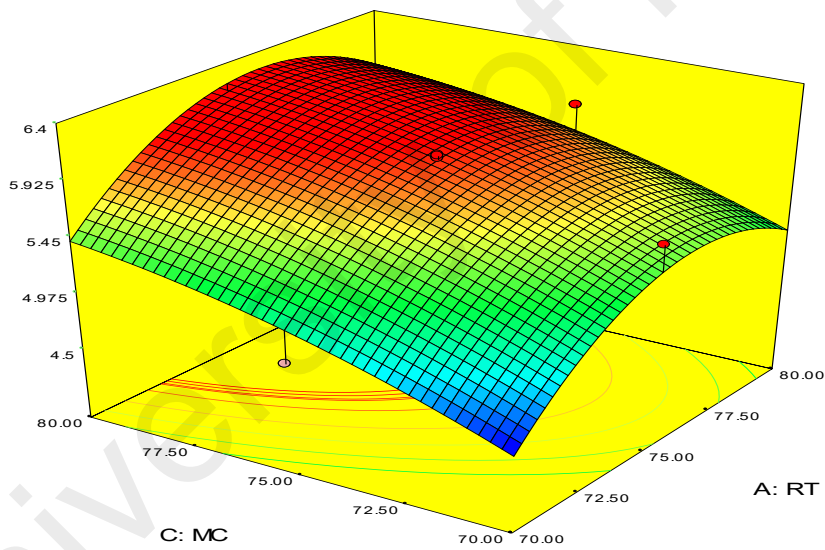




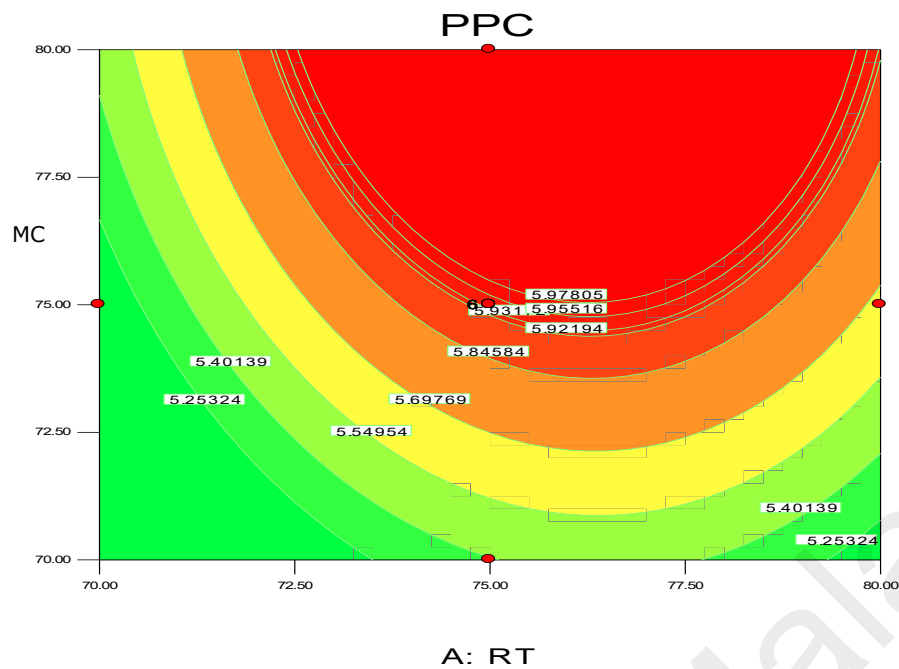


(b)

**Figure 4.3:** 3D Response surface 3(a) with 2D contour plot 3(b) of reaction temperature (RT) and system pressure (SP)



(a)



(b)

**Figure 4.4:** 3D Response surface 4(a) with 2D contour plot 4(b) of reaction temperature (RT) and monomer concentration (MC)

Each combined 3D and 2D figure signifies the optimum results of two independent process variables, where the blue to red coloured line signifies the lowest to highest response level ranges respectively. The highest response value was found on the area separated by the red coloured lines in the 3D and contour diagram. Figures 4.3–4.4 direct the major interactions amid any two process parameters on the polymer conversion, when the other process parameter was fixed at their central points.

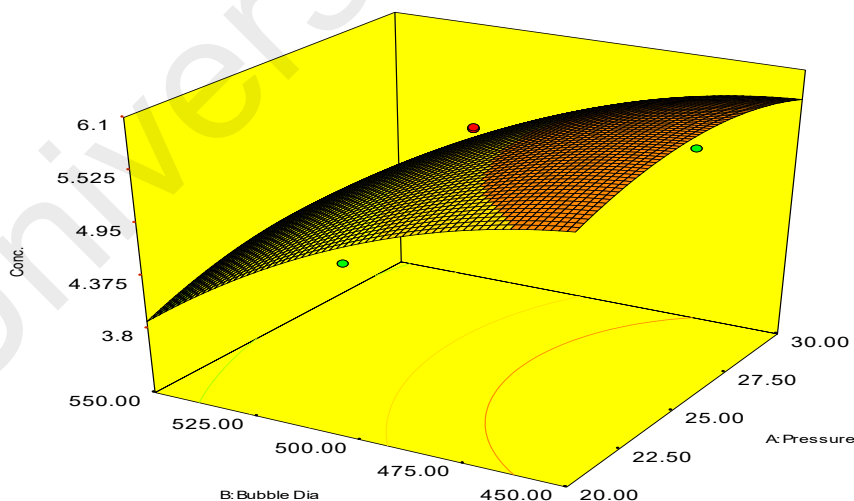
Figure. 4.3 (a)–(b) show the effect of temperature and pressure on the polymer conversion rate. The conversion rate showed a rising trend with increments of reaction temperature and system pressure, up to a certain level. From the response plot, the increment of response values can be clearly seen. At a temperature of 75 °C the response point value is 5.98%, and when the temperature increased to 77.5 °C, it gave the same response value. Further increments in temperature showed a decrease of

response. The conclusion can be drawn that the optimum temperature is 75 °C. However, most of the optimum responses values are at the 25 bar point, noticeable from the contour plots. At 25 bar the propylene polymerisation percentage response value remains at about 5.93–5.98%. The increase in pressure above 25 bar does not show any significant improvement in the response value, whereas the optimum zone starts at 25 bar. In the literature, system pressure fluctuation has been described as an important parameter for olefin polymerisation with the fluidisation technique, as it can affect the bed dynamics (Harshe et al., 2004). Optimum fluidisation yield was studied by researchers at pressure ranges of 1–16 bar (Sidorenko & Rhodes, 2004). Experimental results reported a substantial boost in the total fluidisation performance with pressure increases up to 15 bar (Rietema & Piepers, 1990). However, it is noteworthy that the reports were derived from lab-scale virtual analysis and were not results from real reaction conditions, and a minimum pressure of 20 bar is mandatory to produce industrial grade polypropylene (Shamiri et al., 2012).

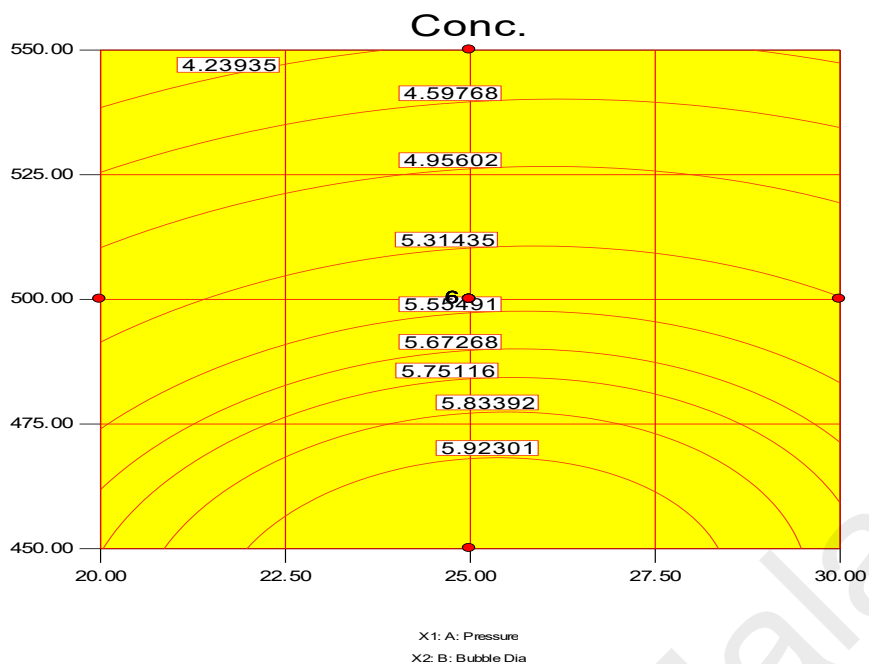
The 3D surface plot in Figure. 4 (a)–(b) express the propylene conversion rate sharply increases due to increments in reaction temperature and monomer concentration. However, a consistent rise of monomer concentration also shows significant changes in the propylene conversion rate. The optimum response value was obtained at 75% MC and further increments did not show any notable changes on response. Therefore, it is concluded that at 75% MC the response value 5.98% is achieved. From the literature, seen through purely mathematical modelling, it is evident better polypropylene production rates can be achieved at the emulsion phase with consistent increments in temperature and propylene concentration (Ibrehem et al., 2009). Some studies (Shamiri et al., 2010; Shamiri et al., 2012) showed at higher emulsion phase temperatures and lower monomer concentrations, the propylene yield was unchanged, which indicates to

a certain extent variation of the monomer concentration does not affect the production rate. The finding strongly supports the result of this study.

A thorough analysis of previous literature regarding gas-phase propylene polymerisation models has indicated that the topic of significant polymerisation examined through the bubble size effect has been neglected so far. According to Shamiri et al. (2010) (Shamiri et al., 2010), however, this catalyst action during the bubble phase is mandatory to be considered when building a model. Both the emulsion and bubble phases witness polymerisation reactions due to the fact that the bubbles also include solids. Figure 4.5 shows estimated total propylene polymerisation with regards to the bubble size and system pressure in the bubble phase. This is so because fluidisation is expected to lead to variation in the bubble size. The diameter of the bubble can vary between  $450 \times 10^{-6}$  m and  $550 \times 10^{-6}$  m. This formula demonstrates that the smaller the bubble size is, the higher the polymerisation percent will be. On the other hand, the highest value of the bubble size ( $450 \times 10^{-6}$  m) along with bar pressure of 25 results in the highest rate of polymerisation (5.92%/pass).



(a)



(b)

**Figure 4.5:** 3D Response surface 4.5(a) with 2D contour plot 4.5(b) of Bubble diameter and pressure on polymerisation.

#### 4.4.2 Effect of Process Conditions on Bed Structure during Reaction:

In this section, the hydrodynamic features under specific operating conditions will be explored. The current study has adopted a fluidised bed reactor from the simulated gas phase, which is identical with the propylene polymerisation reactor in its pilot scale used by the University of Malaya's Department of Chemical Engineering. The fundamental reason for this setup adoption is to examine operating conditions comparable to the ones in the industrial units, as well as olefins' catalytic polymerisation when subjected to high pressure. Section 2.1 elaborates on the pilot plant's specific characteristics. The medium of the fluidisation contains a monomer gas combination of hydrogen, nitrogen, also called inert gas, and propylene.

#### 4.4.3 Boundary conditions

The uniform inlet velocity was conceived as inlet boundary condition, while the top of the bed took the form of fixed pressure outlet. Table 4.4 depicts the thorough plan summary of the fluidised bed reactor's CFD simulation pilot scale. The functional superficial gas velocity was set between 0.5 m/s and 0.75 m/s in the pilot plant, which accounts for its cylindrical geometry. The superficial gas velocity dimension was thus evaluated in terms of rectangular geometry due to the overwhelming calculation expenses, in order to coordinate the accessible plant information with the height of the bed and process parameters. Last but not least, existing literature has deemed 0.5 m/s an appropriate gas velocity value, thus it has been assigned to the experiment. Front and back walls aftermath has been disregarded. The gas phase was assigned no slip wall boundary conditions, while the solid phase got the free-slip ones. For the cases when there is no solid phase, a uniform gas inlet velocity was induced by applying the Dirichlet boundary condition. At  $t$  equalling zero, all velocities were also assigned zero value. The bed's assumed condition was the initial well-mixed one, while the condition of the outlet pressure boundary was given a 25-bar value. The current study operates with one gas phase and three particle ones (quadrature points). The primary phase was assumed to be the gas phase. The particle phases, involving polymer particles, were distinguished by multiple properties, such as volume fraction, particle shape factor, length, density, etc.; the quadrature weights and the variations of the weighted nodes have been nullified. Particle density was assumed to be 910 kg/m<sup>3</sup>, and the viscosity and inlet gas densities as  $1.14 \times 10^{-4}$  Pa s and 23.45. The values were set to match a pilot scale gas-phase polymerisation reactor's characteristics. The packing fraction was assigned a maximum value of 0.75 because the space surrounding the larger particles was presumed to be filled by the smaller ones. The coefficient of the restitution was set to 0.8. Another important inference was that the heat emitted during the reaction has

been thoroughly removed and the bed was able to maintain an isothermal condition (Ahmadzadeh et al., 2008). Table 4.4 presents the simulation and wall boundary conditions accordingly.

#### **4.5 Model Validation and Grid Sensitivity Analysis**

Model validation required time step and grid sensitivity analysis, executed by correlating the information from the pilot scale gas-phase polymerisation reactor and the results from the simulation. Table 4.3 and 4.4 illustrate the conditions of the simulation. The phase formation event determines the median bed high on the basis of its catalyst properties and injection, product separation devices and withdrawal position, particle residence time, and operating condition. Hence, affirmation purposes appealed for propylene conversion inside the reactor. Variations in the bed height are determined by changes in the process parameters, which represent vital fluidisation attributes like bubble hydrodynamic, the bed's operating conditions, and gas turbulence. The bed height and the pressure drop's transient behaviour are compared to the data acquired by the pilot plant, as displayed in Figure 4.7. It is evident that the simulation course comprises start-up and quasi-steady fluidisation stages. Pressure drop oscillation most often occurs within the operational range, which is caused by the attributes of the fluidisation, while the gas-solid flow can witness a steady state of the bed height after 73 s.

**Table 4.4:** Boundary conditions for simulation set ups:

Factors	value	
Reaction zone	Inner diameter	0.1016 m
	Cross sectional area	0.00785 m <sup>2</sup>
	height	1.5 m
	volume	0.011775 m <sup>3</sup>
Disengagement zone	Inner diameter	0.25 m
	Cross sectional area	0.0490625 m <sup>2</sup>
	height	0.25 m
	volume	0.0097 m <sup>3</sup>
Reactor volume	0.0215 m <sup>3</sup>	
Initial bed height (m)	1.5	
Initial void fraction	0.431	
Gas density (kg/m <sup>3</sup> )	23.45	
Gas viscosity (Pa s)	1.14 × 10 <sup>-4</sup>	
Particle density (kg/m <sup>3</sup> )	910	
coefficient of restitution	0.8	
angle of internal friction	30	
Maximum solid packing volume fraction	0.75	
Time step (s)	0.001	
Activation energy, $E$ (J mol <sup>-1</sup> )	7.04 × 10 <sup>4</sup>	
Active site of catalyst (mol m <sup>-3</sup> )	1.88 × 10 <sup>-4</sup>	
Feed monomer concentration (mol m <sup>-3</sup> )	0.75	
Pre-exponential factor, $kp_0$ (m <sup>3</sup> mol <sup>-1</sup> s <sup>-1</sup> )	1.2 × 10 <sup>4</sup>	



### 4.5.1 Grid Independent Analysis

With the help of a 2D analysis and a boundary-and-gradient adaptation technique, it was confirmed that the higher the resolution the more independent of grid the outcome is. In this way, the adjoined mesh points could be situated in high-gradient areas in the inlet and fluidisation regions. The response variations at three mesh resolutions with 50464, 87009, and 101343 node numbers correspond to Figures 4.6 (a) to 6(c). The parameters for the simulation include 1.5m of bed height, 1000 s real time, and 0.5 m/s superficial gas velocity. Figure 4.6 illustrates the three separate grids, which were used to partition the 2D flow domain into square cells.

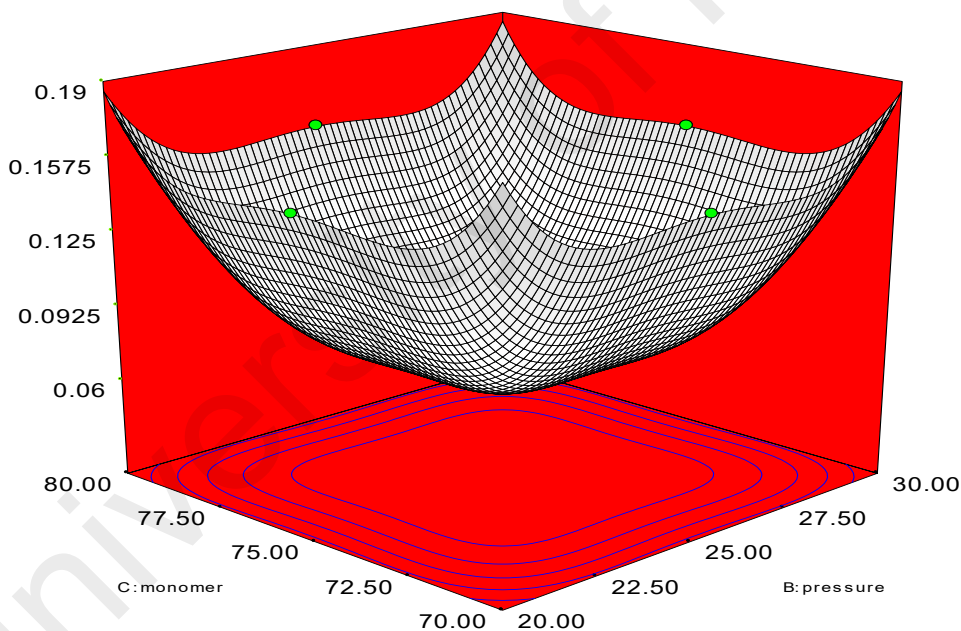


**Figure 4.6 (a)** : Changes of polymerization rate at node number 101,343 at various pressure and amount of monomer (propylene). y-axis indicates the polymerization changes.

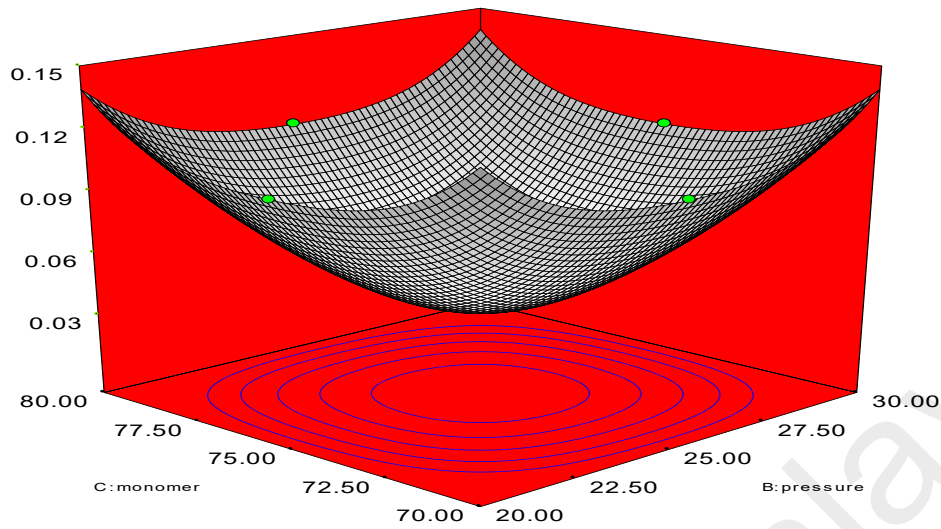


**Figure 4.6 (b) :** Changes of polymerization rate at node number 101,343 at various pressure and amount of monomer (propylene). y-axis indicates the polymerization changes.

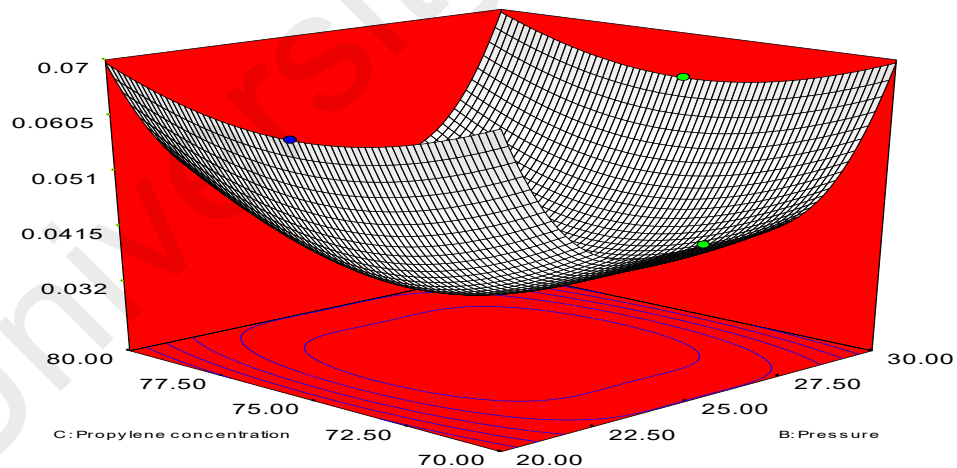


**Figure 4.6 (c) :** Changes of polymerization rate at node number 87,009 , at various pressure and amount of monomer (propylene). y-axis indicates the polymerization changes

It is evident from Figures 4.6 (a) to 6(c) that grid resolution plays a determinative role for the response. Thus, it can be deduced that the polymerisation variation is in the

0.07–0.14% range, according to the nodes variation, which ranges from 87009 to 50464. Nonetheless, with the upsurge of the grid resolution (from node number 87009 to 101343), the response value also increases in the 0.14–0.19% range. Hence, the smaller the variation is, the more accurate the response calculation will be. What is preliminary is this scenario is for a compromise to be established between the time for calculation and the necessary accuracy. As a result, adequate grid convergence with a minute polymerisation difference of 0.07% at 87009 nodes is needed to attain more precise results during the simulation in pilot scale. However, overall computational domain and mesh generation has been depicted in the figure 4.7. Sketch of fluidized bed filled with granulated particle has been shown in figure 4.7 (a). Meshing and the marked domain has been given in the figures 4.7 (b) and 7 (c).

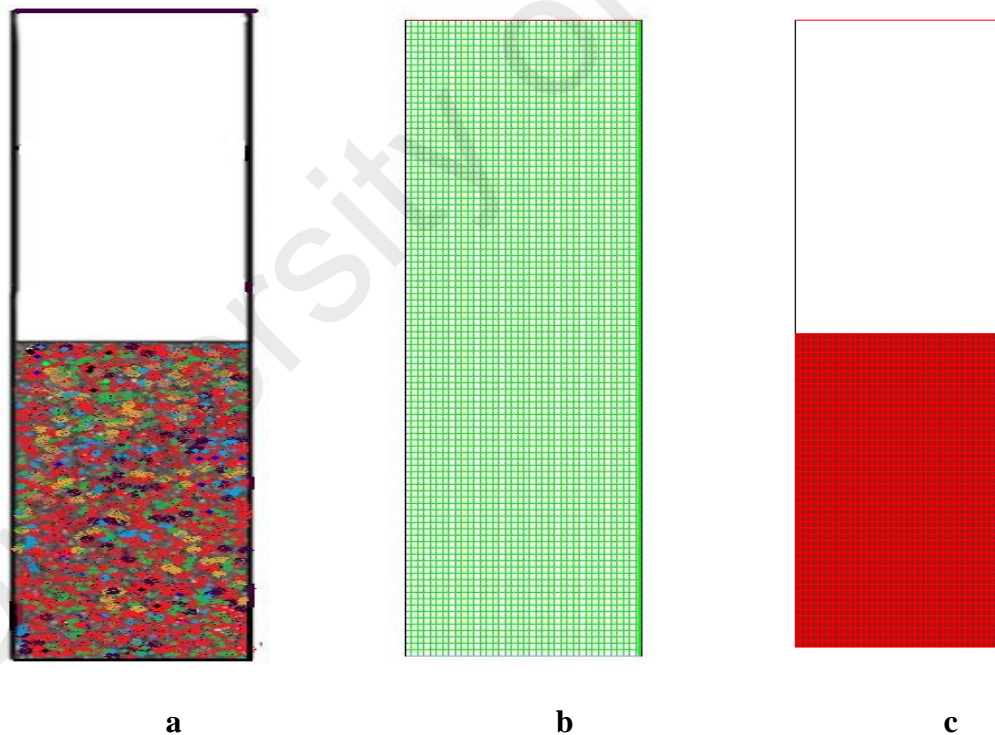


**Figure 4.7:** General computational domain and mesh generation ; (a) Framework of the gas-phase fluidized bed polymerization reactor used in simulation, (b) Generated Mesh for fluidized bed simulation, (c) Computational region marked.

Fourteen sets of process conditions were selected for the simulation study as this combined set of 8 process parameters covered the remarkable range of polymer conversion percentages. The inlet gas mixture velocity was fixed at 0.63 m/s in the simulations, and the corresponding simulated results are shown in Figure 4.8.

Figure 4.8 depicts the solid volume fraction profiles at different fixed gas velocities and time under diverse operating conditions. As clearly indicated in the figures, an alteration in the temperature, pressure and propylene concentration led to a rising trend in the bed expansion height and an increase in the bubble size. It was also obvious that probable negative deviations were noticed over the common parameter space, but strong positive variations were detected for variations in the system pressure, which also led to developments in the bed heights. This suggests that within these ranges the simulations that were exclusive of the presence of variations of pressures forecasted better reactor performance (higher degree of polymerization) even with the much denser (and lower penetrable) emulsion phase. The cause of this fact was best portrayed by animations of the volumetric segment of the two phases, which can also be seen in the figures. Fundamentally, the alteration in the system pressure expressively raised the solid phase trajectories, instigating the bed to act more solid-like to a certain degree. This initiated the appearance of bigger sized bubbles at the reactor inlet point and the construction of consistent channelling for the fluid (gas) through the bed. Individually, these trends reduced the characteristics of the gas–solid contact and hence, lessened the reactor performance. Conversely, however, if the system pressure increased to certain level (from 20 bar to 25 bar), the bed acted very liquid-like. Small bubbles were formed at the inlet and less channelling was observed. The most likely reason is that with the alteration of the bed, the thermo-physical vectors affected the particle movement in the bed sharply and assured more uniform contact between the gas, solid and catalyst. This

would have resulted in an increase in the inter-particle forces (including the drag force) between the gas and solid phases acting on the particles. At a lower system pressure, the particles accumulated in the lower portion of the bed. As the gas pressure increased, the solid volume fraction at the bottom of the bed increased gradually. Thus, the bubble size and the bed expansion height apparently increased. The systematic bubble development and movement are very important for the expected mixing of the solid and the gas, which also ensures the achievement of a better polymer conversion rate (H. R. Norouzi et al., 2011). On the other hand, Figure 4.5 illustrates the bed condition at a comparatively lower pressure (20 bars) and temperature (70<sup>0</sup> C), and expresses a comparatively mediocre bubble orientation. At this set of operating conditions (Run No. 2) the rate of propylene conversion was also lower. As depicted in Figure 4.8, the solid volume fractions became uniformly distributed in the core region across the bed, and significant differences were found at the upper region of the reactor. This means that after the gas had carried the granules to the top of the bed, they were jetted out and the polymer particles were circulated back down along the bubbles for the impact of the bed expanding section. The comparison and analysis of the hydrodynamic characteristics in

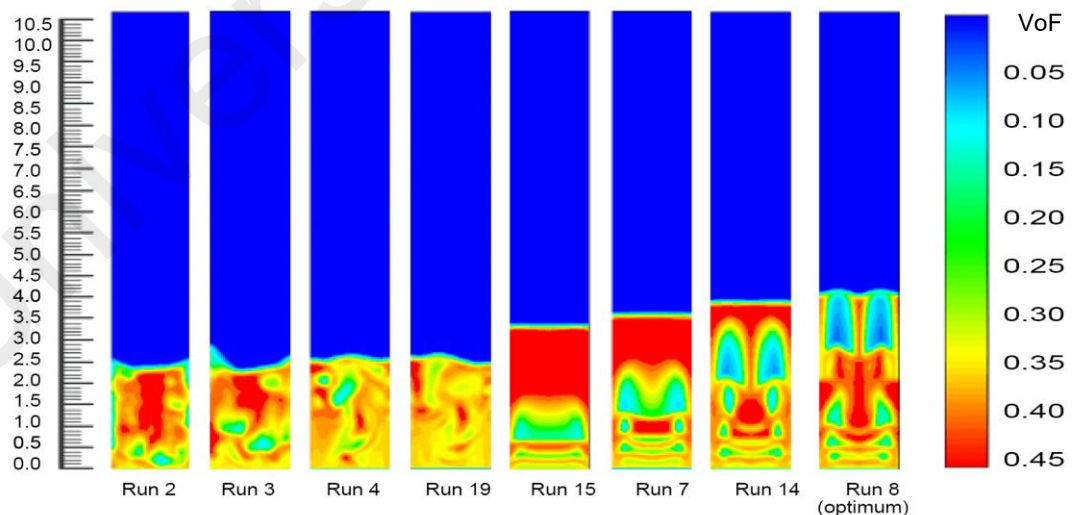


**Figure 4.8:** Bed dynamic conditions at various process combinations at inlet gas velocities

Figure 4.8 shows that when the pressure and temperature were at optimum conditions (run 8) in the bed, the bubble formation and movement, which are responsible for imparting the gas-solid contact, were remarkably changed. The wide-ranging contact is responsible for higher polypropylene production in real conditions (Akbari et al., 2014).

#### 4.6 Examining the model accuracy:

Varying in the response value can take place if the factor level is altered by coding a particular unit, represented by the coefficient of the developed equation. Analysis of variance and  $F$ -value were considered to examine the equation model and the consequence of second-order models at 95% confidence level. In practice, a larger calculated  $F$ -value than tabulated  $F$ -value suggests the null hypothesis should be avoided, as the values of individual regression coefficients trend to zero. The  $F$ -value can be formulated by the following equation:

$$F = \frac{MnS_{RG}}{MnS_{RD}} \quad (4.22)$$

ANOVA findings were used to check model accuracy, together with other significant statistical diagnostic tools. Normal probability and residuals plots for the propylene conversion rate are shown in Figure 4.9. The normal probability test evaluates the data set applied in the model and whether or not it is normally distributed. According to normal distribution theory, the plotted data should be compared to a projected straight line. Any divergence of the plotted data from the projected line would signify a digression from normality. If a linear shape is formed from the plotted data, it can be concluded that the data is distributed normally. In Figure 4.9, the fit of the model data and of the degree of concurrence with the results of the ANOVA are shown, where the residuals calculate the quantity of standard deviations in both experimental and predicted values. Figure 4.9 also suggests that response transformation analysis can be avoided as no further perceptible problem is not found with normality.

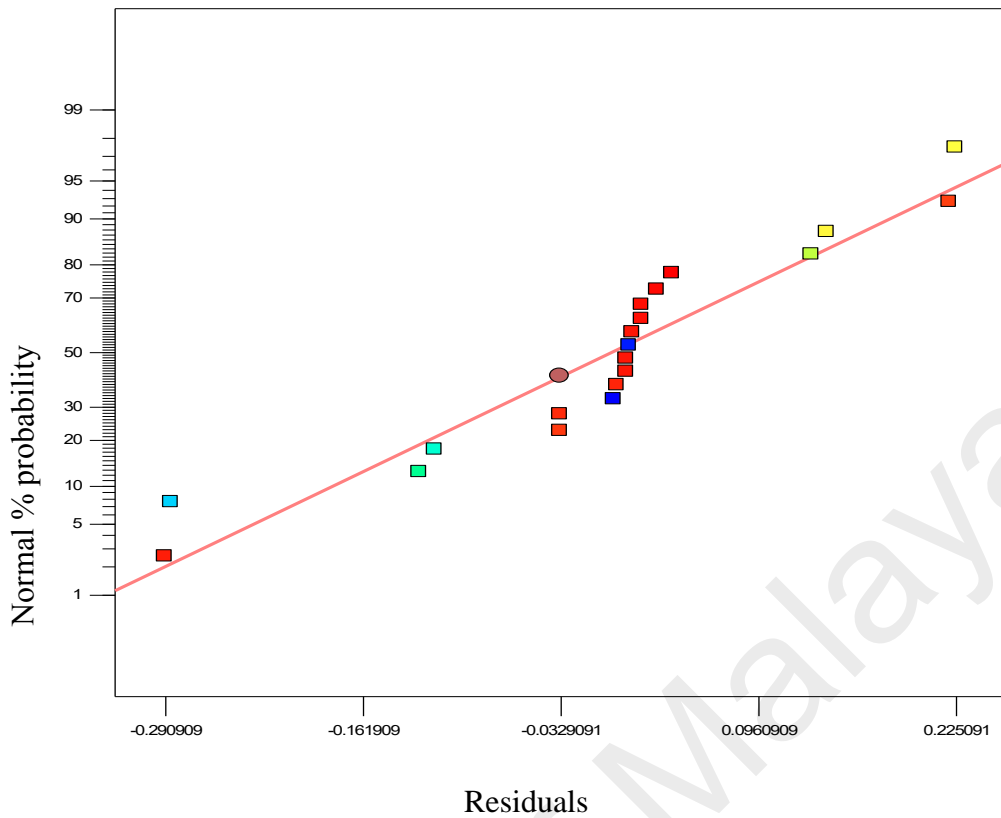


**Figure 4.9:** Normal % probability and residual plot for propylene polymerization (%) .

Residuals are considered as estimations of experimental error, attained by deducting the actual from the estimated response. Theoretically, the estimated response can be determined from the selected model, as the model parameters are assessed from experimental data. Precise investigation on residuals can express whether the hypotheses are satisfactory and the model selection is suitable. In a regression model it is expected that the error should appear randomised. The conclusion would be if the estimates of the model are greater than the actual values, but lesser than the actual with identical probability. Furthermore, the range of the error must also be independent otherwise the scope of the observation may remain predicted. It could be expected that the pattern of the residuals would have a scattered form. Accordingly, graphical methods are important to observe residuals. A randomly scattered plot of residual and predicted values can be seen in Figure 4.10. The collective impression is that as the plot

is randomly scattered, the variance of real observations is stable for each response value. This also suggests there is no need for transformation of the response variable.

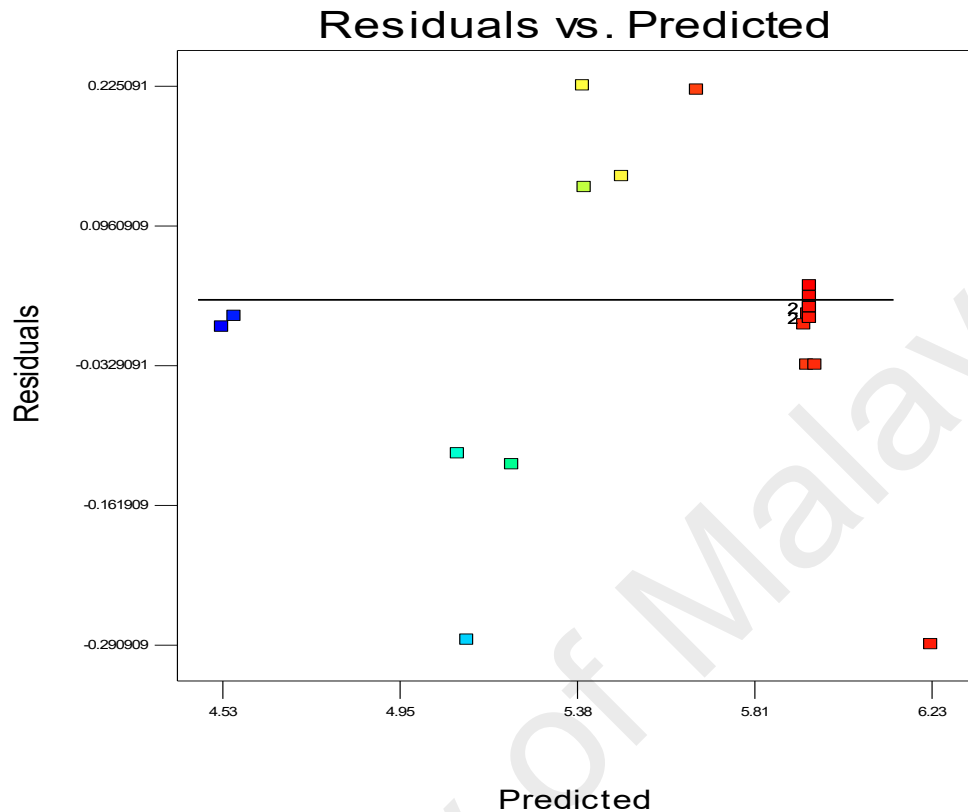


**Figure 4.10:** The residuals and predicted response plot for propylene polymerization.

The measurement of the number of deviation points of experimental values from predicted values is an important step for statistical digenesis of an experimental design. The outlier  $t$  measurement can provide a clear explanation on this matter. Figure 4.11 illustrates the outlier  $t$  plot for propylene polymerisation (%) over the batch reactions carried out. All the standard residuals positioned between  $\pm 3.50$  suggest the estimation of the fitted model towards the response surface was positive, which also suggests data recording errors are negligible. However, any data that falls outside this range indicates the presence of insignificant terms in the model, and further investigation of the nonlinear influence of the specific parameters on response is required. In this type of situation, certain combinations of process parameters need to be repeated.



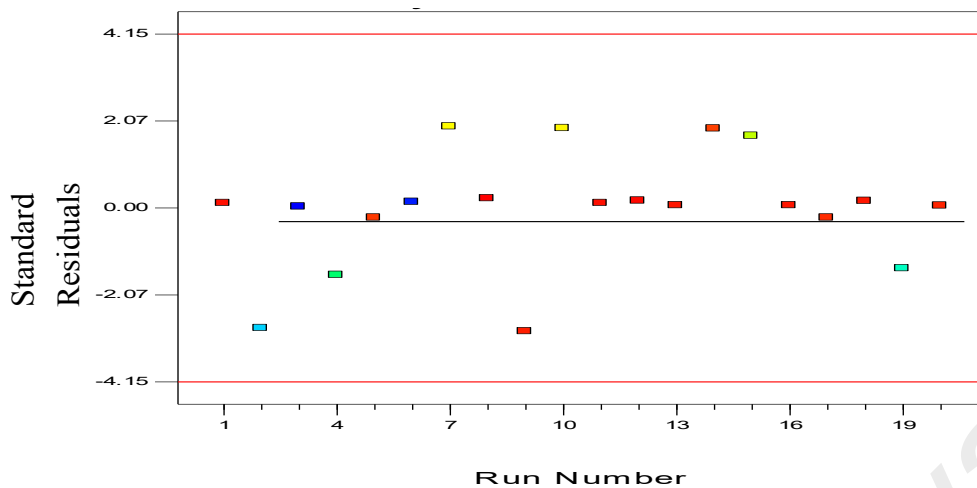


**Figure 4.11:** Outlier  $t$  plot for propylene polymerization (%) per pass.

#### 4.6.1 Interaction graphs

Investigation of the interaction effect among the process variables is essential to make decisions on optimisation in any chemical process. The RSM offers a convenient approach to monitor this issue, as it can clearly characterise the effects of binary arrangement by relating two independent variables. Interaction takes place once a specific factor does not generate the identical effect on the response at discrete levels of a new factor. So, if the graph curves of two factors are running parallel, there is no possibility for interaction to take place. If the interaction graph displays non-parallel

curves, it indicates a relatively robust interaction between the process variables.

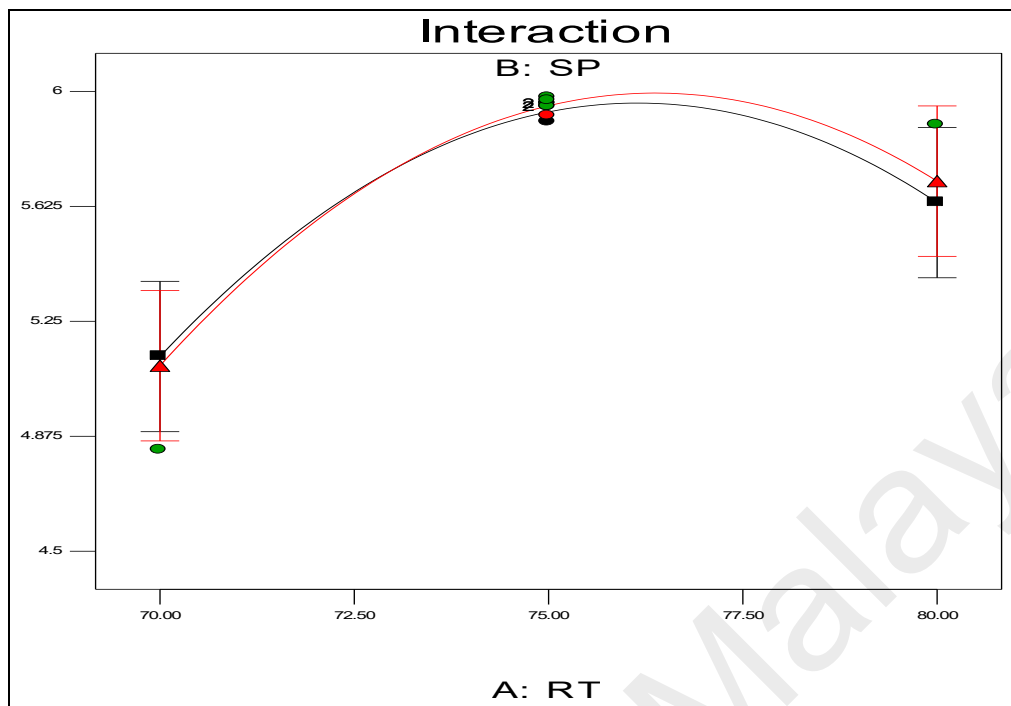


**Figure 4.12:** (a) Interaction between temperature and pressure

Figure 4.12 (a) shows a strong interaction effect between reaction temperature and system pressure, where the effects of binary combination of two independent factors can be easily recognised. However, Figure 4.12 (b)–(c) do not show any non-parallel curves, signifying there was simply no interaction possible during the propylene polymerisation reactions. Figure 4.12 (a)–(c), confirm the process variable interaction for each of the responses.

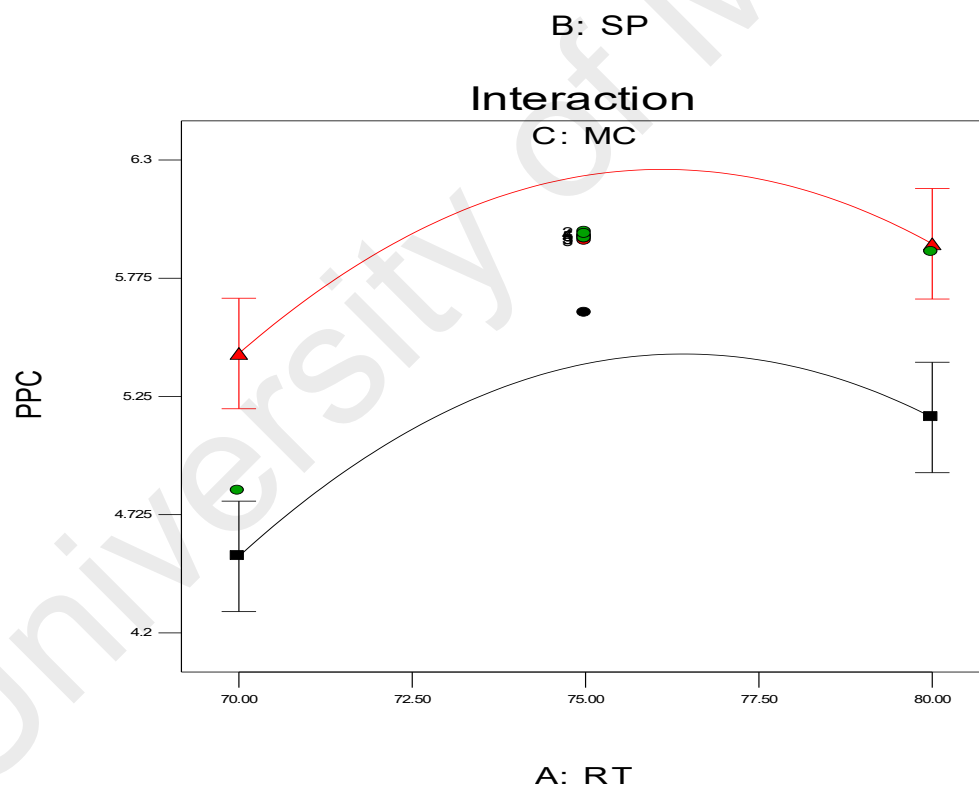
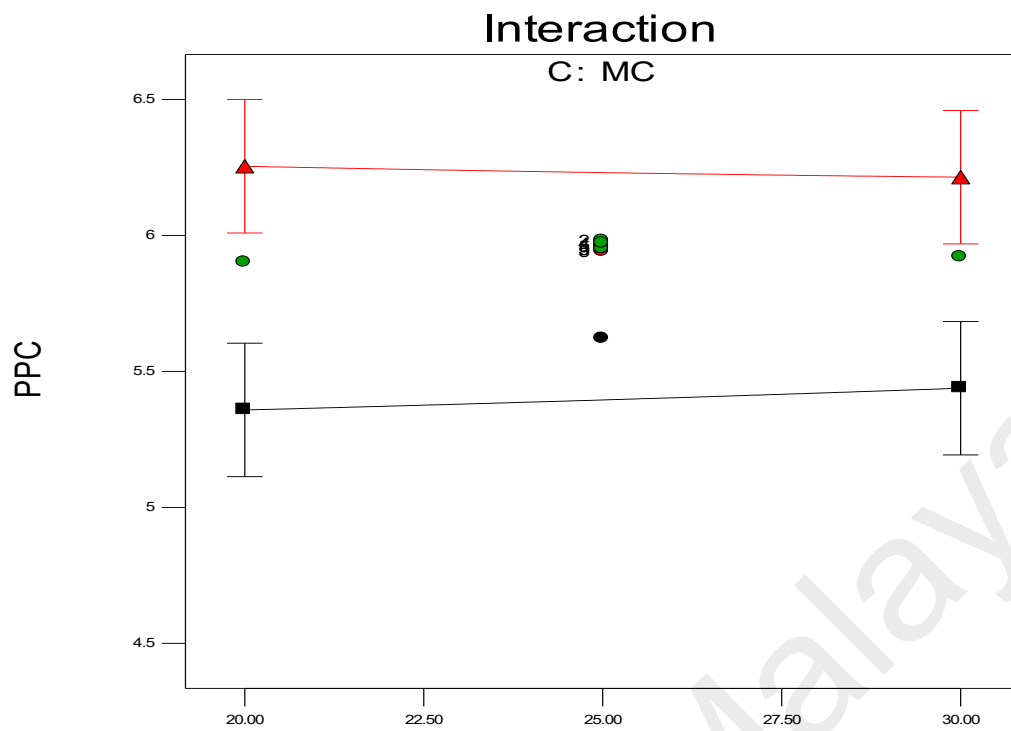


**Figure 4.12** (b) Interaction between temperature and propylene concentrations; (c) Interaction between pressure and propylene concentration

#### 4.6.2 Perturbation graph

The specific effect of every parameter on the response is another important concern in process modelling, which can be shown by a statistical measure termed a perturbation plot. This plot facilitates the comparison of the influences of every process parameter based on the centre point inside the design plot. Figure 4.13 is the perturbation chart for the polymer conversion rate with respect to A, B, and C. The perturbation plot signifies the effect of a certain parameter at a specific designed point of extent. The response, i.e. the polymer conversion rate (in percentage) of propylene is plotted by altering just one process parameter at a time over its extent, while maintaining the two other process parameters constant, at its centre point.

A perturbation plot shows the comparative influences of every independent process parameter on the polymer conversion rate. In Figure 4.13, a sharply bending curve in temperature (A) and monomer concentration (C), confirm that the response polymer conversion productivity was identically sensitive to these two process variables. Comparatively, the semi-flat system pressure curve (B) displays less sensitivity to alter the response efficiency, in respect of a change in propylene concentration. In other words, the monomer concentration has no major function in the polymerisation process, when comparing reaction temperature and pressure.

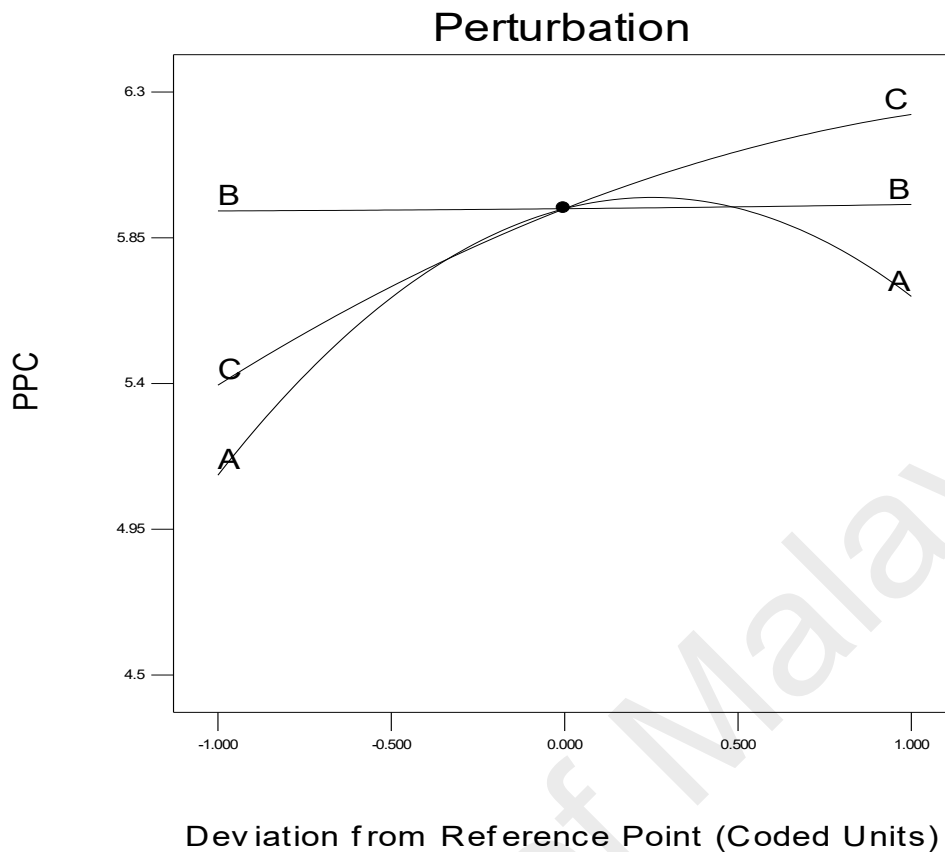


**Figure 4.13:** Deviation of individual parameter from the response

#### 4.7 Statistical diagnosis of the model through ANNOVA analysis

To analyse the most imperative effects and interactions, ANOVA analysis was applied and the results are given in Table 4.4. The  $F$ -value of the model at 14.80 specifies the significance of the model, and there is a negligible chance of error due to noise being present. Smaller  $\text{Prob} > F$  values (less than 0.05%) are a powerful indicator of the significance of model variables. Values greater than 0.1000 determine the model variables are non-significant. In this study, reaction temperature and monomer concentration are significant model variables. As the  $\text{Prob} > F$  values for RT and MC are 0.008 and  $<0.001$  respectively, it gives the idea that the response can be severely affected when the reaction temperature range fluctuates and the monomer concentration is not properly controlled within a specific range.

**Table 4.5:** Statistical parameters for developed model and process parameters.

	df	Mean Square	F-Value	<i>p</i> -value (Prob >F)
Model	9	0.57	14.80	<0.0001
A-RT	1	0.76	22.50	0.0008
B-SP	1	0.003	0.006	0.867
C-MC	1	1.75	51.62	<0.0001
A <sup>2</sup>	1	0.82	24.29	0.0006
B <sup>2</sup>	1	0.009	0.018	<0.9777
C <sup>2</sup>	1	0.044	1.31	<0.2796

R-Squared: 0.9302; Adj. R-Squared: 0.8673; Adequate Precision: 13.091.

In statistical modelling  $R^2$  is considered as one of the measures which results in the reduction of variability of the response. In spite of this, a greater  $R^2$  value does not suggest a better fit for a regression model. Adding more variables increases the  $R^2$  value without considering the statistical significance. The value of  $R^2$  lays fractionally between 0.0 and 1.0 and without units can be determined by Equation 1. Achieving higher values indicates a better fit of the model to the data set. The  $R^2$  value of the model is 0.9302 which is very close to 1, thus it can be agreed the developed model comprises the best fitted data.

The term adjusted  $R^2$  ( $R^2_{\text{adj}}$ ) is applied for the purpose of adjustment of the number of terms in the model. If the addition of model terms does not add any value, then the  $R^2_{\text{adj}}$  value is lower than regular  $R^2$ . In other words, if  $R^2_{\text{adj}}$  is less than regular  $R^2$ , it already indicates there is no necessity to add extra terms in the model. In this study,  $R^2_{\text{adj}}$  is 0.8673, which suggests that the model does not need to consider any additional terms.

Principally, adequate precision is a measure of the signal to noise ratio. This statistical tool can provide information about factors by which the model can be judged through examining if it is adequate to navigate amid the design space, along with being capable to predict the response. The desired value of adequate precision is more than 4.0. In this

case, the value of adequate precision gained is 13.091. This was defined by the following equation:

$$\frac{\max(Y_p) - \min(Y_p)}{\sqrt{\frac{p\omega^2}{n}}} \geq 4 \quad (4.23)$$

#### 4.8 Financial Benefits

As mentioned previously, PETRONAS Malaysia (one of the biggest petrochemical hubs for national and multinational players, such as BASF, Reliance, Kaneka, Eastman and Polyplastics) is the industrial collaboration partner of this research project and the pilot scale reactor is the prototype of the industrial scale reactor. The capacity of this plant is 80,000 TPA (tonnes *per annum*) of Polypropylene production through gas phase catalytic technology. In fact, it is predicted that a 5.98 % increase in production, from this advanced research, will generate extra profits of over € 5.194 million per annum (at a cost of €1,197/metric ton) for this single polyolefin plant in Malaysia. However, a market research has predicted that the global demand for polypropylene will grow to 102 million TPA in 2016 (Pandia, 2014) . From this estimation, the additional 6,411,981.74 TPA of polypropylene can be produced to meet this global demand; which may generate extra profits in the global market, to reach more than € 7,675.14 million in 2016.

#### 4.9 Summary

The process parameters of the optimisation phenomenon in a fluidised bed reactor have been investigated and associated with the prediction of reaction temperature, system pressure, as well as monomer concentration. As gas phase catalytic fluidisation is a complex and exothermic reaction, the polymer production rate and product quality is highly affected by temperature, availability of an appropriate quantity of monomer, and

fluctuations in reactor pressure. Therefore, all of these process parameters are imperative when designing and constructing a fluidised bed reactor. These values need to be controlled as accurately as possible from an engineering point of view. The optimal polymerisation was achieved at 5.98% per pass at a reaction temperature of 75 °C, a system pressure of 25 bar, and with a controlled monomer concentration of 75%. The literature reports a 3–4% polymer conversion per reaction pass, by applying fluidisation technology. Therefore, the findings of this study may be extremely helpful to decision making, not only in the polyolefin sector, but also could open new doors of research in the overall petrochemical industry. Analysis, using the response surface methodology in conjunction with central composite design, has been used to model the influence of three process parameters on propylene polymerisation. Mathematical model equations were derived for the single response by using sets of experimental data and ANOVA. The normal probability test, residual test, and outlier *t* plots, showed the developed model had a significant fit with the experimental outcomes. However, the interaction graphs clearly depicted that only reaction temperature and system pressure show trends to interact with each other. Conversely, the perturbation test showed that reaction temperature and monomer concentration had a very sharp effect on polymerisation. One of the unique findings from this study is the bed structure changes in course of polymer conversion changes. However, system pressure variation did not affect the production rate significantly. Therefore, the model and its correlated findings can be efficiently exercised within the design space, together with an excellent correlation coefficient with a 95% confidence level, on the design and suitable parameters of a fluidised bed reactor system.



## **CHAPTER 5: MULTIPHASIC REACTION MODELING FOR POLYPROPYLENE PRODUCTION IN A PILOT-SCALE CATALYTIC REACTOR**

### **5.1 Introduction**

The operational performance of the Fluidized Bed Reactors (FBRs) depends on their capacity to execute many multiphasic chemical reactions, uniform fluid mixing, a higher rate of heat and mass transfers, and operating in a continuous state (Brosh et al., 2014; Khan et al., 2014; Shaul et al., 2012). Consequently, a lot of interest has been generated by the propylene polymerization model in an FBR (Khan et al., 2014; Ushak et al., 2016; Valdesueiro et al., 2015). In the industrialized gas-phase polypropylene FBR, smaller particles of the Ziegler-Natta catalyst along with triethyl aluminium are continuously charged in the bed reactor and they react with the various reactants for producing a wide distribution of the polymer particles. Several studies have indicated that the foremost aim of engineering the gas-phasic olefin polymerization reaction is to comprehend the way the reaction mechanism works, along with studying the physical transportation process, the reactor configurations and the reactor operational conditions, which can influence the properties of the polymer product (Nguyen et al., 2015; Rault et al., 2015; Umair et al., 2015). It should be noted that the polymer products in the FBRs exhibit several types of properties, such as the morphological property and the molecular property (Ibrehem et al., 2009; Iwamoto et al., 2014; Lin et al., 2015; Pan, et al., 2015; Rault et al., 2015). Generally, the polymerization processes are classified as homogeneous and heterogeneous processes. In the homogeneous polymerization process, the reaction takes place in a single phase, while the polymerization takes place in different phases in a heterogeneous process. Hence, the heat transfer, the inter-phasic mass transfer, and the chemical reaction are very important to study (Bhuiya et al., 2012; Bhuiya et al., 2012; Breault & Guenther, 2010; Khan et al., 2014; Shamiri et al.,

2010; Wu et al., 2014). Moreover, the multiphase properties are connected to the industrial-scale polymerization reactor behavior from the pilot scales and are greatly impacted by the operational conditions of the reactor, such as gas–solid flow fields (*viz.*, the gas and the solid fractions). Due to this, detailed modeling describing the pilot-scale phenomenon is a very difficult task. The modeling of the pilot-scale FBR should take into consideration the complicated two-phase gas–solid flow, the interaction between the particles and the particle-reactor, along with microscale phenomena such as the chemical interactions and the kinetic reactions between catalyst-active sites and the molecular movement and particle collision. A multiphase reaction approach serves to solve the problems described above and establish the relation between the multiphase polymerization rate and the operating conditions.

There have been very few research articles describing the pilot-scale, multiphase olefin chemical polymerization process. In the heterogeneous systems, the polymerization reaction takes place during the occurrence of the various phases that have an inter-phase mass, heat transfer and the chemical reactions. The actual modeling approach should incorporate the complicated gas-solid flow characteristics, kinetics of the heterogeneous polymerization reaction and different heat and mass transfer procedures. There are several protocols that describe the hydrodynamics of the polyolefin FBR. Some researchers (Kiashemshaki et al., 2006; Luo, Su, Shi, et al., 2009; McAuley et al., 1994) took into account the polyolefin FBR along with the well-mixed reactor. The authors compared their model and the uniformly mixed model under steady-state parameters and observed that the even-mixed model did not present any substantial error while predicting the monomer amount in the fluidized bed reactor and the temperature in comparison to the developed mathematical model. In their study (Alizadeh et al, 2004), Alizadeh et al. (2004) described a gas–solid model wherein the reactor consisted of the

emulsion and the bubble phase. They hypothesized that the polymerization took place in the emulsion phase only as the bubble phase was free of solids. A heterogeneous three-phase model was proposed by Caliani et al. (2006) (Caliani et al., 2006), in which they considered the emulsion, bubble, and particulate phase having the plug flow behavior. In their work, Hatzantonis et al. (Hatzantonis et al., 2000) presumed that a reactor which is comprised of the mixed bubble and emulsion phases can be divided into many well-mixed, solid-free sections in a series. Generally, the polymers and the gaseous phases present in the FBR are considered to be evenly mixed. However, in several huge industrial FBRs, particle separation is seen to occur, indicating that particle dispersal varies with relation to the height of the bed. Also, it is noted that particle segregation could appear in the FBRs, which are run at very low gas-flow velocities (*viz.*,  $u_g \approx 0.2$  m/s), when the reactor contains larger particle sizes or greatly differing particle densities. A tank-in-series model was proposed by Satish et al. (2005) (Satish & Pydi Setty, 2005) to depict the reactor hydrodynamics. Harshe et al. (Harshe et al., 2004) developed a thorough mathematical approach which was based on a mixing cell for simulating the transient behavior of the polypropylene FBRs. This model used the population balancing steady-state equations, along with incorporating the complex multisite, multi-monomer, polymerization kinetics. Also, Ibrehem et al. (Ibrehem et al., 2009) suggested that the bed could be comprised of the bubbles, emulsion, cloud, and solid phases and also took into account the polymerization reactions which occurred in the emulsion phase and the solid phase. This model considered the influence of the type of catalyst particle and particle porosity on the reaction rate.

In all of the above-mentioned models, the authors presumed that no chemical reaction occurred in the gas bubble phase. However, Kiashemshaki et al. (Kiashemshaki et al., 2006) presented a study, where they had sectioned the reactor in four serial sections,

where every section contained the bubble gas phase as the plug flow and the emulsion phase as the uniform-dispersed phase. The system was modeled at the steady-state condition and it was hypothesized that the polymerization reaction occurred in the bubble and the emulsion phases.

Dompazis et al. (Dompazis et al., 2005) described a complex multi-scale and multi-compartmental dynamic model for analyzing the degree of solid dispersal in the catalytic olefin-polymerizing FBRs. This model used the “linking” model for four separate time and length scales, *i.e.*, the kinetics model, the single particle model and the multi-zonal mixing models. However, they were unable to couple the four models at their individual scales. Moreover, they implemented the integrated CFD–PBM–PMLM model for describing the gas–solid flow fields in the FBRs.

In our study, we aim to develop a novel polyolefin-based engineering process which minimizes the computational and the experimental attempts in the presence of a novel pilot-scale experimentation design. The study includes a modeling and a pilot-scale experimental validation, for designing a high-performance production system with additional advantages. As the multiphase model helps in the prediction of the relation between the PP (polypropylene) production rate and the reactor operational parameters, it is possible to develop some novel PP production processes that possess very good productivity and it is also possible to obtain their processing parameters in advance, which would help in their industrial and experimental development.

Moreover, in our study we have also employed the homopolymerization CFD scheme for understanding propylene homopolymerization in comparison to the heterogeneous Ziegler-Natta catalyst in the FBRs. We have assumed that the heat and mass transfer

resistance between the emulsion gas and the polymer particles are almost negligible. Hence, we have carried out a comprehensive and extensive study for the gas–solid phase conversion and bubble formation caused by the hydrodynamic behavior, and an improved multiphase model was proposed to examine the effect of major parameters on the presumed bed reactor process variables and the polymer properties.

## **5.2 The Reactions and Kinetic Model for Polymerization**

In our study, we have considered a complex catalytic (Ziegler-Natta catalyst) reaction mechanism for describing the propylene homopolymerization kinetics. The polypropylene production rate factors were explained using the momentum method. The necessary mass balance equations in the case of the reacted monomers (that are described by a sequence of differential and algebraic equations) were applied separately for the different emulsion and the bubble phase, as the plug flow reactor contains the very active sites of the catalyst. This was a better depiction of the situations faced by the heterogeneous Ziegler-Natta catalysts.

The Euler-Euler technique has been introduced for the analysis of the interphase phenomena taking place in the fluidized conditions. In this technique, the phases are mathematically modeled as the interpenetrating continua. As the phase volume is not taken over by other phases, this technique uses the theory of the phase volume fraction. The phase volume fractions are supposed to be a continued function of space and time, with their summation equal to 1. The conservation equations, in the case of every phase, are derived for obtaining the equations, and they have analogous structures for the phases. The equations can be terminated after constitutive relations have been provided, and these are derived from the empirical statistics or by using the kinetic theory based on granular flow (Adamczyk et al., 2014; Herzog et al., 2012). In the ANSYS FLUENT,

two different multiphasic models can be obtained, from which the Volume of Fluid (VOF) model and the Eulerian model are used and integrated to form the mathematical models (Banaei et al., 2015; Che et al., 2015a; Gharibshahi et al., 2015; Julián et al., 2016). One of the most complicated multiphasic models in the ANSYS FLUENT is the Eulerian model. This model contains a group of momentum and continuity equations for every phase. The coupling can be possible by the pressure and the interphase exchange coefficients. The way the model handles the coupling is based on the categories of phases that are involved, *i.e.*, the granular (gas–solid) flows are treated differently as compared to the non-granular (fluid–fluid) flow. This study obtains the properties by applying the kinetic theory for examining the granular flow. The mixture which is being modeled also affects the exchange of momentum between the phases. Moreover, it is highly recommended to use the feature of User-Defined Functions (UDF) that permits the customization of the momentum exchange calculation.

Though the polymerization mechanism is similar in both phases, the reaction rate between the bubble and the emulsion phase are very different. This is mainly because the dynamic two-phase model consists of varying concentrations of the solids in every phase and also differs in the amount of polymer present in the bubble ( $V_{pb}$ ) and emulsion phases, which has been elaborated on in Section 4.2. Variations in the catalyst flow rates in the emulsion and the bubble phases result in differing reaction parameters for both the phases and influence the temperature, and production rate, along with the monomer conversion in these two phases. Applying the Eulerian multiphasic model along with the kinetic model helps in the analysis of the fluidized beds as certain mathematical hypotheses are important for developing the comprehensible reaction models, which are explained in further detail in the subsequent sections.

In our study, we have presumed that the main consumption of the monomer is only in the polymerization reaction and hydrogen consumption is through the transfer of hydrogen to the reaction. Hence, the consumption rate for the components (in the case of the monomer and the hydrogen) is obtained as follows:

The generalized equation describing the rate of the  $r_{th}$  catalytic reaction is as follows:

$$R_r = k_{f,r} \prod_{i=1}^{N_g} [G_i]_{ct}^{\eta'_{i,g,r}} \prod_{j=1}^{N_s} S_j^{\eta'_{j,s,r}} \quad (5.1)$$

For the forward rate coefficient for reaction ( $r_{th}$ ), the  $k_{f,r}$  is computed by using the Arrhenius expression:

$$k_{f,r} = A_r T^{\beta_r} e^{-E_r/RT} \quad (5.2)$$

where

$A_r$  = pre-exponential factor (consistent units)  $\beta_r$  = temperature exponent (dimensionless)

$E_r$  = activation energy for the reaction (J/kmol)

$R$  = universal gas constant

It is logical to use the specific method to characterize the rate expression in pressure-dependent reactions (Balaji et al., 2002; Orava et al., 2015). The gas-phase polymerization reaction is one in which the temperature and pressure are such that the reaction takes place between Arrhenius maximum-pressure and minimum-pressure limits, and as a consequence is no longer exclusively dependent on temperature.

However, based on the above equation, the net molar rate for the consumption or the production of specific species in various phases can be described as:

$$R_{i,j(bu)} = \sum_{r=1}^{N_{bu}} B_{i,r}'' B_{i,r}' \quad i = 1,2,3 \dots N_{bu} \quad (5.3)$$

$$R_{i,j(eu)} = \sum_{r=1}^{N_{eu}} E_{i,r}'' E_{i,r}' \quad i = 1,2,3 \dots N_{eu} \quad (5.4)$$

$$R_{i,j(ct)} = \sum_{r=1}^{N_{ct}} C_{i,r}'' C_{i,r}' \quad i = 1,2,3,\dots,N_{ct} \quad (5.5)$$

For monomer:

$$R_{i,p} = \sum_{j=1}^{N_{gs}} M_i Y(0,j) k_p(j) \quad i = 1 \quad (5.6)$$

For hydrogen:

$$R_{i,h} = \sum_{j=1}^{N_{gs}} M_i Y(0,j) k_h(j) \quad i = 2 \quad (5.7)$$

The reaction rate coefficients were taken from the literature and are given in Table 5.1 (Ibrehem et al., 2009; Shamiri et al., 2010).

**Table 5.1:** Kinetic mechanism of gas-phase catalytic propylene polymerisation

Reaction	Description	Rate coefficient	Unit	Value
$N(0, J) + M_i \xrightarrow{k_i(j)} N(1, j)$	initiation of polymerization	$k_i(j)$	$\text{m}^3 \cdot \text{kmol}^{-1} \cdot \text{s}^{-1}$	54.9
$N(r, J) + M_i \xrightarrow{k_p(j)} N(r+1, j)$	propagation	$k_p(j)$	$\text{m}^3 \cdot \text{kmol}^{-1} \cdot \text{s}^{-1}$	208.6
$N(r, J) + M_i \xrightarrow{k_{im}(j)} N(1, j) + Q(r, j)$	chain transfer to monomer	$k_{im}(j)$	$\text{m}^3 \cdot \text{kmol}^{-1} \cdot \text{s}^{-1}$	0.253
$N_H(0, J) + M_i \xrightarrow{k_h(j)} N(1, j)$	transfer to hydrogen	$k_h(j)$	$\text{m}^3 \cdot \text{kmol}^{-1} \cdot \text{s}^{-1}$	0.1
$N_H(r, j) + H_2 \xrightarrow{k_{fh}(j)} N_H(0, j) + Q(r, j)$	transfer to hydrogen (cocatalyst)	$k_{fh}(j)$	$\text{m}^3 \cdot \text{kmol}^{-1} \cdot \text{s}^{-1}$	7.54
$N(r, J) + M_{cat} \xrightarrow{k_{fcat}(j)} N(1, j) + Q(r, j)$	transfer to catalyst	$k_{fcat}(j)$	$\text{m}^3 \cdot \text{kmol}^{-1} \cdot \text{s}^{-1}$	0.12

In our study, we considered the impact of temperature (*i.e.*, the activation energy) on the polymerization kinetics for the polymerization reactions only. There have been many reports which have stated that in the cases where the Ziegler-Natta particles are very small and their activity is not very high (low or moderate rate of polymerization), then the mass and the heat transfer resistance present in the polypropylene and within the unreacted solid and the gas particles play an insignificant role and they will not influence the reactor behavior or even the polyolefin properties (Zacca et al., 1996).



The FBRs are not very ideal and are tough to characterize due to the presence of complicated mixing and the contact flow patterns, the transportation phenomenon and the various polymerization reactions. Several researchers have tried to model this type of non-ideal system by developing numerous mixing models for describing this kind of behavior. These types of reactors, generally, need to combine the hydrodynamics, kinetics, and transport phenomena for their modeling. In one study, the dynamic performance of the FBR was described by Choi and Ray (Choi & Ray, 1985), wherein they suggested a steady bubble-sized model which comprised the well-mixed emulsion phase along with a plug flow bubble phase. Researchers also developed a very simple evenly mixed model by hypothesizing that the reaction contained an unobstructed transfer of heat and mass within the emulsion and the bubble phases (McAuley et al., 1994). In this study, we have adopted the unified modeling method for studying the gas–solid fluidization. A bubble-emulsion phase flow model has been developed for describing the dynamic behavior, which involves the multidimensional flow pattern and the multifaceted mixing of the polymer, PP, and gaseous phase FBR. For estimating the mean value of the bed voidage and the energy and mass balance equations, we have derived the dual-phasic model by combining the previously described kinetic developments and the dynamic two-phase model.

### **5.2.1. The Multiphasic Hydrodynamic Models**

In this model, it has been assumed that the bubble phase does not contain any solids and the emulsion phase continues at minimal fluidization conditions. However, the emulsion phase voidage may differ from that in the minimum fluidization conditions. Additionally, the bubble phase could also contain different solid particle fractions (H. Cui, Sauriol, & Chaouki, 2003). Using this idea as the basic step, Cui *et al.* (Cui et al., 2003) suggested the dynamic inter-phase flow for studying the hydrodynamics of the fluidized bed (the concentrations of the solid particles vary in the emulsion and the

bubble phases depending on the gas velocity). Hypothesizing the emulsion phase minimal fluidization conditions in the PP reactor (for a conventional two-phase model) is unrealistic, hence, in this study, the dynamic two-phase flow of the fluidized beds, as suggested by Shamiri et al. (Shamiri et al., 2010), has been incorporated along with the CFD model. This would help improve the multiphase model used in our study and would also help in the calculation of the mean bed voidages. The correlation required for the estimation of the bubble volume fraction in the fluidized beds, the emulsion and the bubble phase velocities, the emulsion phase and the bubble phase voidage, and the mass and heat transfer coefficients in the case of the two-phase model and the steady bubble-sized model have been summarized in Table 5.2.

University of Malaya

**Table 5.2:** Dynamic correlations and formulas applied for the multiphasic model (Khan, Hussain, & Mujtaba, 2016; Kunni, 1991; Shamiri et al., 2010)

Parameter	Formula
Bubble velocity	$v_b = v_o - v_e + v_{br}$
Bubble rise velocity	$v_{br} = 0.7119(gd_b)^{1/2}$
Emulsion velocity	$v_e = \frac{v_o - \partial v_b}{1 - \partial}$
Bubble diameter	$d_b = d_{br} [1 + 27(v_o - v_e)]^{1/3} (1 + 6.84H)$ $d_{br} = 0.0085$ (Geldard B category)
Bubble phase fraction	$\partial = 0.534(1 - e^{-\frac{v_o - v_{mf}}{0.413}})$
Emulsion phase porosity	$\chi_e = \chi_{mf} + 0.2 - 0.059e^{-\frac{v_o - v_{mf}}{0.429}}$
Bubble phase porosity	$\chi_b = 1 - 0.146e^{-\frac{v_o - v_{mf}}{0.439}}$
Volume of polymer phase in the emulsion phase	$\zeta_{pe} = AH(1 - \chi_e)(1 - \partial)$
Volume of polymer phase in the bubble phase	$\zeta_{pb} = AH(1 - \chi_b)\partial$
Volume of the emulsion phase	$\zeta_e = AH(1 - \chi_b)$
Volume of the bubble phase	$\zeta_b = A\partial H$
Minimum fluidization velocity	$\beta e_{mf} = \left[ (29.5)^2 + 0.357Ar \right]^{1/2} - 29.5$
Mass transfer coefficient	$K_{sg} = 4.5 \left( \frac{\beta e_{mf}}{d_{pr}} \right) + 5.85 \left( \frac{PPC \cdot g^{1/4}}{d_{pr}^{5/4}} \right)$ $K_{gs} = 6.77 \left( \frac{D_g \cdot 0.45v_b}{d_{pr}^3} \right)$
Momentum exchange coefficient	$K_{mn} = 150 \frac{\alpha_s^2 v_g}{\alpha_g d_{pr}} + 1.75 \frac{\alpha_s \rho_g}{d_{pr}}  v_b - v_e $

### 5.2.2. The Emulsion Phase Model

In their study, Hassani et al. (Hassani et al., 2013) developed a simple well-mixed model in which they assumed that the bubbles are very small and possess an unobstructed heat and mass transfer within the emulsion, and the bubble phases, the composition and the temperature were homogenous in the gaseous phase present in the fluidized bed. A good solid mixing is vital for ensuring a consistent distribution of product quality and maintaining a constant solid temperature or concentration in the bed. Also, the hydrodynamic elements such as bed porosity and bubble motion directly affect the solid flow mixing/pattern in the bed. It is also suggested that developing programming codes based on the requirement to elucidate the unsteady dynamic helps reduce the CPU (central processing unit) time. In this study, coding was developed through the use of user-defined functions (UDF) to serve this purpose. Some significant assumptions also made for this modeling are mentioned below:

The heat and the mass transfer rates in the bubble and the emulsion phase were very high and the bubbles were very small; hence, the polymerization reaction is a single-phase reaction, while the reactor is believed to be a single-phasic (emulsion phase), well-mixed type of reactor.

The emulsion phase continues in minimum fluidization conditions.

The bed consists of uniform composition and temperature.

Considering the above-mentioned assumptions, the energy-balance and the dynamic material equations in the case of the monomer and hydrogen concentration are written depending on the above assumptions. The equation for estimating the mole balance can be calculated as follows:

$$(V_R \varepsilon_{\min}) \frac{d[M_i]}{dt} = U_0 A ([M_i]_{in} - [M_i]) - R_v \varepsilon_{\min} [M_i] - (1 - \varepsilon_{\min}) R_p$$

The energy-balance equation considers the monomer internal energy as negligible. Therefore, the primary conditions that help in solving the equations are described below:

$$\left[ \sum_{i=1}^m [M_i] C_{pi} V \epsilon_{\min} + V (1 - \epsilon_{\min}) \rho_{pp} C_{p,sol} \right] \frac{dT}{dt} = U_o A \sum_{i=1}^m [M_i] C_{pi} (T_{in} - T_r) - U_o A \sum_{i=1}^m [M_i] C_{pi} (T_{in} - T_r) - R_{vol} \left[ \sum_{i=1}^m [M_i] C_{pi} \epsilon_{\min} + (1 - \epsilon_{\min}) \rho_{pp} C_{p,sol} \right] (T - T_r) + (1 - \epsilon_{\min}) \Delta H_R R_p \quad (5.8)$$

### 5.2.3 The Bubble Phase Model

Shamiri et al. (Shamiri et al., 2010) proposed the constant bubble-sized model which assumes that the emulsion phase (or the dense phase) is present in the minimal fluidization conditions. This model was adapted in several earlier reports which studied the gas-phase olefin chemical polymerization reaction.

The hypotheses for the bubble phase model have been described below:

1. The fluidized bed contains two different phases, *i.e.*, the bubble and the emulsion phase, and the chemical reactions generally take place in the emulsion phase only.
2. The emulsion phase is believed to be mixed completely, at minimum fluidization, and it exchanges mass and heat at uniform rates with the bubble phase above the height of the bed.
3. The bubbles are spherically shaped and have varied sizes and are in a plug flow with a constant velocity.
4. The heat and mass transfer resistances which occur between the solid polymer and the gas in the emulsion phase are very small (*i.e.*, presence of very minute catalyst particles, low-to-moderate catalytic activity or very low polymerization rates).

Based on these hypotheses, the energy balance and the steady-state mass can be estimated to describe the difference in the temperature and monomer concentration present in the bubble phases. The equation for the mole balance in the case of hydrogen and the monomer is as described below:

$$\frac{d[M_i]_{bu}}{dt} = \frac{K_{be}}{U_{bu}} ([M_i]_{eu} - [M_i]_{bu}) \quad (5.9)$$

Integration of the neighboring monomer concentration  $[M_i]_b$  present in the bed helps in the estimation of the average concentration for the  $i^{\text{th}}$  monomer present in the bubble phases.

$$\begin{aligned} [\bar{M}_i] &= \frac{1}{H} \int_0^H [M_i]_{bu} dh = [M_i]_{eu} + ([M_i]_{eu(in)} \pm [M_i]_{in}) \\ &\times \frac{U_{bu}}{K_{be} H} (1 \pm \exp(-\frac{K_{be} H}{U_{bu}})) \end{aligned} \quad (5.10)$$

The bubble phase energy balance is expressed by the following equation:

$$\sum_{i=1}^m M_i]_{bu} C_{pi} \frac{dT_{bu}}{dt} = \frac{H_{be}}{U_b} (T_b - T_c) \quad (5.11)$$

Integration of Equation (10) for the overall height of the bed estimates the mean temperature of the bubble phase, which can be expressed as:

$$\bar{T}_{bu} = \frac{1}{H} \int_0^H T_b dh = T_{eu} + (T_{in} - T_{eu}) \frac{U_b \bar{C}_p}{H_{be} H} \left( 1 - \exp(-\frac{H_{be} H}{U_b \bar{C}_p}) \right) \quad (5.12)$$

where the mean heat capacity for the reacting participants is as follows.

$$\bar{C}_p = \sum_{N=1}^{N_i} [\bar{M}_i]_{bu} C_{pM_i} \quad (5.13)$$

The dynamic molar balance for the  $i$ -th component for the emulsion phase may derived as

$$\begin{aligned} (V_{eu} \epsilon_{\min}) \frac{d[M_i]_{eu}}{dt} &= U_{eu} A_{eu} \epsilon_{\min} ([M_i]_{eu,in} - [M_i]_{eu}) \\ &+ \frac{V_{eu} \alpha_{eu} K_{be}}{(1 - \alpha_{eu})} ([M_i]_{bu} - [M_i]_{eu}) - R_v \epsilon_{\min} [M_i]_{eu} - (1 - \epsilon_{\min}) R_i \end{aligned} \quad (5.14)$$

The emulsion phase energy balance was expressed as

$$\begin{aligned}
 & \left[ \sum_{i=1}^m V_{eu} \varepsilon_{\min} [M_i]_{eu} C_{pi} + V_{eu} (1 - \varepsilon_{\min}) \rho_{pol} C_{p,sol} \right] \frac{dT_{eu}}{dt} = - \sum_{i=1}^m V_{eu} \varepsilon_{\min} C_{pi} \frac{d[M_i]_{eu}}{dt} (T_e - T_r) \\
 & + U_{eu} A_{eu} \varepsilon_{\min} \sum_{i=1}^m [M_i]_{eu,in} C_{pi} (T_e, in - T_r) - \frac{V_{eu} \varepsilon_{\min} H_{be}}{(1 - \varepsilon_{\min})} (T_e - T_r) \\
 & + R_v ((1 - \varepsilon_{\min}) \rho_{pol} C_{p,sol} + \varepsilon_{\min} \sum_{i=1}^m [M_i]_{eu,in} C_{pi}) (T_e - T_r) + (1 - \varepsilon_{\min}) \nabla H_r R_p
 \end{aligned} \tag{5.15}$$

The following equations have been used as initial conditions:

$$[M_i]_{bu,z=0} = [M_i]_{in}$$

$$T_b(z=0) = T_{in}$$

$$[M_i]_{eu,t=0} = [M_i]_{in}$$

$$T_e(t=0) = T_{in}$$

#### 5.2.4 The Inter-Phase Hydrodynamic Model

Generally, in the traditional constant bubble-sized and the well-mixed models, it is assumed that the emulsion would remain at its minimum fluidization ( $\varepsilon_{eu} = \varepsilon_{\min}$ ) condition and the bubbles would be solid-free ( $\varepsilon_{bu} = 1$ ). However, these assumptions do not permit the prediction of the impact of the gas-solid dispersal on the actual reactions along with the mass/heat transfer rate which would be present in the beds at velocities which are greater than the minimal fluidization velocities. On the other hand, experimental and theoretical data have shown the presence of the solids in the bubble phase (Gilbertson & Yates, 1996). Also, (Abrahamson and Geldart, 1980) (Gilbertson & Yates, 1996) stated that the emulsion phase would not stay at the minimal fluidization condition and it would also a greater gas concentration at greater velocities. When these two phases get mixed properly, it leads to an increased number of solid particles which

enter the bubble phase and also more gas (propylene) that enters the emulsion phase, whereas it also leads to an increase in superficial gas velocities in the bed. The phase interface(s) can be tracked by applying the continuity equation to the volume fraction for one or more than one phase. The equation can be calculated for the  $i^{\text{th}}$  phase as follows:

$$\left[ \frac{1}{M_i} \right]_{\text{in}} \frac{d}{dt} (\alpha_i M_i) + \nabla \cdot (\alpha_i M_i \bar{v}_i) = S_{\alpha_i} + \sum_{j=1}^n (\dot{m}_{i,j} \pm \dot{m}_{j,i}) \quad (5.16)$$

where  $(\dot{m}_{i,j})$  refers to the mass transfer from the  $i$  phase to the  $j$  phase. By default, the source term on the right side of the equation would always be  $S_{\alpha_i} = 0$ ; however, it could also be stipulated by the constant value or by the user-defined mass source value for every phase particulate loading

$(\ell_{\text{pt}})$ , which also affects the phase interactions. Particulate loading can be defined as the emulsion phase's mass density ratio to the mass density ratio for the bubble phase:

$$(\ell_{\text{pt}}) = \frac{[M_i]_{\text{eu}} \rho_{\text{eu}}}{[M_i]_{\text{in}} \rho_{\text{pp}}} \quad (5.17)$$

The multiphase model was studied for determining the behavior of the dynamic fluidized bed for the various important process parameters. This was conducted by using the software ANSYS 16.1 (ANSYS Inc., Berkeley, CA, USA), as this software provided a parallel and well-integrated computational service for estimating complicated multiphase flows and the effect of the process parameters on the propylene production rate. We have applied the Eulerian-Eulerian method for simulating dynamic phase behavior. The built-in mathematical PBM (Population Balance Model) and the moment methodology were applied for evaluating the production rate of the polymer in actual reaction environments. To explain further, the second-order time method is applied for all transport equations, which include the mixture-phase momentum equations, all the species transport equations, the energy equations, the turbulence



model, the phase volume fraction equation, the pressure-correction equation, and the granular flow model. It should be noted that solving a multiphase system is quite complicated and it could encounter several stability and convergence issues. Instabilities generally arise from the poor initial field, and, hence, this requires a stable initial field. Moreover, the CPU time also poses a concern with respect to the transient issues; therefore, we considered the PC-SIMPLE option. In this study, the momentum equation which was used depends on the fraction volume of all the phases throughout the material characteristics. We have suggested the multiphase mass transfer model which considers the mass transfer occurring between the species that belong to various other phases. In the model, rather than having a matrix type of data input, one needs to input the several mass transfer procedures.

**Table 5.3:** Transport equations for dynamic multiphase fluidized bed reaction system

No.	Type of equations	Equations
1	General transport equation	$\frac{d(\alpha\rho\phi)}{dt} + \nabla \cdot (\alpha\rho\vec{v}\phi) = \nabla \cdot \tau'' + S\phi$
2	The volume fraction dual-phase density	$\rho = \alpha_2\rho_2 + (1 - \alpha_2)\rho_1$
3	Momentum Equation	$\frac{d}{dt}(\rho\vec{v}) + \nabla \cdot (\rho\vec{v}\vec{v}) = -\nabla p + \nabla \cdot \mu I(\nabla \cdot \vec{v} + \vec{v}^T) + \rho\vec{g} + \vec{F}$
4.	The energy equation shared between the phases	$\frac{d}{dt}(\rho E) + \nabla \cdot (\vec{v}(\rho E + p)) = \nabla \cdot (k_{eff} \nabla T) + S_h$
5.	Inter-phase species transport equations	$\frac{d}{dt}(\rho Y_i) + \nabla \cdot (\rho\vec{v}Y_i) = -\nabla \cdot \vec{J}_i + R_i + S_i$
6.	Mass transfer in bubble phase	$S_b = R_{bi} (M_b \pm_i M_{bp})$
7.	Mass transfer in emulsion phase	$S_{eu} = R_{ei} (M_e \pm_i M_{ep})$
8.	The net velocity of the reactants	$\vec{u}_{net} = \frac{\sum r_j^r M_j^r \vec{u}_{r,j}}{\sum r_j^r M_j^r}$
9.	Momentum transfer for the bubble phase	$S_{bu}^{\vec{U}} = \mathfrak{R}_{i,p} (M_b \vec{U}_{net} - M_{bp} \vec{U}_i)$
10	Momentum transfer for the emulsion phase	$S_{eu}^{\vec{U}} = \mathfrak{R}_{i,p} (M_{eu} \vec{U} - M_{eu} \vec{U}_i)$

Every procedure then describes the mass transfer occurrence from a particular entity to other entities. An entity refers to either some species present in the phase or to the overall bulk phase if this phase contains no mixture in it. The mass transfer phenomena have been described using the user-defined functions, which have been developed. The dynamic multiphase fluidized bed requirements have been explained using the following transport equations in table 5.3.

In our present study, we have used the dynamic multiphase model, which was partially suggested by Khan et al. (Khan et al., 2016), and this model provided a better knowledge of the various hydrodynamic phenomena and also improved the quantitative knowledge of the real process. In any bubbling FBR, the upward movement of the bubbles can lead to better mixing of the solid particles within the emulsion or the dense phase. This can lead to a uniform concentration of the different particles and even temperature within the dense phase. Hence, a CFD-based pseudo-homogeneous model is also adopted for this phase. The gas bubbles move upwards in the bed with a fixed velocity while the particles move downwards, and they display an increase in size and mass when they flow in the downward direction. This justifies the use of the plug flow within the bubble phase. We have made the following assumptions for developing equations for the proposed improved model:

1. The polymerization reaction takes place in both the emulsion and the bubble phases.
2. The emulsion phase would be well mixed and it would not stay at minimal fluidization conditions.
3. We have assumed that the bubbles are spherically shaped and possess a uniform size. They have also been assumed to travel upwards in the fluidized bed in a plug flow with constant velocities.

4. The resistance of the mass and heat transfer within the gas and the solid particles present in the bubble and the emulsion phases have been assumed to be negligible (refers to very low or moderate catalytic activities).
5. The agitation which results from the upwards flow of the bubbles leads to negligible radial concentrations and temperature gradient in the FBR.
6. Elutriation of the solids on the upper layer of the FBR is considered to be negligible.
7. It has been assumed that the size of the particles is constant within the bed.
8. The reactor uses materials that flow in a pseudo-homogeneous phase. The hydrodynamic features of the bed are defined using the average hydrodynamic properties of the existing phases (emulsion and bubble).

Considering the above-mentioned assumptions, we present the dynamic material balance equations for all components present in the FBR:

For bubbles:

$$\begin{aligned}
 & [M_i]_{bu,(in)} U_{bu} A_{bu} - [M_i]_{bu} U_{bu} A_{bu} - R_v \varepsilon_{bu} [M_i]_{bu} - K_{be} ([M_i]_{bu} - [M_i]_{eu}) V_{bu} \\
 & - (1 - \varepsilon_{bu}) \frac{A_{bu}}{V_{br}} \int R_{i,bu} dt = \frac{d}{dt} (V_b \varepsilon_{bu}) [M_i]_{bu}
 \end{aligned} \tag{5.18}$$

For emulsion:

$$\begin{aligned}
 & [M_i]_{eu,(in)} U_{eu} A_{eu} - [M_i]_{eu} U_{eu} A_{eu} - R_v \varepsilon_{eu} [M_i]_{eu} - K_{be} ([M_i]_{bu} - [M_i]_{eu}) V_{eu} \\
 & - \left( \frac{1}{1 - \varepsilon_{eu}} \right) R_{i,eu} = \frac{d}{dt} (V_b \varepsilon_{bu}) [M_i]_{eu}
 \end{aligned} \tag{5.19}$$

Moreover, we have assumed that the mass transfer direction is from the bubble phase to the emulsion phase. The energy balances can be expressed as for bubbles:

$$\begin{aligned}
& U_{bu} A_{bu} (T_{bu,(in)} - T_r) \sum_{i=1}^m [M_i]_{bu,(in)} C_{pi} - U_{bu} A_{bu} (T_{bu} - T_r) \sum_{i=1}^m [M_i]_{bu} C_{pi} - R_v (T_{bu} - T_r) \\
& \left( \sum_{i=1}^m \varepsilon_{bu} C_{pi} [M_i]_{bu} + (1 - \varepsilon_{bu}) \rho_{pol} C_{p,pol} \right) + H_{be} (T_e - T_b) V_b - V_b \varepsilon_b (T_{bu} - T_r) \sum_{i=1}^m C_{pi} \frac{d}{dt} [M_i]_{bu} \quad (5.20) \\
& = \left( V_b \left( \varepsilon_{bu} \sum_{i=1}^m C_{pi} \frac{d}{dt} [M_i]_{bu} + (1 - \varepsilon_{bu}) \rho_{pol} C_{p,pol} \right) \right) \frac{d}{dt} (T_{bu} - T_r)
\end{aligned}$$

For emulsion:

$$\begin{aligned}
& U_{eu} A_{eu} (T_{eu,(in)} - T_r) \sum_{i=1}^m [M_i]_{eu,(in)} C_{pi} - U_{eu} A_{eu} (T_{eu} - T_r) \sum_{i=1}^m [M_i]_{eu} C_{pi} - R_v (T_{eu} - T_r) \\
& \left( \sum_{i=1}^m \varepsilon_{eu} C_{pi} [M_i]_{eu} + (1 - \varepsilon_{eu}) \rho_{pol} C_{p,pol} \right) - (1 - \varepsilon_{eu}) R_{p,eu} \Delta H_R + H_{be} V_{eu} \left( \frac{\alpha_{bu}}{1 - \alpha_{bu}} \right) (T_e - T_b) - V_b \varepsilon_b (T_{eu} - T_r) \sum_{i=1}^m C_{pi} \frac{d}{dt} [M_i]_{eu} \quad (5.21) \\
& = \left( V_{eu} \left( \varepsilon_{eu} \sum_{i=1}^m C_{pi} \frac{d}{dt} [M_i]_{eu} + (1 - \varepsilon_{eu}) \rho_{pol} C_{p,pol} \right) \right) \frac{d}{dt} (T_{eu} - T_r)
\end{aligned}$$

### 5.2.5 Coupling Steps of Multiphasic CFD-Based Reaction Model

To correlate the turbulence, population balance and energy equations in a multi-fluid UDF framework, a systematic CFD reaction kinetic coupled modeling framework application of multiphase polymerization in the fluidized bed reactor was executed. The CFD-based coupled model constitutes a flexible platform. Hence, its applications can be expanded to different polydisperse multiphasic FBRs by altering the geometry and constitutive equation. The generic model comprises four main steps, as shown in Figure 5.1:

- Problem definition
- Problem specification
- Model structure/solution
- Model applications

The concentrations of the species (propylene) for which the source term is a nonlinear function determine the stability of the UDF-coupled CFD simulation. This shows that

the reaction rate is highly sensitive, and hence cannot be eliminated in the multiphase reaction simulation procedure.

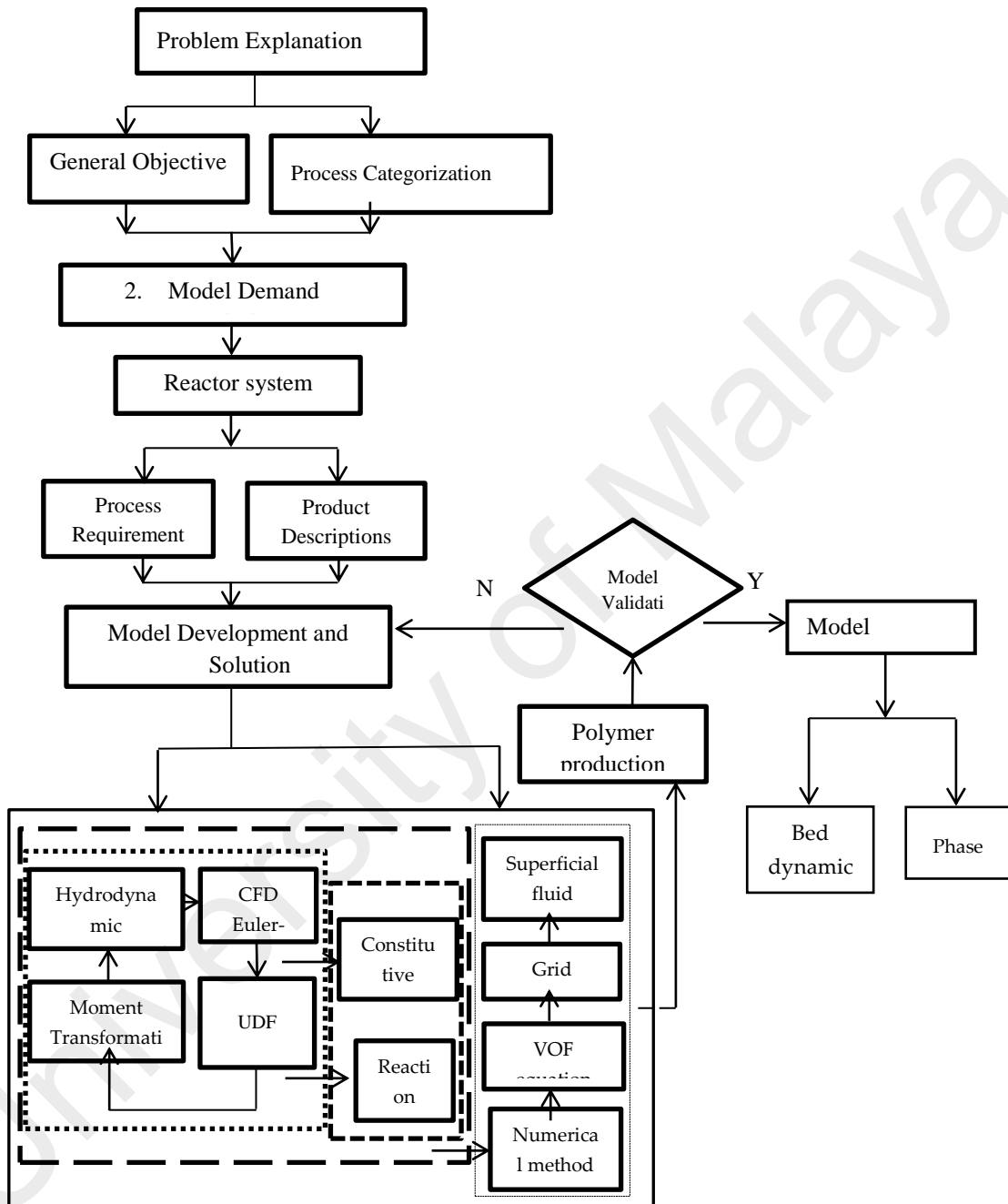


**Figure 5.1:** Steps of CFD-based multiphase reaction model development.

### 5.2.6. Grid Sensitivity Analysis

The greater the resolution, the more independent the grid outcome is. This was confirmed with the help of a two-dimensional (2D) analysis that employs the boundary-and-gradient adaptation technique. In this procedure, the adjoined mesh points could be present in high-gradient areas in the inlet and fluidization regions. The response variations at three mesh resolutions with 56,834, 89,101 and 111,143 node numbers are shown in Figure 5.2a–c. The parameters considered for the simulation include 1.5 m of bed height, 1000 s real time and 0.2 m/s superficial gas velocity. Figure 5.1 demonstrates the three separate grids used to divide the 2D flow domain into square cells. Hence, it can be said that grid resolution plays an influential role for the response, as evident in Figure 5.2 a–c.

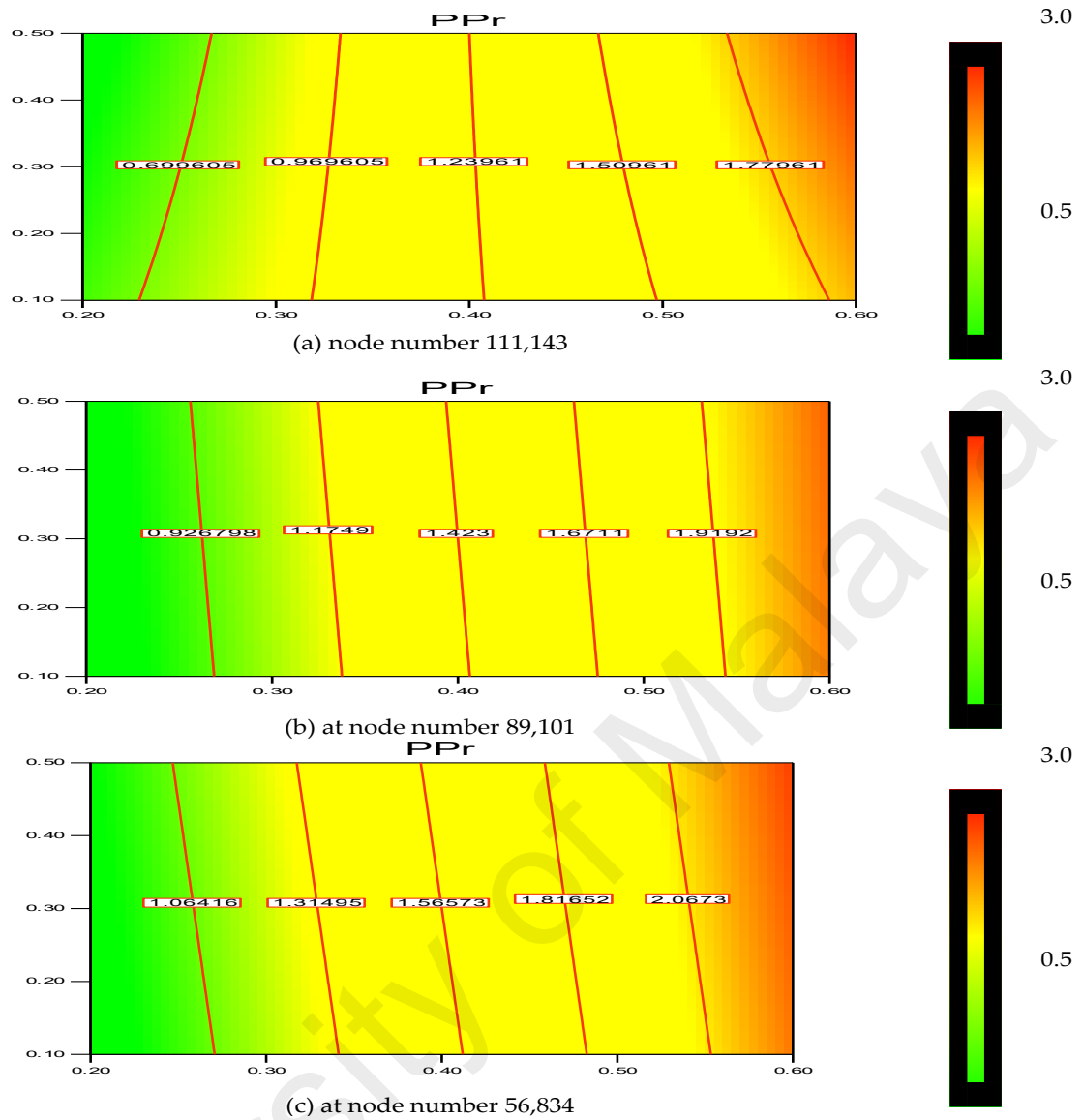


**Figure 5.2:** (a) Changes of the polymerization rate at node number 111,143 at various superficial gas velocities. Contour lines indicate the polymerization (%) changes; (b) Changes of the polymerization rate at node number 89,101 at various superficial gas velocities. Contour lines indicate the polymerization (%) changes; (c) Changes of the polymerization rate at node number 56,834, at various superficial gas velocities. Contour lines indicate the polymerization (%) changes.

Thus, according to the nodes' variation, it is found that the polymerization percentage variation is in the range of 0.699%–1.779% when the node number is at 111,143. However, with the decrease in grid resolution (from node number 111,143 to 89,101), the response value also reaches a range of 0.926%–1.919%. Hence, the response calculation becomes less accurate as the node number decreases. Moreover, at node number 56,834 the polymerization percentage varies in wider range from 1.064%–

2.067%. In this scenario, it has been verified that node number 111,143 should be considered as a compromised establishment for calculation and necessary accuracy. Thus, during the simulation on the pilot scale, sufficient grid convergence with a small polymerization difference from 0.699% to 1.779% at 111,143 nodes is required to achieve a more precise outcome. Figure 5.3 depicts the overall computational domain and mesh generation.

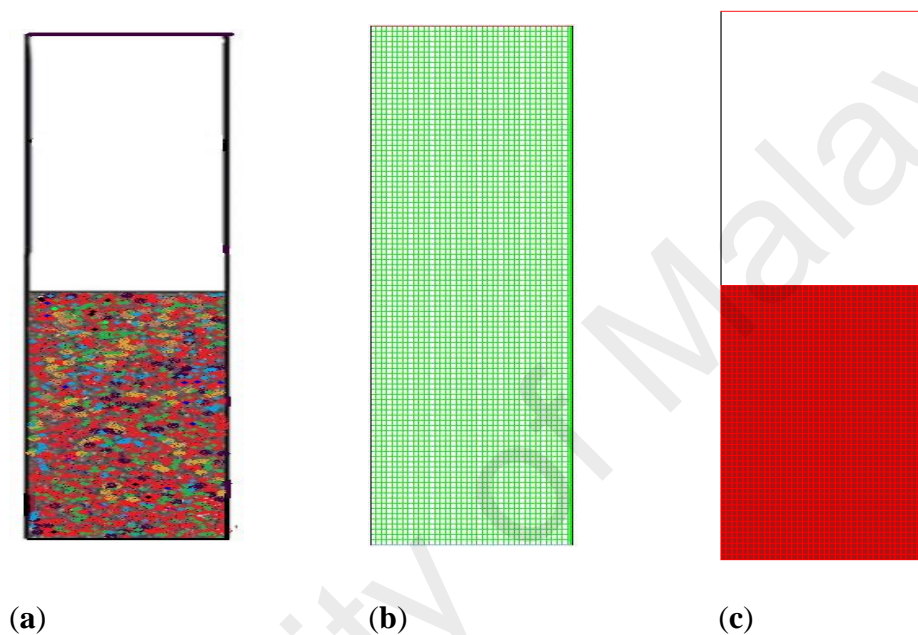


**Figure 5.3:** General computational domain and mesh generation. (a) Framework of the gas-phase fluidized bed polymerization reactor used in the simulation; (b) Generated mesh for the fluidized bed simulation; (c) Computational region marked.

Figure 5.3a shows a sketch of the fluidized bed packed with granulated particles. The meshing and the marked domain are shown in Figure 5.3 b & c respectively.

### 5.3 Experimental Facilities

A pilot-level fluidized bed reactor has been built in the pilot-scale Research Laboratory at the University of Malaya. The major aim of constructing this kind of experimental unit was to examine the catalytic polymerization reaction of the olefins at actual operating conditions which are similar to industrial parameters. In Figures 5.4–5.6, we



have described the picture, the data acquisition method and a detailed diagram of the pilot-level fluidized bed reactor.

This reactor consists of the fluidized bed and the product discharge zone. The reactor has an inner diameter of 10 cm while the fluidized bed zone height is 150 cm. Both the diameter and the height of the discharge zone are 25 cm. The catalyst particles have been introduced into the fluidized bed in the form of an injection at 9 cm above the gas distribution point. The product specimens were then withdrawn from three separate locations, *i.e.*, at the points which were 16, 26, and 40 cm above the position of the distributor plate. The polymer that is produced is discharged in a semi-continuous manner by opening the valve that is attached to the vessel at the point which is 5 cm over the gas distribution point. The gas distributor consists of a stainless steel plate which is perforated and consists of a fine mesh. The gas flow is controlled with the help of the control valve and is measured using the flow meter situated in front of the reactor. The fluidized bed reactor has one important requirement, wherein the recycled gas stream velocity should be enough so that the bed is always in a fluidized state.

Very pure quality raw material is needed for the catalytic olefin polymerization reaction to prevent the catalyst from being poisoned. The nitrogen, hydrogen and propylene have been purified in different purification systems (*i.e.*, Entegris Gate Keeper gas purifiers) for removing any traces of impurities of water vapor, oxygen, or carbon monoxide. For measuring the flow of hydrogen, nitrogen and propylene, three separate mass flow meters (Brooks, Hatfield, PA, USA) have been applied in the fresh feed streams.

For temperature measurements, it is hard to combine a high enough sample frequency to obtain a dynamic signal with the robustness of the equipment needed for industrial measurements. To overcome this problem we have fabricated seven temperature sensors at various points of the reactor. Secure and resilient pressure sensors with a high

frequency of response have been set up at four positions (see in Figure 5.6). If a probe of appropriate size is selected, direct contact between the fluidized particles and the sensor can be prevented without interrupting the temperature and pressure signal. Also, the interaction between the highly reactive gaseous chemicals and the probe can be averted by directing a small purgative gas flow.

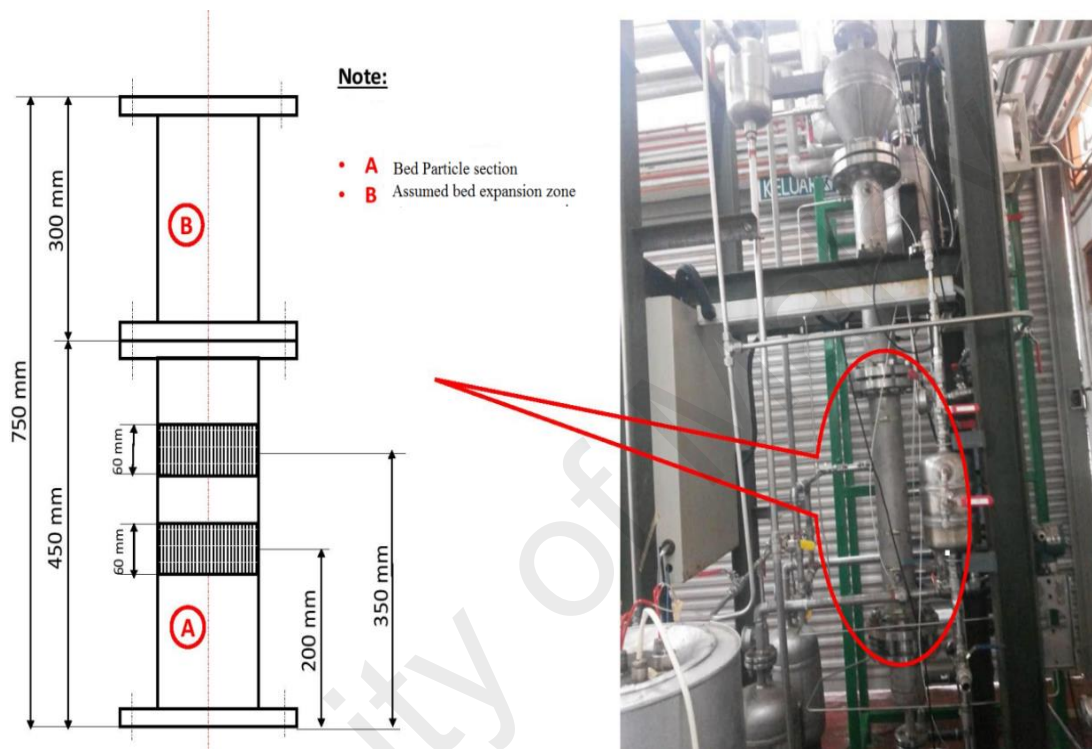
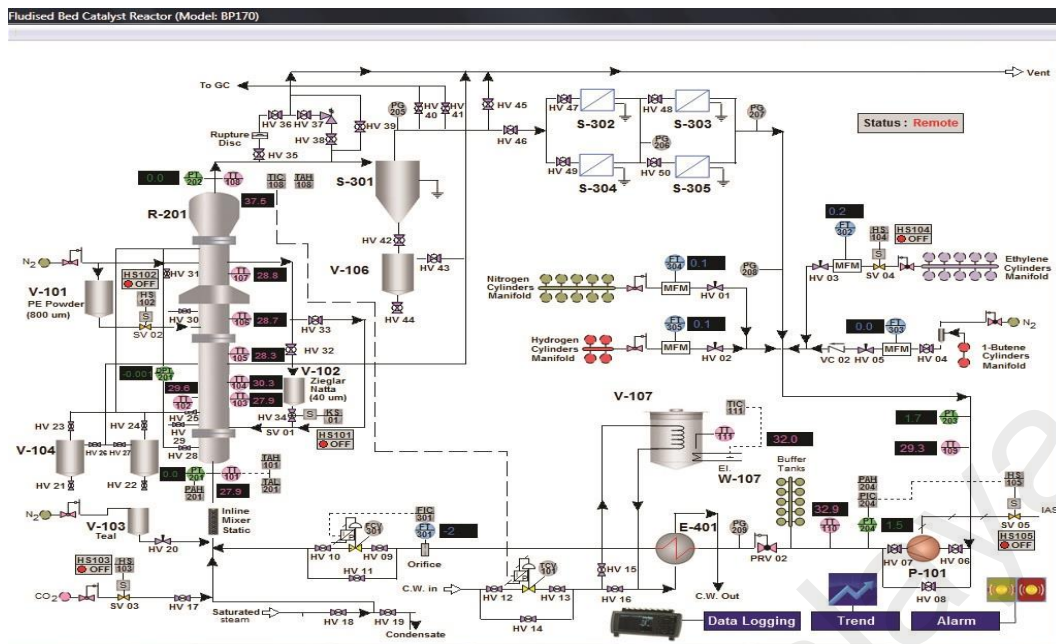


**Figure 5.4:** Image of the pilot-scale FBCR for polypropylene production where the experiments were conducted for this study (detailed dimensions have been shown in mm).



<b>V-101</b> PP Powder Feed Tank Stain less steel 304 0.20 m (D)×0.35 m(H) Capacity Approx. 10-L	<b>V-102</b> Catalyst Feed Tank Stain less steel 304 0.10 m (D)×0.15 m (H) Capacity Approx. 2-L	<b>V-103</b> CO-Catalyst Feed Tank Stain less steel 304 0.10 m (D)×0.15 m(H) Capacity Approx. 500mL	<b>V-104</b> Product discharge Tank 1 Stain less steel 304 0.20 m (D)×0.35 m(H) Capacity Approx. 10-L	<b>V-105</b> Product discharge Tank 2 Stain less steel 304 0.20 m (D)×0.35 m(H) Capacity Approx. 10-L	<b>V-106</b> Cyclone Hooper Stain less steel 304 0.15m (D)×0.15 m(H) Capacity Approx. 2.5-L	<b>V-107</b> Thermal Oil Bath Heater 4kW Capacity Approx. 20-L
<b>R-201</b> Fluidized Bed Reactor Stain less steel 304 4" (D)×1.5 m(H) Disengagement 10" (D) ×10" (H)	<b>S-301</b> Cyclone Hooper Stain less steel 304 Body Dia 0.06 m	<b>S-302/S-304</b> Inline Filters Aluminum casing; SS wire mesh Max Operating Pressure 40 bar Max particle size 40 micron	<b>E-401</b> Gas cooler Shell & Tube Heat Exchanger Carbon Steel Exchange area Approx. 0.8 m <sup>2</sup>	<b>P-101</b> Gas Booster Type: Air Driven Piston Pump Max Outlet Pressure 55 bar	<b>W-107</b> Cartridge Heater	

**Figure 5.5:** A Real-time data acquisition system for the pilot-scale FBCR for polypropylene production.

### 5.3.1 The Catalyst Dosing Measurement System

In the actual world, engineers find the measurement of the catalyst dosing in high pressure and heated polymerization reactor systems very difficult. In this report, we have reported the first device that was designed in the Department of Chemical Engineering, University of Malaya (UM). KROHNE Messtechnik GmbH, Germany, manufactured the specialized solid powder measurement device according to the request of UM. All the device features and components are presented in Table 5.4 and Figure 5.7. The device has been designed according to the FMCW (Frequency Modulated Continuous Wave), a radar level meter for measuring level, distance, volume and mass for several powder sizes, granules and all other solids. This form of measurement is more stable as compared to the pulse radar and is also better suited for dusty procedures.

This device operates at high and low temperature values when the chemical process-connecting temperature values have been fulfilled.

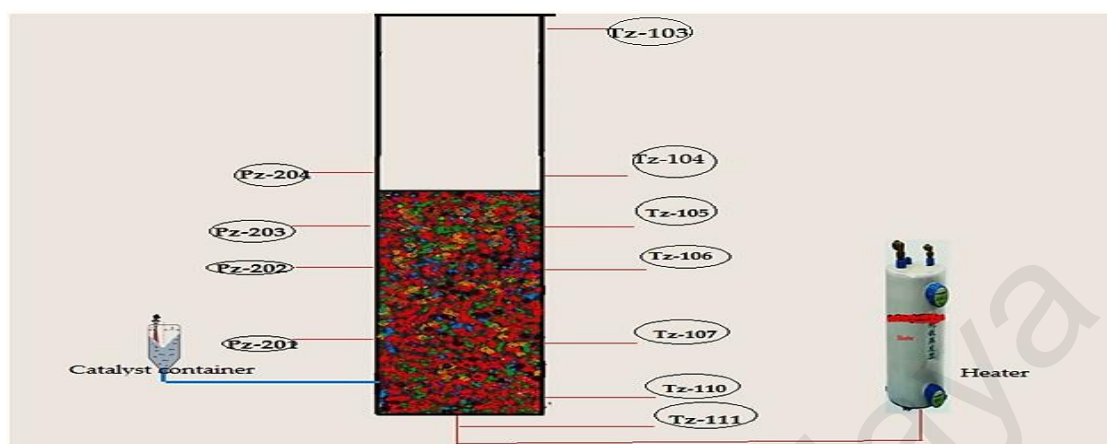


**Figure 5.6:** Pressure and temperature profile measurement scheme for real-time data acquisition system (fluidized bed has been shown before gas mixer introduction in the system).

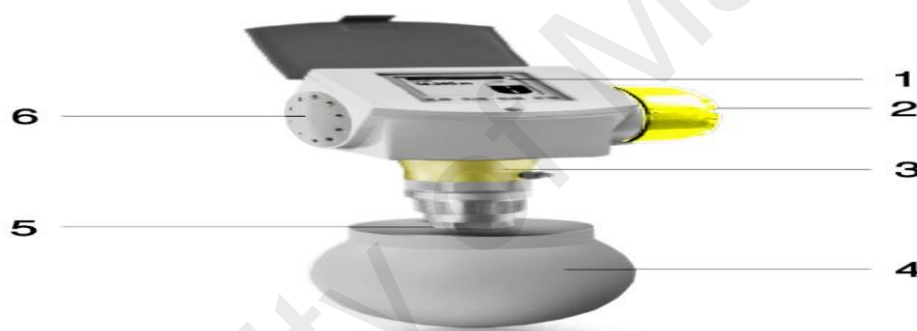


**Figure 5.7:** The catalyst dosing measurement device. (1) An elective touchscreen with a dose-controlling optional button; (2) A dual-wire reading meter; (3) A changeable and a rotatable converter consisting of a rapid connector technique; (4) Horn antennas (made of stainless steel); (5) A flange plate protector (needed for aggregating products) with extension services; (6) A single converter for many applications.

**Table 5.4:** Features of the catalyst dosing system.

Issues	Condition
accuracy	standard accuracy, $\pm 10$ n.gm (nano gram)/ $\pm 0.4\%$
Inserted antenna/sensors	The shape prevents unexpected product build-up in complex dusty applications
Stability in extreme reaction conditions	Sensors can sustain at $200\text{ }^{\circ}\text{C}$ ( $392\text{ }^{\circ}\text{F}$ ) temperature and 40 bar/580 psig pressure
Measuring range	Wide-ranged measurement capacity (up to 80 m/260 ft)
Data acquisition facility	Directly accessible graphic touchscreen/wizard (option 1) and optional second station (connected desktop computer) output
Prioritized particle	Ziegler-Natta catalyst

#### 5.4 Results and Discussion

Using the improved multiphasic phase and conventional mathematical model, the phenomena of gas-solid reaction with dynamic fluidization behavior modeling and simulation investigations of the propylene polymerization in the pilot scale fluidized bed reactor was conducted to prove the effects on the dynamic response and phase shift of the process of various hydrodynamic sub-models, model assumptions, and mixing conditions. To calculate the effect of key parameters like  $U_0$ , catalyst dosing rate, monomer feed concentrations on the polypropylene production rate and fluidized bed dynamic situation during real reaction conditions, comparative and comprehensive simulations were done. Table 5.5 shows the operating conditions where simulations were carried out.

University of Malaya

**Table 5.5:** System boundary and operating conditions used for simulation.

<b>Factors</b>	<b>Value</b>
Reactor volume	0.0215 m <sup>3</sup>
Initial bed height (m)	1.5
Initial void fraction	0.431
Gas density (kg/m <sup>3</sup> )	23.45
Catalyst diameter	3.0 × 10 <sup>-4</sup> m
Gas viscosity (Pa·s)	1.14 × 10 <sup>-4</sup>
Mole fraction of hydrogen	2000 ppm
Cocatalyst concentration (mol/L)	0.01
Solid density (kg/m <sup>3</sup> )	1039 m <sup>3</sup>
Coefficient of restitution	0.8
Angle of internal friction	30
Maximum solid packing volume fraction	0.75
Time step (s)	0.001
Activation energy, $E$ (J·mol <sup>-1</sup> )	7.04 × 10 <sup>4</sup>
Active site of catalyst (mol·m <sup>-3</sup> )	1.88 × 10 <sup>-4</sup>
Feed monomer concentration (mol·m <sup>-3</sup> )	1.0
Hydrogen concentration (mol·m <sup>-3</sup> )	0.02
Inner diameter (Reaction zone)	0.1016 m
Cross sectional area	0.00785 m <sup>2</sup>
Height	1.5 m
Volume	0.011775 m <sup>3</sup>
Inner diameter (Disengagement zone)	0.25 m
Cross sectional area	0.0490625 m <sup>2</sup>
Height	0.25 m
Volume	0.0097 m <sup>3</sup>

Given the advantages that the improved multiphasic model has over the prior ones, one can expect the improved model to give a result that is more realistic when compared to the conventional mathematical model. Moreover, it is worth noting that experimental validation of this type of model has been done for the first time. The results obtained exhibited the fact that this system's improved multiphasic model agrees well with the experimental data.

#### 5.4.1 Hydrodynamic Model in the Absence of Polymerization

In the process of devising an FBR, the pressure fluctuations are considered a critical parameter. They help determine the bubble dynamics in the system and quantify the intensity of the fluidization regime, even at oscillated velocity levels, by adjusting the bed height. At the pre-polymerization phase, bed height and pressure drop are vital parameters to examine the overall fluidization structure. To validate the proposed model, a CFD simulation between literature data and the developed model of the bed height *versus* superficial gas velocity are compared thoroughly. In this model, the top of the bed was set as a constant pressure outlet and the uniform inlet velocity was designed keeping in mind the inlet boundary conditions. The pilot-scale reactor has a cylindrical geometry containing the operational superficial gas with the velocity ranging from 0.2 to 0.6 m/s. We did not take into account the effects of front and back walls in this model. A no-slip wall boundary condition was used for the gas phase and a free-slip wall boundary condition was used for the solid phase. We assume that the bed is in the initial well-mixed condition and all velocities were set to zero at  $t = 0$ . The value of the void fraction was 0.53 and the static bed height was 1.5 m. The outlet pressure boundary condition was set at 25 bar. A detailed list of boundary conditions is provided in Table 5.5 and a dynamic correlation among these conditions is presented in Table 5.2.

It was evident that a surge in the superficial gas velocity resulted in an increase in the bed height (see Figure 5.8).

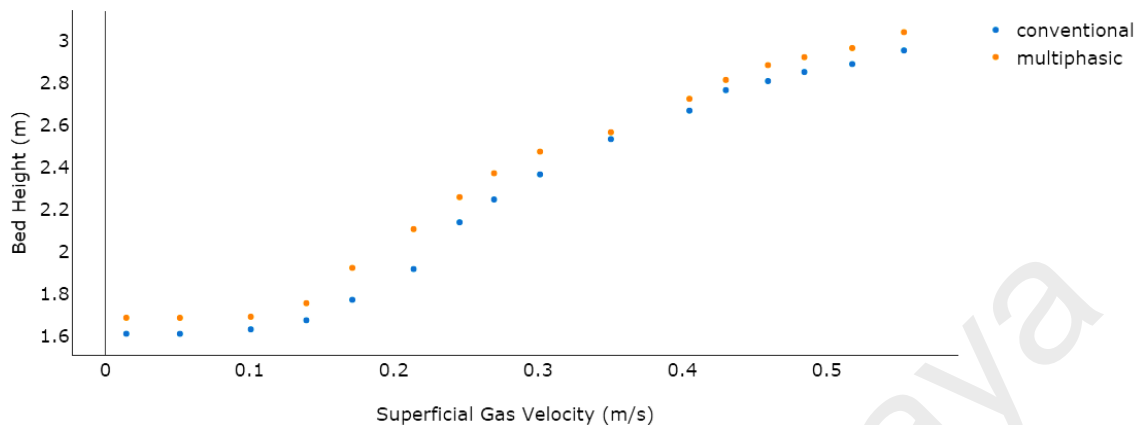


**Figure 5.8:** Dynamic bed behavior analysis between multiphasic and conventional model (without reaction).

Both the models proved to be in a good agreement with regards to bed expansion and the initial bed was predicted at 1.5 m in both. It was also noted that on increasing the superficial gas velocity, the maximum bed expansion for the available literature model reached 2.9104 m, while the multiphasic model's highest bed expansion was found to be 3.1203 m, which proves the good agreement between the two models.

#### 5.4.2. Bubble Emulsion Phase Distribution and Model Verification

Optimum propylene polymerization during the previous work Khan, et al. (Khan et al., 2016) was discovered to have reached levels of around 6% per pass during the initial fluidization stage (Table 5.5 lists the simulated profiles). However, the very vital dynamic effects on the reaction rate were not considered in that work. By taking into consideration the dynamic parameters that are deemed as very significant process parameters for industrial-scale and commercial-grade propylene polymerization, this study has covered up that gap. As the reaction and fluidization proceed, the Ziegler-Natta catalyst, the catalyst feed rate, the superficial fluid velocity, and the monomer



concentration in the reactor would change the fluidization dynamics. How these parameters are distributed in the reactor should therefore be investigated.

Polypropylene concentration distribution and bubble and emulsion phase formation in FBR at  $U_0 = 0.2, 0.25, 0.3, 0.35, 0.4, 0.45, 0.50$  and  $0.55$  m/s can be seen in Figure 5.9. Because the inlet reactants have the highest concentration, the heat supplied from the system heating source heats up the particles when the mixed gases come in contact with the bed particles. The figures clearly show that the gas-solid distribution exhibits significant dynamic changes in the reactor. These simulation-derived results can also give clear information on the conception of bubble and emulsion phase formation. Figure 5.9 clearly demonstrates that the change distribution and the bubble size are greatly altered with a variation in the  $U_0$  value. The bubbles present at  $U_0 = 0.2$  m/s are lesser than those in other situations. Herein, the bubbles form and move upwards in the reactor system but there was no bubble breakage. This ensured that there were more options present for the solid and the gas phase to come into closer contact. On the other hand, by the continued increments of the superficial fluid flow rate, the phenomenon of the bubble collapse can be clearly noted, which leads to a lesser chance for the close contact of the solid and gas phase. Theoretically, this phenomenon has been previously supported (Che et al., 2015b). In this study, we have observed that the fluidized bed dynamics show a similar attitude when it reaches the  $U_0$  value of  $0.4$  m/s and continue until the value of  $U_0$  reaches  $0.55$  m/s. Figure 5.9 also shows the solid (bed particle) volume fraction development in the reactor where the average value is observed at  $0.65$  m/s. However, it is very important to determine if the  $U_0$  value has any impact on the propylene production rate or not. These issues have been highlighted in the subsequent section.

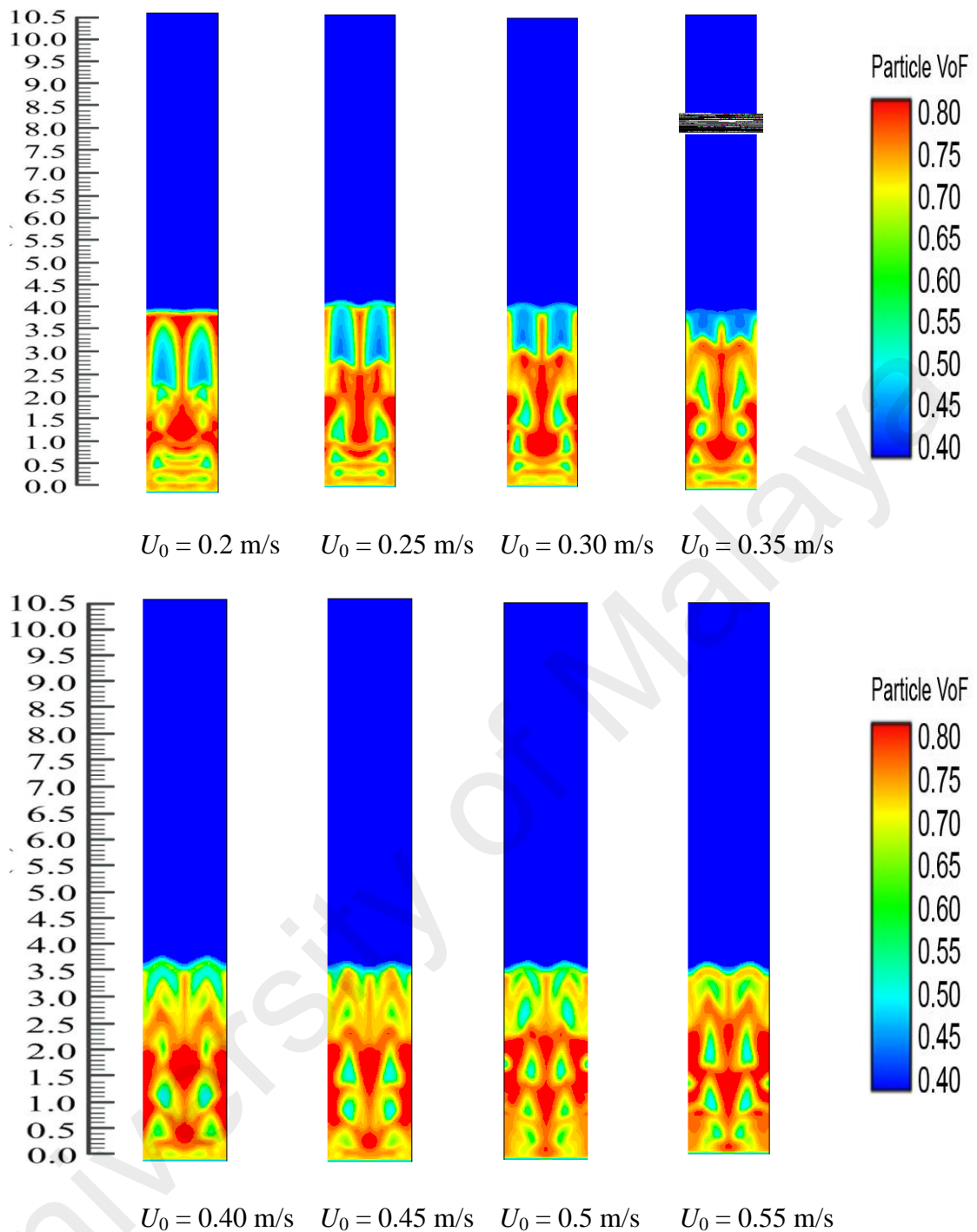


**Figure 5.9:** Dynamic effect of superficial gas velocity on phase (bubble and emulsion) formation before catalyst injection.

The fluidized bed dynamics after the catalyst's injection in the system are depicted in Figure 5.10. Catalyst dosing immediately starts the exothermic reaction and releases energy from the reaction. The heat transfer from the particles then heats up the gases surrounding the bed particles and also results in differences in the production rates of the polymer. Thus, throughout the reaction system, there is a change in the mass

fraction of the polymerized particle. Figure 5.10 shows the upward movement towards the bed of the polymer particle with the greater mass fraction. The figures also show the dynamic distribution in the FBR of the PP content profiles. This is due to the close positive relations among the reaction parameters. This also proves that dynamic catalyst activity determines the change in the gas/particle mass fraction in polymerization.

Figure 5.10 shows how, at the initial stage, the entire FBR has an identical propylene mass fraction distribution. The consumption of propylene and hydrogen and the generation of PP take place as the polymerization reactions go on. The distribution of the propylene mass fraction shifts until the flows of emulsion and bubble phases and the polymer distribution reach a stationary state (*i.e.*, 8 s). Along with the reactor height, the propylene mass fraction increases. This could be due to the fact that the hydrogen feed is limited and is consumed quickly to a relatively low level. Moreover, hydrogen has a significant impact on the reaction and deactivation rates. Under industrial conditions, a chain transfer with hydrogen is typically used to control the polypropylenes' molecular weight, as this method is considered the most efficient. The ratio between the overall propagation rate and the total chain transfer rate determines the molecular weight of a polymer sample. However, this weight is not influenced by the polymerization activity. During this period, a relatively small amount of low molecular weight polymers are produced through the supplement of a large amount of hydrogen to the system. At higher temperatures, degradation reactions of cocatalyst compounds may generate chain termination agents.

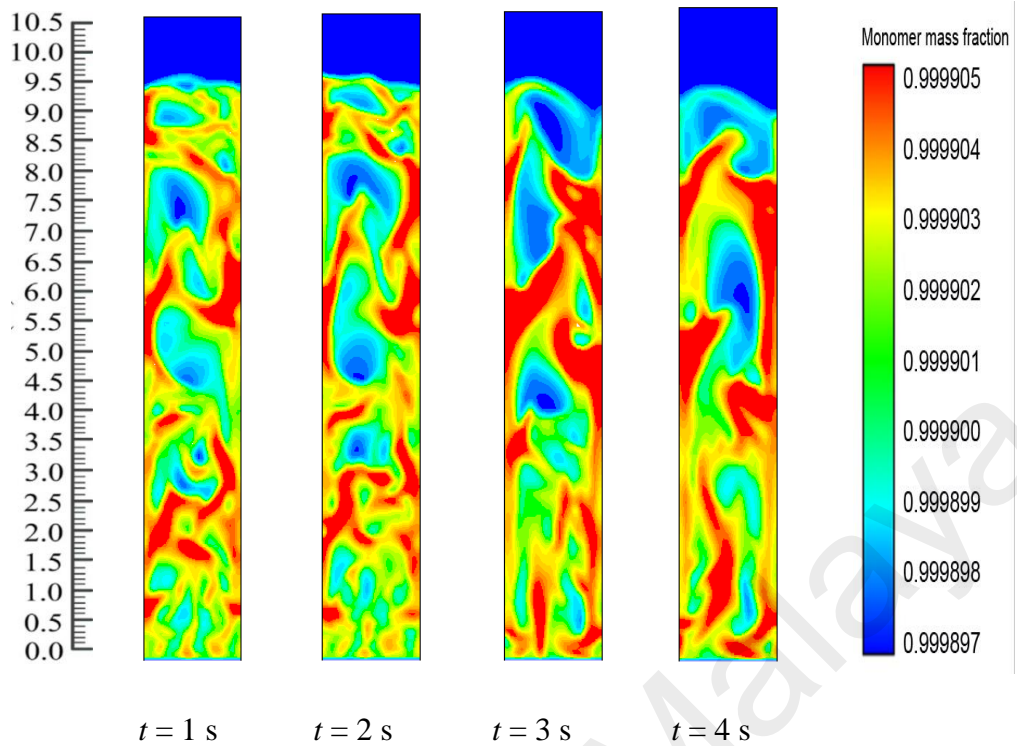


**Figure 5.10:** *Cont.*

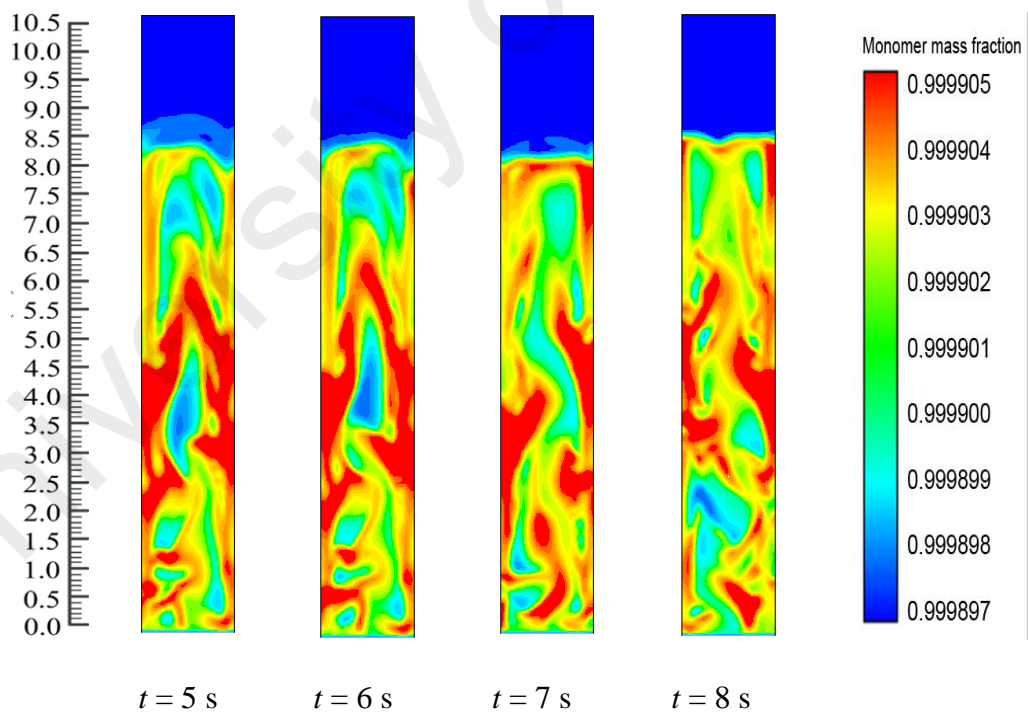


**Figure 5.10:** Mass fraction of monomer (propylene) during reaction at  $U_0 = 0.2$  m/s.

On the other hand, there is continuous polymerization to form PP. Moreover, since the FBR bottom has the highest catalyst concentration, the propylene mass fraction obtains

a minimum at the FBR bottom, and shows a slight increase due to the decreases of the hydrogen mass fraction. The dynamic mass fraction for the hydrogen gas is illustrated in Figure 5.11. The hydrogen mass fraction goes on changing from the reactor bottom and it moves upwards in the system continuously. However, eventually, the mass fraction stabilizes at  $t = 1.2$  s. However, it is worth mentioning that Figures 5.10 and 5.11 illustrate the dynamic distributions of monomer (propylene) and hydrogen mass fractions, correspondingly. Additionally, one can also clearly compare the dominance of the propylene presence against hydrogen in the system from these snapshots, as it is very important in real reaction conditions to get a clear idea of this phenomenon. In literature it has been mentioned that the sum of the mass fraction values of propylene and hydrogen is near 1, which is in close agreement to our finding (Chen et al., 2011; Chen et al., 2011; Zheng et al., 2011).

#### **5.4.3 Model Validation Based on the Effect of Superficial Gas Velocity**

The superficial gas velocity is an important process parameter because of its direct relationship to the propylene production rate, monomer residence time in the system, fluidization conditions, and particle mixing. It is therefore vital to study what effects it has on these process conditions. Figure 12 illustrates the various models that have predicted the impact of superficial gas velocity on the polymerization rate in the system. As  $U_0$  increases, the polypropylene production rate drops. The monomer mean residence time decreases when there is an increase in the  $U_0$ , which causes the monomer conversion and polymer production rate to decrease. Because the dominant emulsion phase is operating at conditions greater than the minimum fluidization velocity of gas, the production rate projected by the developed multiphasic model is greater than the conventional mathematical model. This leads to the emulsion phase having a lower void fraction and higher production rate. Compared to the predicted values of this

multiphasic model, the experimental values were a little bit higher. Similar trends of production rates were also revealed. However, due to the fact that the emulsion phase starts at conditions beyond the minimum fluidization velocity of fluid, the polymerization rate projected by the conventional model is lower. As a result, the emulsion phase has a greater void fraction and lower reaction rate.

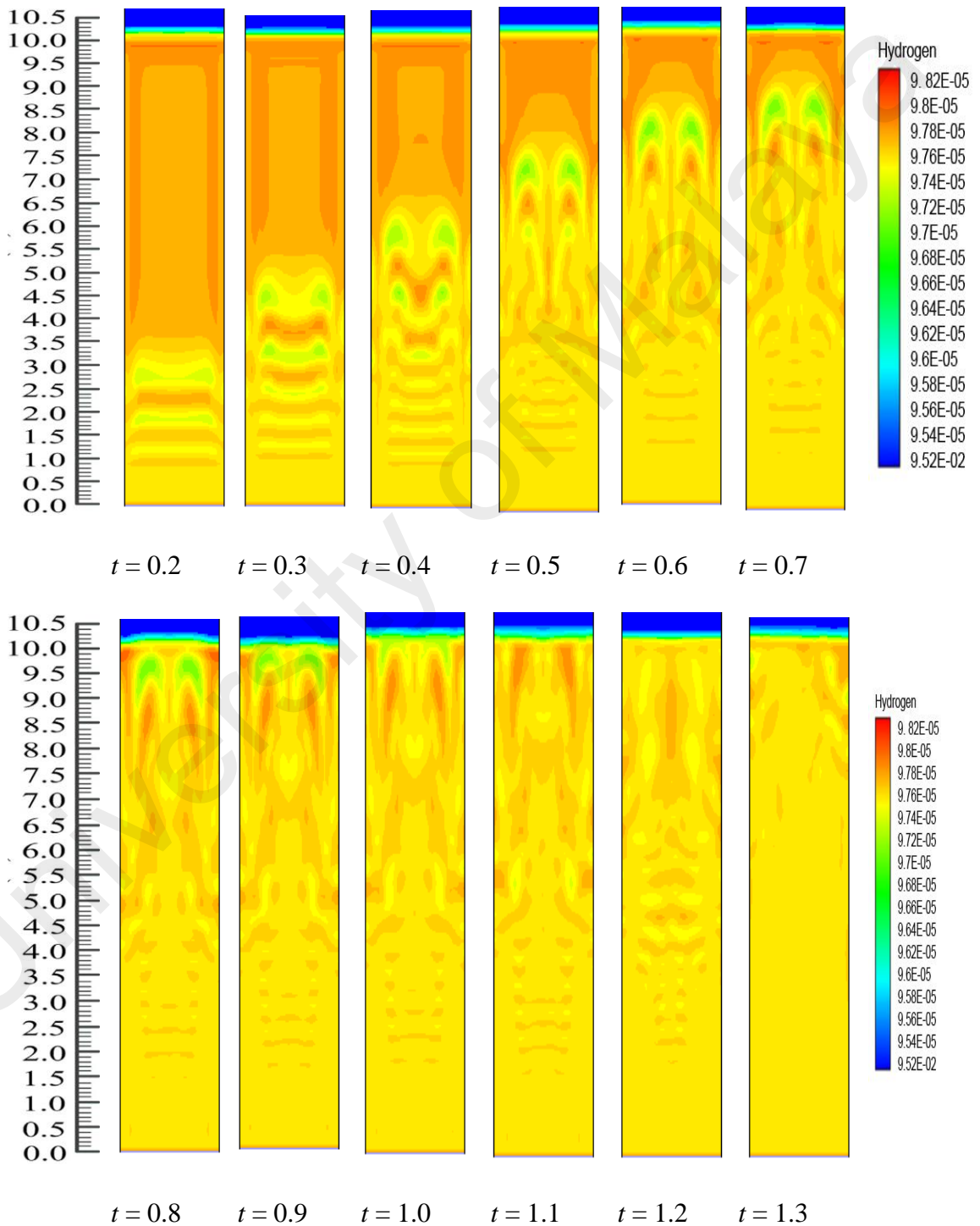


**Figure 5.11:** The dispersal transformation of hydrogen mass fraction due to alteration of time in the FBR at  $U_0 = 0.2$  m/s.

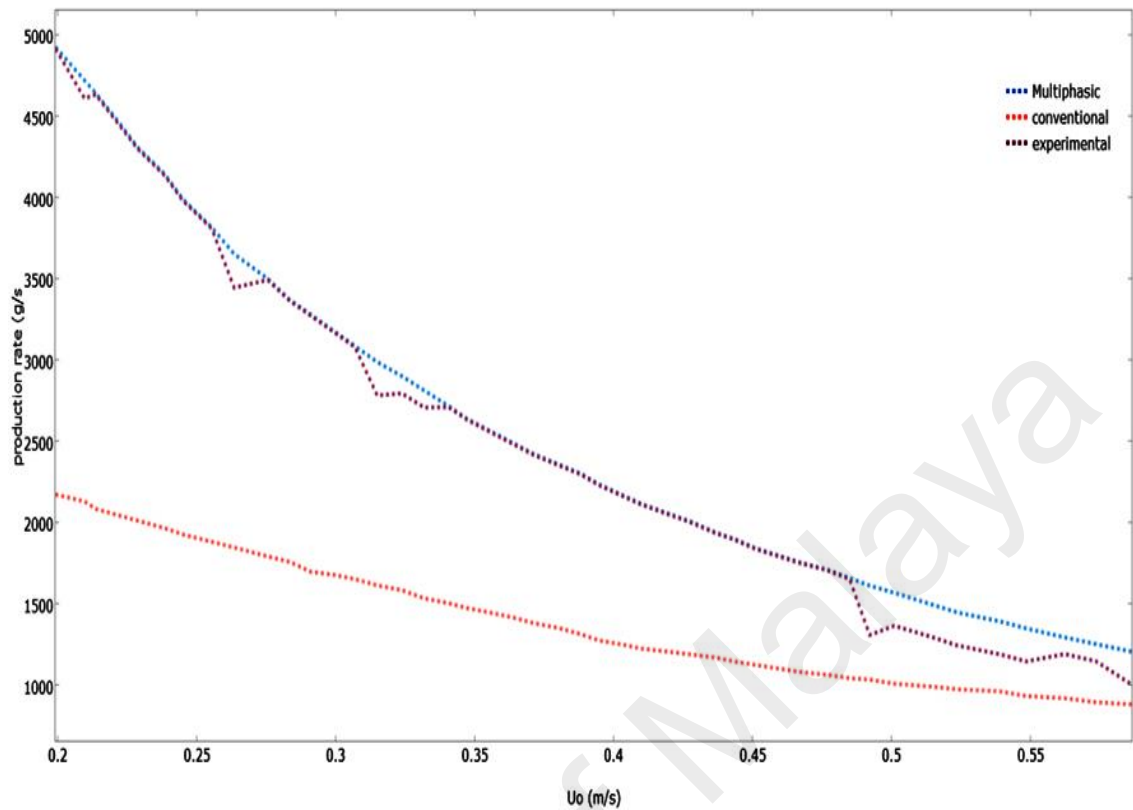


**Figure 5.12:** Effect of superficial gas velocity on the production rate (at optimum catalyst dosing 0.2 g/s).

Figure 5.13 illustrates the effect that  $U_0$  has on the polymerization rate of emulsion and bubble phases at varying Ziegler-Natta feed rates calculated by the multiphase model. The polymer production rate in the emulsion and bubble phases decreases when there is an increase in the value of  $U_0$ , because the monomer mean residence time is decreased. This results in a lower polymer production rate.

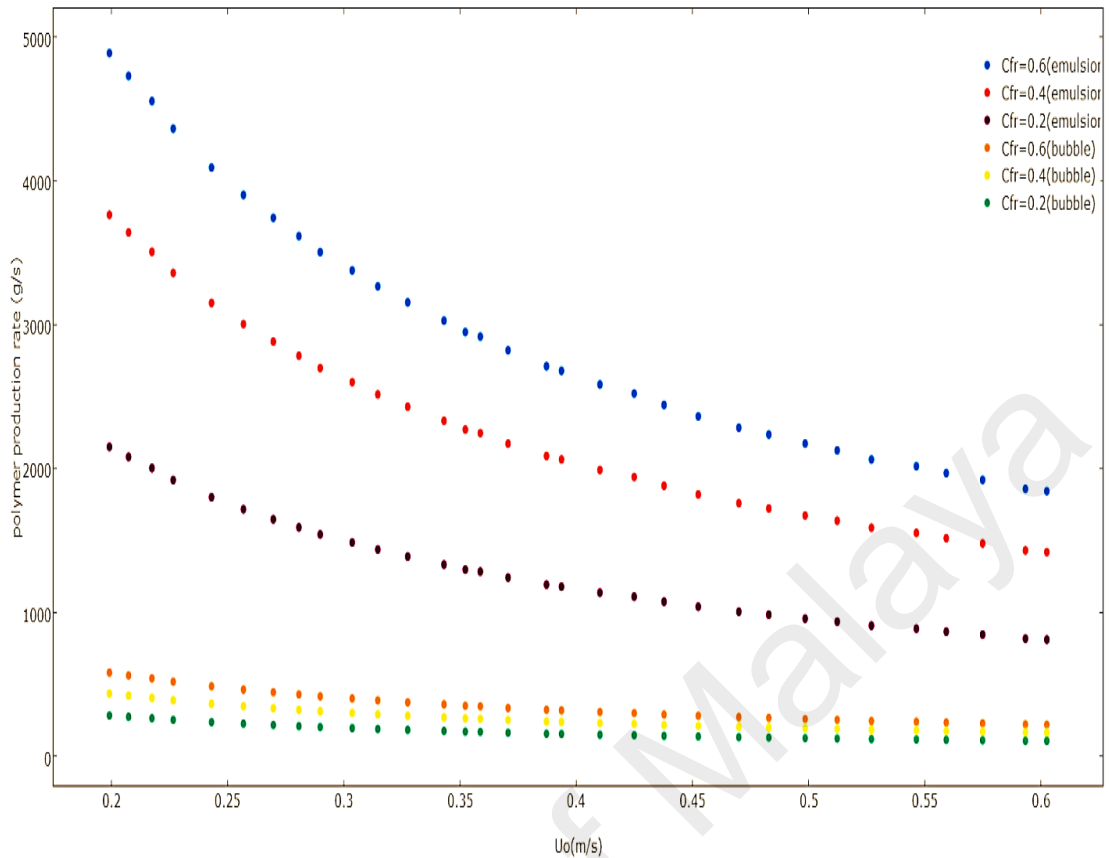


**Figure 5.13:** Effect of superficial gas velocity on the production rate of emulsion phases at various catalyst feed rates predicted by the multiphase model.

The multiphase model was also used to predict the effect of superficial gas velocity on the polymer production rate by considering the proportion of the bubble phase polymerization rate to the overall polymerization rate, which is shown in Figure 5.14. The figure reveals how the increase of the superficial gas velocity results in an increase in the proportion of polymerization in the bubble phase over the total polymerization rate. When the superficial gas velocity is increased, more fresh reactant and solids enter the bubbles. This leads to a rise in the bubble impact on the polymerization rate. The bubble influence on the overall polymerization is approximately 9%–11%. This is already a noteworthy amount and it should be taken under consideration for a more consistent model projection. This model has underestimated the polymerization rate in the bubble, because, based on the bed hydrodynamics, it can clearly be observed that most of the reaction zone is occupied with a well-mixed emulsion phase. It is logical to



assume that increased gas-solid contact results in the presence of larger amounts of catalyst. More space of contact between mixed active gases (propylene, hydrogen, and nitrogen) and catalyst can lead to an improved production rate.

To reduce the risks of agglomeration, high gas velocities are needed. However, the monomer conversion per pass through the reactor bed is reduced by high gas velocities and can result in greater elutriation of small particles from the bed.

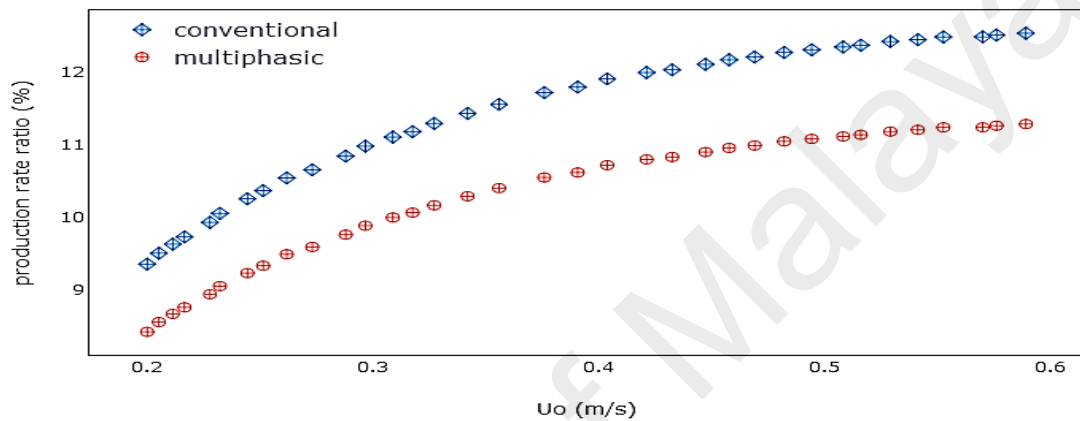


**Figure 5.14:** The ratio of polymer production in the bubble phase to the total production rate.

#### 5.4.4. Effect of Catalyst Feed Rate

Another key process parameter in the controlling of polypropylene FBCRs is the catalyst feed rate. Simplified hydrodynamic models do not take into account the presence of catalyst in the bubbles and consider that polymer production only takes place in the emulsion. However, the use of the multiphasic model made it possible to see that the emulsion phase contained about 91.7% of the catalyst while the bubbles had about 8.3% of the catalyst that was continuously charged into the reactor. The part of the reaction that takes place in the bubbles is therefore significant and must be considered.

When the fluidization is at a stable state, the polymerization reactions are at a steady state as well. In this case, the coupled model of the reacting flow can be verified using the product concentrations that are found in the FBR.

Figure 5.15 shows the catalytic dynamics. In the starting stage, catalyst particles that possess high active sites are produced at the bed bottom. Afterwards, particles with varying amounts are evenly mixed with gas. Solid also flows. In this situation, more polymer chain formation takes place by coordinating the monomer to the remaining active site of the Ziegler-Natta catalyst subsequently to insertion. Termination happens within a  $\beta$ -hydride elimination process; consequently, the highest number of the chains is comprised of a terminal double bond. In this case, the sum of  $\text{CH}=\text{CH}_2$  groups is equivalent to the amount of methyl groups, which indicates that the chain transfer is progressing by  $\beta$ -hydride elimination. The activity of the catalyst particles in the FBR has been assumed to be taking place at a stable rate, but a snapshot of the catalyst dosing dynamics reveals that the activity is actually changing at a relatively slow pace because of the decentralized catalyst particles and unstable motion of the bubble. When hydrogen is consumed and its concentration along the bed height decreases, the rate of polymerization throughout the bed becomes high and results in a slightly higher catalyst presence on the upper part of the bed.

One of the great aspects of this model is that the selectivity of ethylene and propylene, and even the other species of conversion catalytic reactions, is almost identical in the FBR during the propylene polymerization process, given the real reaction conditions of higher active catalyst. Despite being deduced at a pilot scale, this CFD-kinetic model can still be utilized for industrial-scale reactors because the reactor type's influence on the bulk reaction mechanisms can be neglected. The simulated data can be validated using the experimental data obtained from a practical FBR.

In Figure 5.16, the effect that the catalyst feed rate has on the polymerization rate that the two models predicted, and the production dispersal rate in the phases that was

calculated by the multiphasic model, can be observed. One can clearly observe how the polymer production rate and the catalyst feed rate are directly proportional. The polymer production rate increases when there is an increase in the catalyst feed rate because of the increase in the available active sites.

The improved multiphasic model predicts a polymer production rate that is lower than the conventional models in the bubble phase compared to the emulsion phase. This is because the improved dual-phase model takes into account the excess gas in the emulsion phase. This excess gas increases the void fraction and results in a decreased polymer production rate compared to the conventional models, which assume an emulsion phase that takes place at minimum fluidization. It can be seen in the improved dual-phase model that there is a higher rate of changes of production in the emulsion phase than that of the bubble phase. This is primarily due to the fact that there is more catalyst in the emulsion phase than in the bubble phase.

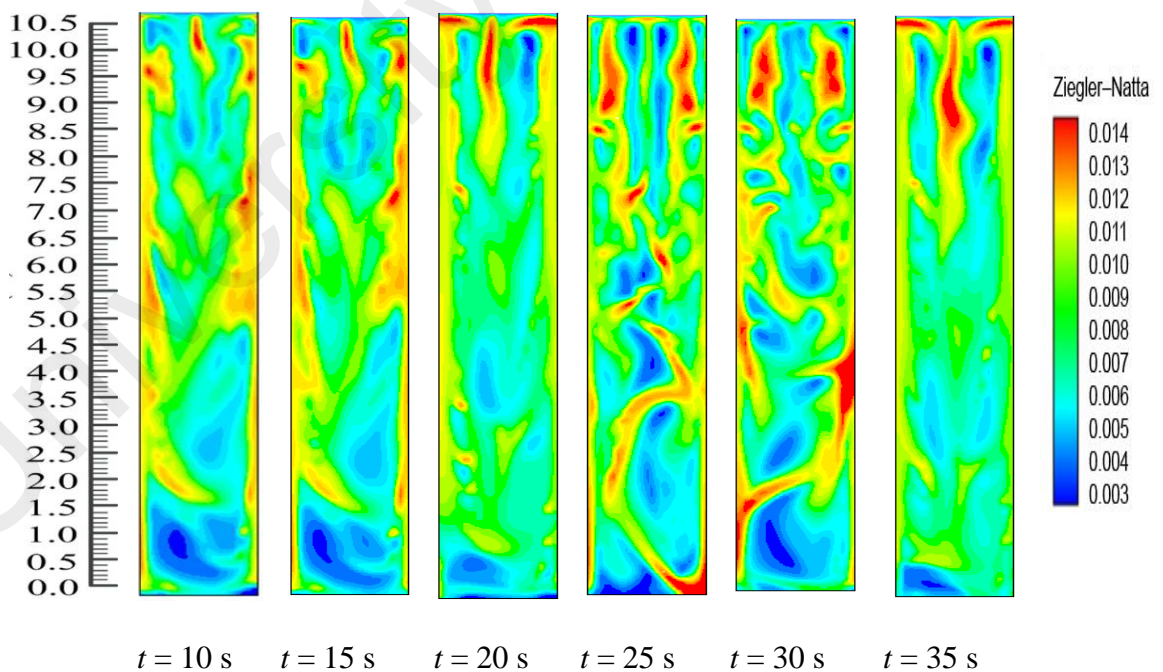


**Figure 5.15:** Snapshot of the solid volume fraction of catalyst particles with different time intervals in the FBR.

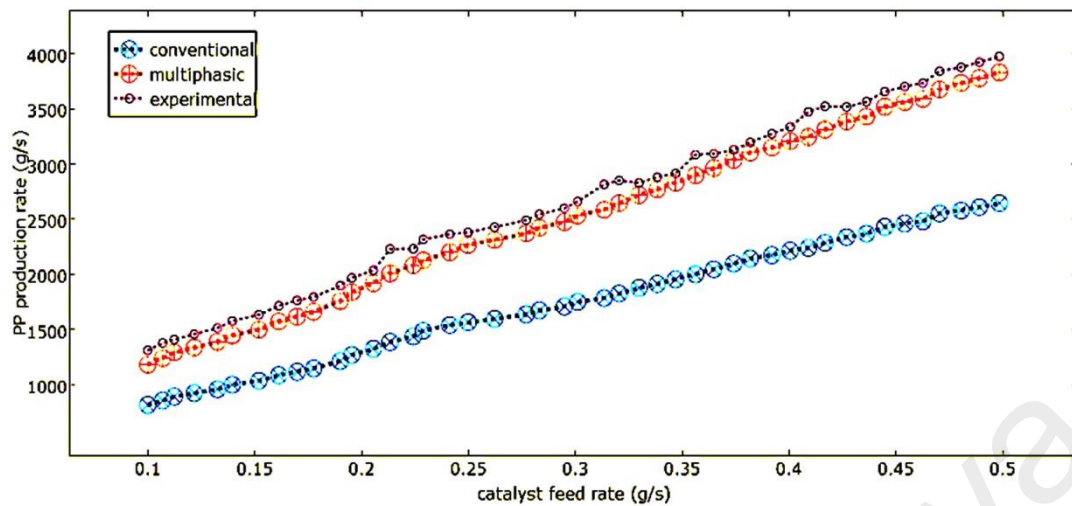


**Figure 5.16:** Effect of catalyst feed rate on polypropylene production comparison and validation.

#### 5.4.5 Effect of the Feed Composition

Figure 5.17 demonstrates the comparison between the multiphasic and the conventional model results for the pilot plant data with respect to the propylene concentration within the reactor. As seen in the Figure 5.17, the predicted data for the multiphasic model agrees well with our experimental results, especially in the case of the long gap of the time points. The multiphasic model takes into account the solid particles present in the bubbles and the fact that the emulsion phase is at a condition which is beyond the minimal fluidization; hence, it provides more accurate and realistic results. On the other hand, the multiphasic model under-predicts the experimental results for shorter time durations. This is due to the fact that there is a very high heat and mass transfer rate between the bubble and emulsion phases in the beginning of the process, where the difference in the concentrations between both the phases is maximal. This situation, present in the initial fluidization stage, changes the reactor approach hydrodynamics to a well-mixed condition (McAuley et al., 1994). However, this type of mechanism becomes unrealistic further in the process as more and more bubbles are formed and the heat and mass transfer rate is decreased. The maximal variation that is seen between our experimental results and the predicted values for the multiphasic and the conventional

model is approximately 3.0 and 4.5 mol %, respectively. This difference results because of the influence of the inert gases on the fluidized bed reactor's hydrodynamic behavior.

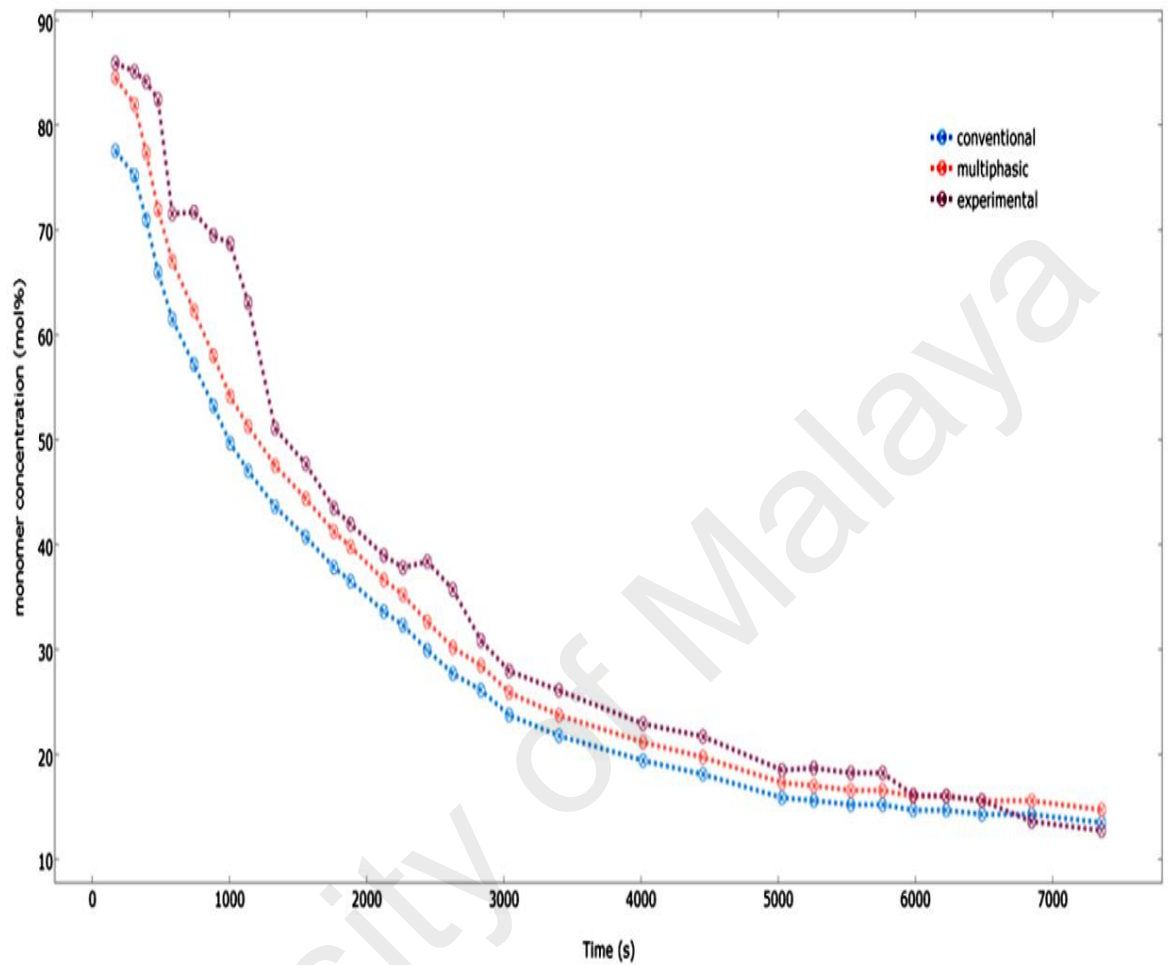


**Figure 5.17:** Effect of monomer composition (mol %) on polypropylene production.

## 5.5 Summary

A coupled CFD-dynamic mathematical model that assimilates the sub-models which describe the polypropylene production resulting from phase transition and gas–solid flow behavior in a gas-phase fluidized bed reactor was formulated. The dynamic bubble and emulsion phase concepts of fluidization served as bases for the hydrodynamics of the fluidized bed reactor of polypropylene production. This model was able to successfully capture the important flow features in a pilot-scale catalytic FBR. These features include the superficial fluid velocity, monomer-hydrogen concentration, catalyst feed rate, and the product concentrations inside the reactor at reacting-flow conditions. Moreover, analyses of the polymerization rate in individual phases, the monomer concentration in individual phase distributions in the reactor, and the ratio of polymer production in the bubble phase to the total production rate were done. An analysis of the effects of the main operation parameters on the reacting flow field was also done. A summary of the findings can be seen below.

- (1) With the use of the multiphase model, an investigation of the evolution of hydrodynamic phenomena in the FBR in typical fluidization states with different gas velocities was done. The developed model was also able to capture the gas–solid flow pattern, especially the solid flow pattern, something that was unobtainable using only the Eulerian–Eulerian method. This particular particle flow pattern promotes exceptional particle mixing, catalyst activation efficiency, and heat transfer, all of which are essential to the FBCR since the catalytic propylene polymerization process is an exothermic one.
- (2) Under reaction-flow conditions, the simulation by the multiphase model was conducted. Moreover, the effects of catalyst dosing, product mass fractions in the FBR at different regions, and the PP content bubble and emulsion phases were obtained. The results showed that the parameter distributions at different regions

have significant differences for the polymerization process. The dynamic particle density distribution in the FBR is determined after injecting the catalyst and at various times. Because there is excellent contact within the catalyst and the solid and gas capability of the FBR, there is a uniform product fraction distribution in FBR.

- (3) The conventional model was discovered to have predicted a lower emulsion phase production rate and propylene concentration under typical operating conditions. On the other hand, the improved multiphase model agreed better with the experimental values. Compared to the conventional model, the improved multiphase model also predicted a narrower and safer operation window at the same operating conditions. The improved multiphase model showed that if one considers the practical range of the superficial gas velocity from 0.2 to 0.55 m/s and the catalyst feed rate from 0.2 to 0.6 g/s, the ratio of polymer production in the bubble phase to the total production rate will be calculated at around 9.4%–10.89%. This amount is significant and should be considered in the model. Moreover, it was revealed that the hydrodynamics and the reaction rate are strongly affected by the superficial gas velocity and catalyst feed rate. As a result, there is greater variation in the total production rate ratio. The improved multiphase model reveals that, at the beginning of polymerization, there is dynamic behavior that is close to the experimental results, but those figures also start to differ as the time increases.

In summary, this work has shown that a multiphase polypropylene production model can be a useful guide in integrating process engineering efforts with reactor design efforts in the field of chemical engineering.

## **CHAPTER 6: EFFECT OF DYNAMIC PROCESS PARAMETERS ON PRODUCTION RATE OF POLYPROPYLENE AND THEIR MECHANICAL FEATURES: FROM VALIDATING MODELS TO PRODUCT ENGINEERING**

### **6.1 Introduction**

To eventually attain complete operational safety and consistent high quality of production, it is imperative to set up an effective process parameters monitoring system. The necessity to design processes and equipment in the chemical industry resulted in the origin of chemical engineering (Charpentier et al., 2002). It emerged as a discipline and was formally instituted more than a century ago. Customarily, the prime intent of chemical process engineering is to transform raw materials to functional products by using process design and analysis. On the other hand, chemical product engineering largely comprises the design of the product and the production process so as to meet the requirements of the customer and foster the competitiveness of the businesses. (Hill et al., 2009; Santos et al., 2014). At present, it is very crucial for modern chemical corporations to develop chemical products with unique properties. Hence, both process engineering and product engineering are commonly identified as the two principal constituents of chemical engineering. Product engineering has become a fast evolving concept and it is inviting a great deal of interest from both academia and industry (Kim et al., 2004; Kim et al., 2011; Park et al. 2003; Yang et al., 2014). However, it has to be considered that the advancement of product engineering is dependent on the fundamental theories of chemical process engineering.

So far, new chemical products have been developed conventionally with modelling and simulation techniques based on the knowledge of prevailing products (Dubey et al., 2016; Hadi et al., 2015; Khan et al., 2014). When product quality is of utmost



importance and the available knowledge on the development of industrial scale reaction system is inadequate, then product design essentially depends on real-time experimental data. Besides, the experimental expenses might significantly increase if industrial scale utilities are considered for trial and error-based experiments. Due to this, developing a systematic product design technique that can minimise experimental work in the absence of comprehensive data has become a difficult task. Hence, pilot scale experiments are commonly proposed by scientists and engineers for this purpose (Khan et al., 2014; Khan et al., 2016; Wang & Yuan, 2014). An industrial prototype that can create real reaction environments to establish the all-inclusive relationships between product properties and processing conditions from micro- to macro-scales can prove to be a promising tool for new and innovative chemical product development (Bayat et al., 2015; Jang et al., 2010; Mahmud et al., 2008; Shum et al., 2008). In this research, the formation of commercial grade polypropylene (PP) was studied to explain the efficiency of our unique product development approach.

For many years, intensive studies have been conducted to understand the mechanical properties of polymers. This class of materials has garnered a great deal of attention from the industry and academia solely due to its unique properties and immense potential for alteration of properties (Aharonovich et al., 2013; Krajenta & Rozanski, 2015; Shim et al., 2002). Specifically for the automotive industry, the mechanical properties resulting from quasi-static tests are of importance (Schoßig et al., 2006). The mechanical properties of polymers, which also include plastic behaviour, are most significant for various applications of polymers (Ha, & Han, 2016; Wu et al., 2016). The effects of process parameters on supermolecular structures formed during polymerisation need to be considered to completely describe plastic deformation of such materials (Pešić et al., 2016). In most studies, the impact of real-time process

parameters, such as the system pressure and reaction temperature, was not evaluated. Only a few reports indicate the importance of impact of controlling the concentration of hydrogen on production rate but not on the structure and physical state of polypropylene (Hu et al., 2016; Nojiri et al., 2016). To meet this objective, the mechanical tests that are performed in the plastic industries are considered. As APLACO, Saudi Arabia, is one of our research collaborators (product quality aspects), we have carried out the mechanical properties testing as APLACO practicing.

However, fluidised bed reactors (FBRs) are one of the most widely used commercial reactors to develop polyolefin (Banaei et al., 2015; Che et al., 2015a, 2015b; Guidolini et al., 2016). Hence, high-performance product development is performed using FBRs. Meanwhile, some of the extremely important mechanical properties, such as Dynamic Mechanical Analysis (DMA), Tensile Strength, Hardness Test and Izod Impact Testing, and Melt Flow Index (MFI) are intensely impacted by the operating environments of the reactor, for example, the gas-solid fractions (that is, the gas and solid flow field) and are directly associated with the FBR behaviour of multi-scale polymerisation. It is already acknowledged that the polymerisation kinetics, along with the mechanical properties of the polymer product, are affected by hydrogen (Nojiri et al., 2016).

In spite of this, it is challenging to perform a comprehensive experimental observation on multi-scale process parameters. In a complete real-time experimental project for a pilot scale reactor, it is necessary to consider composite gas-solid two-phase flow, and particle-reactor and particle-particle interactions, along with dynamic trends that include pressure, system temperature and hydrogen content.

Four new concepts are presented in this study. The first would be the evolution of dynamic process parameters in combination with reaction models developed for olefin

polymerisation. A single experimental report is available which involved gaseous phase propylene homopolymerisation in fluidised-bed reactors, wherein polymerisation in batch was performed, in a basic dynamically-balanced scheme with a single phase as suggested by Meier et al. From this, a compartmented reactor scheme was developed from smaller-scale in their study and not just pilot-level reaction processes. Second, our research is the pioneering research where comprehensive processing parameters have illustrated the results of non-linear reaction conditions in reactors at pilot scale. Profiles of temperatures in seven varied zones of reactions are reported, while the profiles of pressures were also taken in four varied areas. The literature on propylene polymerisations has until recently only reported on explorations of profiled averaged temperatures and pressures. Third, the regulation of catalytic doses is seen as the most critical task in estimating propylene polymerisation. A distinct method for controlling catalytic doses has been evolved for our pilot-level production process, as well as the associated rules for dose estimations. And finally, industrial-standards characterisation studies on controlling hydrogen throughout the process have been carried out. Product-quality trial studies involving hydrogen concentrations in the actual conditions of reactions have not been previously conducted.

It is therefore our goal to provide clear-cut dynamic explanations of the concurrent process parameters and how these influence the physical properties of commercial-grade polypropylenes, in order to assist industrial-engineering and academic specialists in their decision-making.

## 6.2 Choice of measurement technique

In literature, it has been stated that because the industrial fluidised beds characterise harsh conditions, the only standard measurement methodologies in industrial fluidised bed reactors consist of pressure and temperature measurements. However, measuring and observing average pressures and temperatures does not always provide sufficient information (van Ommen et al., 2011). Ommen et al. (Ommen et al., 2004) gave an example of average pressure and temperature measurements being insufficient for a process operator of a fluidised bed reactor to recognize the abnormal behaviour of multiphase fluid dynamic problems that took place in the bed. Bartels et al. (Bartels et al., 2015) presented that without the occurrence of defluidisation, the average decrease in pressure does not ascertain the rate of production and clustering of plastic particles in a laboratory-level fluidised bed at high temperature.

More advanced measurement techniques could be used to obtain better data on the fluidized bed hydrodynamics in order to improve the operation quality. Many of these techniques are very local, i.e., they give information about a small measurement volume. Examples are capacitance and optical measurements for solids volume concentration, heat transfer measurements, and solids flow measurements by suction probes (Bartels et al.). Another possibility is provided by image analysis techniques for particle size measurements (Saayman et al., 2013). A point of attention is that some of these techniques may disturb the flow, and could consequently give measurement results that are not representative for the undisturbed hydrodynamics. Moreover, these techniques are less useful for obtaining a general impression of the overall state of the hydrodynamics in the whole fluidized bed (or at least in a substantial part of the bed) due to the small measurement volume. Rather than moving to other measurement techniques, one can also try to extract more information from the only two measurement

techniques that are routinely applied: pressure and temperature measurements (Khan et al., 2014). In our present research we have add another dominant process parameter, hydrogen, to measure. So far, there is not a single study has been reported on the combination of these three dynamic process parameters. By performing pressure, temperature or hydrogen measurements at a high enough data sampling frequency, dynamic information can be obtained instead of average data only. For temperature measurements, it is hard to combine a high enough sample frequency to obtain a dynamic signal with the robustness of the equipment needed for industrial measurements. To overcome this problem we have fabricated seven temperature sensors at various point of the reactor. Secure and resilient pressure sensors with high frequency of response have been set up at four positions [see in Figure-6.1].

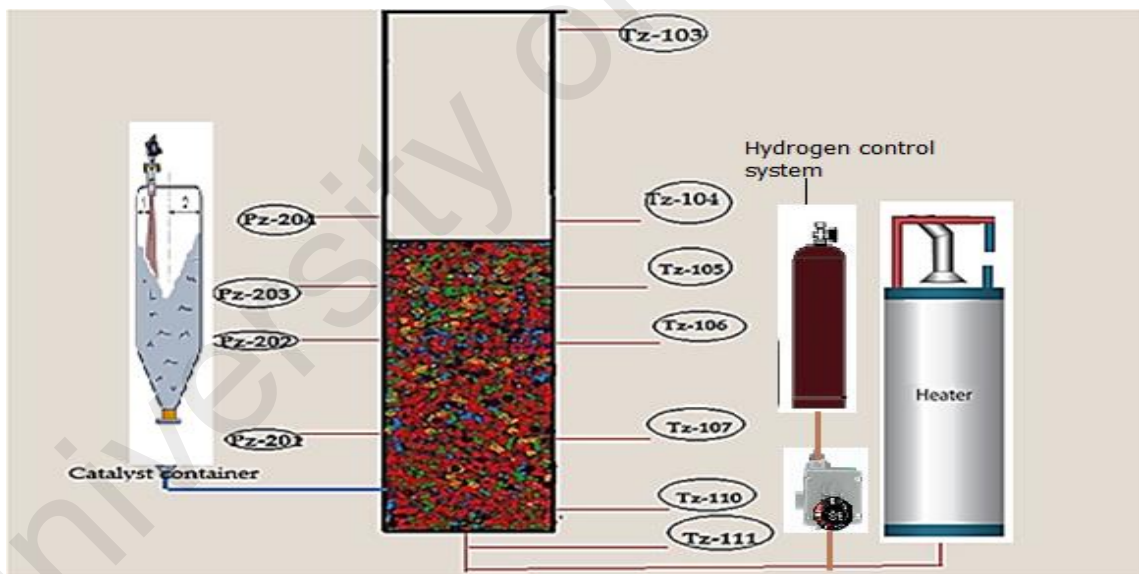
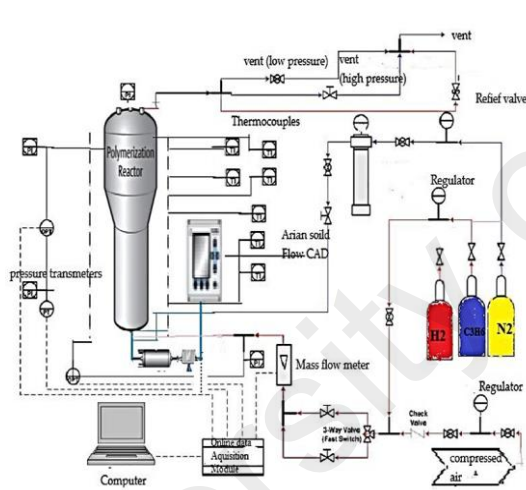


**Figure 6.1** : Pressure and temperature profile measurement scheme for real-time data acquisition. (fluidised bed has been shown before gas mixer introduction in the system)

### 6.3 Experimental setups :

The experimental setup is illustrated in Figure-6.2. The experimental setup constituted of a pilot level fluidised bed reactor (150 cm long and 10 cm internal diameter) designed and developed by the Polyolefin Research Group of University of Malaya,

Malaysia and the Research and Development Centre of Malaysian National Petroleum Corporation (PETRONAS Research Sdn Bhd). The reactor with reactant gases that has the potential of operating at pressures up to 30 bar and temperatures up to 200 °C, was externally heated using electrical heater and regulated by an integrated control system (that enables control of flow, temperature, pressure and feeding control). A gas purifier ENTEGRIS (0.003 micron) is used for supplying gases, such as, Hydrogen, Nitrogen and Propylene. For the calculation of rate of gas flow, a calibrated ADMAG AXF (YOKOGAWA-Japan) flow meter was installed with the adoption of the Dual Frequency Excitation (DFE) technique.



2 (a)



2(b)

**Figure 6.2:** Detailed schematics of the pilot scale fluidised bed reactor for polypropylene production , 2 (a) and pilot scale fluidised bed reactor at University of Malaya, 2 (b) .

Moreover, this enhanced Dual Frequency Excitation has been added to tackle more severe applications. The gas mixture was introduced into through the metal meshed gas distributor. The column was constructed of stainless steel. At seven points, the temperature of the fluidisation gas was recorded using Tz10X series thermocouples (SRU3G-F/C-60 model, Willium Inc. USA) temperature sensors. The pressure was measured in four points using pressure transmitters (PzX1000). The Dactron's RT Pro

Dynamic Signal Analysis Series Software, BP-170, program was used to log all the data collected from the temperature, pressure, and gas meter in a data file.

The rate of reaction can be computed from the rate of hydrogen feed necessary for keeping the pressure and temperature constant throughout the experiment. This procedure was followed for producing the polypropylene for analysing mechanical properties. Only hydrogen concentration was varied. To be able to carry out experiments up to 25 bar, the liquid propylene in the system is maintained at a minimum temperature of 70°C. Also, all the channels of the propylene supply system are kept at 70°C, to avoid condensation of propylene.

#### **6.4 Model development**

We have taken the complex catalytic reactions under consideration for explaining the kinematic factors of propylene homopolymerisation. Factors for production rates of polypropylenes were described with the kinematic-momentum approach. In the cases of reactive monomers (as expressed in sequences of differential- and algebraic-type equation sets), the required mass-balance equations were independently employed in the various bubble/emulsions phases, for fluidized bed reactors contain the highly active catalyst sites. This resulted in an improved representation of the conditions confronting the diverse catalysts (Ziegler-Natta).

This model comprises a set of continuity and momentum equation for the bubble/emulsions phases. Couplings of reaction rates and active parametric functions are achieved in the determinations of each pressure- and interphase-exchange coefficient. The manner in which the scheme manages the couplings is dependent on the phase classes which are included. For example, granular gases-to-solids flows are

handled differently in comparison to that of non-granulated or fluid-to-fluid flows. These properties were obtained by employing dynamic theories in the examinations of granular flows, and the modelled mixtures also influence momentum exchanges between each phase. The User-Defined Function, or UDF, of ANSYS FLUENT, which allows customisations of the momentum-exchange computations, was used in this study.

The application of both multi-phasic and kinematic models supports the analyses of fluidised-bed reactions. As some mathematical theories are critical to the development of understandable models of reactions, their details are therefore further covered in the following parts.

It was assumed in our research that the propylene are mainly consumed in the polymerisation reactions and the hydrogen is consumed in the hydrogen transfers to the reactions. A reasonable use of the specific approach typifies the expressions of rates in each pressure-sensitive reaction. That said, the pressure-base rate of reaction equations can be explained by considering following assumptions:

1. Polymerisation reactions occur in dual emulsion/bubbling phases.
2. Emulsion phases would be well homogeneously mixed and will not remain in a minimally fluidised condition.
3. The assumption is that each bubble is spherical in shape. Most are also assumed to rise up in the fluidised bed in plug flows and with fixed velocity.
4. The resistance within the gaseous and the solid particulates occurring in each bubbling and emulsion phase to the mass and thermal transfers is expected to be insignificant, with reference to very low-to-moderate catalyst reactions (S Floyd et al., 1986).



5. Gas-solid distribution resulting from the rising flows of bubbles will lead to minor temperature declines/inclines in temperatures and radial concentrations in the FBR but will affect the pressure significantly.
6. The assumption is that particle sizes within the bed are unvarying.
7. The reactions consume components which flow in phases displaying pseudo-homogeneity. The hydrodynamic structures of the fluidised beds are delineated in the averaged properties of the occurring emulsion/bubbling phases.
8. Adhesion forces between particles are assumed to be insignificant for the purposes of simplifying the problem in its thermal features
9. Observed properties such as thermal capacities, thermal conductivities, viscosities, and densities of the gases and particulates are presumed to be physically unvarying. Values are determined for initial and final temperatures at 70 °C and 80 °C, respectively.
10. Heat losses via reactor walls are disregarded
11. Conduction of heat in bubbling phases is disregarded
12. All particles exhibit consistent temperatures
13. For gas-particle local thermal transfer coefficients, the Ranz-Marshall correlations are utilised for local particle conditions

In consideration of the aforementioned assumptions, we offer here the important equation set for every necessary component occurring in the FBR. Mathematical terms are listed in the nomenclatures as well as in the manuscript.

For Ti-Mg based (Ziegler–Natta) catalytic reactions, the reaction rate equation of Floyd et al. (1986) is conveniently applicable, and is described according to catalytic volumes and transformed to the ensuing equation for single-polymer particles:

$$R_{pd} = k_{pex} \exp\left(-\frac{E}{RT_{pl}}\right) p_{gs} \quad (6.1)$$

Where  $k_{pex}$  denotes the pre-exponential constants of polymerisation rate coefficients,  $E$  denotes activation energies for polymerisations, and  $p_{gs}$  symbolises reactor pressures. The  $k_{pex}$  and  $E$  parameters were established from the work of Kaneko et al (1999). In current expressions, the particle-size transitions are rendered insignificant due to the need to simplify the model. Transitions in temperatures therefore dominate transitions in reaction rates. In later modelling of instances featuring broad distributions of polymer particle sizes, equations of the kinetics which incorporate resistances of dilution monomers may need to be employed.

Monomer mass balances correspond to:

$$m \frac{dy_{H_2}}{dt} = F_{in}(y_{H_2,in} - y_{H_2}) - R_{H_2} \quad (6.2)$$

Where  $m$  represents the total masses in each of the reaction mediums, where  $y_{H_2}$  represents hydrogen weight fractions in gH<sub>2</sub>/kg, and  $R_{H_2}$  represents their hydrogenation consumption rates. These seeming consumption rates are employed given that the reaction-rate factors for hydrogen reaction transfers and for reactivations of inactive sites are not available for the system of catalysts utilised in this research.

The term  $\frac{dy_{H_2}}{dt}$  for stability calculations is governed by this associated expression of Tsuji et al. (1993):

$$\frac{dy_{H_2}}{dt} = \frac{1}{5} 2\pi \sqrt{\frac{m}{k}} \quad (6.3)$$

The energy balances for particles follow the expression:

$$V_p c_{p,p} \frac{dT_p}{dt} = R_p (-\Delta H_r) - \{h_p\} (T_p - T_g) S_p \quad (6.4)$$

Wherein  $v_p$  represents volumes of particles,  $c_{p,p}$  represents the specific heats of solids,  $\Delta H$  represents polymerisation heats, and  $S_p$  represents the exterior surface areas of particles. In fully-fluidised conditions, the appropriate Anderson & Jackson's equation set (1967) for application is for application is:

Continuity equation

$$\frac{\partial \varepsilon}{\partial t} + \frac{\partial (\varepsilon u_i)}{\partial x_i} = 0 \quad (6.5)$$

Momentum equation:

$$\rho_{gas} \frac{d(\varepsilon u_i)}{dt} + \rho_{gas} \frac{d(\varepsilon u_i u_j)}{dx_j} = \varepsilon \frac{\partial p_i}{\partial x_i} - f_i + \varepsilon \rho_g g \quad (6.6)$$

For the motions of particles in fluidised-bed reactors, the appropriate expression for application is:

$$m \frac{dv}{dt} = mg + F_{pi} - V_p \nabla p_i + F_n + F_t \quad (6.7)$$

Rotation:

$$I \frac{d\omega}{dt} = |F_t| r_p \quad (6.8)$$

For gas-particle interactions, the forces applied to fluid cells  $f_i$  Eq. (6) are provided by Eq. (9) which results from the Ergun correlation for  $\varepsilon < 0.8$  or for  $\varepsilon \geq 0.8$  via Eq. (10) which is derivative of Wen & Yu's correlation.

$$f_i = \left( 150 \frac{(1 \pm \varepsilon) \mu_g (u - \bar{v})}{\varepsilon^2 d_p^2} \right) + 1.75 \frac{1 + \varepsilon}{\varepsilon} \frac{\rho_g (u - \bar{v}) |u - \bar{v}|}{d_p} \quad (\varepsilon < 0.8) \quad (6.9)$$

$$f_i = \sum_8^{\pi} C'_{Dl} \rho_g \varepsilon^2 (u - v_1) |u - v_1| d^2 (\varepsilon \geq 0.8) \quad (6.10)$$

$$C_{Dl} = \varepsilon^{-4.65} \frac{24}{R_{el}} \left( 1 + 0.15 R_{el}^{0.687} \right) (R_{el} \leq 1000) \quad (6.11)$$

$$C'_{Dl} = \varepsilon^{-4.65} 0.44 (R_{el} \geq 1000) \quad (6.12)$$

Where  $R_{el} = (\rho_g \varepsilon d_p / \mu_g) / |u - v_l|$ ,  $\mu_g$  corresponds to gas viscosities,  $C'_{DI}$  corresponds to revised drag coefficients,  $\bar{v}$  corresponds to average particle velocities in fluid cells, and  $v_l$  corresponds to the velocities of discrete particles. It must be noted that both voidages and gaseous pressures are delineated at the centres of computational domains, while gas velocities are delineated at the centres of the boundary planes between cell units to maintain quantitative stability, i.e. staggered-grid.

The terms  $(u - \bar{v})$  and  $|u - \bar{v}|$  in equation can be determined with the appropriate equation set:

$$(u - \bar{v})_x = 0.5(u_x(i, j) + u_x(i-1, j)) \pm \frac{1}{n_c} \sum v_{xl} \quad (6.13)$$

$$(u - \bar{v})_y = 0.5(u_y(i, j) + u_y(i-1, j)) \pm \frac{1}{n_c} \sum v_{yl} \quad (6.14)$$

$$|u \pm \bar{v}| = \left\{ (u - \bar{v})_x^2 + (u - \bar{v})_y^2 \right\}^{1/2}$$

Where  $(u - \bar{v})_x$  and  $(u - \bar{v})_y$  correspond to the component x and y values signifying the relative velocities between gases and particles,  $n_c$  corresponds to the particle counts in fluid cells  $v_{yl}$ , and  $v_{xl}$  correspond to the component x and y velocity values of  $l$  particles.

In evaluating  $\nabla p_i$  in Eq. (7), it is presumed that pressure gradients nearly equal those in beds which are adequately mixed at voidages,  $\varepsilon$ . These involve the presumption that the acceleration terms of gaseous elements are insignificant in comparison to others. The left side of Eq. (6) therefore approximately equals 0 where we gain:

$$V_p \nabla p_i = \left( V_p \left( -\frac{f_i}{\varepsilon} + \rho_g g \right) \right) = \frac{1-\varepsilon}{n} \left( \left( -\frac{f_i}{\varepsilon} \right) + \rho_g g \right) \quad (6.15)$$

Where  $n$  corresponds to the particle counts. Similar techniques were assumed by Mikami et al. (Mikami et al. 1998), but were not examined fully. As the aim of the current research is to explore the temperature behaviours of gas-phase polymerisation reactors, the further enhancement and advancement of phase-formation simulations is beyond our current area of emphasis, and phase-change details have been covered in prior research by Khan et al. (Khan et al., 2016).

For energy balances, the proper derivative expression is:

$$\frac{\partial \varepsilon T_g}{\partial t} + \frac{\partial (\varepsilon u_i T_g)}{\partial x_i} = \frac{Q_g}{\rho_s C_{pg}} \quad (6.16)$$

Where  $C_{pg}$  corresponds to the thermal capacities of gases,  $T_g$  corresponds to gas temperatures, and  $Q_g$  corresponds to the rates of thermal transfers between gases and particles in unit volumes, which is stated in the ensuing expression in accordance with above mentioned presumptions .

$$Q_g = \frac{6(1-\varepsilon)}{d_p} \|h_p((T_p)-T_g)\| \quad (6.17)$$

Where  $h_p$  represents the coefficient of thermal transfers between gases and particles,  $d_p$  represents particle diameters, and  $T_p$  represents particle temperatures in fluid cells.

The coefficient of thermal transfers  $h_p$  is approximated with the appropriate Ranz-Marshall correlations (Ranz, 1952):

$$Nu = 2.0 + 0.6Pr^{1/3} Re_p^{1/2} \quad (6.18)$$

Where,

$$Nu = h_p d_p / \lambda_g \quad (6.19)$$

$$Pr = C_{p,g} \mu_g / \lambda_g \quad (6.20)$$

$$\text{Re}_p = \frac{\rho_g d_g |u - v_l|}{\mu_g} \quad (6.21)$$

Where  $\lambda_g$  denotes the thermal conductivities of the gases,  $c_{p,g}$  denotes the thermal capacities of the gases,  $\mu_g$  denotes the gaseous viscosities, and  $|u - v_l|$  denotes particle-to-gas relative velocities.

Gas velocities are delineated at the centres of boundary planes between cell units in order to eliminate quantitative instability. Voidages as well as gaseous temperatures and pressures are delineated at the centre of cells. To resolve calculations for fluidic motion in Eqs. (5), (6), and (16), SIMPLE (Semi-Implicit Methods for Pressure Linked Equations) algorithms and explicit techniques using the upwind-order system were applied. The dynamic process parametric sets and coefficients assumed in this research can be located in the specified literature of Shamiri et al (2010), with quantitative conditions and computational details provided in Table -6.1. In this research, the influence of temperatures, or the activation energies, on polymerisation dynamics was studied for the propylene polymerisation reactions. Many research findings have shown that in those instances when Ziegler-Natta particulates are tiny and do not exhibit high levels of activity due to low-to-moderate rates of polymerisation, the existing resistances to thermal and mass transfers within the polypropylene and the un-reacted particulate solids and gases have inconsequential roles which would not affect reactor behaviours or the properties of the polyolefins. We have also utilised the active dual-phase scheme that had been partly recommended by Khan et al. (Khan et al., 2016). This offers a superior description of the many hydrodynamic events as well as enhanced our quantifiable understanding of the actual processes.

**Table 6.1** : Computational conditions for modelling**Initial flow conditions:**

Fluids	Mass Flow rate (kg/hr)
Propylene	145
Hydrogen	0.414
Nitrogen	73.87
<b>Bed materials</b>	
particle density (kg/m <sup>3</sup> )	950
Particle diameter, (μm)	500
Restitution coefficient, <i>e</i>	0.9
Friction coefficient, <i>k</i>	0.3
<b>System specifications</b>	
Reactor inner cross sectional area, m <sup>2</sup>	0.00785
Reactor inner diameter, m	0.1016
Bed height at minimum fluidization, m	0.17
Bed height, m	0.24
Height of reaction zone, m	1.5
maximum cross-sectional area of the disengagement zone, m <sup>2</sup>	0.0490625
Reactor disengagement zone diameter, m	0.25
Height of disengagement zone, m	0.31
reactor volume, m <sup>3</sup>	0.0215
<b>Bubble</b>	
Maximum bubble diameter, m	0.08
Types of distributor	perforated plate (stainless steel)
Number of fluid cells	41 × 10 <sup>5</sup>
Time step, s	1.298 × 10 <sup>-5</sup>
<b>Process Parameters</b>	
Reaction temperature	70 <sup>0</sup> -80 <sup>0</sup> C
System pressure	20-30 bar
Propylene concentration (% wt)	75
Hydrogen concentration (% wt)	2
Nitrogen concentration (% wt)	23
Overall heat transfer coefficient, rate constant	410.22
activation energy	8.948 × 10 <sup>-6</sup>
heat of polymerization	10585
viscosity	2.51 × 10 <sup>3</sup>
thermal conductivity,	0.01412
	0.03623

In all bubbling FBRs, the rising movements of bubbles can result in improved blending of the particulate solids in the emulsions or the denser phases. This can bring about uniform concentrations of the various particulates as well as temperatures in the denser phases. Thus a CFD-derived scheme displaying pseudo-homogeneity is also implemented for these phases. The gaseous bubbles rise in the bed with set velocities

while particulates fall, exhibiting mass and sizing increases as they stream downwards, thus validating the usage of plug flows in the bubbling phases.

### 6.5 Sample preparation for mechanical testing

For mechanical property analysis, polypropylene samples (see figure-6.4.a ) were prepared by compression moulding method. In the compression moulding approach, the polymer was melted at 180°C, compressed by hot press and after 2 min cooled by blowing the air. Compressed polypropylene sheets had 1 mm thickness.



6.4. a



6.4. b

**Figure 6.4:** Produced granular Polypropylene (6.4.a) and dog-bone shape polypropylene bars (6.4.b) for thermo-mechanical testing



Samples for mechanical test were cut out from sheets. The sample was a long bar and had a dog-bone shape (figure 6.4.b), with a gauge length of 25 mm, width of 9 mm and thickness of 1 mm. In these samples, the formation and propagation of neck was not restricted by the shape of specimens.

An Instron® Universal Materials testing machine was used for tensile testing. In this process, a specimen was stretched and the weight bore by the specimen was measured to check the tensile strength. Consequently, a stress-strain curve was derived from the load and deflection data that are determined from the specimen dimensions. The stress-strain curve presents different types of tensile properties. The standard tests were carried out in accordance with the ASTM D638-03 procedure.

### **6.5.1 Impact property testing of plastics**

ASTM impact tester model 43-02 was used to carry out Izod impact tests. These tests were done at the room temperature on notched specimens, which were sliced with a 6.8-J hammer from the far-end and gate-end of injection moulded Izod bars at an impact velocity of 3.5 m/s. Mostly, the Izod impact strength at the far-end was similar to that at the gate-end; in case the former is a little lower than the latter, an average of the two values was considered.

### **6.5.2 Dynamic mechanical analysis**

One of the several configurations was used to carry out dynamic mechanical analysis. In this analysis, stress was applied in tension, compression, shear, flexure or torsion. Dynamic mechanical analysis experiments were executed at a temperature range of room temperature to 180 °C, typically at a 5 °C/min heating rate. The type of modulus estimated depends on the mode of the analysis used. Temperature sweep testing refers to the measurement of modulus across a varied range of temperatures. In the dynamic

mechanical analysis, the resultant modulus is continuous across the temperature range of interest, which is an advantage of this method over conventional tensile or flexural testing methods. The third generation Dynamic Mechanical Analyser (DMA), Q800 series from TA instrument comprising with ultramodern linear drive technology was used to get the detailed, accurate control of stress, and air bearings for lesser friction support. Every factor was measured by using optical encoder technology that offers supreme sensitivity as well as resolution.

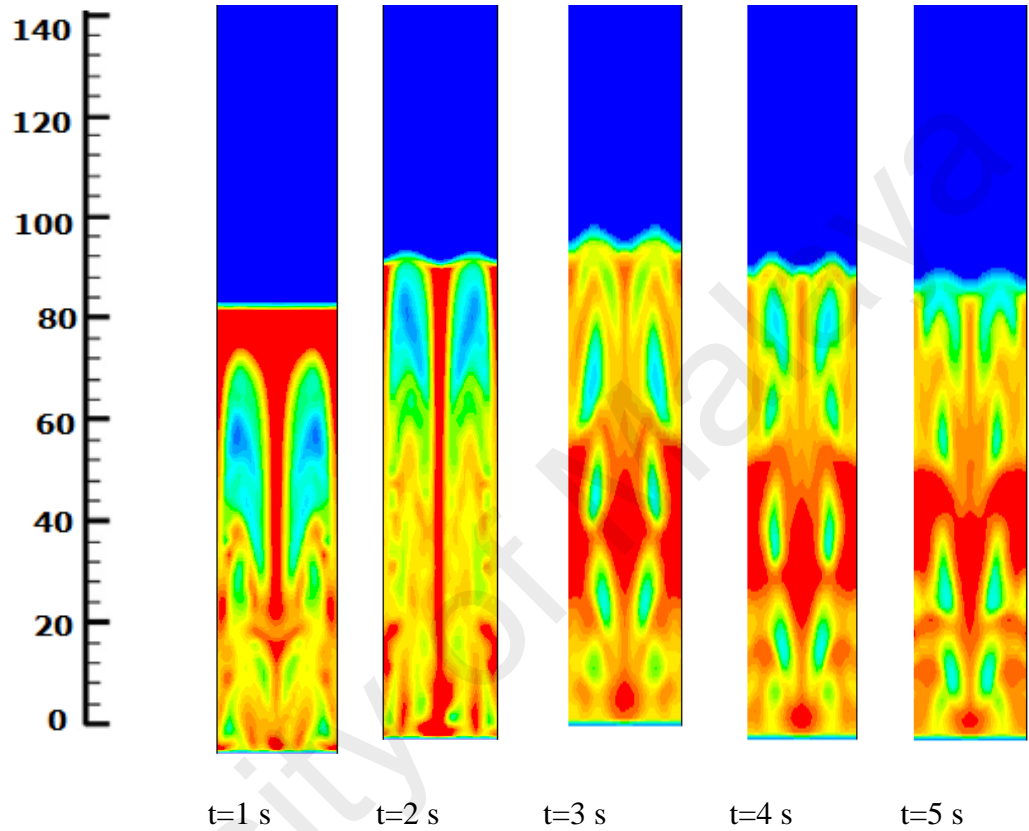
## **6.6 Results and Discussion**

### **6.6.1 Dual phase (bubble-emulsion) dynamics behaviour:**

The motive behind this phase modelling is to give a clearer idea of the dynamic bubble movement during reaction. As the bubble formation and headway plays a vital role in gas-solid mixing which can significantly affect the polymerisation rate in real reaction conditions. Conversely, pressure fluctuation in the different portion of the reactor may be altered due to the variability of the bubble shape. Snapshots of the patterns of phases (bubble and emulsion) transformation found in the pseudo-2D fluidised beds at various points in time can be useful in analysing their bubbling behaviours. These shots were caught at a similarly superficial velocity ( $u_0=0.25$  m/s) after thermal steady-states were reached in the simulated models. The general formation of phases and changes in bed elevations were also utilised to measure time-varying effects on the hydrodynamic properties.

Once inlet gas velocities are fixed(in minimal fluidisation) and the simulation time interval varied as in the initial snapshot in Figure 6.5, small spherically-shaped bubbles are observed to stream to the bed surfaces. Increases the times lead to increases in the size of bubbles due to rate increases in coalescence. The fluidised bed displays

chaotically disordered movements. When bed fully fluidised (at  $t=3\text{s}$  and onwards), bubbles are difficult to distinguish discretely. Owing to severe disintegrating and coalescing behaviours among bubbles, particulate movements in the bed do not display characteristic bubbling features, and instead manifest odd-shaped void structures.



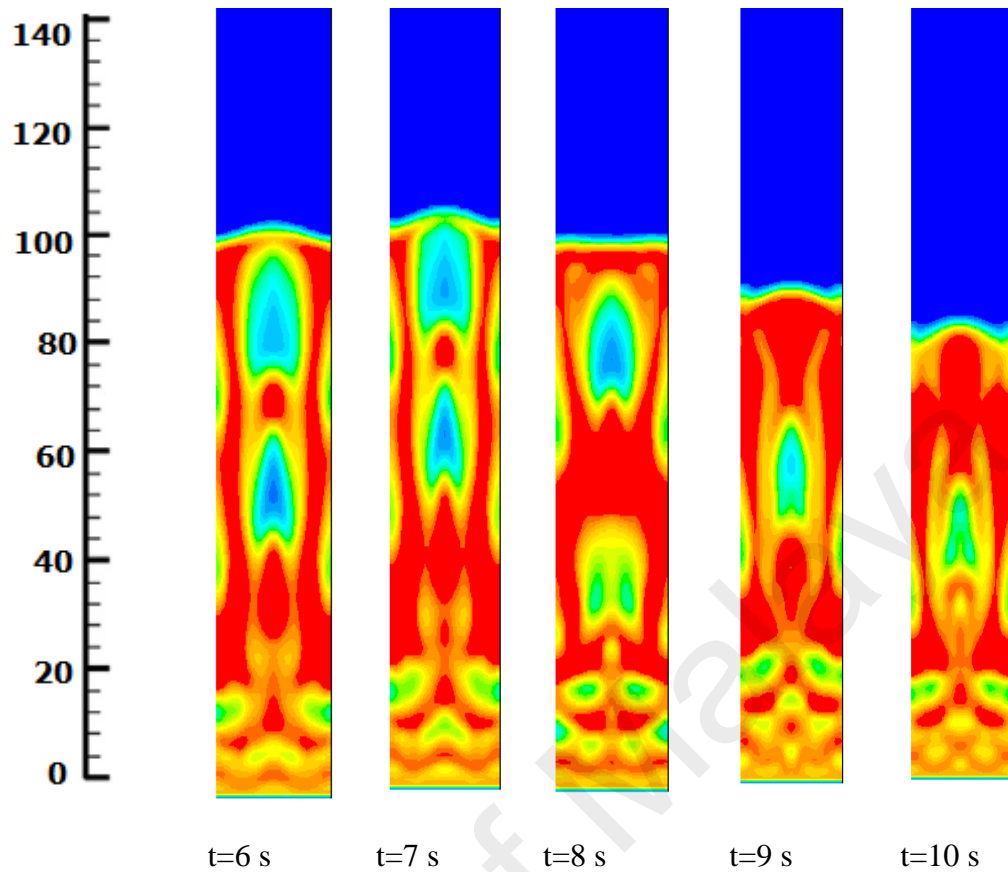


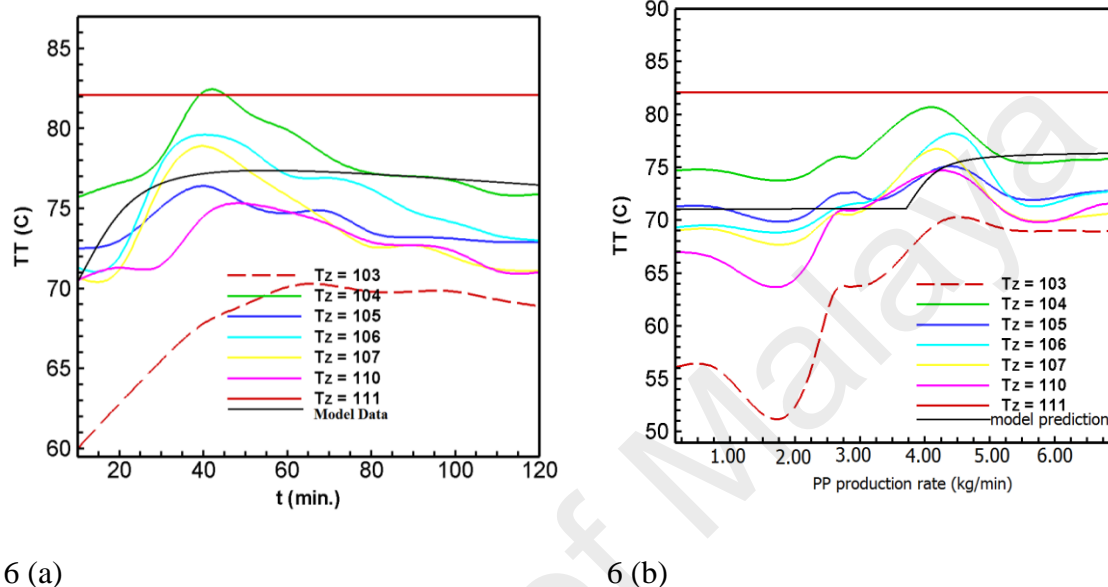
**Figure 6.5:** Dynamic phase transformation of fluidised bed during propylene polymerisation

It should be noted that bubble movements and distributions have critical roles in mediating fluctuating reactor temperatures and pressures. Accordingly, these occurrences can influence aggregate rates of production, which has been demonstrated in the following sections.

### 6.6.2 Dynamics of temperature on reaction system and production rate

The dynamic profile of temperature during polymerisation has been examined at different temperatures at 25 bar pressure and 2 mol% of hydrogen. As shown in figure 6, the dynamic temperature oscillation along with the polymer production rate vary at certain section of the reactor. The experimental results showed a higher temperature at the point, Tz 104, at the section where gas-solid possible uniform mixing is considered

to be took place. The two thermocouples T 104 and T106 showed a substantially higher temperature compared to other thermocouples in the bed, which shows that there has been relatively high polymerisation activity in the proximity of the exothermic nature of the reaction.



6 (a)

6 (b)

**Figure 6.6:** Online temperature monitoring during reaction and effect on reaction rate. (system pressure 25 bar and hydrogen concentration at 2 mol%)

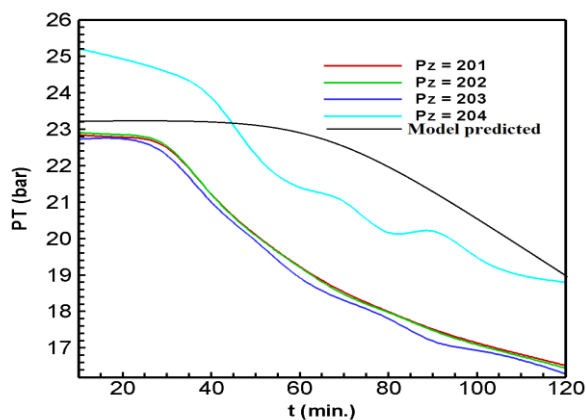
It is well documented that catalytic activities significantly influence the reaction rate temperature dynamics in the olefin polymerisation. But, the performance of catalyst symmetrically depends upon the uniform mixing of solid particle and the gases. Once the catalyst injections are performed, there is a quick rise in the temperature, which attains the highest limit after approximately 45 minutes. The next step involves the deactivation of the catalyst, which subsequently leads to a dip in the temperature inside the reactor that returns to its initial value after about 90 minutes. The highest temperature attained in this experiment was about 82°C. However, model predicted consequences exhibited that temperature increased sharply from 70°C to 75°C at 30 minutes of residence time, after that a stationary phase demonstrated.

There is a high probability for chemical reactions among different catalyst components owing to high reaction temperature. Shamiri et al. (Shamiri et al., 2011) suggest that for gas phase polymerisation that uses a Ziegler-Natta catalyst, the catalyst is deactivated quickly when the temperature exceeds a certain limit. Moreover, a micro level thermal runaway can be avoided by prepolymerisation. In the prepolymerisation step (at the zone T-103), the reaction rate is much lower than that in the main polymerisation, which gives particles enough time to grow to a size where the exterior surface is large enough to eliminate all the reaction heat.

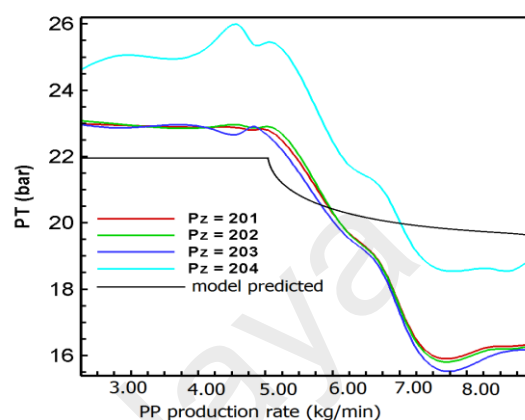
### **6.7 Real-time pressure profile during reaction**

Pressure fluctuation measurements do not give a direct measure of some fluidization characteristics, such as the local solids flux or the voidage profile; however, they help to determine various important gas-solid fluidisation dynamics like, bubble motion direction, bubble coalescence, and bubble bursting (Jang et al., 2010). While pressure fluctuations between two nearby points indicate local hydrodynamic phenomena (like the flow of a bubble through the measurement points), oscillations in absolute pressure largely indicate overall hydrodynamic behaviour, which can be measured anywhere in the system (like eruption of bubble on the surface of the bed). As this study focuses on the global characterisation of hydrodynamics, we consider real-time pressure fluctuations to arrive at the results. The deviations observation of high-pressure reaction at different part inside the reactor has not been found in the works published before. It should be stressed here that monitoring based on pressure fluctuations should not be seen as a replacement of the current routine measurements of average temperature and pressure drop, but as a valuable analysing tool for observing the fluidization state of industrial fluidized beds.

The dynamic pressure consequence was studied between 20 and 26 bar at 75°C. The hydrogen concentration was set constant at 2 mol%, which is consistent with the value used for the temperature series. The maximum pressure rising has been observed at the reactor zone, z-204, which escalates at 25.2 bar and falls at 20 bar. This is a very significant finding as it has been found out from this experimental study that reaction took place as full range at specific reaction zone, z-204 within 2 hours. Theoretically, this statement is supportable as the polypropylene gas-phase fluidization reaction needs minimum 20 bar system pressure and only at the z-204 reaction pressure sustains from 25.2 to 20 bar (Shamiri et al., 2010). In the case of other reaction zones (z-201, z-202 and z-204) the highest pressure raises until 23 bar but after 32 min a sharp pressure drop is observed which continues until 57 min to reach at 20 bar. After 1 hour the system pressure starts to drop below 20 bar and perpetual falloff reached at 16 bar at 2 hours, which proves that no reaction took place after 1 hour at other three reaction zones. Figure 6.7 depicts a first-order reaction kinetics, in which the polymer production rate rises in line with the system pressure variation.



7 (a)



7(b)

**Figure 6.7:** Real-time pressure dynamics profile of propylene polymerisation in a pilot scale fluidised bed reactor at 75 °C temperature and 2 mol% of hydrogen.

High polymerization rates, which involve high monomer concentrations or bulk temperatures, result in chemical deactivation reactions. This can be attributed to the fact that at high polymerisation rates, particle temperature tends to be considerably higher than the bulk temperature. If the maximum polymerisation activity of particle excess temperature behaviour is identical to that of the pressure series, then the actual particle temperature will likely be the same for both the pressure and temperature series.

### 6.8 Hydrogen flow rate profile:

It is widely known that the hydrogen/fresh feed gas ratio yields specific polymer grades in terms of polymer microstructure. In this study, the effect of control of hydrogen concentration during reaction on polymerization rate was measured in the first stage. It is worth to mention that hydrogen concentration was maintained at 3 different concentrations 2 mol%, 4 mol% and 8 mol%. Polypropylene produced at different hydrogen concentrations i.e. 2, 4 and 8 mol% were termed as PP-2, PP-4 and PP-8



respectively in the next sections. In second phase of analysis, the polymer grade was defined by conducting characterization study. More specifically, we are interested in the thermal and physical characterizations of various grades of polypropylene. The hydrogen to monomer ratio is set constant by a predefined value through a controller to achieve the required thermoplastic properties. However, when commercial grade polypropylene mechanical properties maintaining is required, the task is challenging as it demands precisely controlled and uninterrupted hydrogen supply during polymer formation.

In this study, real-time hydrogen consumption rate was determined for the first time. Figure 6.8 shows that highest amount hydrogen intake took place from 30 min. to 60 min. At 60 min. the hydrogen inflow rate was at maximum 4.0 LPM scfm (standard cubic feet per minute) in the reactor. This finding strongly endorses the previous findings of this study i.e. the findings of dynamic temperature and pressure. Both phenomena shows maximum reaction rate in similar time duration. This value was measured by a specially designed online RGA (Refinery Gas Analyser) (designed at University of Malaya, Malaysia and commissioned by Perkin Elmer, USA). However, the developed model showed also the similar trend of hydrogen consumption rate in the system.

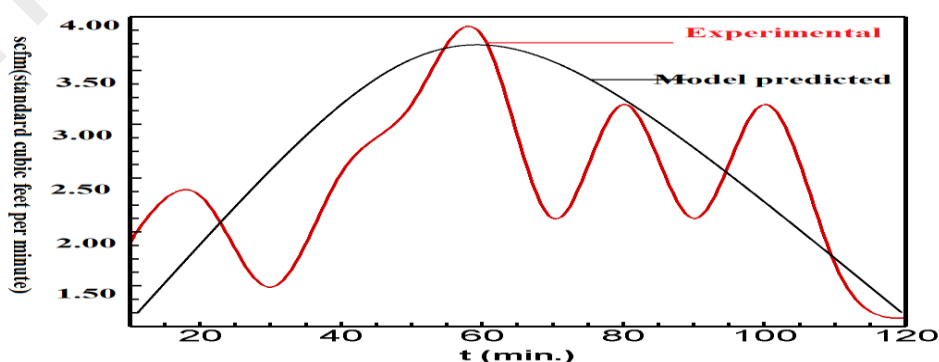


**Figure 6.8:** Real-time Hydrogen consumption dynamics in the pilot scale fluidised polymerisation reactor

Though hydrogen is believed to exert some influence on catalytic activities, the activation method by hydrogen is yet to be proved (Khan et al., 2016). While many theories exist, the majority believes that the uneven addition of monomers results in the formation of dormant or sleeping sides, which are reactivated by hydrogen. This boosts the overall catalyst activity. Generally, the most successful method is the chain transfer with hydrogen. This method controls the molecular weight of PP under real reaction conditions. The proportion between the total propagation rate and the total chain transfer rates determines the mechanical properties of a polymer sample, which generally do not depend on the polymerisation activity. A detailed characterisation findings of hydrogen amount controlled polypropylene have been discussed in the subsequent sections.

### **6.9 Mechanical and thermal characterisations**

The enhancement of mechanical properties is also related to the processing conditions. There are many mechanical tests to examine plastics and polymers; however, they primarily do not form a rational set. The entire set of mechanical tests can be classified into various logical sets using definite methods. One such classification groups the mechanical methods into tests that examine long-term properties and tests that examine short-term properties. Short-term tests constitute tests such as tensile tests, flexural tests, and the determination of impact resistance, which measure material properties. Though these tests are easy to perform and infer, they do not have the capability to calculate or gauge the long-term performance properties of a material. Short-term tests are most often listed on material data sheets. The following section will focus on some specific mechanical testing, which are routinely carried out by commercial grade plastic manufacturers.

### 6.9.1 Izod impact strength

In fact, almost all polymer components are exposed to impact loads. Many polymers are capable of taking this type of loading owing to their tough and strong properties. Nevertheless, even the most plastic materials like polypropylene sometimes are unable to bear the load under certain conditions. Such kind of failures tends to take place at high deformation rates. Designers generally use impact tests to evaluate the relative impact resistance. These tests are generally used for quality check as well. The standard test, ASTM D256-06, was selected for Izod impact strength of our produced polypropylene. The energy per unit length or per unit area represents the impact resistance. The impact strength of different grades of polypropylene can be determined using these impact tests.

Figure 6.9 shows plots of Izod impact strength for PP with the various hydrogen concentration designated as those having an MFI of 1.0. As seen in Figure 6.9, the impact strength for PP with 2 wt % hydrogen has shown 'super-tough' behaviour, which leads to a strong increase in the impact strength up to 692 J/m. However, further increase in the hydrogen concentration in PP displayed a sharp decrease of impact. At 4 wt % of hydrogen in PP, the observed Izod value was around 635 J/m, whereas another two specimens (for 6 wt % and 8 wt %) showed the Izod strength value at 618 J/m and 593 J/m, respectively.

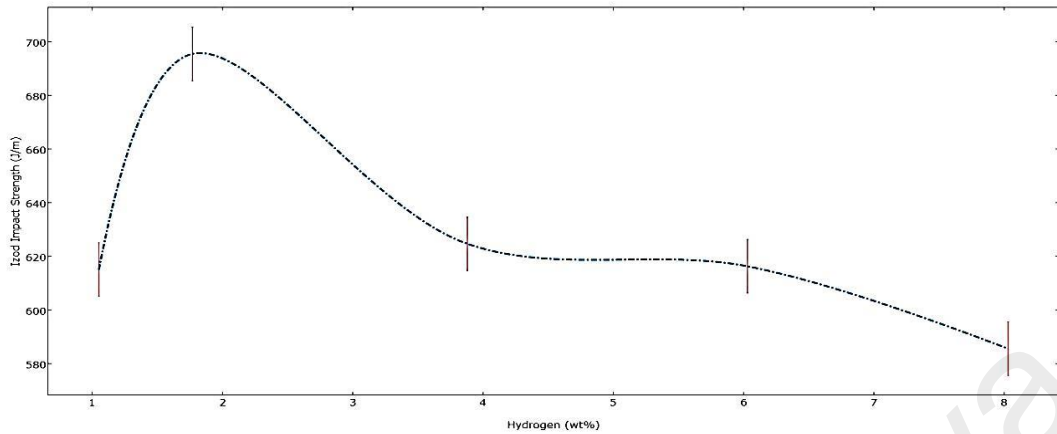


**Figure 6.9:** Izod strength profile of different grades of polypropylene (PP-2, PP-4 and PP-8)

Various plastics do not consist of the desired impact resistance, which is required for its intended use. Instead of changing to a different kind of plastic, they can be modified to suit the requirement. Alteration of hydrogen concentration during PP manufacture can significantly affect the impact resistance.

### 6.9.2 Tensile and flexural properties

The tensile test is one of the most frequently used mechanical methods to examine material properties of plastics. A dumbbell-shaped specimen is used in the test that is outlined in ASTM D 638. Apart from providing information such as the fracture properties as tensile strength at break and elongation at break, the yield point in the form of yield strength and elongation at yield, and the stiffness of the material as elastic modulus, tensile testing yields data about the proportional limit.

This study aims at finding the influence of strain rate on stress–strain behaviour of polypropylene. The tensile strain-stress curves obtained in this study are shown in figure 6.10. The range indicated by points on the curve for different PP samples can be described as follows:

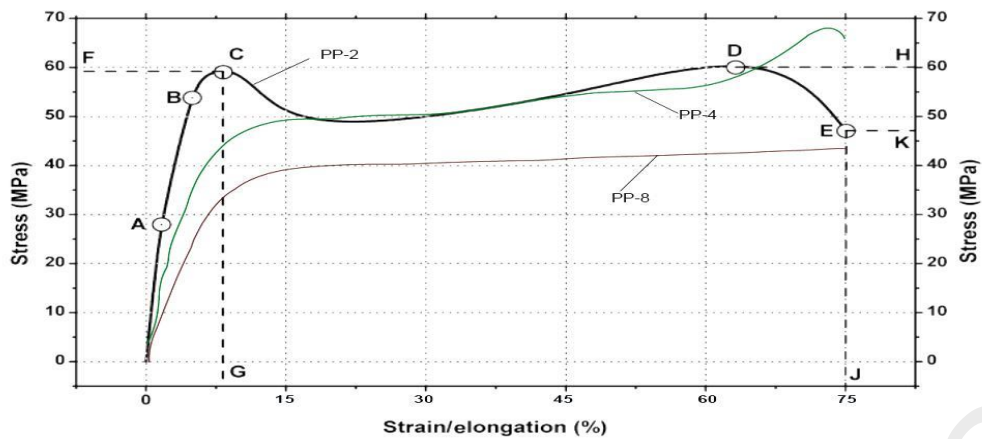


**Figure 6.10:** Tensile strength analysis of PP-2, PP-4 and PP-8 (ASTM D 638)

‘A’ represents the ‘proportional limit’, which is the end of the region in which the PPs demonstrate the linear stress-strain behaviour. In this case, all the PPs show similar trend of linear behaviour. ‘B’ represents the ‘unacceptable elastic limit’ after which the part is constantly distorted when the ASTM-recommended strain is eliminated. No PP sample considered for this study was deformed at an early stage. ‘C’ constitutes the ‘yield point’ after which the material will deform without any more rise in strain. PP-4 and PP-8 showed the bearable response to strain at 60 mpa and 53 mpa, respectively, whereas PP-2 did not show any deformation response at this point, which means that at the standard yield point, PP-2 will not be deformed. ‘D’ represents the ‘ultimate strength’, which is the highest stress on the curve. This point forms the main feature of the thermoplastic characterisation study.

Our three products showed very surprising mechanical phenomena. PP-2 showed the ‘stiff and tough’ trends. Here, it is worth mentioning that toughness is the extent to which a material can undergo deformation before fracture, i.e. how much energy a PP sample can absorb while deforming before it breaks. Stiffness is the extent to which an object resists deformation in response to an applied force. Strength is a degree of the extent of a material's elastic range or a combination of elastic and plastic ranges

together. PP-4 showed the ‘stiff and strong’ trends. On the other hand, PP-4 showed soft and tough characteristics. ‘E’ is the ‘breakpoint’, at which the plastic materials should permanently break.

### 6.9.3 Morphological transformations

Figure 6.11 (a) shows the surface structure of PP-2. This compact grain configuration confirms a reinforced matrix, ensuring the increased stiffness and tensile strength as examined before. This structure also indicates identical high stress tolerance zones, which specifies the improved reinforcement of the polymer matrix. Here, structural elements may be related to the intensification in the tensile modulus as well as tensile strength. Figure 6.11 (b) shows the smooth surface with existence of few inner bubbles. The surface shows a fairly homogenous polydispersity with some extent of early deformation stress zones. There is a noticeable change in the surface structure of PP-8 (figure 6.11 (c)) compared to the other PP samples. Some lighter lines aligned with the grey background and some narrow wrinkle type structures are visible.

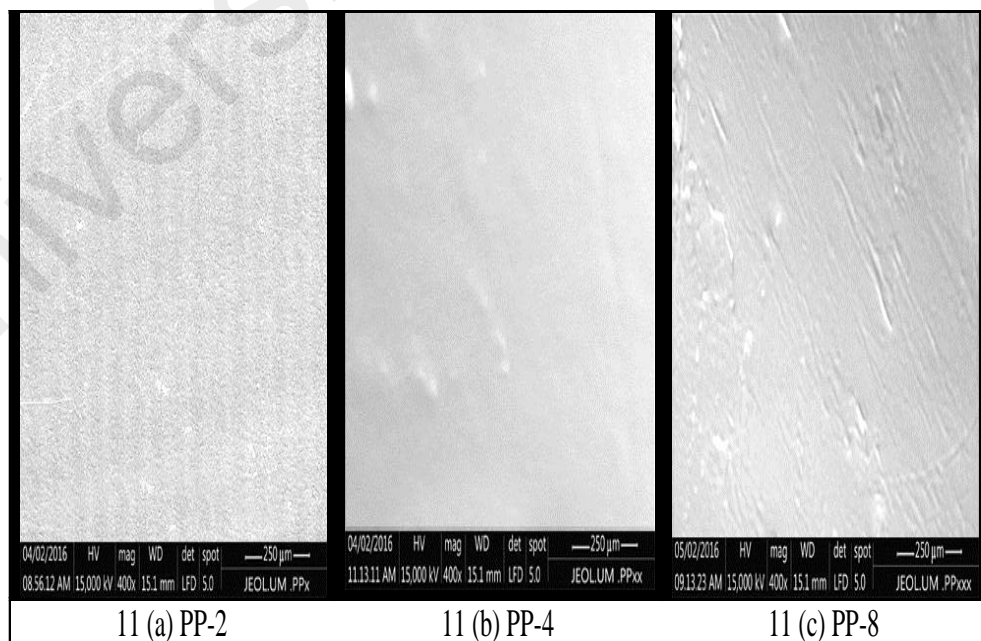


**Figure 6.11:** SEM images on morphological changes of produced polypropylene

The improvement in tensile strength may be as a result of the homogenous and fibrillated transformation in morphology where Chow et al. (Chow et al., 2005) mentions that superior interfacial adhesion develops the improvement of tensile properties.

#### **6.9.4 Dynamic Mechanical Analysis (DMA)**

The sinusoidal oscillatory test, also called the dynamic-mechanical-analysis (DMA) test, is one of the most useful mechanical tests for polymers. In this test, a fixed frequency stress input is used to stimulate a specimen, which is then noted along with the strain response. Different tests have different testing processes and varied shapes of the test specimens. ASTM D4065 explains the different tests and their corresponding specimen shapes and ASTM D4092 describes the terminology. The typical responses assessed in these dynamic tests are a storage modulus and a loss modulus. The storage modulus is associated with the elastic modulus of the polymer at the loading frequency and the loss modulus is connected to the damping or dissipative component seen during loading. The loss modulus can also be written in terms of loss tangent delta ( $\tan \delta$ ). Being a thermoanalytical technique, dynamic mechanical analysis (DMA) evaluates the viscoelastic properties of materials. Polymeric substances exhibit both elastic and viscous behaviour concurrently. The equilibrium between the elastic recovery and viscous flow varies with temperature. DMA results provide the storage modulus, loss modulus, and the tangent of the phase-angle delta ( $\tan \delta$ ). Though this analysis is not always used as a failure analysis technique, it can impart valuable material information. A vital application of DMA is the temperature-dependent behaviour of polymeric substances. The results of a standard temperature-sweep test depict the loss modulus, storage modulus, and the  $\tan \delta$  as a function of temperature. The capacity of a substance to contain stress across a temperature range is referred to as storage modulus.

At different temperature ranges, changes in molecular structures occur, which subsequently results in property changes, such as the glass transition and other secondary transitions. The loss modulus and tan delta impart information on these temperature changes that are otherwise not detectable by other thermal analyses. It is well noted that for evaluating the glass transition, DMA is considered advantageous over DSC (differential scanning calorimeter) and TMA(thermal mechanical analysis) . In addition, DMA can calculate the capability of a plastic-moulded component to maintain its properties over the service temperature range. Secondary transitions of lesser magnitude can relate to material properties like impact resistance; hence, they are also vital considerations.

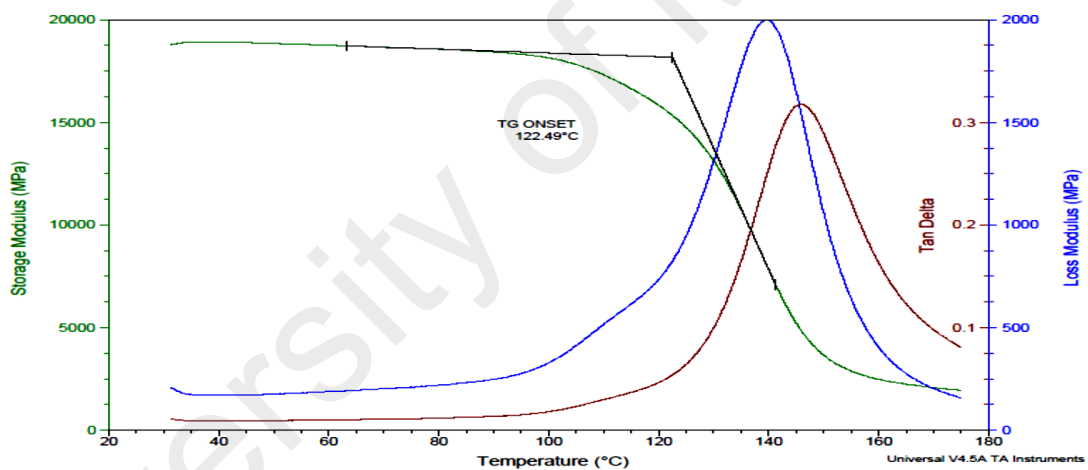


**Figure 6.12 (a):** DMA analysis of PP-2 (s=Sample Size: 17.5000 x 10.2000 x 2.4200 mm, Method: SOP 05202, Single Cantilever Ramp 5.00 °C/min, Instrument: DMA Q800 V20.24 Build 43)



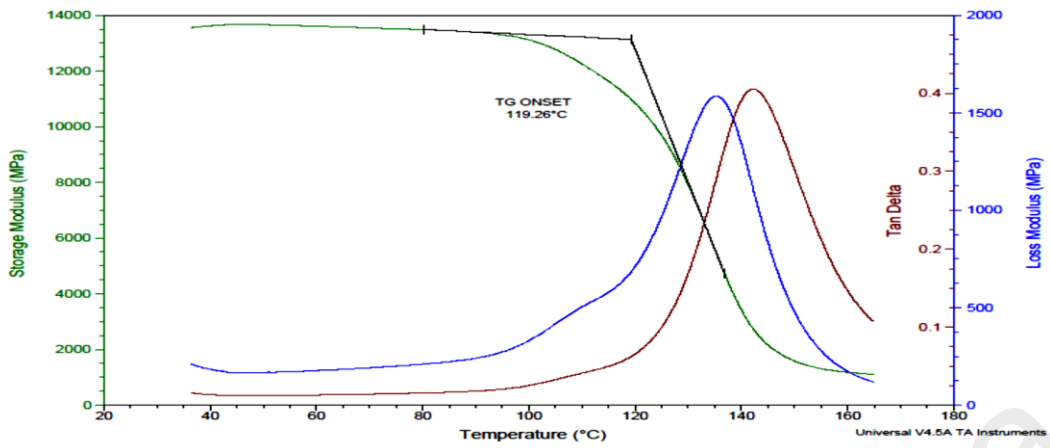


**Figure 6.12 (b):** DMA analysis of PP-4 (s=Sample Size: 17.5000 x 10.2000 x 2.4200 mm, Method: SOP 05202, Single Cantilever Ramp 5.00 °C/min, Instrument: DMA Q800 V20.24 Build 43)

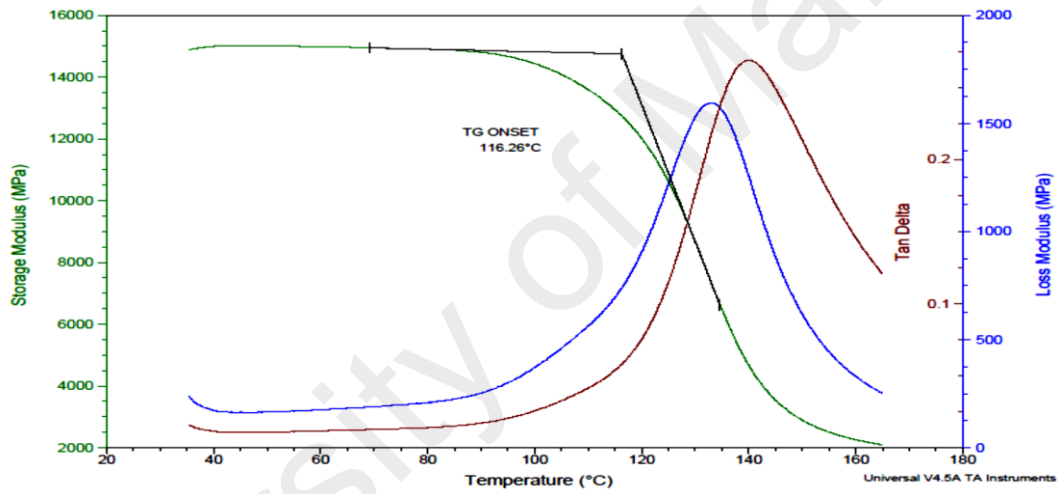


**Figure 6.12 (c) :** DMA analysis of PP-8 (s=Sample Size: 17.5000 x 10.2000 x 2.4200 mm, Method: SOP 05202, Single Cantilever Ramp 5.00 °C/min, Instrument: DMA Q800 V20.24 Build 43)

Figure 6.12 (a-c) shows the glass transition, the elastic shear modulus and the loss factor for various polypropylene grades considering the following parameters:

**Storage modulus:**

Figures 6.12 (a-c) show the graphs of storage modulus versus temperature for PP-2, PP-4 and PP-8. All the samples showed the nearly constant values storage modulus from room temperature to 80 °C, this shows a glassy regime in the range for polypropylene. While a sharp decrease of storage modulus was observed between 80 °C to 145 °C, 150°C and 145 °C for PP-2, PP-4 and PP-8 respectively with the rise of temperature, i.e., the material transforms from glassy to rubber transition phase from temperature range of 80 °C to 150 °C.

At the last stage, a straight stripe and the values approximately tend to zero was observed for each samples, which indicates a rubbery typography directing degradation of the moduli above 150 °C. An important finding has been derived from this stage, among three samples only PP-8 was reached to the complete rubbery phase. Value of storage modulus for PP-2 is exceptionally higher than that of PP-4 and PP-8. The highest storage modulus vale for PP-2 was 18,750 mpa, whereas, for PP-4 and PP-8 the values were 13,500 mpa and 14,897 mpa respectively. The higher values in primary stage and clear decline in the values in middle stage indicates the notion that the material is in glass transition condition at which a transition from glass state into rubber-elastic condition may turn up. When the dynamic molecular motion overlaps with that of mechanical bend, every oscillation is transformed into the highest- achievable non-elastic deformation.

**Loss modulus:**

Figure 6.12 (a-c) also shows the loss modulus of various grade of PP in Dynamic Mechanical Analysis (DMA) spectrum. With the increase in the value of temperature in primary stage the loss modulus of each PP samples slightly increases from room

temperature to 100<sup>0</sup>C with similar trends, whereas in the middle stage the value of loss modulus attains a peak value which again decreases with the increase in temperature in region. However, the loss modulus value for PP-2 has been observed at 2000 mpa at the temperature 140<sup>0</sup>C , which is the highest among all samples. On the contrary, same loss modulus values at 1595 mpa at same temperature of 130<sup>0</sup>C were observed for PP-4 AND PP-8.

#### **Tan delta:**

Figures 6. 12 (a-c) show the behaviour of the damping factor for PP-2, PP-4 and PP-8 with the increase in the temperature. While comparing the graphs of three samples, the similar values of tan delta were obtained for three samples. The peak value of tan delta indicates that the elasticity of the materials. In terms of elasticity all the polypropylene samples showed the similar mechanical behavior in wide range of thermal fluctuations.

#### **6.10 Summary**

Gas-phase polymerisations of propylene in a globally unique pilot-scale catalytic reactor, facilitated with online data logger, have been carried out at different temperatures, pressures and hydrogen concentrations. The model calculated reaction rate has been explained and validated with experimental results, which considers the effects of real-time temperature, pressure and hydrogen concentration variation in the reactor. It is argued that the developed online process parameters effect observation strategy is capable of providing not only clear pictures on ‘where and when’ reaction takes place but also the reaction rate.

At high polymerisation rates, deviations have been observed from the experimental study, which is attributed to the real-time thermal and pressure dynamics. The maximum reaction rates were observed at a pressure of 25.1 bar and a temperature of 75<sup>0</sup>C. However, large deviations were seen not only at higher temperature and pressure

ranges but also due to other reaction parameters zone for prepolymerisation time of 45 min to 1 hour. Obviously, the effect of hydrogen flow rate on polymerisation was taken into account.

The polypropylene industry produces polymers with definite mechanical and rheological characteristics. The microstructure of the manufactured polymer determines these characteristics. Of all the different process parameters, hydrogen concentration control during polymerisation was considered for the first time as one of the major factors that determines its mechanical properties. It was found that the thermomechanical properties of polypropylene were highly affected by the regulation of hydrogen concentration in the reaction system. The hydrogen content inside the reactor was regulated by modifying the hydrogen feed rate to the monomer ratio. Over a span of time, the ratio is manipulated in such a way that produced a polymer with desired properties. The influence of hydrogen on the polymerisation characteristics has been studied at concentrations of 2, 4 and 8 mol%. The produced polypropylene showed different physical properties like stiffness, toughness and thermoplastic behaviour due to alteration of hydrogen mass in the reaction system. As this real-time experimental and characterisation study was conducted in a pilot scale reactor (which is a prototype of an industrial-scale plant) and used state-of-the-art equipment, the findings will be significantly helpful for decision making for both industrialists and academia.

## CHAPTER 7: CONCLUSIONS AND RECOMMENDATIONS

### 7.1 Conclusions

We tried to come up with several conclusions and recommendations in this chapter based on the results of this study. We created an experimental statistically based design model via a set of equations which was validated with experimental data for the production of polypropylene. Independent variables, namely temperature, pressure and hydrogen concentration, were classified as the vital factors that need to be set to augment the production of polypropylene. From this study, the optimum environment for polypropylene production included a temperature of 75°C, pressure of 25 bar and hydrogen concentration of 2%. The anticipated polypropylene production from the statistical model was 5.2% while the experimental data was 5.82%. In this study, the relationship between system pressure and reaction initiation temperature indicated that the interaction between them and the outcome of various applied statistical techniques demonstrated that the suggested model was an exceptional substitute to established first principle models.

A hybrid model was created by meshing the statistical model with CFD (computational fluid dynamic) method to rationalise the detailed phenomena of the process parameter effects on fluidised bed hydrodynamics and reaction rate. To this end, a series of experiments were conducted to validate the developed model. The composite design, and emphasis on constructing an adequate precision ratio, the analysis of variance (ANOVA), and the significance of second-order models, determined by the F-value, normal percentage probability and an interaction graph of the hybridization model were the main points used to justify its validity. The optimum polypropylene production was set at a monomer concentration of 75%. Also discussed were bed expansion, bubble dynamics and grid sensitivity at various process conditions were.

A coupled CFD-dynamic mathematical model, that integrated the sub-models that described the polypropylene production resulting from phase transition and gas–solid flow behaviour in a gas-phase fluidized bed reactor, was devised. This model was well suited to obtain the vital flow parameters in a pilot-scale catalytic FBR. These parameters included the superficial fluid velocity, monomer-hydrogen concentration, catalyst feed rate, and the product concentrations inside the reactor at reacting-flow conditions. Furthermore, analysis of the polymerization rate in individual phases, the monomer concentration in individual phase distributions in the reactor, and the ratio of polymer production in the bubble phase to the total production rate were also carried out. With respect to the experimental extent of the superficial gas velocity and the Ziegler-Natta feed rate, it was observed that the ratio of the polymer produced as compared to the overall rate of production was approximately in the range of 9%–11%. This was a major sum and it should be looked into seriously.

Real-time data for important process parameters like pressure, temperature and feed rate of hydrogen on the dynamics of polypropylene (PP) production were obtained from a universally distinctive online data acquisition system. To examine the effects of the process parameters on the quality of polypropylene, an industrial standard characterisation study was conducted. The qualitative relationships were also recognised between the operating environments and the multi-scale properties. The results indicated that the findings of real-time dynamics could be applied to steer a multi-scale generalisation of the polymer from chemical process to product engineering. The effects of hydrogen on the polymerisation features were studied at concentrations of 2, 4 and 8 mol%. The produced polypropylene exhibited various physical properties like stiffness, toughness and thermoplastic characteristics due to the alteration of hydrogen mass in the reaction system.

## 7.2 Recommendations and future works

Based on the study that was carried out, the following are recommendations for future research to improve the modelling, optimization and pilot scale validation of this polymerization process engineering.

1. Electrical capacitance tomography (ECT) is a non-invasive imaging technique for multiphase flows like those found in fluidised beds. It is worth mentioning that an ECT system is to be installed and commissioned at the existing pilot plant. It is highly suggested that a validation study of CFD simulation results with ECT be carried out.
2. Various kinds of catalysts and co-catalyst can be evaluated to reduce operational costs, enhance plant safety and attain optimum conditions for high quality production.
3. In the next few years, Big-Data management research in the petrochemical industries is expected to be the hot topic. There are various matters related to Big-Data management in olefin polymerization when real-time data acquisition is very important for very delicate industrial judgements like scale up. The border between the use of pilot scale data, industrial scale data and Internet of Things (IoT) is sometimes very thin for organizations that adopt Big-Data with the intent of allowing better access, performance and efficiency of analysing the data and understanding the data analysis.

## REFERENCES

- Acosta-Iborra, A., Sobrino, C., Hernández-Jiménez, F., & de Vega, M. (2011). Experimental and computational study on the bubble behavior in a 3-D fluidized bed. *Chemical Engineering Science*, 66(15), 3499-3512. doi: 10.1016/j.ces.2011.04.009
- Addagatla, S. K. (2008). *Computational study of Gas-Solid flow in riser section of circulating fluidized beds*. (Master Of Science), Texas A&M University-Kingsville.
- Ahmadzadeh, A., Arastoopour, H., Teymour, F., & Strumendo, M. (2008). Population balance equations' application in rotating fluidized bed polymerization reactor. *Chemical Engineering Research and Design*, 86(4), 329-343.
- Ahuja, G. N., & Patwardhan, A. W. (2008). CFD and experimental studies of solids hold-up distribution and circulation patterns in gas–solid fluidized beds. *Chemical Engineering Journal*, 143(1–3), 147-160.
- Aktaş, N., Boyacı, İ. H., Mutlu, M., & Tanyolaç, A. (2006). Optimization of lactose utilization in deproteinated whey by *Kluyveromyces marxianus* using response surface methodology (RSM). *Bioresource Technology*, 97(18), 2252-2259.
- Al-Adel, M. F., Saville, D. A., & Sundaresan, S. (2002). The Effect of Static Electrification on Gas–Solid Flows in Vertical Risers. *Industrial & Engineering Chemistry Research*, 41(25), 6224-6234. doi: 10.1021/ie010982w
- Aldaco, R., Garea, A., & Irabien, A. (2007). Modeling of particle growth: Application to water treatment in a fluidized bed reactor. *Chemical Engineering Journal*, 134(1–3), 66-71. doi:
- Ali Farhangiyani Kashani, H. A., Mohammad Reza Kalae. (2011). Simulation of an Industrial Linear Low Density Polyethylene Plant *Chemical Product and Process Modeling*, 6(1), 1934-2659.
- Almendros-Ibáñez, J. A., Pallarès, D., Johnsson, F., & Santana, D. (2010). Voidage distribution around bubbles in a fluidized bed: Influence on throughflow. *Powder Technology*, 197(1–2), 73-82.
- Alobaid, F., & Epple, B. (2013). Improvement, validation and application of CFD/DEM model to dense gas–solid flow in a fluidized bed. *Particuology*, 11(5), 514-526.
- Alobaid, F., & Epple, B. Improvement, validation and application of CFD/DEM model to dense gas–solid flow in a fluidized bed. *Particuology*
- Alobaid, F., Ströhle, J., & Epple, B. (2013). Extended CFD/DEM model for the simulation of circulating fluidized bed. *Advanced Powder Technology*, 24(1), 403-415.
- Alshaiban, A., & Soares, J. B. P. (2012). Effect of Hydrogen, Electron Donor, and Polymerization Temperature on Poly(propylene) Microstructure. *Macromolecular Symposia*, 312(1), 72-80. doi: 10.1002/masy.201100023



- Anderson, T. B., & Jackson, R. (1967). Fluid Mechanical Description of Fluidized Beds. Equations of Motion. *Industrial & Engineering Chemistry Fundamentals*, 6(4), 527-539. doi: 10.1021/i160024a007
- Ankamma Rao, D., & Sivashanmugam, P. (2010). Experimental and CFD simulation studies on power consumption in mixing using energy saving turbine agitator. *Journal of Industrial and Engineering Chemistry*, 16(1), 157-161.
- Arastoopour, H., Huang, C. S., & Weil, S. A. (1988). Fluidization behavior of particles under agglomerating conditions. *Chemical Engineering Science*, 43(11), 3063-3075.
- Arencón, D., & Velasco, J. I. (2009). Fracture Toughness of Polypropylene-Based Particulate Composites. *Materials*, 2(4), 2046-2094.
- Asegehegn, T. W., Schreiber, M., & Krautz, H. J. (2012). Influence of two- and three-dimensional simulations on bubble behavior in gas–solid fluidized beds with and without immersed horizontal tubes. *Powder Technology*, 219(0), 9-19.
- Ashrafi, O., Mostoufi, N., & Sotudeh-Gharebagh, R. (2012). Two phase steady-state particle size distribution in a gas-phase fluidized bed ethylene polymerization reactor. *Chemical Engineering Science*, 73(0), 1-7.
- Ashrafi, O., Nazari-Pouya, H., Mostoufi, N., & Sotudeh-Gharebagh, R. (2008). Particle Size Distribution in Gas-phase Polyethylene Reactors. *Advanced Powder Technology*, 19(4), 321-334. doi:
- Ayeni, A. O., Hymore, F. K., Mudliar, S. N., Deshmukh, S. C., Satpute, D. B., Omoleye, J. A., & Pandey, R. A. (2013). Hydrogen peroxide and lime based oxidative pretreatment of wood waste to enhance enzymatic hydrolysis for a biorefinery: Process parameters optimization using response surface methodology. *Fuel*, 106(0), 187-194.
- Azadi, M. (2011). Multi-fluid Eulerian modeling of limestone particles' elutriation from a binary mixture in a gas–solid fluidized bed. *Journal of Industrial and Engineering Chemistry*, 17(2), 229-236. doi:
- Balow, M. J. (2003). *Handbook of polypropylene and polypropylene composites*. New York, NY, USA: CRC Press.
- Basesme, E. A., & Levy, E. K. (1992). Solids exchange between the bubble wake and the emulsion phase in a two-dimensional gas-fluidized bed. *Powder Technology*, 72(1), 45-50.
- Basiri Parsa, J., Merati, Z., & Abbasi, M. (2013). Modeling and optimizing of electrochemical oxidation of C.I. Reactive Orange 7 on the Ti/Sb–SnO<sub>2</sub> as anode via response surface methodology. *Journal of Industrial and Engineering Chemistry*, 19(4), 1350-1355.
- Behjat, Y., Shahhosseini, S., & Hashemabadi, S. H. (2008). CFD modeling of hydrodynamic and heat transfer in fluidized bed reactors. *International Communications in Heat and Mass Transfer*, 35(3), 357-368.

- Bhuiya, M. M. K., Chowdhury, M. S. U., Ahamed, J. U., Khan, M. J. H., Sarkar, M. A. R., Kalam, M. A., . . . Shahabuddin, M. (2012). Heat transfer performance for turbulent flow through a tube using double helical tape inserts. *International Communications in Heat and Mass Transfer*, 39(6), 818-825.
- Bhuiya, M. M. K., Chowdhury, M. S. U., Islam, M., Ahamed, J. U., Khan, M. J. H., Sarker, M. R. I., & Saha, M. (2012). Heat transfer performance evaluation for turbulent flow through a tube with twisted wire brush inserts. *International Communications in Heat and Mass Transfer*, 39(10), 1505-1512.
- Bi, H. T. (2007). A critical review of the complex pressure fluctuation phenomenon in gas–solids fluidized beds. *Chemical Engineering Science*, 62(13), 3473-3493. doi:
- Bi, H. T., Ellis, N., Abba, I. A., & Grace, J. R. (2000). A state-of-the-art review of gas–solid turbulent fluidization. *Chemical Engineering Science*, 55(21), 4789-4825.
- Bin, Y., Zhang, M. C., Dou, B. L., Song, Y. B., & Wu, J. (2002). Discrete Particle Simulation and Visualized Research of the Gas–Solid Flow in an Internally Circulating Fluidized Bed. *Industrial & Engineering Chemistry Research*, 42(1), 214-221.
- Bikiaris, D. (2010). Microstructure and Properties of Polypropylene/Carbon Nanotube Nanocomposites. *Materials*, 3(4), 2884-2946.
- Boemer, A., Qi, H., & Renz, U. (1997). Eulerian simulation of bubble formation at a jet in a two-dimensional fluidized bed. *International Journal of Multiphase Flow*, 23(5), 927-944. doi:
- Bokkers, G. A., van Sint Annaland, M., & Kuipers, J. A. M. (2004). Mixing and segregation in a bidisperse gas–solid fluidised bed: a numerical and experimental study. *Powder Technology*, 140(3), 176-186. doi:
- Boland, D., & Geldart, D. (1972). Electrostatic charging in gas fluidised beds. *Powder Technology*, 5(5), 289-297.
- Briens, C. L., Bergougnou, M. A., Inculet, I. I., Baron, T., & Hazlett, J. D. (1992). Size distribution of particles entrained from fluidized beds: Electrostatic effects. *Powder Technology*, 70(1), 57-62. doi:
- Brown, S. L., & Lattimer, B. Y. (2013). Transient gas-to-particle heat transfer measurements in a spouted bed. *Experimental Thermal and Fluid Science*, 44(0), 883-892. doi:
- Busciglio, A., Vella, G., Micale, G., & Rizzuti, L. (2009). Analysis of the bubbling behaviour of 2D gas solid fluidized beds: Part II. Comparison between experiments and numerical simulations via Digital Image Analysis Technique. *Chemical Engineering Journal*, 148(1), 145-163.
- Busciglio, A., Vella, G., Micale, G., & Rizzuti, L. (2010). Experimental analysis of bubble size distributions in 2D gas fluidized beds. *Chemical Engineering Science*, 65(16), 4782-4791.

- C. Guenther, M. S., M. Syamlal, J. Longanbach, D. Cicero, and P. Smith. (2002). *CFD modeling of a transport gasifier*. Paper presented at the 19th Annual Pittsburgh Coal Conference, Pittsburgh, Pa, USA.
- C. Tagliaferri, L. M., P. Lettieri, A. Marzocchella, G. Olivieri, P. Salatino, . (2013). CFD simulation of bubbling fluidized bidisperse mixtures: Effect of integration methods and restitution coefficient,. *Chemical Engineering Science*
- Cabezas Gómez, L., & Milioli, F. E. (2003). Numerical study on the influence of various physical parameters over the gas–solid two-phase flow in the 2D riser of a circulating fluidized bed. *Powder Technology*, 132(2–3), 216-225.
- Canu, P., & Vecchi, S. (2002). CFD simulation of reactive flows: Catalytic combustion in a monolith. *AIChE Journal*, 48(12), 2921-2935. doi: 10.1002/aic.690481219
- Caspar, J. V., & Meyer, T. J. (1983). Application of the energy gap law to nonradiative, excited-state decay. *The Journal of Physical Chemistry*, 87(6), 952-957. doi: 10.1021/j100229a010
- Chalermssinsuwan, B., Chanchuey, T., Buakhao, W., Gidaspow, D., & Piumsomboon, P. (2012). Computational fluid dynamics of circulating fluidized bed downer: Study of modeling parameters and system hydrodynamic characteristics. *Chemical Engineering Journal*, 189–190(0), 314-335. doi:
- Chalermssinsuwan, B., Gidaspow, D., & Piumsomboon, P. (2011). Two- and three-dimensional CFD modeling of Geldart A particles in a thin bubbling fluidized bed: Comparison of turbulence and dispersion coefficients. *Chemical Engineering Journal*, 171(1), 301-313. doi:
- Chang, J., Wang, G., Gao, J., Zhang, K., Chen, H., & Yang, Y. (2012). CFD modeling of particle–particle heat transfer in dense gas-solid fluidized beds of binary mixture. *Powder Technology*, 217(0), 50-60. doi:
- Chatterjee, S., Kumar, A., Basu, S., & Dutta, S. (2012). Application of Response Surface Methodology for Methylene Blue dye removal from aqueous solution using low cost adsorbent. *Chemical Engineering Journal*, 181–182(0), 289-299.
- Chatzidoukas, C., Perkins, J. D., Pistikopoulos, E. N., & Kiparissides, C. (2003). Optimal grade transition and selection of closed-loop controllers in a gas-phase olefin polymerization fluidized bed reactor. *Chemical Engineering Science*, 58(16), 3643-3658. doi:
- Chen, G., Chen, J., Srinivasakannan, C., & Peng, J. (2012). Application of response surface methodology for optimization of the synthesis of synthetic rutile from titania slag. *Applied Surface Science*, 258(7), 3068-3073.
- Chen, X.-Z., Luo, Z.-H., Yan, W.-C., Lu, Y.-H., & Ng, I. S. (2011). Three-dimensional CFD-PBM coupled model of the temperature fields in fluidized-bed polymerization reactors. *AIChE Journal*, 57(12), 3351-3366. doi: 10.1002/aic.12548
- Chen, X.-Z., Shi, D.-P., Gao, X., & Luo, Z.-H. (2011). A fundamental CFD study of the gas–solid flow field in fluidized bed polymerization reactors. *Powder Technology*, 205(1–3), 276-288. doi:

- Cheung, S. C. P., Yeoh, G. H., & Tu, J. Y. (2007). On the numerical study of isothermal vertical bubbly flow using two population balance approaches. *Chemical Engineering Science*, 62(17), 4659-4674. doi:
- Chiesa, M., Mathiesen, V., Melheim, J. A., & Halvorsen, B. (2005). Numerical simulation of particulate flow by the Eulerian–Lagrangian and the Eulerian–Eulerian approach with application to a fluidized bed. *Computers & Chemical Engineering*, 29(2), 291-304. doi:
- Choi, K. Y., & Ray, W. H. (1988). The dynamic behavior of continuous stirred-bed reactors for the solid catalyzed gas phase polymerization of propylene. *Chemical Engineering Science*, 43(10), 2587-2604. doi:
- Cloete, S., Johansen, S. T., & Amini, S. (2012). An assessment of the ability of computational fluid dynamic models to predict reactive gas–solid flows in a fluidized bed. *Powder Technology*, 215–216(0), 15-25.
- Cooper, S., & Coronella, C. J. (2005). CFD simulations of particle mixing in a binary fluidized bed. *Powder Technology*, 151(1–3), 27-36.
- Cui, Z., & Fan, L. S. (2004a). Energy Spectra for Interactive Turbulence Fields in a Bubble Column. *Industrial & Engineering Chemistry Research*, 44(5), 1150-1159.
- Cui, Z., & Fan, L. S. (2004b). Turbulence energy distributions in bubbling gas–liquid and gas–liquid–solid flow systems. *Chemical Engineering Science*, 59(8–9), 1755-1766. doi:
- D. Gidaspow, Academic Press. (1994). *Multiphase Flow and Fluidization: Continuum and Kinetic Theory Descriptions*. New York, NY, USA.
- D. Kunii, O. L. ( 1991). *Fluidization Engineering* ( 2nd ed.). Boston: Butterworth-Heinemann.
- Dahl, S. R., & Hrenya, C. M. (2005). Size segregation in gas–solid fluidized beds with continuous size distributions. *Chemical Engineering Science*, 60(23), 6658-6673. doi:
- Darelius, A., Rasmuson, A., van Wachem, B., Niklasson Björn, I., & Folestad, S. (2008). CFD simulation of the high shear mixing process using kinetic theory of granular flow and frictional stress models. *Chemical Engineering Science*, 63(8), 2188-2197.
- Davidson, J. F. H., D. . ( 1963). *Fluidized Particles*: Cambridge University Press.
- Dehnavi, M. A., Shahhosseini, S., Hashemabadi, S. H., & Ghafelebashi, S. M. (2008). CFD based evaluation of polymer particles heat transfer coefficient in gas phase polymerization reactors. *International Communications in Heat and Mass Transfer*, 35(10), 1375-1379. doi:
- Dehnavi, M. A., Shahhosseini, S., Hashemabadi, S. H., & Ghafelebashi, S. M. (2010). CFD simulation of hydrodynamics and heat transfer in gas phase ethylene polymerization reactors. *International Communications in Heat and Mass Transfer*, 37(4), 437-442.

- Delva, L., Ragaert, K., Degrieck, J., & Cardon, L. (2014). The Effect of Multiple Extrusions on the Properties of Montmorillonite Filled Polypropylene. *Polymers*, 6(12), 2912.
- Demim, S., Drouiche, N., Aouabed, A., Benayad, T., Couderchet, M., & Semsari, S. Study of heavy metal removal from heavy metal mixture using the CCD method. *Journal of Industrial and Engineering Chemistry* 115(4), 115-122 .
- Di Natale, F., Lancia, A., & Nigro, R. (2009). Surface-to-bed heat transfer in fluidised beds of fine particles. *Powder Technology*, 195(2), 135-142.
- Di Renzo, A., Cello, F., & Di Maio, F. P. (2011). Simulation of the layer inversion phenomenon in binary liquid--fluidized beds by DEM--CFD with a drag law for polydisperse systems. *Chemical Engineering Science*, 66(13), 2945-2958.
- Ding, J., & Gidaspow, D. (1990). A bubbling fluidization model using kinetic theory of granular flow. *AIChE Journal*, 36(4), 523-538. doi: 10.1002/aic.690360404
- Dong, L., Zhao, Y., Luo, Z., Duan, C., Wang, Y., Yang, X., & Zhang, B. (2013). A model for predicting bubble rise velocity in a pulsed gas solid fluidized bed. *International Journal of Mining Science and Technology*, 23(2), 227-230.
- Dora, D. T. K., Mohanty, Y. K., & Roy, G. K. (2013). Hydrodynamics of three-phase fluidization of a homogeneous ternary mixture of regular particles— Experimental and statistical analysis. *Powder Technology*, 237(0), 594-601.
- Doroodchi, E., Galvin, K. P., & Fletcher, D. F. (2005). The influence of inclined plates on expansion behaviour of solid suspensions in a liquid fluidised bed—a computational fluid dynamics study. *Powder Technology*, 156(1), 1-7.
- Eriksson, E. J. G., & McKenna, T. F. (2004). Heat-Transfer Phenomena in Gas-Phase Olefin Polymerization Using Computational Fluid Dynamics. *Industrial & Engineering Chemistry Research*, 43(23), 7251-7260.
- Eriksson, E. J. G., & McKenna, T. F. L. (2009). A Study of Particle-Surface Interactions During Olefin Polymerisation in Gas Phase Reactors. *Macromolecular Symposia*, 285(1), 28-34.
- Esmaili, E., & Mahinpey, N. (2011). Adjustment of drag coefficient correlations in three dimensional CFD simulation of gas--solid bubbling fluidized bed. *Advances in Engineering Software*, 42(6), 375-386.
- F.P. Incropera, D. P. D., T.L. Bergman, A.S. Lavine. ( 2007.). *Fundamentals of Heat and Mass Transfer* (6th ed ed.). New York,: John Wiley & Sons,.
- Faldi, A., & Soares, J. B. P. (2001). Characterization of the combined molecular weight and composition distribution of industrial ethylene/ $\alpha$ -olefin copolymers. *Polymer*, 42(7), 3057-3066.
- Fan, L. a. C. Z. (1998). *Principles of Gas-Solid Flows*. Cambridge, UK: Cambridge University Press.
- Fan, L. S. Z. (2005). *Principles of Gas-Solid Flows*. New York,: Cambridge University Press.

- Fan, R., & Fox, R. O. (2008). Segregation in polydisperse fluidized beds: Validation of a multi-fluid model. *Chemical Engineering Science*, 63(1), 272-285.
- Fang, W., Jingdai, W., & Yongrong, Y. (2008). Distribution of Electrostatic Potential in a Gas-Solid Fluidized Bed and Measurement of Bed Level. *Industrial & Engineering Chemistry Research*, 47(23), 9517-9526.
- Feng, Y., Swenser-Smith, T., Witt, P. J., Doblin, C., Lim, S., & Schwarz, M. P. (2012). CFD modeling of gas-solid flow in an internally circulating fluidized bed. *Powder Technology*, 219(0), 78-85.
- Fernandes, F. A. N., & Ferrareso Lona, L. M. (2001). Fluidized-bed reactor modeling for polyethylene production. *Journal of Applied Polymer Science*, 81(2), 321-332.
- Floyd, S., Choi, K. Y., Taylor, T. W., & Ray, W. H. (1986). Polymerization of olefins through heterogeneous catalysis. III. Polymer particle modelling with an analysis of intraparticle heat and mass transfer effects. *Journal of Applied Polymer Science*, 32(1), 2935-2960. doi: 10.1002/app.1986.070320108
- FLUENT 14.5.7 2013). User guide*
- Frassoldati, A., Frigerio, S., Colombo, E., Inzoli, F., & Faravelli, T. (2005). Determination of emissions from strong swirling confined flames with an integrated CFD-based procedure. *Chemical Engineering Science*, 60(11), 2851-2869.
- Fung, A. S., & Hamdullahpur, F. (1993). A gas and particle flow model in the freeboard of a fluidized bed based on bubble coalescence. *Powder Technology*, 74(2), 121-133.
- Galli, P., & Vecellio, G. (2004). Polyolefins: The most promising large-volume materials for the 21st century. *Journal of Polymer Science Part A: Polymer Chemistry*, 42(3), 396-415. doi: 10.1002/pola.10804
- Gamwo, I. K., Soong, Y., & Lyczkowski, R. W. (1999). Numerical simulation and experimental validation of solids flows in a bubbling fluidized bed. *Powder Technology*, 103(2), 117-129.
- Geldart, D. (1986). *Gas Fluidization Technology*. Chichester,: Wiley & Sons.
- Geldart, D., & Kelsey, J. R. (1972). The use of capacitance probes in gas fluidised beds. *Powder Technology*, 6(1), 45-50.
- Geldart, D., Abdullah, E. C., & Verlinden, A. (2009). Characterisation of dry powders. *Powder Technology*, 190(1-2), 70-74
- Gera, D., & Gautam, M. (1995). Bubble rise velocity in two-dimensional fluidized beds. *Powder Technology*, 84(3), 283-285.
- Gerogiorgis, D. I., & Ydstie, B. E. (2005). Multiphysics CFD Modelling for Design and Simulation of a Multiphase Chemical Reactor. *Chemical Engineering Research and Design*, 83(6), 603-610. doi:

- Gharibshahi, R., Jafari, A., Haghtalab, A., & Karambeigi, M. S. (2015). Application of CFD to evaluate the pore morphology effect on nanofluid flooding for enhanced oil recovery. *RSC Advances*, 5(37), 28938-28949. doi: 10.1039/C4RA15452E
- Gibilaro, L. G., & Rowe, P. N. (1974). A model for a segregating gas fluidised bed. *Chemical Engineering Science*, 29(6), 1403-1412.
- Gidaspow, D. (1994). *Multiphase Flow and Fluidization: Continuum and Kinetic Theory Descriptions*. New York: Academic Press.
- Giffin, A., & Mehrani, P. (2010). Comparison of influence of fluidization time on electrostatic charge build-up in the bubbling vs. slugging flow regimes in gas-solid fluidized beds. *Journal of Electrostatics*, 68(6), 492-502.
- Glauß, B., Steinmann, W., Walter, S., Beckers, M., Seide, G., Gries, T., & Roth, G. (2013). Spinnability and Characteristics of Polyvinylidene Fluoride (PVDF)-based Bicomponent Fibers with a Carbon Nanotube (CNT) Modified Polypropylene Core for Piezoelectric Applications. *Materials*, 6(7), 2642-2661.
- Gobin, A. N., H.; Simonin, O.; Llinas, J.; Reiling, V.; Selo, J. . ( 2012). *In Numerical Simulation of a Gas-Phase Polymerisation Reactor*. Paper presented at the European Congress on Computational Methods in Applied Sciences and Engineering ECCOMAS Computational Fluid Dynamics Conference 2012, Vienna.
- Gobin, A. N., H.; Simonin, O.; Llinas, J.; Reiling, V.; Selo, J. In in ; . (2001). *Numerical Simulation of a Gas-Phase Polymerisation Reactor; European Congress on Computational Methods*. Paper presented at the Computational Fluid Dynamics Conference 20012, Wales.
- Godlieb, W., Deen, N. G., & Kuipers, J. A. M. (2008). On the relationship between operating pressure and granular temperature: A discrete particle simulation study. *Powder Technology*, 182(2), 250-256.
- Goh, Y. R., Zakaria, R., Yang, Y.B., Nasserzadeh, V. and Swithenbank, J. (2003). Reduction of NOX during incineration of municipal solid waste by a fundamental combustion technique. *Journal of the Institute of Energy*, 76((508)), 72-79.
- Gonzalez-R, P. L., Framinan, J. M., & Ruiz-Usano, R. (2011). A response surface methodology for parameter setting in a dynamic Conwip production control system. *International Journal of Manufacturing Technology and Management*, 23(1), 16-33.
- Gröger, T., Tüzün, U., & Heyes, D. M. (2003). Modelling and measuring of cohesion in wet granular materials. *Powder Technology*, 133(1-3), 203-215.
- Guastalla, G., & Giannini, U. (1983). The influence of hydrogen on the polymerization of propylene and ethylene with an MgCl<sub>2</sub> supported catalyst. *Die Makromolekulare Chemie, Rapid Communications*, 4(8), 519-527.
- Gunn, D. J. (1978). Transfer of heat or mass to particles in fixed and fluidised beds. *International Journal of Heat and Mass Transfer*, 21(4), 467-476.

- Guo, Y., Wu, C. Y., & Thornton, C. (2013). Modeling gas-particle two-phase flows with complex and moving boundaries using DEM-CFD with an immersed boundary method. *AIChE Journal*, 59(4), 1075-1087.
- H. Zhao, G. S. P. C., I.I. Incullet, A.G. Bailey, . (2000). Bipolar charging in polydisperse polymer powders in industrial processes. *IEEE* 2, 835–841.
- Hafizi, A., Ahmadpour, A., Koolivand-Salooki, M., Heravi, M. M., & Bamoharram, F. F. (2013). Comparison of RSM and ANN for the investigation of linear alkylbenzene synthesis over H14[NaP5W30O110]/SiO<sub>2</sub> catalyst. *Journal of Industrial and Engineering Chemistry*, 19(6), 1981-1989.
- Hamidipour, M., Chen, J., & Larachi, F. (2012). CFD study on hydrodynamics in three-phase fluidized beds—Application of turbulence models and experimental validation. *Chemical Engineering Science*, 78(0), 167-180.
- Hamzehei, M., & Rahimzadeh, H. (2009). Experimental and Numerical Study of Hydrodynamics with Heat Transfer in a Gas–Solid Fluidized-Bed Reactor at Different Particle Sizes. *Industrial & Engineering Chemistry Research*, 48(6), 3177-3186.
- Harshe, Y. M., Utikar, R. P., & Ranade, V. V. (2004). A computational model for predicting particle size distribution and performance of fluidized bed polypropylene reactor. *Chemical Engineering Science*, 59(22–23), 5145-5156.
- Hassani, M. A., Zarghami, R., Norouzi, H. R., & Mostoufi, N. (2013). Numerical investigation of effect of electrostatic forces on the hydrodynamics of gas–solid fluidized beds. *Powder Technology*, 246(0), 16-25.
- Hatzantonis, H., Goulas, A., & Kiparissides, C. (1998). A comprehensive model for the prediction of particle-size distribution in catalyzed olefin polymerization fluidized-bed reactors. *Chemical Engineering Science*, 53(18), 3251-3267.
- Hatzantonis, H., Yiannoulakis, H., Yiagopoulos, A., & Kiparissides, C. (2000). Recent developments in modeling gas-phase catalyzed olefin polymerization fluidized-bed reactors: The effect of bubble size variation on the reactor's performance. *Chemical Engineering Science*, 55(16), 3237-3259.
- Hayes, R. E. a. K., S.T. (1997). *Introduction to Catalytic Combustion*. USA: Gordon and Breach Science Publishers
- Hendrickson, G. (2006). Electrostatics and gas phase fluidized bed polymerization reactor wall sheeting. *Chemical Engineering Science*, 61(4), 1041-1064.
- Hernández-Jiménez, F., Gómez-García, A., Santana, D., & Acosta-Iborra, A. (2013). Gas interchange between bubble and emulsion phases in a 2D fluidized bed as revealed by two-fluid model simulations. *Chemical Engineering Journal*, 215–216(0), 479-490.
- Herzog, N., Schreiber, M., Egbers, C., & Krautz, H. J. (2012a). A comparative study of different CFD-codes for numerical simulation of gas–solid fluidized bed hydrodynamics. *Computers & Chemical Engineering*, 39(0), 41-46.



- Hisayuki, N., Dodik, K., Toshiaki T., Minoru, T. (2008). Degradation behavior of polymer blend of isotactic polypropylenes with and without unsaturated chain end group. *Science and Technology of Advanced Materials*, 9, 1-6.
- Hjertager, B. F. M. a. B. H. ( 1976). *On mathematical models of turbulent combustion with special emphasis on soot formation and combustion*. Paper presented at the In 16th Symp. (Int'l.) on Combustion, The Combustion Institute, USA.
- Hosseini, S. H., Shojaee, S., Ahmadi, G., & Zivdar, M. (2012). Computational fluid dynamics studies of dry and wet pressure drops in structured packings. *Journal of Industrial and Engineering Chemistry*, 18(4), 1465-1473.
- Hosseini, S. H., Zhong, W., Esfahany, M. N., Pourjafar, L., & Azizi, S. (2010). CFD Simulation of the Bubbling and Slugging Gas-Solid Fluidized Beds. *Journal of Fluids Engineering*, 132(4), 041301-041301.
- Hou, Q.-F., Zhou, Z.-Y., & Yu, A.-B. (2012). Computational Study of the Effects of Material Properties on Heat Transfer in Gas Fluidization. *Industrial & Engineering Chemistry Research*, 51(35), 11572-11586.
- Huilin, L., Gidaspow, D., Bouillard, J., & Wentie, L. (2003). Hydrodynamic simulation of gas–solid flow in a riser using kinetic theory of granular flow. *Chemical Engineering Journal*, 95(1–3), 1-13. doi:
- Huilin, L., Wentie, L., Feng, L., Guangbo, Z., & Yurong, H. (2002). Eulerian simulations of bubble behaviour in a two-dimensional gas–solid bubbling fluidized bed. *International Journal of Energy Research*, 26(15), 1285-1293.
- Hull, A. S., Chen, Z., Fritz, J. W., & Agarwal, P. K. (1999). Influence of horizontal tube banks on the behavior of bubbling fluidized beds: 1. Bubble hydrodynamics. *Powder Technology*, 103(3), 230-242. doi:
- Hulme, I., & Kantzas, A. (2004). Determination of bubble diameter and axial velocity for a polyethylene fluidized bed using X-ray fluoroscopy. *Powder Technology*, 147(1–3), 20-33.
- Hulme, I., Clavelle, E., van der Lee, L., & Kantzas, A. (2005). CFD Modeling and Validation of Bubble Properties for a Bubbling Fluidized Bed. *Industrial & Engineering Chemistry Research*, 44(12), 4254-4266.
- Hutchinson, R. A., & Ray, W. H. (1987). Polymerization of olefins through heterogeneous catalysis. VII. Particle ignition and extinction phenomena. *Journal of Applied Polymer Science*, 34(2), 657-676.
- Ibrehem, A. S. (2009). Hybrid Modeling of Modified Mathematical Model for Gas Phase Olefine in Fluidized Bed Catalyst Reactors Using Artificial Neural Networks. *Chemical Product and Process Modeling*, 4(1), 1934-2659.
- Ibrehem, A. S., Hussain, M. A., & Ghasem, N. M. (2009). Modified mathematical model for gas phase olefin polymerization in fluidized-bed catalytic reactor. *Chemical Engineering Journal*, 149(1–3), 353-362.
- Islam, M. A., Hussein, I. A., & Atiqullah, M. (2007). Effects of branching characteristics and copolymer composition distribution on non-isothermal

crystallization kinetics of metallocene LLDPEs. *European Polymer Journal*, 43(2), 599-610.

- J.R. Mountain, M. K. M., R.A. Sims, D.L. Wankum, T. Chasser, P.H. Pettit Jr. (2001). Triboelectric charging of polymer powders in fluidization and transport processes. *IEEE*, 37, 778–784.
- Jakobsen, H. A., Grevskott, S., & Svendsen, H. F. (1997). Modeling of Vertical Bubble-Driven Flows. *Industrial & Engineering Chemistry Research*, 36(10), 4052-4074. doi: 10.1021/ie970276o
- Jalalinejad, F., Bi, X. T., & Grace, J. R. (2012). Effect of electrostatic charges on single bubble in gas–solid fluidized beds. *International Journal of Multiphase Flow*, 44(0), 15-28. doi:
- Jang, H. T., Park, T. S., & Cha, W. S. (2010). Mixing–segregation phenomena of binary system in a fluidized bed. *Journal of Industrial and Engineering Chemistry*, 16(3), 390-394. doi:
- Jarullah, A. T., Mujtaba, I. M., & Wood, A. S. (2011). Kinetic parameter estimation and simulation of trickle-bed reactor for hydrodesulfurization of crude oil. *Chemical Engineering Science*, 66(5), 859-871.
- Jarullah, A. T., Mujtaba, I. M., & Wood, A. S. (2012). Improving fuel quality by whole crude oil hydrotreating: A kinetic model for hydrodeasphaltenization in a trickle bed reactor. *Applied Energy*, 94(0), 182-191.
- Javad, H., Nayef, M. G., & Wan. (2004). Effects of the Temperature and Mixing Rate on Foaming in a Polymerization Reaction To Produce Fatty Polyamides in the Presence of Catalyst. *Industrial & Engineering Chemistry Research*, 43(19), 6048-6054.
- Jenck, J. F. (1991). Gas - Liquid - Solid Reactors for Hydrogenation in Fine Chemicals Synthesis. In J. B. C. B. D. D. G. P. R. M. M. Guisnet & C. Montassier (Eds.), *Studies in Surface Science and Catalysis* (Vol. Volume 59, pp. 1-19): Elsevier.
- Jiang, Y., Khadilkar, M. R., Al-Dahhan, M. H., & Dudukovic, M. P. (2002). CFD of multiphase flow in packed-bed reactors: I. k-Fluid modeling issues. *AIChE Journal*, 48(4), 701-715.
- Jiradilok, V., Gidaspow, D., & Breault, R. W. (2007). Computation of gas and solid dispersion coefficients in turbulent risers and bubbling beds. *Chemical Engineering Science*, 62(13), 3397-3409.
- Jiradilok, V., Gidaspow, D., Breault, R. W., Shadle, L. J., Guenther, C., & Shi, S. (2008). Computation of turbulence and dispersion of cork in the NETL riser. *Chemical Engineering Science*, 63(8), 2135-2148.
- Jiradilok, V., Gidaspow, D., Damronglerd, S., Koves, W. J., & Mostofi, R. (2006). Kinetic theory based CFD simulation of turbulent fluidization of FCC particles in a riser. *Chemical Engineering Science*, 61(17), 5544-5559.

- Jung, J., Gidaspow, D., & Gamwo, I. K. (2005). Measurement of Two Kinds of Granular Temperatures, Stresses, and Dispersion in Bubbling Beds. *Industrial & Engineering Chemistry Research*, 44(5), 1329-1341
- Jung, J., Gidaspow, D., & Gamwo, I. K. (2006). BUBBLE COMPUTATION, GRANULAR TEMPERATURES, AND REYNOLDS STRESSES. *Chemical Engineering Communications*, 193(8), 946-975
- Kaneko, Y., Shiojima, T., & Horio, M. (1999). DEM simulation of fluidized beds for gas-phase olefin polymerization. *Chemical Engineering Science*, 54(24), 5809-5821.
- Karimi, S., Mansourpour, Z., Mostoufi, N., & Sotudeh-Gharebagh, R. (2011). CFD-DEM Study of Temperature and Concentration Distribution in a Polyethylene Fluidized Bed Reactor. *Particulate Science and Technology*, 29(2), 163-178.
- Kashyap, M., Gidaspow, D., & Koves, W. J. (2011). Circulation of Geldart D type particles: Part I – High solids fluxes. Measurements and computation under solids slugging conditions. *Chemical Engineering Science*, 66(2), 183-206.
- Kaushal, P., & Abedi, J. (2010). A simplified model for biomass pyrolysis in a fluidized bed reactor. *Journal of Industrial and Engineering Chemistry*, 16(5), 748-755. doi:
- Kemmere, M. F., Meuldijk, J., Drinkenburg, A. A. H., & German, A. L. (2001). Emulsification in batch-emulsion polymerization of styrene and vinyl acetate: A reaction calorimetric study. *Journal of Applied Polymer Science*, 79(5), 944-957.
- Kennedy, J. F., & Knill, C. J. (1994). Multicomponent polymer systems. Edited by I. S. Miles and S. Rostami. Longman Scientific & Technical, Harlow, 1992. pp. 435, price £65.00. ISBN 0-582-03785-9. *Polymer International*, 33(3), 342-342.
- Khan Wardag, A. N., & Larachi, F. (2012). Stability analysis of flat- and corrugated-wall bubbling fluidized beds: Differential pressure, heat transfer coefficient, digital image analysis and CFD simulations. *Chemical Engineering Journal*, 179(0), 349-362.
- Khongprom, P., Aimdilokwong, A., Limtrakul, S., Vatanatham, T., & Ramachandran, P. A. (2012). Axial gas and solids mixing in a down flow circulating fluidized bed reactor based on CFD simulation. *Chemical Engineering Science*, 73(0), 8-19.
- Kiashemshaki, A., Mostoufi, N., & Sotudeh-Gharebagh, R. (2006). Two-phase modeling of a gas phase polyethylene fluidized bed reactor. *Chemical Engineering Science*, 61(12), 3997-4006.
- Kolaczowski, S. T., Chao, R., Awdry, S., & Smith, A. (2007). Application of a CFD Code (FLUENT) to Formulate Models of Catalytic Gas Phase Reactions in Porous Catalyst Pellets. *Chemical Engineering Research and Design*, 85(11), 1539-1552.
- Kolhapure, N. H., & Fox, R. O. (1999). CFD analysis of micromixing effects on polymerization in tubular low-density polyethylene reactors. *Chemical Engineering Science*, 54(15-16), 3233-3242.:

- Kotoulas, C., & Kiparissides, C. (2006). A generalized population balance model for the prediction of particle size distribution in suspension polymerization reactors. *Chemical Engineering Science*, 61(2), 332-346.
- Krishna, R., & van Baten, J. M. (2001). Using CFD for scaling up gas–solid bubbling fluidised bed reactors with Geldart A powders. *Chemical Engineering Journal*, 82(1–3), 247-257.
- Kuipers, J. A. M., van Duin, K. J., van Beckum, F. P. H., & van Swaaij, W. P. M. (1993). Computer simulation of the hydrodynamics of a two-dimensional gas-fluidized bed. *Computers & Chemical Engineering*, 17(8), 839-858.
- Kukreja, T. R., Kumar, D., Prasad, K., Chauhan, R. C., Choe, S., & Kundu, P. P. (2002). Optimisation of physical and mechanical properties of rubber compounds by response surface methodology—Two component modelling using vegetable oil and carbon black. *European Polymer Journal*, 38(7), 1417-1422.
- Kumar, R. N., Nagarajan, R., Chee Fun, F., & Leng Seng, P. (2000). Effect of process variables on the exothermicity during the production of phenol–formaldehyde resins – modeling by response surface methodology. *European Polymer Journal*, 36(11), 2491-2497.
- Kuwagi, K., & Horio, M. (2002). A numerical study on agglomerate formation in a fluidized bed of fine cohesive particles. *Chemical Engineering Science*, 57(22–23), 4737-4744.
- Laborde-Boutet, C., Larachi, F., Dromard, N., Delsart, O., & Schweich, D. (2009). CFD simulation of bubble column flows: Investigations on turbulence models in RANS approach. *Chemical Engineering Science*, 64(21), 4399-4413.
- Laux, H. J., S. T. . (1998). *Computer simulation of bubble formation in a gas-solid fluidized bed*. Paper presented at the Ninth Engineering Foundation Conference on Fluidization, Durango, CO.
- Lesage, F., Nedelec, D., Descales, B., & Stephens, W. D. (2012). Dynamic Modelling of a Polypropylene Production Plant. In B. Ian David Lockhart & F. Michael (Eds.), *Computer Aided Chemical Engineering* (Vol. Volume 30, pp. 1128-1132): Elsevier.
- Lettieri, P., Cammarate, L., Micale, G. D. M., & Yates, J. . (2003). CFD simulations of gas fluidized beds using alternative Eulerian–Eulerian modelling approaches. *International Journal of Chemical Reactor Engineering*, , 1, 1542-6580.
- Li, J., & Kuipers, J. A. M. (2002). Effect of pressure on gas–solid flow behavior in dense gas-fluidized beds: a discrete particle simulation study. *Powder Technology*, 127(2), 173-184.
- Li, P., Lan, X., Xu, C., Wang, G., Lu, C., & Gao, J. (2009). Drag models for simulating gas–solid flow in the turbulent fluidization of FCC particles. *Particuology*, 7(4), 269-277.

- Li, S., Marshall, J. S., Liu, G., & Yao, Q. (2011). Adhesive particulate flow: The discrete-element method and its application in energy and environmental engineering. *Progress in Energy and Combustion Science*, 37(6), 633-668.
- Li, T., Garg, R., Galvin, J., & Pannala, S. (2012). Open-source MFIX-DEM software for gas-solids flows: Part II — Validation studies. *Powder Technology*, 220(0), 138-150.
- Li, Y., Yang, G. Q., Zhang, J. P., & Fan, L. S. (2001). Numerical studies of bubble formation dynamics in gas-liquid-solid fluidization at high pressures. *Powder Technology*, 116(2-3), 246-260.
- Li, Y., Zhang, J., & Fan, L.-S. (1999). Numerical simulation of gas-liquid-solid fluidization systems using a combined CFD-VOF-DPM method: bubble wake behavior. *Chemical Engineering Science*, 54(21), 5101-5107.
- Liao, C.-C., Hsiau, S.-S., & Huang, T.-Y. (2011). The effect of vibrating conditions on the electrostatic charge in a vertical vibrating granular bed. *Powder Technology*, 208(1), 1-6.
- Lim, E. W. C., Zhang, Y., & Wang, C.-H. (2006). Effects of an electrostatic field in pneumatic conveying of granular materials through inclined and vertical pipes. *Chemical Engineering Science*, 61(24), 7889-7908.
- Limtrakul, S., Rotjanavijit, W., & Vatanatham, T. (2007). Lagrangian modeling and simulation of effect of vibration on cohesive particle movement in a fluidized bed. *Chemical Engineering Science*, 62(1-2), 232-245.
- Liu, B., Wang, L., Liu, Y., Qian, B., & Jin, Y.-H. (2010). An effective hybrid particle swarm optimization for batch scheduling of polypropylene processes. *Computers & Chemical Engineering*, 34(4), 518-528.
- Liu, D., Bu, C., & Chen, X. Development and test of CFD-DEM model for complex geometry: A coupling algorithm for Fluent and DEM. *Computers & Chemical Engineering*(0).
- Liu, M., Zhang, Y., Bi, H., Grace, J. R., & Zhu, Y. (2010). Non-intrusive determination of bubble size in a gas-solid fluidized bed: An evaluation. *Chemical Engineering Science*, 65(11), 3485-3493.
- Londono, A., Londono, C., Molina, A., & Chejne, F. (2007). *Simulation of gas-solid fluidized bed hydrodynamics using OpenFOAM*. Paper presented at the OpenFOAM International Conference Beaumont House, UK.
- Lun, C. K. K., Savage, S. B., Jeffrey, D. J., & Chepuriniy, N. (1984). Kinetic theories for granular flow: inelastic particles in Couette flow and slightly inelastic particles in a general flowfield. *Journal of Fluid Mechanics*, 140, 223-256.
- Luo, Z.-H., Su, P.-L., Shi, D.-P., & Zheng, Z.-W. (2009). Steady-state and dynamic modeling of commercial bulk polypropylene process of Hypol technology. *Chemical Engineering Journal*, 149(1-3), 370-382.

- Luo, Z.-H., Su, P.-L., You, X.-Z., Shi, D.-P., & Wu, J.-C. (2009). Steady-state particle size distribution modeling of polypropylene produced in tubular loop reactors. *Chemical Engineering Journal*, 146(3), 466-476.
- Lyczkowski, R. W., Bouillard, J. X., Gamwo, I. K., Torpey, M. R., & Montrone, E. D. (2009). Experimental and CFD Analyses of Bubble Parameters in a Variable-Thickness Fluidized Bed. *Industrial & Engineering Chemistry Research*, 49(11), 5166-5173.
- M. J. H. Khan, M. A. H., Z. Mansourpour, N. Mostoufi, N. M. Ghasem, E. C. Abdullah. (2014). CFD Simulation of Fluidized Bed Reactors for Polyolefin Production - A Review. *Journal of Industrial and Engineering Chemistry*.
- M. Syamlal, S. V., and S. M. Cho., ( 1996). *Modeling of coal conversion in a carbonizer*,. Paper presented at the 13th Annual International Pittsburgh Coal Conference,.
- Mansourpour, Z., Karimi, S., Zarghami, R., Mostoufi, N., & Sotudeh-Gharebagh, R. (2010). Insights in hydrodynamics of bubbling fluidized beds at elevated pressure by DEM–CFD approach. *Particuology*, 8(5), 407-414. doi: 10.1016/j.partic.2010.03.017
- Mansourpour, Z., Mostoufi, N., & Sotudeh-Gharebagh, R. (2013). A mechanistic study of agglomeration in fluidised beds at elevated pressures. *The Canadian Journal of Chemical Engineering*, 91(3), 560-569.
- Martinez Prata, D., Schwaab, M., Luis Lima, E., & Carlos Pinto, J. (2010). Simultaneous robust data reconciliation and gross error detection through particle swarm optimization for an industrial polypropylene reactor. *Chemical Engineering Science*, 65(17), 4943-4954.
- Mason, R. L., Gunst, R. F., & Hess, J. L. (2003). *Statistical design and analysis of experiments: with applications to engineering and science* (Vol. 474): Wiley.com.
- Mazzei, L., Casillo, A., Lettieri, P., & Salatino, P. (2010). CFD simulations of segregating fluidized bidisperse mixtures of particles differing in size. *Chemical Engineering Journal*, 156(2), 432-445.
- Mazzei, L., Marchisio, D. L., & Lettieri, P. (2012). New quadrature-based moment method for the mixing of inert polydisperse fluidized powders in commercial CFD codes. *AIChE Journal*, 58(10), 3054-3069.
- McAuley, K. B., MacGregor, J. F., & Hamielec, A. E. (1990). A kinetic model for industrial gas-phase ethylene copolymerization. *AIChE Journal*, 36(6), 837-850. doi: 10.1002/aic.690360605
- McAuley, K. B., Talbot, J. P., & Harris, T. J. (1994). A comparison of two-phase and well-mixed models for fluidized-bed polyethylene reactors. *Chemical Engineering Science*, 49(13), 2035-2045.
- McKenna, T. F., & Soares, J. B. P. (2001). Single particle modelling for olefin polymerization on supported catalysts: A review and proposals for future developments. *Chemical Engineering Science*, 56(13), 3931-3949.

- McKenna, T. F., Cokljat, D., & Wild, P. (1998). CFD Modelling of heat transfer during gas phase olefin polymerisation. *Computers & Chemical Engineering*, 22, Supplement 1(0), S285-S292.
- Mickley, H. S., & Fairbanks, D. F. (1955). Mechanism of heat transfer to fluidized beds. *AIChE Journal*, 1(3), 374-384
- Mikami, T., Kamiya, H., & Horio, M. (1998). Numerical simulation of cohesive powder behavior in a fluidized bed. *Chemical Engineering Science*, 53(10), 1927-1940.
- Miroliaei, A. R., Shahraki, F., Atashi, H., & Karimzadeh, R. (2012). Comparison of CFD results and experimental data in a fixed bed Fischer–Tropsch synthesis reactor. *Journal of Industrial and Engineering Chemistry*, 18(6), 1912-1920.
- Mishra, B. K., Thornton, C., & Bhimji, D. (2002). A preliminary numerical investigation of agglomeration in a rotary drum. *Minerals Engineering*, 15(1–2), 27-33.
- Mitra-Majumdar, D., Farouk, B., & Shah, Y. T. (1997). Hydrodynamic modeling of three-phase flows through a vertical column. *Chemical Engineering Science*, 52(24), 4485-4497.
- Montgomery, D. C. (2006). *Design and analysis of experiments*: Wiley. com.
- Moritz, H. U. (1989). Increase in viscosity and its influence on polymerization processes. *Chemical Engineering & Technology*, 12(1), 71-87.
- Mostafazadeh, M., Rahimzadeh, H., & Hamzei, M. (2013). Numerical analysis of the mixing process in a gas–solid fluidized bed reactor. *Powder Technology*, 239(0), 422-433.
- Moughrabiah, W. O., Grace, J. R., & Bi, X. T. (2008). Effects of Pressure, Temperature, and Gas Velocity on Electrostatics in Gas–Solid Fluidized Beds. *Industrial & Engineering Chemistry Research*, 48(1), 320-325.
- Mudde, R. F., Groen, J. S., & Van Den Akker, H. E. A. (1997). Liquid velocity field in a bubble column: LDA experiments. *Chemical Engineering Science*, 52(21–22), 4217-4224.
- Myers, R. H., & Anderson-Cook, C. M. (2009). *Response surface methodology: process and product optimization using designed experiments* (Vol. 705): Wiley. com.
- N.N. Li, A. G. F., W.S.W. Ho. ( 2008). *Advanced Membrane Technology and Application*. New York, USA.: John Wiley & Sons Inc.
- Nguyen, T.-A., Gregersen, Ø., & Männle, F. (2015). Thermal Oxidation of Polyolefins by Mild Pro-Oxidant Additives Based on Iron Carboxylates and Lipophilic Amines: Degradability in the Absence of Light and Effect on the Adhesion to Paperboard. *Polymers*, 7(8), 1468.
- Norouzi, H. R., Mostoufi, N and Sotoudeh-Gharebagh, R. . (2012). Segregation behavior of particles in gas solid fluidized beds at elevated pressure. *Journal of Chemical and Petroleum Engineering*, 46, 111-121.

- Norouzi, H. R., Mostoufi, N., & Sotudeh-Gharebagh, R. (2012). Effect of fines on segregation of binary mixtures in gas–solid fluidized beds. *Powder Technology*, 225(0), 7-20.
- Norouzi, H. R., Mostoufi, N., Mansourpour, Z., Sotudeh-Gharebagh, R., & Chaouki, J. (2011). Characterization of solids mixing patterns in bubbling fluidized beds. *Chemical Engineering Research and Design*, 89(6), 817-826.
- O'Brien, M. S. a. T. J. (1989). *Computer Simulation of Bubbles in a Fluidized Bed*. Paper presented at the AIChE Symp. Series.85.
- Onishi, R., Takahashi, K., & Vassilicos, J. C. (2013). An efficient parallel simulation of interacting inertial particles in homogeneous isotropic turbulence. *Journal of Computational Physics*, 242(0), 809-827.
- Pain, C. C., Mansoorzadeh, S., & de Oliveira, C. R. E. (2001). A study of bubbling and slugging fluidised beds using the two-fluid granular temperature model. *International Journal of Multiphase Flow*, 27(3), 527-551.
- Panneerselvam, R., Savithri, S., & Surender, G. D. (2007). CFD based investigations on hydrodynamics and energy dissipation due to solid motion in liquid fluidised bed. *Chemical Engineering Journal*, 132(1–3), 159-171.
- Passalacqua, A., & Fox, R. O. (2011). Implementation of an iterative solution procedure for multi-fluid gas–particle flow models on unstructured grids. *Powder Technology*, 213(1–3), 174-187.
- Patankar, S. V. (1980). *Numerical Heat Transfer and Fluid Flow* (First ed.). Washington, DC: Hemisphere Publishing.
- Patel, H., Ein-Mozaffari, F., & Dhib, R. (2010). CFD analysis of mixing in thermal polymerization of styrene. *Computers & Chemical Engineering*, 34(4), 421-429.
- Patil, D. J., Smit, J., van Sint Annaland, M., & Kuipers, J. A. M. . (2006). Wall-to-bed heat transfer in gas–solid bubbling fluidized beds. *AIChE Journal*, 52(1), 58-74.
- Paul, E. L., Atiemo-Obeng, V. A., & Kresta, S. M. (2004). *Handbook of industrial mixing*. New York: John Wiley.
- Peirano, E., Delloume, V., & Leckner, B. (2001). Two- or three-dimensional simulations of turbulent gas–solid flows applied to fluidization. *Chemical Engineering Science*, 56(16), 4787-4799.
- Peng, B., Zhu, J., & Zhang, C. (2011). A New Approach To Specify the Inlet Boundary Conditions for Computational Fluid Dynamics (CFD) Modeling of Hydrodynamic Behavior of a Circulating Fluidized Bed (CFB) Riser. *Industrial & Engineering Chemistry Research*, 51(4), 2152-2165. doi: 10.1021/ie200916c
- Pracella, M., Haque, M. M.-U., & Alvarez, V. (2010). Functionalization, Compatibilization and Properties of Polyolefin Composites with Natural Fibers. *Polymers*, 2(4), 554.
- Prasetya, A., Liu, L., Litster, J., Watanabe, F., Mitsutani, K., & Ko, G. H. (1999). Dynamic model development for residence time distribution control in high-



- impact polypropylene copolymer process. *Chemical Engineering Science*, 54(15–16), 3263-3271.
- Puettmann, A., Hartge, E. U., & Werther, J. (2012). Application of the flowsheet simulation concept to fluidized bed reactor modeling. Part I: Development of a fluidized bed reactor simulation module. *Chemical Engineering and Processing: Process Intensification*, 60(0), 86-95.
- R. Elsdon, F. R. G. M. (1976). Contact electrification of polymers. *Journal of Physics D: Applied Physics*, 9, 1445–1460.
- R. Elsdon, F. R. G. M. (1976). Contact electrification of polymers. *Journal of Physics D: Applied Physics*, 9, 1445–1460.
- R. Fan, R. O. F., M.E. Muhle. (2007). *Role of intrinsic kinetics and catalyst particle size distribution in CFD simulations of polymerization reactors*. Paper presented at the The 12th International Conference on Fluidization,, Vancouver, Canada.
- R. R.B. Bird, W. E. S., E.N. . (2002). *Transport Phenomena* (2nd ed. ed.). Lightfoot, New York,: Jonh Wiley & Sons, Inc.
- R.C. Darton, R. D. L., J.F. Davidson, D. Harrison. (1977). Bubble growth due to coalescence in fluidized beds. *Transactions of the Institutions of Chemical Engineers*, 55, 274–280.
- Rabinovich, E., & Kalman, H. (2011). Flow regime diagram for vertical pneumatic conveying and fluidized bed systems. *Powder Technology*, 207(1–3), 119-133.
- Rajković, K. M., Avramović, J. M., Milić, P. S., Stamenković, O. S., & Veljković, V. B. (2013). Optimization of ultrasound-assisted base-catalyzed methanolysis of sunflower oil using response surface and artificial neural network methodologies. *Chemical Engineering Journal*, 215–216(0), 82-89.
- Ranade, V. (2001). *Computational Flow Modeling for Chemical Reactor Engineering*. New York Academic Press.
- Rathore, S. K., & Das, M. K. (2013). Comparison of two low-Reynolds number turbulence models for fluid flow study of wall bounded jets. *International Journal of Heat and Mass Transfer*, 61(0), 365-380.
- Reh, L. (1999). Challenges of circulating fluid-bed reactors in energy and raw materials industries. *Chemical Engineering Science*, 54(22), 5359-5368.
- Reuge, N., Cadoret, L., Coufort-Saudejaud, C., Pannala, S., Syamlal, M., & Caussat, B. (2008). Multifluid Eulerian modeling of dense gas–solids fluidized bed hydrodynamics: Influence of the dissipation parameters. *Chemical Engineering Science*, 63(22), 5540-5551.
- Rhodes, M. J., Wang, X. S., Nguyen, M., Stewart, P., & Liffman, K. (2001). Study of mixing in gas-fluidized beds using a DEM model. *Chemical Engineering Science*, 56(8), 2859-2866.:

- Rokkam, R. G., Fox, R. O., & Muhle, M. E. (2010). Computational fluid dynamics and electrostatic modeling of polymerization fluidized-bed reactors. *Powder Technology*, 203(2), 109-124.
- Roy, S., Dhotre, M. T., & Joshi, J. B. (2006). CFD Simulation of Flow and Axial Dispersion in External Loop Airlift Reactor. *Chemical Engineering Research and Design*, 84(8), 677-690.
- Rudniak, L., Machniewski, P. M., Milewska, A., & Molga, E. (2004). CFD modelling of stirred tank chemical reactors: homogeneous and heterogeneous reaction systems. *Chemical Engineering Science*, 59(22-23), 5233-5239.
- Ryu, J.-B., Jung, C.-Y., & Yi, S.-C. (2013). Three-dimensional simulation of humid-air dryer using computational fluid dynamics. *Journal of Industrial and Engineering Chemistry*, 19(4), 1092-1098.
- Sahu, J. N., Chava, V. S. R. K., Hussain, S., Patwardhan, A. V., & Meikap, B. C. (2010). Optimization of ammonia production from urea in continuous process using ASPEN Plus and computational fluid dynamics study of the reactor used for hydrolysis process. *Journal of Industrial and Engineering Chemistry*, 16(4), 577-586.
- Salama, F., Sowinski, A., Atieh, K., & Mehrani, P. (2013). Investigation of electrostatic charge distribution within the reactor wall fouling and bulk regions of a gas-solid fluidized bed. *Journal of Electrostatics*, 71(1), 21-27.
- Sassi, K. M., & Mujtaba, I. M. (2013). MINLP based superstructure optimization for boron removal during desalination by reverse osmosis. *Journal of Membrane Science*, 440(0), 29-39.
- Sedighikamal, H., & Zarghami, R. (2013). Dynamic characteristics of bubbling fluidization through recurrence rate analysis of pressure fluctuations. *Particuology*, 11(3), 282-287.
- Setiabudi, H. D., Jalil, A. A., Triwahyono, S., Kamarudin, N. H. N., & Jusoh, R. (2013). Ir/Pt-HZSM5 for n-pentane isomerization: Effect of Si/Al ratio and reaction optimization by response surface methodology. *Chemical Engineering Journal*, 217(0), 300-309.
- Seyyed Hossein Hosseini, M. Z., Rahbar Rahimi, M., Abdolreza Samimi. (2009). CFD Simulation of Solid Hold-Up in Gas-Solid Fluidized Bed at High Gas Velocities, *Chemical Product and Process Modeling*, 4(1), 1934-2659.
- Shamiri, A., Azlan Hussain, M., Sabri Mjalli, F., Mostoufi, N., & Saleh Shafeeyan, M. (2011). Dynamic modeling of gas phase propylene homopolymerization in fluidized bed reactors. *Chemical Engineering Science*, 66(6), 1189-1199.
- Shamiri, A., Hussain, M. A., Mjalli, F. S., & Mostoufi, N. (2010). Kinetic modeling of propylene homopolymerization in a gas-phase fluidized-bed reactor. *Chemical Engineering Journal*, 161(1-2), 240-249.
- Shamiri, A., Hussain, M. A., Mjalli, F. S., & Mostoufi, N. (2010). Improved single phase modeling of propylene polymerization in a fluidized bed reactor. *Computers & Chemical Engineering*, 36(0), 35-47.

- Sharmene Ali, F., Adnan Ali, M., Ayesha Ali, R., & Inculet, I. I. (1998). Minority charge separation in falling particles with bipolar charge. *Journal of Electrostatics*, 45(2), 139-155.
- Shen, L., Johnsson, F., & Leckner, B. (2004). Digital image analysis of hydrodynamics two-dimensional bubbling fluidized beds. *Chemical Engineering Science*, 59(13), 2607-2617.
- Shi, D.-P., Luo, Z.-H., & Guo, A.-Y. (2010). Numerical Simulation of the Gas–Solid Flow in Fluidized-Bed Polymerization Reactors. *Industrial & Engineering Chemistry Research*, 49(9), 4070-4079.
- Shih, Y. T., Gidaspow, D., & Wasan, D. (1987). Hydrodynamics of electroluidization: Separation of pyrites from coal. *AIChE Journal*, 33(8), 1322-1333.
- Shuaeib, F. M., Hamouda, A. M. S., Wong, S. V., Umar, R. S. R., & Ahmed, M. M. H. M. (2007). A new motorcycle helmet liner material: The finite element simulation and design of experiment optimization. *Materials & Design*, 28(1), 182-195.
- Shuai, W., Zhenhua, H., Huilin, L., Goudong, L., Jiaying, W., & Pengfei, X. (2012). A bubbling fluidization model using kinetic theory of rough spheres. *AIChE Journal*, 58(2), 440-455.
- Sitnai, O. (1982). Utilization of the pressure differential records from gas fluidized beds with internals for bubble parameters determination. *Chemical Engineering Science*, 37(7), 1059-1066.
- Soliman, M. A., Aljarboa, T., & Alahmad, M. (1994). Simulation of free radical polymerization reactors. *Polymer Engineering and Science*, 19(34), 1454.
- Sowinski, A., Mayne, A., & Mehrani, P. (2012). Effect of fluidizing particle size on electrostatic charge generation and reactor wall fouling in gas–solid fluidized beds. *Chemical Engineering Science*, 71(0), 552-563.
- Sowinski, A., Miller, L., & Mehrani, P. (2010). Investigation of electrostatic charge distribution in gas–solid fluidized beds. *Chemical Engineering Science*, 65(9), 2771-2781.
- Sowinski, A., Salama, F., & Mehrani, P. (2009). New technique for electrostatic charge measurement in gas–solid fluidized beds. *Journal of Electrostatics*, 67(4), 568-573.
- Srivastava, D. (2002). Optimization studies on the development of methylmethacrylate (mma)-grafted nylon-6 fibers with high percentage grafting *Journal of Polymer Engineering* (Vol. 22, pp. 457).
- Stewart, P. H., Larson, C. W., & Golden, D. M. (1989). Pressure and temperature dependence of reactions proceeding via a bound complex. 2. Application to  $2\text{CH}_3 \rightarrow \text{C}_2\text{H}_5 + \text{H}$ . *Combustion and Flame*, 75(1), 25-31.
- Sun, J., Wang, J., & Yang, Y. (2012). CFD simulation and wavelet transform analysis of vortex and coherent structure in a gas–solid fluidized bed. *Chemical Engineering Science*, 71(0), 507-519.

- Sun, J., Zhou, Y., Ren, C., Wang, J., & Yang, Y. (2011). CFD simulation and experiments of dynamic parameters in gas–solid fluidized bed. *Chemical Engineering Science*, 66(21), 4972-4982.
- Syamlal, M. (1994). MFIX Documentation, User's Manual. Springfield, Va, USA: National Technical Information Service.
- Syamlal, M., O'Brien, T. J., Benyahia, S., Gel, A., & Pannala, S. (2008). Open-Source Software in Computational Research: A Case Study. *Modelling and Simulation in Engineering*, 2008.
- Syamlal, M., & Gidaspow, D. (1985). Hydrodynamics of fluidization: Prediction of wall to bed heat transfer coefficients. *AIChE Journal*, 31(1), 127-135.
- Syamlal, M., & O'Brien, T. J. (2003). Fluid dynamic simulation of O<sub>3</sub> decomposition in a bubbling fluidized bed. *AIChE Journal*, 49(11), 2793-2801. doi: 10.1002/aic.690491112
- Syamlal, M., O'Brien, T. (1989). *Computer simulation of bubbles in a fluidized bed*. Paper presented at the A.I.Ch.E. Sympisium Series 85.
- Syamlal, M., Rogers, W., & O'Brien, T. J. (1993). MFIX documentation theory guide *Other Information: PBD: Dec 1993* (pp. Medium: ED; Size: 49 p.).
- Syamlal, M., Rogers, W., & O'Brien, T. J. (1993). MFIX documentation: Theory guide (Technical Note). (DOE/METC-95/1013 and NTIS/DE95000031). from National Energy Technology Laboratory, Department of Energy
- Tagami, N., Mujumdar, A., & Horio, M. (2009). DEM simulation of polydisperse systems of particles in a fluidized bed. *Particuology*, 7(1), 9-18.
- Taghipour, F., Ellis, N., & Wong, C. (2005). Experimental and computational study of gas–solid fluidized bed hydrodynamics. *Chemical Engineering Science*, 60(24), 6857-6867.
- Tian, Z., Xue-Ping, G., Feng, L.-F., & Guo-Hua, H. (2013). A model for the structures of impact polypropylene copolymers produced by an atmosphere-switching polymerization process. *Chemical Engineering Science*, 101(0), 686-698.
- Tioni, E., Broyer, J. P., Spitz, R., Monteil, V., & McKenna, T. F. L. (2009). Heat Transfer in Gas Phase Olefin Polymerisation. *Macromolecular Symposia*, 285(1), 58-63.
- Tiyapiboonchaiya, P., Gidaspow, D., & Damronglerd, S. (2012). Hydrodynamics of Electrostatic Charge in Polypropylene Fluidized Beds. *Industrial & Engineering Chemistry Research*, 51(25), 8661-8668.
- Trambouze, P. (1993). Computational Fluid Dynamics Applied to Chemical Reaction Engineering. In P. A. Pilavachi (Ed.), *Energy Efficiency in Process Technology* (pp. 1122-1131): Springer Netherlands.
- Tsuchiya, K., Song, G.-H., & Fan, L.-S. (1990). Effects of particle properties on bubble rise and wake in a two-dimensional liquid—solid fluidized bed. *Chemical Engineering Science*, 45(5), 1429-1434.

- Umair, S., Numada, M., Amin, M., & Meguro, K. (2015). Fiber Reinforced Polymer and Polypropylene Composite Retrofitting Technique for Masonry Structures. *Polymers*, 7(5), 963.
- van Sint Annaland, M., Bokkers, G. A., Goldschmidt, M. J. V., Olaofe, O. O., van der Hoef, M. A., & Kuipers, J. A. M. (2009). Development of a multi-fluid model for poly-disperse dense gas–solid fluidised beds, Part II: Segregation in binary particle mixtures. *Chemical Engineering Science*, 64(20), 4237-4246.
- van Wachem, B. G. M., Schouten, J. C., Krishna, R., & van den Bleek, C. M. (1998). Eulerian simulations of bubbling behaviour in gas-solid fluidised beds. *Computers & Chemical Engineering*, 22, Supplement 1(0), S299-S306.
- Vegendla, S. N. P., Heynderickx, G. J., & Marin, G. B. (2011). Comparison of Eulerian–Lagrangian and Eulerian–Eulerian method for dilute gas–solid flow with side inlet. *Computers & Chemical Engineering*, 35(7), 1192-1199.
- Vejahati, F., Mahinpey, N., Ellis, N., & Nikoo, M. B. (2009). CFD simulation of gas–solid bubbling fluidized bed: A new method for adjusting drag law. *The Canadian Journal of Chemical Engineering*, 87(1), 19-30.
- Villarreal–Marroquín, M. G., Castro, J. M., Chacón–Mondragón, Ó. L., & Cabrera–Ríos, M. (2013). Optimisation via simulation: a metamodelling–based method and a case study. *European Journal of Industrial Engineering*, 7(3), 275-294.
- Vun, S., Naser, J., Witt, P. J., & Yang, W. (2010). Measurements and numerical predictions of gas vortices formed by single bubble eruptions in the freeboard of a fluidised bed. *Chemical Engineering Science*, 65(22), 5808-5820.
- Wadnerkar, D., Utikar, R. P., Tade, M. O., & Pareek, V. K. (2012). CFD simulation of solid–liquid stirred tanks. *Advanced Powder Technology*, 23(4), 445-453.
- Wang, L., Zhang, B., Wang, X., Ge, W., & Li, J. (2013). Lattice Boltzmann based discrete simulation for gas–solid fluidization. *Chemical Engineering Science*, 101(0), 228-239.
- Wang, S., Liu, G., Lu, H., Sun, L., & Xu, P. (2012). CFD simulation of bubbling fluidized beds using kinetic theory of rough sphere. *Chemical Engineering Science*, 71(0), 185-201.
- Wang, T., Wang, J., & Jin, Y. (2006). A CFD–PBM coupled model for gas–liquid flows. *AIChE Journal*, 52(1), 125-140.
- Wang, W., & Li, J. (2007). Simulation of gas–solid two-phase flow by a multi-scale CFD approach—of the EMMS model to the sub-grid level. *Chemical Engineering Science*, 62(1–2), 208-231.
- Wang, W., Lu, B., & Li, J. (2007). Choking and flow regime transitions: Simulation by a multi-scale CFD approach. *Chemical Engineering Science*, 62(3), 814-819.
- Wang, W., Lu, B., Zhang, N., Shi, Z., & Li, J. (2010). A review of multiscale CFD for gas–solid CFB modeling. *International Journal of Multiphase Flow*, 36(2), 109-118.

- Wang, X. S., & Rhodes, M. J. (2004). Mechanistic study of defluidization by numerical simulation. *Chemical Engineering Science*, 59(1), 215-222.
- Wang, Y., & Yuan, F. The basic study of methanol to gasoline in a pilot-scale fluidized bed reactor. *Journal of Industrial and Engineering Chemistry*(0).
- Wardag, A. N. K., & Larachi, F. (2012). Bubble behavior in corrugated-wall bubbling fluidized beds—Experiments and CFD simulations. *AIChE Journal*, 58(7), 2045-2057.
- Warnecke, H. J., Schäfer, M., Prüss, J., & Weidenbach, M. (1999). A concept to simulate an industrial size tube reactor with fast complex kinetics and absorption of two gases on the basis of CFD modeling. *Chemical Engineering Science*, 54(13–14), 2513-2519.
- Wei, L.-H., Yan, W.-C., & Luo, Z.-H. (2011). A preliminary CFD study of the gas–solid flow fields in multizone circulating polymerization reactors. *Powder Technology*, 214(1), 143-154.
- Wells, G. J., & Ray, W. H. (2005). Mixing effects on performance and stability of low-density polyethylene reactors. *AIChE Journal*, 51(12), 3205-3218. doi: 10.1002/aic.10544
- Witt, P. J., Perry, J. H., & Schwarz, M. P. (1998). A numerical model for predicting bubble formation in a 3D fluidized bed. *Applied Mathematical Modelling*, 22(12), 1071-1080.
- Wu, C.-l., & Zhan, J.-m. (2007). Numerical prediction of particle mixing behavior in a bubbling fluidized bed. *Journal of Hydrodynamics, Ser. B*, 19(3), 335-341.
- Xie, J., Zhong, W., Jin, B., Shao, Y., & Huang, Y. (2013). Eulerian–Lagrangian method for three-dimensional simulation of fluidized bed coal gasification. *Advanced Powder Technology*, 24(1), 382-392.
- Xie, T., McAuley, K. B., Hsu, J. C. C., & Bacon, D. W. (1994). Gas Phase Ethylene Polymerization: Production Processes, Polymer Properties, and Reactor Modeling. *Industrial & Engineering Chemistry Research*, 33(3), 449-479.
- Xiong, Q., Li, B., Zhou, G., Fang, X., Xu, J., Wang, J., Li, J. (2012). Large-scale DNS of gas–solid flows on Mole-8.5. *Chemical Engineering Science*, 71(0), 422-430.
- Xu, X., Wu, Y., Qiu, Y., Dong, C., Wu, G. y., & Wang, H. (2006). Study on cationic polymerization of isobutylene using electrochemical method. *European Polymer Journal*, 42(10), 2791-2800.
- Xuejing Zheng, M. S. P., G' unterWeickert, Joachim Loos. (2006). Study the porosity effects of Ziegler–Natta catalyst on polymerization system,. *European Polymer Journal*, 68 ,680–688.
- Yan, W.-C., Chen, G.-Q., & Luo, Z.-H. (2012). A CFD Modeling Approach to Design a New Gas Barrier in a Multizone Circulating Polymerization Reactor. *Industrial & Engineering Chemistry Research*, 51(46), 15132-15144.

- Yan, W.-C., Li, J., & Luo, Z.-H. (2012). A CFD-PBM coupled model with polymerization kinetics for multizone circulating polymerization reactors. *Powder Technology*, 231(0), 77-87.
- Yan, W.-C., Luo, Z.-H., Lu, Y.-H., & Chen, X.-D. (2012). A CFD-PBM-PMLM integrated model for the gas–solid flow fields in fluidized bed polymerization reactors. *AIChE Journal*, 58(6), 1717-1732.
- Yang, G. Q., Du, B., & Fan, L. S. (2007). Bubble formation and dynamics in gas–liquid–solid fluidization—A review. *Chemical Engineering Science*, 62(1–2), 2-27.
- Yang, R. Y., Yu, A. B., Choi, S. K., Coates, M. S., & Chan, H. K. (2008). Agglomeration of fine particles subjected to centripetal compaction. *Powder Technology*, 184(1), 122-129.
- Yang, W. C. (2003). *Handbook of Fluidization and Fluid-Particle Systems*. New York: Marcel Dekker, Inc.
- Yao, L., Bi, H. T., & Park, A.-H. (2002). Characterization of electrostatic charges in freely bubbling fluidized beds with dielectric particles. *Journal of Electrostatics*, 56(2), 183-197.
- Yiannoulakis, H., Yiagopoulos, A., & Kiparissides, C. (2001). Recent developments in the particle size distribution modeling of fluidized-bed olefin polymerization reactors. *Chemical Engineering Science*, 56(3), 917-925.
- Yiwei Zhong, Z. W., Zhancheng Guo, Qing Tang. (2013). Prediction of defluidization behavior of iron powder in a fluidized bed at elevated temperatures: Theoretical model and experimental verification. *Powder Technology*, 76(5), 117-123.
- Yu, C.-Y. W. a. Y. H. ( 1966). "*Mechanics of Fluidization*". Paper presented at the Chem. Eng. Prog. Symp. Series. 62.
- Yu, X., Li, W., Xu, Y., Wang, J., Yang, Y., Xu, N., & Wang, H. (2009). Effect of Polymer Granules on the Electrostatic Behavior in Gas–Solid Fluidized Beds. *Industrial & Engineering Chemistry Research*, 49(1), 132-139.
- Yusuf, R., Halvorsen, B., & Melaaen, M. C. (2012). Computational fluid dynamic simulation of ethylene hydrogenation in a fluidised bed of porous catalyst particles. *The Canadian Journal of Chemical Engineering*, 90(3), 544-557.
- Zacca, J. J., Debling, J. A., & Ray, W. H. (1996). Reactor residence time distribution effects on the multistage polymerization of olefins—I. Basic principles and illustrative examples, polypropylene. *Chemical Engineering Science*, 51(21), 4859-4886.
- Zavala, V. M., Flores-Tlacuahuac, A., & Vivaldo-Lima, E. (2005). Dynamic optimization of a semi-batch reactor for polyurethane production. *Chemical Engineering Science*, 60(11), 3061-3079.
- Zhang, J., Li, Y., & Fan, L.-S. (2000). Numerical studies of bubble and particle dynamics in a three-phase fluidized bed at elevated pressures. *Powder Technology*, 112(1–2), 46-56.

- Zhang, K., Brandani, S., & Bi, J. (2005). Computational fluid dynamics for dense gas-solid fluidized beds. *Progress in Natural Science*, 15(sup1), 42-51.
- Zhang, K., Brandani, S., Bi, J., & Jiang, J. (2008). CFD simulation of fluidization quality in the three-dimensional fluidized bed. *Progress in Natural Science*, 18(6), 729-733.
- Zhang, S. X., & Ray, W. H. (1997). Modeling of imperfect mixing and its effects on polymer properties. *AIChE Journal*, 43(5), 1265-1277.
- Zhang, Y., Jin, B., & Zhong, W. (2009). Experimental investigation on mixing and segregation behavior of biomass particle in fluidized bed. *Chemical Engineering and Processing: Process Intensification*, 48(3), 745-754.
- Zhang, Y., Jin, B., Zhong, W., Ren, B., & Xiao, R. (2010). DEM simulation of particle mixing in flat-bottom spout-fluid bed. *Chemical Engineering Research and Design*, 88(5-6), 757-771.
- Zhong, H., Gao, J., Xu, C., & Lan, X. (2012). CFD modeling the hydrodynamics of binary particle mixtures in bubbling fluidized beds: Effect of wall boundary condition. *Powder Technology*, 230(0), 232-240.
- Zhou, Y., Ren, C., Wang, J., Yang, Y., & Dong, K. (2013). Effect of hydrodynamic behavior on electrostatic potential distribution in gas-solid fluidized bed. *Powder Technology*, 235(0), 9-17.
- Zhou, Z. Y., Yu, A. B., & Zulli, P. (2009). Particle scale study of heat transfer in packed and bubbling fluidized beds. *AIChE Journal*, 55(4), 868-884.
- Zhuang, Y.-Q., Chen, X.-M., Luo, Z.-H., & Xiao, J. (2014). CFD-DEM modeling of gas-solid flow and catalytic MTO reaction in a fluidized bed reactor. *Computers & Chemical Engineering*, 60(0), 1-16.



## LIST OF PUBLICATIONS

### Academic Journals (Published)

(1) **M.J.H. Khan**, M.A. Hussain, Z. Mansourpour, N. Mostoufi, N.M. Ghasem, E.C. Abdullah; CFD simulation of fluidized bed reactors for polyolefin production – A review, *Journal of Industrial and Engineering Chemistry*, 2014 (ISI cited *Tier-1* journal) (**CHAPTER-II**)

(2) **M. J. H. Khan** , M.A. Hussain , I.M.Mujtaba; Polypropylene production optimization in Fluidized Bed Catalytic reactor (FBCR)–statistical modeling and pilot scale experimental validation, *Materials*, February, 2014 (ISI cited *Tier-1* journal)

(**CHAPTER-III**)

(3) **M. J. H.Khan**, M.A. Hussain , I.M.Mujtaba; Multiphasic Reaction Modeling for Polypropylene Production in a Pilot-Scale Catalytic Reactor, *Polymers*, 2016, 8, 220; (ISI cited *Tier-1* journal) (**CHAPTER-IV**)

(4) **M.J.H.Khan**, M.A. Hussain , I.M.Mujtaba; Developed Hybrid Model for Propylene Polymerisation at Optimum Reaction Conditions, *Polymers* 2016, 8, 47; (ISI cited *Tier-1* journal) (**CHAPTER-V**)

### **Under Review**

(5) **M. J. H. Khan**, M. A. Hussain, I. M. Mujtaba and H. Al-Rashid, Effect of Dynamic Process Parameters on Production Rate of Polypropylene and Their Mechanical Features: From Validating Models to Product Engineering, *Advances in Production Engineering & Management (APEM)*, (Under Review) , (ISI cited *Tier-1* journal) (**CHAPTER-VI**)

(6) **M. J. H. Khan** , M.A. Hussain , I.M.Mujtaba, M.M.Rashid, M.A.Kalam; Fluidization Application in the Energy Sector: A Review, (ready for submission)

### Conference proceedings

(1) **M. J. H. Khan** , M.A. Hussain , I.M.Mujtaba : Integrated optimization modeling for propylene polymerization, WPOC & APO 2015, 23<sup>rd</sup> November to 27 November, 2015, Tokyo, *Japan*

(2) **M. J. H. Khan** , M.A. Hussain , I.M.Mujtaba : Process parameters optimization for polypropylene production in a pilot scale fluidized bed catalytic reactor, Chemeca , 2014 conference, 28 September to 1<sup>st</sup> October, 2014, Perth, *Australia*.

(3) **M. J. H. Khan** , M.A. Hussain , I.M.Mujtaba : Identification of optimum process parameters for propylene polymerization in pilot scale fluidized bed catalytic reactor (FBCR), 23rd International Symposium on Chemical Reaction Engineering (ISCRE 23)Centara Grand & Bangkok Convention Centre (BCC) at Central World, Bangkok, **Thailand**

(4) **M. J. H. Khan** , M.A. Hussain ' A review on CFD modeling of fluidization bed gas phase reactor for polyolefin production, Regional Symposium on Chemical Engineering (RSCE, 2014), November 12-13, 2013, Bohol, **Philippines**

(5) **M. J. H. Khan**, M.A. Hussain , M.F.Irfan, A review on modeling and control system of fluidization bed gas phase reactor for polyethylene production, 4<sup>th</sup> Regional Conference on Chemical Engineering, Armanda Hotel, Selangor, *Malaysia*, 9-10<sup>th</sup> February 2012.

University of Malaya